Supercritical Carbon Dioxide for Green Polymer Chemistry

Silvio Curia, MSci, BSci

Thesis submitted to the University of Nottingham
in fulfilment of the requirements for the degree of
Doctor of Philosophy



The University of Nottingham

UNITED KINGDOM · CHINA · MALAYSIA

The University of Nottingham
School of Chemistry, May 2016

Disclaimer

All the work presented in this thesis is the original work of the author, with the exception of results referenced to other sources. It has not been submitted as part of any other degree or professional qualification.

Date:_____ Signed:_____

Silvio Curia

Acknowledgments

I would like to first thank my supervisor, Professor Steve Howdle, for the opportunity to undertake this PhD, for his fatherly guidance, encouragement and research freedom provided throughout my research, and for sharing his expertise about English football with me. I must also thank Dr Derek Irvine for his co-supervision and advice. I am also infinitely grateful to Helen Carson, and the other secretaries, for the organisation of travels, conferences, expenses *etc.*: thanks for replying to all the interminable emails I sent you in these years!

Mark Guyler, Rich Wilson, Pete Fields, Martin Dellar and all the other guys in the workshop deserve a great deal of gratitude for their priceless technical support and for coming up with solutions for every imaginable problem: thank you, I would have made no progress without you!

Thank you to all of our collaborators for sharing their expertise with me and for the fruitful discussions: Dr Davide De Focatiis (The University of Nottingham), Professor Mats Johansson and Susana Torron (KTH Royal Institute of Technology), Professor Juan Francisco Rodríguez Romero and Dr Cristina Gutierrez Muñoz (University of Castilla-La Mancha), and all the FP7-REFINE partners (the research leading to these results has received funding from the People Programme (Marie Curie Actions) of the European Union's Seventh Framework Programme FP7/2007-2013/under REA grants agreement No. [289253]).

Thank you to everyone in B10 for the help, scientific (and non-scientific) discussions and for making my time in Nottingham so enjoyable (in particular those who introduced me to the joy of life: gravy). There are too many of you to name, but special thanks to (in alphabetical order so that nobody gets offended!) Amy, Mariana, Simon and Tom, who helped me a lot during the writing process, and to the MSci students (Charlie and Andy), who helped me in developing my research.

Finally, a special thanks goes to my family and Giada. Without their support and patience, I could have not done any of this. Grazie.

List of Publications

- C.G. Muñoz, M.T. Garcia, **S. Curia**, S.M. Howdle, J.F. Rodriguez, "The effect of CO_2 on the viscosity of polystyrene/limonene solutions", *The Journal of Supercritical Fluids* (88), **2014**, 26-37

- **S. Curia**, D.S.A. De Focatiis and S.M. Howdle, "High-pressure rheological analysis of CO_2-induced melting point depression and viscosity reduction of poly(ε-caprolactone)", *Polymer* (69), **2015**, 17-24 (arisen from Chapter 3)

- **S. Curia**, A.F. Barclay, S. Torron, M. Johansson and S.M. Howdle, "Green process for green materials: viable low temperature lipase-catalysed synthesis of renewable telechelics in supercritical CO_2", *Philosophical Transactions of the Royal Society A: Mathematical, Physical and Engineering Sciences* (373), **2015**, 1-16 (arisen from Chapter 4)

- **S. Curia** and S.M. Howdle, "Towards sustainable polymeric nano-carriers and surfactants: facile low temperature enzymatic synthesis of bio-based amphiphilic copolymers in scCO_2", *Polymer Chemistry* (7), **2016**, 2130-2142 (arisen from Chapter 5)

Overview

This thesis details novel research on the design of new approaches that might lead to a more sustainable polymer industry by combining the use of supercritical carbon dioxide, a commercially available immobilised enzyme and renewable monomers.

First, the key themes explored in this thesis are outlined. Green polymer chemistry, biodegradable and renewable polymers, biocatalysts for polymerisations (*i.e.* enzymes) and supercritical carbon dioxide as a reaction medium for polymer synthesis and processing are introduced (Chapter 1).
Then, the high-pressure equipment and characterisation techniques are detailed. The reaction vessel used extensively in this research work is meticulously described. The high-pressure fixed-volume view cell and the high-pressure rheometer are also detailed (Chapter 2). This chapter includes also the standard operating procedure (SOP) for each piece of equipment.
In the first research chapter, the carbon dioxide-induced melting point depression of poly(ε-caprolactone) is investigated; thorough rheometric studies are used to provide a rheological viewpoint to this phenomenon (Chapter 3). Shear-viscosity studies were performed in order to assess the advantages that high-pressure carbon dioxide could deliver for semi-crystalline polymer processing. Visual observations of the polymer plasticisation and comparisons with high-temperature studies are also shown.
In the subsequent chapter, the development of a novel enzymatic low-temperature approach for the preparation of functional low molecular weight polyesters is detailed (Chapter 4). By exploiting the unique properties of supercritical carbon dioxide and an enzyme catalyst, polymerisations ordinarily conducted using metal catalysts in excess of 200 °C were successfully conducted at milder conditions. Functional molecules could be used to end-cap the chains, thus producing green telechelics.
Then, this innovative synthetic approach was extended to the preparation of bio-based amphiphilic polymers, which could be useful for drugs encapsulation and as surfactants in detergent formulations (Chapter 5). Specifically, the self-assembly

of these novel polymers and the stability of the aggregated structures in water were investigated in detail. Additionally, encapsulation of a highly lipophilic molecule (Coumarin-6) and surface tension studies provided a clear demonstration of the usefulness of these polymers for a wide range of applications.

The final part of the thesis sums up the overall conclusions obtained from this research work and outlines possible opportunities for future research in this area (Chapter 6).

List of abbreviations

ATR	→	Attenuated total reflection
CAC	→	Critical aggregation concentration
CaLB	→	*Candida antarctica* Lipase B
CNT	→	Carbon nanotube
DCM	→	Dichloromethane
DCTB	→	trans-2-[3-(4-tert-Butylphenyl)-2-methyl-2-propenylidene]malononitrile
DLS	→	Dynamic light scattering
DP	→	Degree of polymerisation
DPH	→	1,6-diphenyl-1,3,5-hexatriene
DSC	→	Differential scanning calorimetry
E_a	→	Activation energy for viscous flow
EGDMA	→	Ethylene glycol dimethacrylate
EPDM	→	Ethylene propylene diene monomer rubber
EU	→	European Union
FDA	→	Food and Drug Administration (US)
FTIR	→	Fourier transform infrared
G'	→	Storage modulus
G''	→	Loss modulus
GPC	→	Gel permeation chromatography
HEMA	→	2-hydroxyethyl methacrylate
HSA	→	12-hydroxy stearic acid
MALDI-TOF	→	Matrix-assisted laser desorption/ionisation-time of flight mass spectroscopy
MPEG	→	Methoxy poly(ethylene glycol)
M_n	→	Number average molecular weight
M_n^{GPC}	→	Number average molecular weight (through GPC)
M_n^{NMR}	→	Number average molecular weight (through ^{1}H-NMR)
M_n^{th}	→	Theoretical number average molecular weight
MW	→	Molecular weight
M_w	→	Mass average molecular weight

NIST	→	National institute of standards and technology
NMR	→	Nuclear magnetic resonance
NRV	→	Non-return valve
PBAT	→	Poly(butylene adipate-*co*-terephthalate)
p_c	→	Critical pressure
PC	→	Poly(carbonate)
PCL	→	Poly(ε-caprolactone)
PDMS	→	Poly(dimethyl siloxane)
PE	→	Poly(ethylene)
PEG	→	Poly(ethylene glycol)
PEO	→	Poly(ethylene oxide)
PET	→	Poly(ethylene terephthalate)
PGA	→	Poly(glycolic acid)
PHA	→	Poly(hydroxyalkanoate)
PHAz	→	Poly(hexylene azelate)
PLA	→	Poly(lactic acid)
PLGA	→	Poly(lactic-*co*-glycolic acid)
PP	→	Poly(propylene)
PPG	→	Poly(propylene glycol)
PVA	→	Poly(vinyl alcohol)
PVC	→	Poly(vinyl chloride)
RES	→	Reticuloendothelial system
ROP	→	Ring opening polymerisation
rpm	→	Revolutions per minute
RT	→	Room temperature
SA	→	Sorbic alcohol
$ScCO_2$	→	Supercritical carbon dioxide
SCF	→	Supercritical fluid
SFC	→	Supercritical fluid chromatography
$Sn(Oct)_2$	→	Tin (II) octanoate
SOP	→	Standard operating procedure
Tan δ	→	Damping factor (G''/G')
T_c	→	Critical temperature
TEM	→	Transmission electron microscopy

T_g	→	Glass transition temperature
THF	→	Tetrahydrofuran
T_m	→	Melting temperature
TMPO	→	Trimethylolpropane oxetane
UA	→	Uranyl acetate
USDA	→	United States Department of Agriculture
UV	→	Ultraviolet
Vis	→	Visible
VOC	→	Volatile organic compound
X_c	→	Degree of crystallinity

$Đ$	→	Dispersity (M_w/M_n)
$\dot{\gamma}$	→	Shear rate
$\dot{\gamma}_{cr}$	→	Critical shear rate
δ_c	→	Critical density
ΔH_f	→	Enthalpy of fusion
ΔH_f^0	→	Enthalpy of fusion for a 100% crystalline polymer
ε-CL	→	ε-caprolactone
η	→	Viscosity
η_0	→	Zero-shear viscosity
η_0^{amb}	→	Zero-shear viscosity at ambient pressure
$\eta_0^{300 bar CO_2}$	→	Zero-shear viscosity at 300 bar (in CO_2)
λ	→	Relaxation time

Contents

1 Introduction 1

1.1 Modern plastic production and green polymer chemistry: some facts 2

1.1.1 Green polymer chemistry 4

1.2 Bio-based and biodegradable polymers 5

1.2.1 Biodegradable polymer functional groups 6

1.2.1.1 Aliphatic polyesters 6

1.2.1.2 Polyethers 10

1.2.1.3 Other biodegradable polymers 10

1.3 Synthesis of polyesters 11

1.3.1 Polycondensations for polyester synthesis 12

1.3.1.1 Enzyme-catalysed polycondensations 14

1.3.1.2 Conventional catalysts 18

1.3.2 Ring opening polymerisation (ROP) of cyclic esters 19

1.4 Supercritical fluids 20

1.4.1 Supercritical carbon dioxide 22

1.4.1.1 Interaction of $scCO_2$ with polymers 23

1.5 Research aims 25

1.6 References 27

2 Experimental: high-pressure techniques 32

2.1 General high-pressure setup 33

2.1.1 MK III Clamp sealed autoclaves 34

2.1.1.1 Standard operating procedure (SOP) for MK III clamp sealed polymerisations autoclave 38

2.1.2 High-pressure fixed volume view cell 39

2.1.2.1 Standard operating procedure for clamp-sealed 100 mL view cell 41

2.1.3 High-pressure rheometer 43

2.1.3.1 Standard operating procedure for high-pressure rheometric studies 47

2.2 References 49

3 High-pressure rheological analysis of CO_2-induced melting point depression and viscosity reduction of poly(ε-caprolactone) 50

3.1 Introduction 52

3.1.1 Melt processing in CO_2 56

3.1.1.1 Rheology of polymers in CO_2 56
3.1.2 Poly(ε-caprolactone) and aims of the study 57
3.2 Experimental 60
3.2.1 Materials 60
3.2.2 Methods 60
3.2.2.1 T_m depression analysis 60
3.2.2.2 Shear viscosity high-pressure analyses 61
3.2.2.3 Viscosity *vs* Temperature studies at ambient pressure and under high-pressure 62
3.2.2.4 Transient shear experiment studies 62
3.2.2.5 View cell plasticisation study 63
3.2.2.6 Differential Scanning Calorimetry (DSC) 63
3.3 Results 65
3.3.1 T_m of PCL10 at ambient pressure 65
3.3.2 Effect of pressure on T_m of PCL10 67
3.3.2.1 Soaking time study 67
3.3.2.2 T_m depression in CO_2 72
3.3.3 Effect of pressure and MW on the viscosity of PCL 76
3.3.3.1 Viscosity of PCL10 and PCL80 under CO_2 77
3.3.3.2 Viscosity of PCL10 and PCL80 under N_2 83
3.3.3.3 Relaxation time analysis 86
3.3.3.4 Transient shear viscosity analyses: is the CO_2 solubility changing while shearing? 87
3.4 Conclusions 92
3.5 References 94
4 Green process for green materials: viable low temperature lipase-catalysed synthesis of renewable telechelics in supercritical CO_2 98
4.1 Introduction 100
4.1.1 Green functional polymers 100
4.1.2 Lipase-catalysed polymerisations 102
4.1.3 $ScCO_2$ as a polymerisation medium, azelaic acid and 1,6-hexanediol as building blocks: aims of the study 104
4.2 Experimental 108
4.2.1 Materials 108
4.2.2 Methods 108
4.2.2.1 Enzymatic synthesis of telechelic poly(hexylene azelate) (PHAz) 108

4.2.2.2 Cross-linking procedure 110
4.2.2.3 ^{1}H and ^{13}C-NMR analysis. 111
4.2.2.4 Gel permeation chromatography (GPC) 113
4.2.2.5 Differential scanning calorimetry (DSC) 113
4.2.2.6 Matrix-assisted laser desorption/ionisation-Time of flight mass spectrometry (MALDI-TOF) 114
4.2.2.7 Real time Fourier Transform Infrared (FTIR) 114
4.2.2.8 Melt (high-temperature) synthesis 115
4.2.2.9 Enzyme recycling test 115
4.3 Results 117
4.3.1 Low temperature enzymatic route to telechelic PHAz in $scCO_2$ 117
4.3.2 Thermal properties 121
4.3.3 Structural characterisation 123
4.3.3.1 NMR studies 123
4.3.3.2 MALDI-TOF analyses 132
4.3.4 Effect of enzyme concentration 135
4.3.5 Enzyme recycling 138
4.3.6 Cross-linking tests 141
4.3.6.1 FTIR studies 141
4.3.6.2 DSC studies on cross-linked samples 146
4.4 Conclusions 148
4.5 References 150

5 Towards sustainable polymeric nano-carriers and surfactants: facile low temperature enzymatic synthesis of bio-based amphiphilic copolymers in $scCO_2$ 154

5.1 Introduction 155
5.1.1 Amphiphilic block copolymers: an overview 155
5.1.1.1 Polymeric nanoparticles preparation 160
5.1.1.2 Critical Aggregation concentration (CAC) 161
5.1.1.3 Characteristic size 163
5.1.2 Low temperature enzymatic synthesis of bio-based amphiphilic copolymers: aims of the study 165
5.2 Experimental 166
5.2.1 Materials 166
5.2.2 Methods 166
5.2.2.1 Enzymatic synthesis MPEG-*b*-PHAz-*b*-MPEG 166

5.2.2.2 ^{1}H and ^{13}C-NMR analysis 168
5.2.2.3 Gel permeation chromatography (GPC) 170
5.2.2.4 Differential scanning calorimetry (DSC) 170
5.2.2.5 Preparation of polymer nanoparticles 171
5.2.2.6 Dynamic light scattering (DLS) 171
5.2.2.7 Transmission electron microscopy (TEM) 171
5.2.2.8 Coumarin-6 (C6) incorporation 172
5.2.2.9 UV-Vis quantification of C6 incorporation 172
5.2.2.10 Critical aggregation concentration (CAC) determination 173
5.2.2.11 Maximum bubble pressure test 174
5.3 Results 176
5.3.1 Copolymers synthesis and structural characterisation 176
5.3.1.1 Thermal analyses 179
5.3.2 Aqueous self-assembly studies 181
5.3.2.1 NMR analyses 181
5.3.2.2 Size investigations: DLS and TEM 183
5.3.3 UV-Vis studies 187
5.3.3.1 C6 incorporation 187
5.3.3.2 CAC determination 190
5.3.4 Surface tension reduction 192
5.4 Conclusions 194
5.5 References 196
6 Conclusions and future investigations 200
6.1 Conclusions 201
6.2 Future work 203
6.3 References 207
A Appendix 1: Additional Information for Chapter 4 208
A.1 ^{1}H-NMR spectra of functional PHAz polymers with DP6 208
A.2 ^{1}H-NMR spectra of the polymer synthesised without CO_2 in the melt at high temperature (110 °C) 210
A.3 ^{1}H-NMR spectra for enzyme recycling tests (synthesis of propyl oleate) 214
B Appendix II: Additional Information for Chapter 5 218
B.1 ^{1}H-NMR of MPEGs and copolymers 218
B.2 DLS studies 222
B.2.1 Intensity and volume distribuions 222

B.2.2 DLS distribution of (b) $MPEG_{12}$-$PHAz_6$-$MPEG_{12}$: temperature study 225
B.2.3 DLS distribution of (b) MPEG-$_{12}$-$PHAz_6$-$MPEG_{12}$ micelles produced from nano-precipitation from DCM 227
B.3 Additional TEM images 228
B.4 CMC studies 229

1 Introduction

The aim of this chapter is to provide an essential background for the subjects presented in this thesis. The chapter gives an introduction to the general aspects of modern polymer chemistry and some specific synthetic procedures, including common polymerisation techniques. An emphasis will be placed on green polymer chemistry and polyesters, which will be the main focus of the research presented in this thesis.

The chapter also introduces the use of supercritical carbon dioxide as a clean, cheap, green alternative to conventional solvents in polymer synthesis.

Finally, the general aims of this work are defined.

1.1 Modern plastic production and green polymer chemistry: some facts

In 2014 around 59 million tonnes of plastics were produced within the European Union (EU). Although European plastic production is currently stable, the global production is constantly rising (Figure 1.1) [1]. A growing trend can clearly be observed, with the global plastic production increasing by around 90 million tonnes over the timespan of 10 years (from 2004 to 2013).

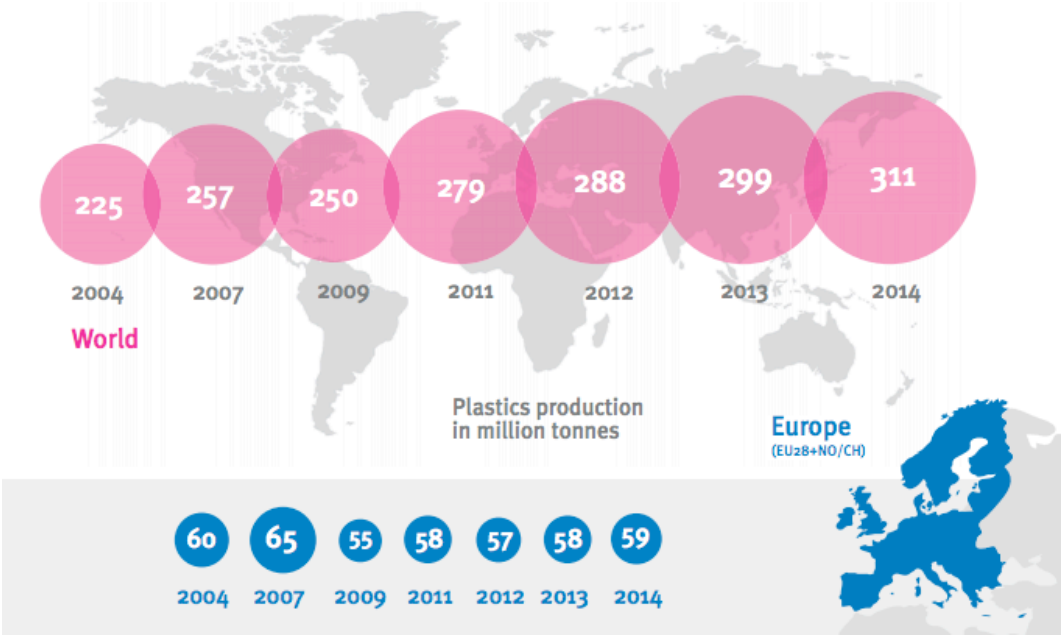


Figure 1.1 - World (pink circles) and European (blue circles) plastic production from 2004 to 2014. In the EU the production stabilised after 2011 to around 58 Mtonnes. On the contrary the global production is characterised by a continuous growth. Figure reproduced from reference [1].

Most commercial polymers are derived from petroleum-based precursors. Therefore, they are synthesised using non-renewable raw materials (*i.e.* resources that are not replenished by natural means on a human time-scale) and the majority of them will not be biodegradable at the end of their life cycle [2].

In 2013, poly(ethylene) (PE) and poly(propylene) (PP) accounted for approximately 50% of polymer demand in the EU, with poly(vinyl chloride) (PVC) being the third one at 10%. These polymers are used in a wide range of applications, such as packaging (the largest end use market segment with a 39.5%

share), building and construction (20.1%) and automotive parts (8.6%) (Figure 1.2) [1].

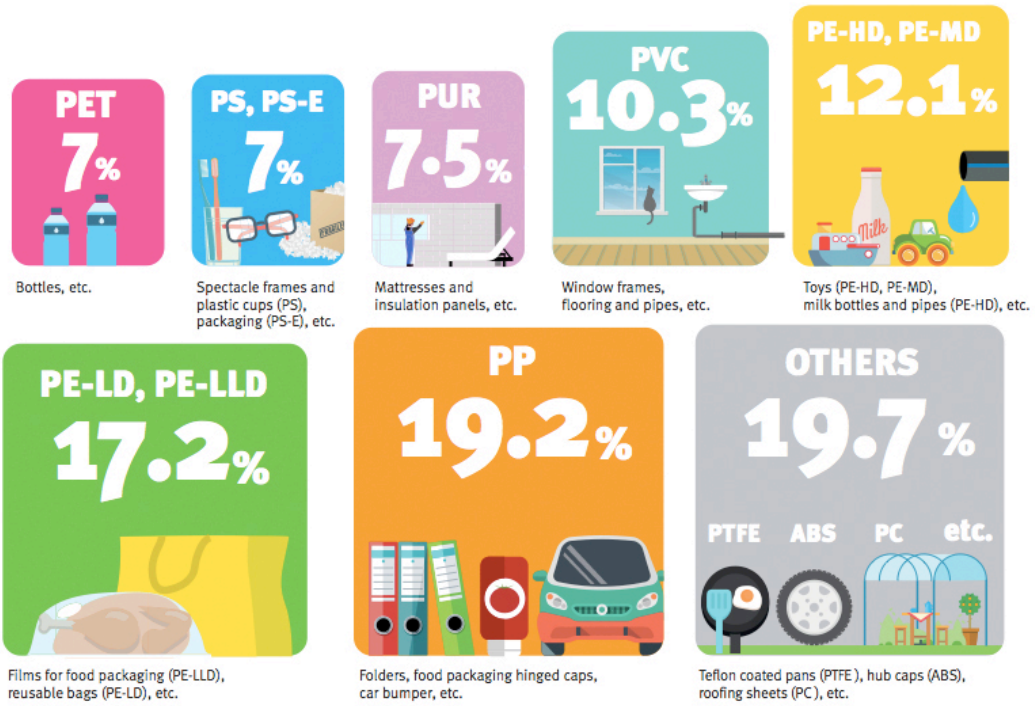


Figure 1.2 - European plastic demand by polymer type in 2014. PE, PP and PVC represent the most used polymers (around 60% of the global demand) [1].

Recycling of these polymers is possible; however, the vast majority of them is buried in landfill sites or incinerated at the end of their useful life [2]. In fact, only 6.6 million tonnes of plastic wastes were recycled in 2012 in the EU [1]; whilst over 30 million and 15 million tonnes of non-degradable polymeric waste are produced each year in the United States and in the EU respectively [2].

This is clearly not environmentally acceptable and for this reason many European countries have imposed, or are imposing, a ban on landfill [1]. In more detail, the first countries that banned landfill were Netherlands (1996) and Denmark (1997). These were followed by Austria (2004), Germany and Sweden (2005), Belgium and Switzerland (2006), Norway (2009) and Scotland (2014). Future landfill bans are expected in Finland and Poland by the end of 2016.

Furthermore, it has been estimated that currently we are exploiting petroleum at a non-sustainable rate, around 10^5 times faster than the nature can produce it. Therefore, continuing with this rate of consumption, the current petroleum reserves will be exhausted in around 60 years [2].

Consequently, the employment of renewable, naturally-derived materials is expected to grow dramatically in the future years [3-5].

1.1.1 Green polymer chemistry

Green chemistry emerged in the 1990s and has become a crucial area of modern science [6, 7]. Several reasons contribute to this drive, including increased public awareness, the request for cleaner manufacturing processes from governments and a sense of industrial responsibility towards environmental issues.
Since the word "green" first started being placed in front of the word "chemistry", many debates regarding the right meaning of "green chemistry" have been held. In general, green chemistry is defined as the design of chemical processes and products that reduce or eliminate the use or the production of hazardous substances [8]. In 1998 Anastas and Warner published a 12-principle list that aimed to guide the practice of green chemistry. In a nutshell, these principles established crucial concepts such as:

- Utilisation of safe and environmentally benign chemicals;
- Design of synthetic processes that maximise the amount of raw material that ends up in the product (atom economy);
- Prevention of waste rather than waste management;
- Use of renewable raw materials and minimisation of the energy consumption [9].

Therefore, the general scope of green chemistry goes beyond concerns over hazards from chemical toxicity and includes waste reduction, energy conservation and sustainability. Unsurprisingly these concepts apply to all the different branches of chemistry, and polymer chemistry is not an exception. Therefore, investigations on biodegradable and bio-based polymers, greener synthetic approaches and more environmentally friendly catalysts have attracted increasing

attention in the last two decades [2, 4, 10-19]. These can lead to the achievement of a more sustainable and environmentally friendly polymer and plastic industry.

1.2 Bio-based and biodegradable polymers

The expressions "bio-based polymer" and "renewably sourced (or renewable) polymer" have the same meaning [20]. They refer to materials containing carbon originating from renewable natural sources (*e.g.* plants, trees, algae *etc.*).

Bio-based polymers (also known as biopolymers) are therefore derived from plant-based raw materials and tend to be biodegradable. They typically contain oxygen and/or nitrogen atoms in their backbone, which are responsible for their biodegradability [2, 4].

The category of bio-based polymers can be further divided into two subcategories: natural biopolymers and synthetic biopolymers. The former category includes bio-based polymers found directly in nature, such as: lignin, suberin, proteins, bacterial polyesters like poly(hydroxyalkanoate)s (PHAs), and carbohydrates (*e.g.* cellulose, starch, chitin, carrageenan *etc.*) [4].

On the other hand, synthetic biopolymers are those polymers that are not found directly in nature but are produced by exploiting precursors that are found abundantly in nature (*e.g.* carbohydrates) [2]. The most significant examples of this class of biopolymers are poly(lactic acid) (PLA), poly(glycolic acid) (PGA) and their copolymer poly(lactic-co-glycolic acid) (PLGA) (see Section 1.2.1.1) [2].

Biodegradable polymers are generally defined as those polymers that decompose in natural aerobic and anaerobic environments [2]. Typically, physical degradation leads to partial degradation through hydrolysis and photodegradation; microorganisms will then take the smaller fragments (monomers and oligomers) and break them down into even simpler units (*e.g.* biomass, water and gases) [2, 21]. Therefore, these polymers do not accumulate in the environment at the end of their life cycle.

Hence, the terms "biodegradable polymers" refer to both bio-based and petroleum-based polymers that are susceptible to degradation through the action of enzymes and/or living organisms [22]. In fact, biodegradability depends not only on the origin of the polymer precursors, but also on the final chemical composition and structure of the chains. For example, poly(ε-caprolactone) (PCL) and poly(ethylene glycol) (PEG) are two biodegradable petroleum-based polymers that are used in a wide range of applications [23, 24].
Furthermore, in recent years investigations on novel routes to derive the polymers and polymer precursors from natural sources have been attracting much attention [4, 25, 26]. For instance, the production of bio-based PEGs, which are derived from sugarcane waste, has been announced by Acme-Hardesty Company [27, 28]. For this reason, the class of synthetic biopolymers is in continuous expansion: polymers that are not considered bio-based nowadays might be considered green and renewable in future years.

1.2.1 Biodegradable polymer functional groups

Generally, biodegradable polymers contain hydrolysable functional groups (such as esters and amides), or groups susceptible to oxidation (such as ethers) [22, 24]. For this reason, vinyl polymers are hardly degradable since they are neither susceptible to hydrolysis, nor easily oxidised in the absence of catalysts or harsh conditions [2, 22, 29]. One exception is represented by poly(vinyl alcohol) (PVA), which can be easily degraded by some enzymes and microorganisms [22, 30, 31].
The next sections give information on the most important classes of biodegradable polymers with a major emphasis on aliphatic polyesters, since it is on these that the presented research will predominantly focus.

1.2.1.1 Aliphatic polyesters

At present, aliphatic polyesters represent the most commonly known and studied class of biodegradable polymers. This class includes PLA, PCL, PHAs, PGA,

PLGA etc. [22, 32]. These polymers are characterised by the presence of ester linkages in the backbone (Figure 1.3).

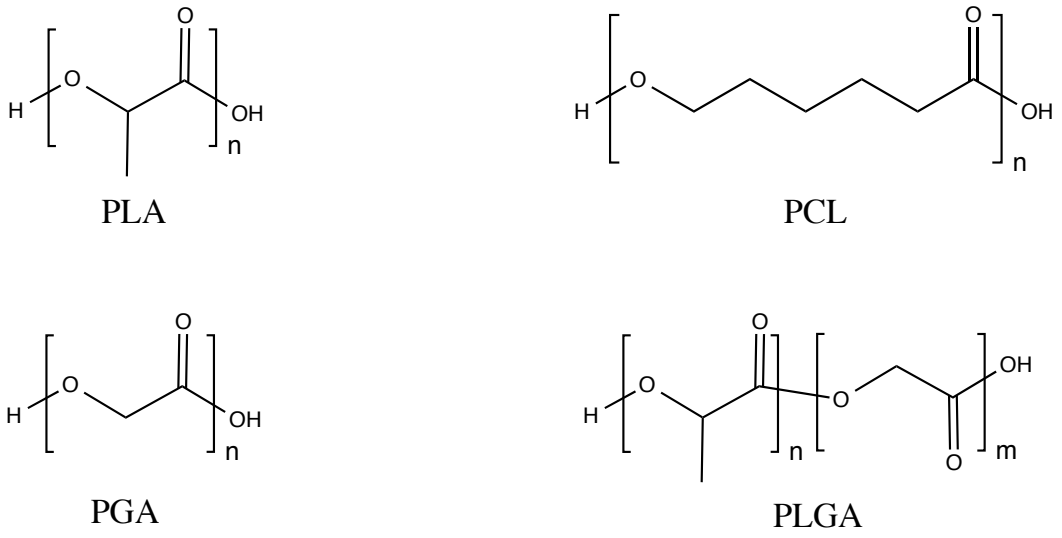
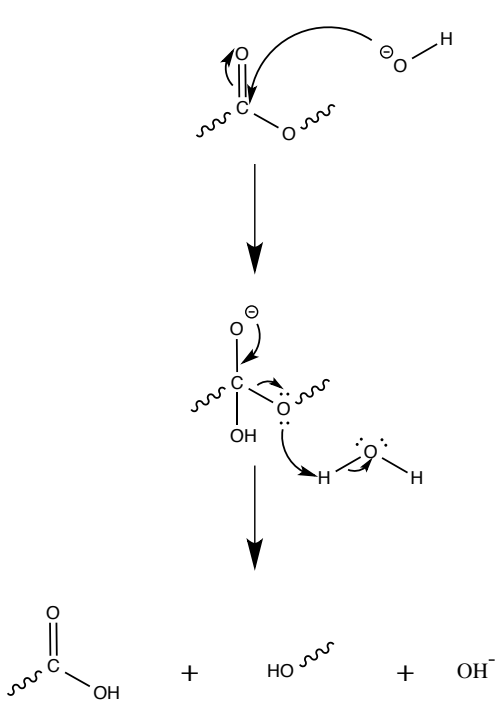


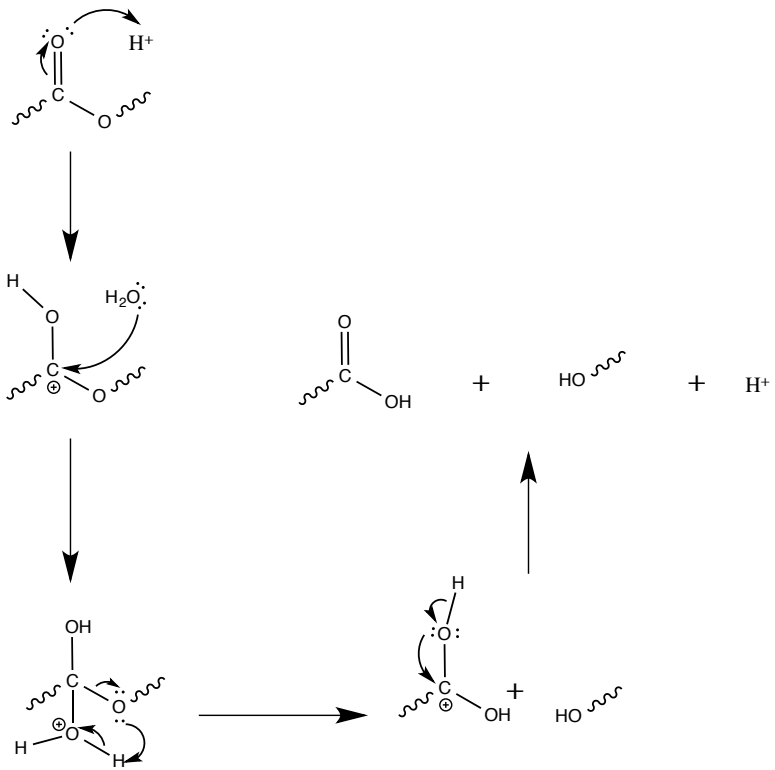
Figure 1.3 - The most common aliphatic polyesters: PLA, PCL, PGA and PLGA. The backbone of these polymers is characterised by the presence of hydrolysable ester bonds.

This bond is easily hydrolysed in acidic or basic conditions (Figure 1.4). Furthermore, enzyme-catalysed hydrolysis and degradation by microorganisms have been widely described [4, 5, 33].

The rate of their degradation depends on several factors, such as: degree of crystallinity (X_c), chain flexibility, macroscopic structure (surface area/porosity) and molecular weight [21, 34, 35]. For instance, if a chain is more flexible, more sites will be accessible to water for hydrolysis and the polymer chain can fit more easily into the active site of enzymes; these factors will increase the biodegradation rate. Furthermore, water does not diffuse well through crystalline regions [34]. For this reason, amorphous regions are degraded preferentially over the crystalline ones and there is an inverse relationship between the melting temperature (T_m) of the polyester and the rate of biodegradation [35, 36].



(a)



(b)

Figure 1.4 - Schematic mechanism of base (a) and acid (b) catalysed hydrolysis of polyesters. In these schemes the wavy lines represent the remainder of the polymer chain structure.

A vast variety of monomers can be used to prepare aliphatic polyesters, and several synthetic routes can be exploited [5, 22, 36-38] (see Section 1.3).
Generally, these polymers have decent mechanical properties so they can be used for packaging and other applications [4, 39]. However, their performances are significantly worse than those of aromatic polyesters (*e.g.* poly(ethylene terephthalate) (PET)), which, on the other hand, are not easily biodegraded [35, 40]. For this reason, aliphatic-aromatic copolyesters have been prepared to obtain polyesters with improved mechanical features and a good biodegradability (*e.g.* poly(butylene adipate-*co*-terephthalate) (PBAT), Figure 1.5) [40].

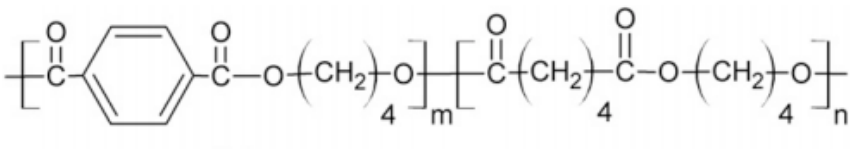


Figure 1.5 – Chemical structure of poly(butylene adipate-*co*-terephtalate) (PBAT).

Moreover, the functional characteristics of aliphatic polyesters can also be modified or improved by blending or copolymerising them with other polymers, or by dispersing inorganic nanofillers into them [32, 41-46].
Finally, a key feature is that PLA, PCL and PLGA are biocompatible and bioresorbable: hence, they are approved for use in humans by the Food and Drug Administration (FDA). Accordingly, these polymers (and their copolymers) are widely used for drug delivery, tissue engineering and other medical applications [45-50].

Aliphatic polyesters will be the main focus of this thesis (see Section 1.5):

- Chapter 3 focuses on the analysis of the mechanical and rheological properties of PCL under supercritical carbon dioxide ($scCO_2$);
- Chapter 4 describes the use of $scCO_2$ to design a novel green synthetic route to produce functional polyesters;
- Chapter 5 shows the extension of this synthetic route for the preparation of innovative bio-based amphiphilic polymers.

1.2.1.2 Polyethers

Polyethers are polymers that contain ether groups in their backbone. This class includes polymers such as PEG and PPG (Figure 1.6).

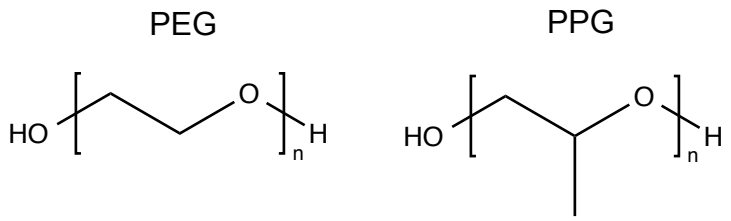


Figure 1.6 – PEG and PPG are by far the most commonly used polyethers. Polyethers have generally low viscosity and low T_m.

Since ether groups cannot form hydrogen bonds with each other, these polymers are generally characterised by low T_m and low viscosity [37, 51].

PEG - also known as poly(ethylene oxide) (PEO) - is a water soluble polymer that finds application as a lubricant, plasticiser, and building block for surfactants to name just a few [52, 53]. Owing to its low toxicity and biocompatibility, it is widely used also in cream formulations and varied medical applications [54, 55].

PEG is metabolised by several bacteria [56]. The microbial degradation of this polyether is indeed widely described in literature and it has been repeatedly ascertained that lower molecular weights favour biodegradation whilst PEGs with molecular weight higher than 4000 g mol^{-1} are typically more resistant to biodegradation [24, 56-58].

In the fifth chapter of this thesis low molecular weight PEG blocks will be used as a hydrophilic segments to prepare new green amphiphilic low molecular weight copolymers through a novel synthetic approach.

1.2.1.3 Other biodegradable polymers

The list of polymers that can be degraded, more or less readily, is rather long. Therefore, this small final section gives some information and references to find more in-depth details about other commercially relevant biodegradable polymers.

Polyanhydrides are characterised by the presence of anhydride bonds in the backbone and are degraded by hydrolysis [59]. The rapid degradation of aliphatic

anhydrides results in instability; because of this, storage of these polyanhydrides requires freezing with liquid nitrogen [60]. As a result, aliphatic anhydrides are mainly used for medical and pharmaceutical applications where short-term release of bioactive molecules is required [59-61].

Polypeptides and polyamides are commonly used biodegradable polymers. These polymers contain amide linkages that enzyme and microorganisms can break down [2, 58]. Furthermore, copolymers containing ester and amide bonds (*i.e.* polyester-amides) are readily degraded [62].

Polyurethanes contain urethane linkages within their backbone and are synthesised using diisocyanates and diols (or hydroxyl-ended low molecular weight polymers such as polyethers and polyesters) [63]. Hence, they are composed of different parts that will determine the physical properties (*e.g.* crystallinity, flexibility *etc.*) and the biodegradation rate [22].

Other important biodegradable polymers are represented by biopolymers such as proteins (*e.g.* collagen) and polysaccharides (*e.g.* starch, cellulose, chitosan). More details on these biopolymers and other biodegradable polymers can be found in the specific literature [2-5, 22, 58, 64].

1.3 Synthesis of polyesters

Polyesters will be the main focus of this thesis. Therefore, a more detailed description and additional references on the synthetic procedures employed to prepare this type of polymers are presented in this section.

Two different routes can be used to synthesise polyesters:

- Polycondensation of difunctional monomers (Figure 1.7 upper);
- Ring opening polymerisation (ROP) of cyclic esters (Figure 1.7 lower).

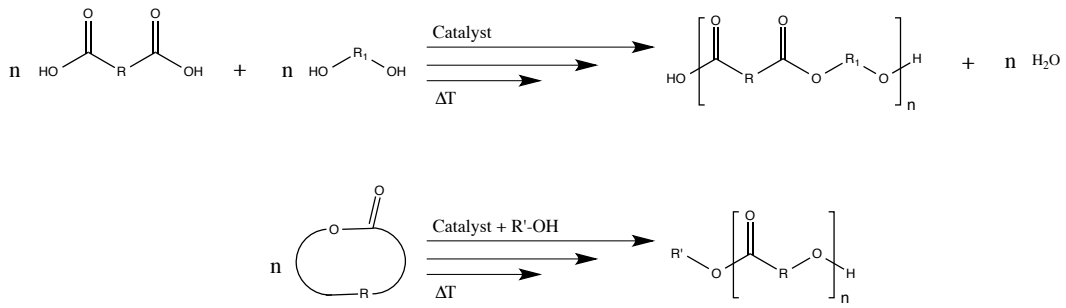


Figure 1.7 – Schematic synthesis of polyesters through polycondensation (upper) and ring opening polymerisation (lower).

The next sections give further information on these approaches, with a particular emphasis on enzymatic polycondensation, since this will be the polymerisation technique employed in Chapter 4 and 5.

1.3.1 Polycondensations for polyester synthesis

Polyester synthesis can be accomplished by a step-growth polymerisation reaction occurring between difunctional reactants. This condensation reaction is accompanied by the formation of a low molecular weight by-product; for instance, when diacids and diols are used, the condensation by-product is H_2O (Figure 1.7 upper).

Esterifications are equilibrium reactions; therefore, an effective removal of the condensate will prevent depolymerisation and will shift the synthesis towards the formation of high molecular weight polymers (*e.g.* up to 40-80 kg mol^{-1} for PET) [65, 66].

Transesterifications of dimethyl esters with diols are also widely used. In this case, the by-product will be methanol and this alcohol can be more efficiently eliminated from the reaction system [37]. In addition, diesters are typically characterised by a lower T_m and an increased solubility and, hence, they are easier to handle [67].

Furthermore, diacyl chlorides can also be used: not only are these molecules more reactive than dicarboxylic acids, but also the by-product (HCl) is gaseous and,

hence, easy to remove (or neutralised with a base). However, these chlorinated derivatives are significantly more expensive and hazardous than the diacids [63].

Esterification and transesterification polymerisations are typically rather slow at low temperature and must therefore be carried out at high temperature, preferably in the presence of a catalyst (see Sections 1.3.1.1 and 1.3.1.2 for more details) [63, 68]. A combination of vacuum and sparging is generally applied to ensure successful removal of the reaction condensate. Alternatively, molecular sieves (nano-porous crystalline metal aluminosilicates) can be used to adsorb the low molecular weight by-product [69, 70].

Another crucial requirement in order to obtain high molecular weight polyester through polycondensation is an exact end-group stoichiometry: imbalance in the monomer feed ratio will limit the average degree of polymerisation (DP). However, this effect can also be used to voluntarily target specific polymer chain lengths. Similarly, mono-functional molecules can be used to end-cap the polymer and target specific molecular weights. Furthermore, the end-capper molecule can possess specific functional groups (*e.g.* epoxy, methacrylate *etc.*) capable of subsequent reaction [71-73]. In this way, di-end-functional polyesters (*i.e.* telechelic polyesters) can be prepared. This approach will be used in Chapter 4 and 5 to prepare novel functional polyesters.

Typical side reactions that can occur during polycondensations are: intramolecular cyclisation (ring closure), hydrolysis, reaction with mono-functional impurities and inter-chain transesterification. These competing reactions can significantly affect the molar mass and molecular weight distribution of the polymer [37].

To sum up, polycondensations are normally slow and require high temperature, controlled stoichiometry and efficient removal of the condensate. Additionally, condensation reactions are characterised by low atom efficiency (or atom economy) due to the formation of by-products.

Nonetheless, condensation polymerisations have attracted increasing attention recently. There are several reasons for this drive. In particular, a wide diversity of diacids with different structures is available from natural resources and these can be employed as building blocks for the preparation of bio-based polyesters [68, 72, 74-76]. Furthermore, the possibility of carrying out enzymatic polycondensations preserving the specific moieties of monomers and end-cappers has opened up for

the facile preparation of functional polyesters through chemo-selective condensation polymerisations [67, 69, 71, 73, 77, 78].

1.3.1.1 Enzyme-catalysed polycondensations

Over the last two decades enzyme-catalysed polycondensations have become an important synthetic approach for the production of polyesters [19, 78-80]. Enzymes are proteins that are characterised by a high catalytic activity and specificity towards a particular chemical reaction.

The enzymes responsible for the cleavage of bonds by hydrolysis belong to a class referred to as hydrolases. One specific group of hydrolases that assumed an important role in polymer chemistry are lipases [80].

Candida antarctica Lipase B (CaLB) is a lipase responsible for the hydrolysis of fatty esters in nature; however, in anhydrous conditions this enzyme is active in the reverse reaction and can accept alcohols as nucleophiles. Hence, esterifications and polyesterifications can be carried out using this enzyme *in vitro* in organic solvents or in the melt with a good selectivity toward primary alcohols [73, 75]. The active site of CaLB is situated in the core of the protein at the bottom of a funnel-like structure characterised by a highly hydrophobic surface. The hydrophobicity and the limited available space in the active site explain its high selectivity [69].

For CaLB, the best reactivity is normally observed in hydrophobic solvents such as hexane, toluene and diphenylether. Hydrophilic polar solvents like methanol lead to significant modifications in enzyme conformation and, hence, to a dramatic decrease in its activity [81].

For synthetic applications, CaLB is normally immobilised onto an inert and insoluble material. CaLB immobilised on cross-linked acrylic resin beads (*i.e.* poly(methyl methacrylate-*co*-divinylbenzene)) is known with the commercial name of Novozym 435 (10% by weight of lipase). Immobilisation provides several advantages, in particular: immobilised enzymes generally have increased thermal and pH stability, higher activity and they are more easily separated from the products, thus facilitating the recycling of the catalyst at the end of the synthesis [73, 80].

CaLB can also catalyse the hydrolysis (or alcoholysis) of polyesters, therefore the condensation by-products need to be removed during poly-esterifications in order to drive the equilibrium of the reaction towards product formation and avoid undesired side-reactions. This is typically achieved by application of vacuum, sparging or using molecular sieves (or a combination of these) [19, 69].

The suggested temperature range for Novozym 435 is between 30 °C and 60 °C (declared by the supplier) [82]; however, this immobilised lipase has been shown to be able to catalyse reactions at temperatures up to 100 °C [14, 73]. Nonetheless, a significant decrease in its activity (~35%) was observed when Novozym 435 was incubated for 24 hours in toluene at temperatures higher than 70 °C. This has been attributed to swelling of the acrylic support and possible leaching of the enzyme [83].

To sum up, compared with conventional routes, enzymatic polycondensations have several advantages, such as: mild reaction conditions, high chemo-selectivity and elimination of issues associated with the presence of residues from metallic catalysts [80]. Therefore, enzymes provide a good platform for the development of green condensation polymerisation processes.

The catalytic triad of CaLB is composed of serine, histidine and aspartate (Ser105, His224 and Asp187). For better understanding, the first steps of the CaLB-catalysed polycondensation mechanism are described (Figure 1.8).

In the first step, the nucleophilic Ser105 residue attacks one carbonyl of the substrate (*i.e.* a diacid if R=H or a diester if R≠H). The substrate acts as the acyl donor and the first tetrahedral intermediate (THI-1) is formed. The negative charge in THI-1 is stabilised by three hydrogen bonds (represented by the dashed lines) within the oxyanion hole, which is a pocket in the active site formed by two amino acids that can stabilise negative charges. The positive charge on His224 is stabilised by interaction with Asp187 [19].

Afterwards, proton transfer from the His224 to the alkyl oxygen of the substrate takes place and the leaving group is released (*i.e.* H_2O if R=H, an alcohol if R≠H). This results in the formation of the acyl-enzyme complex (AEC). In the next step, the AEC is attacked by the incoming nucleophile (*i.e.* the diol HO-B-OH). A proton is transferred from the diol to the His224 residue and a second tetrahedral intermediate (THI-2) is formed. This is again stabilised by hydrogen-bond interactions with the oxyanion hole [19].

In the final step, the enzyme is de-acylated to form the ROOC-A-CO-O-B-OH ester, which is released.

The propagation of the polymerisation occurs through alternating binding of diacids (or diesters) and diols. Later in the reaction, oligomers and whole polyester chains can be linked together.

Furthermore, it is important to remark that the ester bonds within the polymer chains can also undergo nucleophilic attack by the Ser105 residue of the lipase, resulting in the cleavage of the chain [69]. Additionally, the polymerisation by-product (ROH) can also act as a nucleophile; for this reason, it should be carefully removed to avoid undesired reactions.

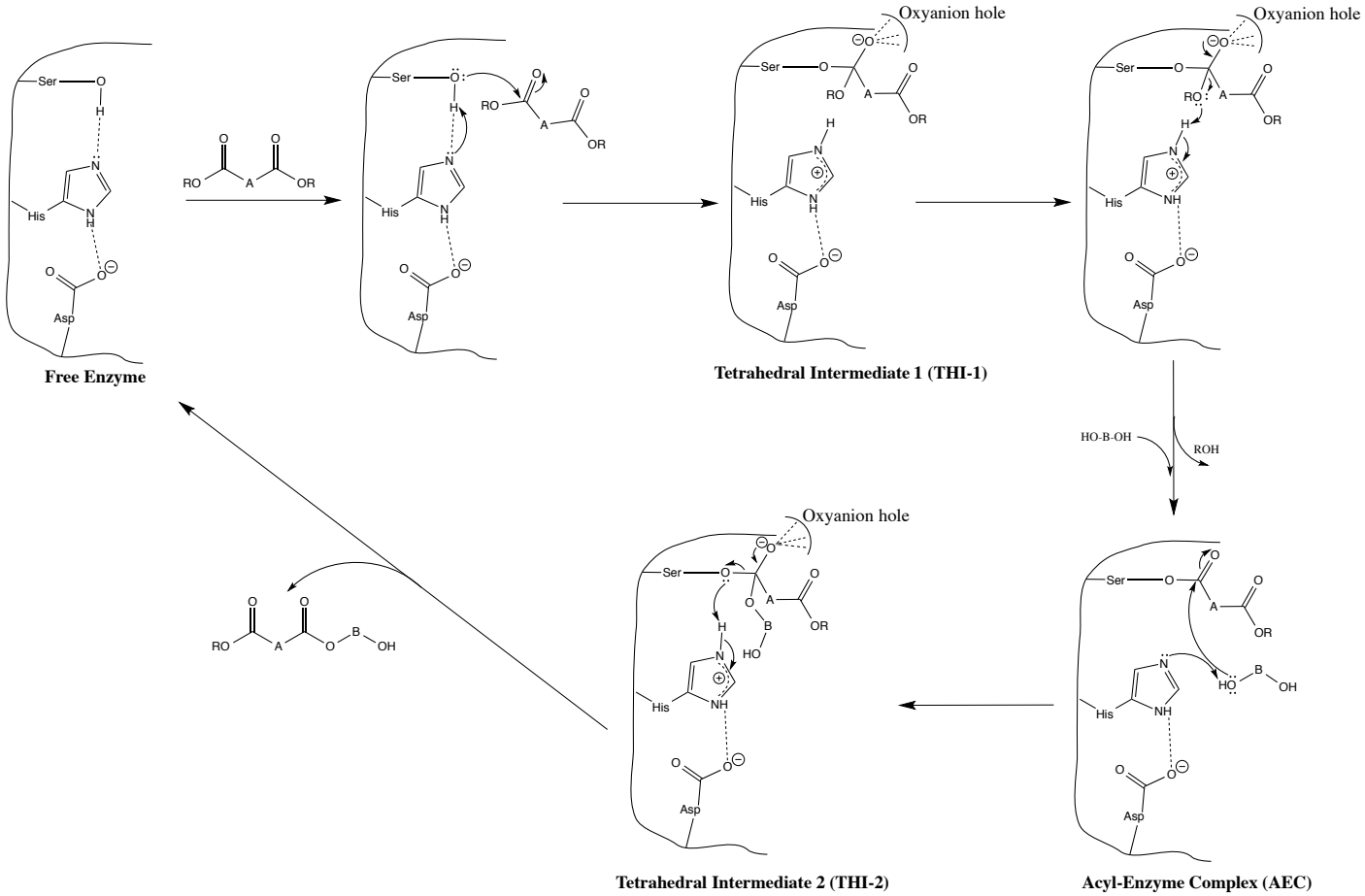


Figure 1.8 – Schematic for the CaLB-catalysed condensation of the monomers ROOC-A-COOR and HO-B-OH.

1.3.1.2 Conventional catalysts

The synthesis of polyesters can be accomplished also through acid-catalysed poly-esterifications. An acid (*e.g.* para-toluenesulfonic acid) can be added to the monomers (external catalysis) or, alternatively, the acid functional group of the diacid monomer can catalyse the reaction (self-catalysis) [63]. In all the cases the use of high temperature (typically from 110 to 290 °C) is normally required to increase the rate of the reaction, aid the removal of the condensation by-product and lower the viscosity of the melt. However, strong acids also catalyse a significant number of side reactions at elevated temperatures [65].

In industrial settings polyesters are generally prepared using metal-based catalysts (*e.g.* alkoxides of antimony and titanium or acetates of manganese, zinc and cobalt) at temperatures ranging from 180 to 290 °C [65, 68, 78]. In-depth description of the mechanism of these metal-catalysed reactions and the typical procedures used to obtain high molecular weight polymers is beyond the scope of this thesis; the interested reader is referred to the specific literature of the field for more information [65, 84].

By conducting polycondensations at high temperatures it is possible to polymerise high-melting monomers and significantly reduce the melt viscosity (increasing the diffusivity of the reactive species). Hence, the lack of enzymes with adequate stability and activity at temperatures higher than 100 °C is somehow limiting [78]. On the other hand, high temperature processes are energy intensive and can easily be affected by undesired side-reactions (*e.g.* dehydration of diols and β-scission of polyesters) [78]. Furthermore, the use of high temperatures is particularly undesirable when using molecules containing thermally labile functional moieties (such as vinyl groups) or bio-molecules (*e.g.* drugs and hormones) [78, 85]. Therefore, this limits the range of polymers that can be prepared through high temperature melt polycondensations.

Finally, the lack of selectivity of metal catalysts can lead to uncontrolled side-reactions [86] and additional serious concerns are represented by metal traces, which are difficult to remove from the final product and are not acceptable for biomedical applications [87].

1.3.2 Ring opening polymerisation (ROP) of cyclic esters

The ROP of cyclic esters (*e.g.* lactide, ε-caprolactone, glycolide *etc.*) is generally carried out in bulk, solution, emulsion or dispersion [88]. The temperature of bulk polymerisations ranges from 60 °C to 150 °C (depending on the monomer) [38, 88], whilst in solution much lower temperatures (0-25 °C) have been used [88, 89]. ROPs are normally performed in the presence of a catalyst and an initiator. The reaction mechanism depends on catalyst/initiator system chosen for the polymerisation. Anionic and coordination-insertion are the most widely employed ROPs of cyclic esters [88].

Tin (II) octanoate ($Sn(Oct)_2$) is by far the most common catalyst for the ROP of lactone monomers [38, 87]. This catalyst follows a coordination-insertion mechanism and is used together with an active hydrogen compound (*e.g.* alcohol) acting as an initiator [87]. Recently, the use of a novel tin alkoxide initiating system ($OctSn\text{-}OCH_2CH_2OCH_2CH_2O\text{-}SnOct$), which gives a better control over the polymerisation, has been described [45].

Problems associated with condensation polymerisations, such as the essential requirement of a controlled stoichiometry and the removal of low molecular weight by-products (*e.g.* water, alcohols), are avoided in ROPs [38].

Lipase-catalysed ROPs have been also described [38, 80]. Lipases have been shown to catalyse ROP of a wide range of lactones. These reactions have been performed in the bulk or in hydrophobic solvents (*e.g.* toluene) [80, 86, 90]. Similarly to enzyme-catalysed polycondensations, enzyme-catalysed ROPs have several positive features, such as low reaction temperature, non-toxic catalysis and high selectivity. For these reason these are generating a growing interest [69, 80]. Nonetheless, the variety of cyclic esters available for the preparation of polyesters through enzymatic ROP is much more limited compared to that of diacids and diols available for polycondensation [80].

1.4 Supercritical fluids

Generally, a supercritical fluid (SCF) is defined as a substance above its critical pressure (p_c) and critical temperature (T_c) (Figure 1.9) [10, 91].
However, this description does not give any information about the density of the substance. Therefore, a more practical definition describes a SCF as a substance above its critical point and with a density close to or higher than its critical density (δ_c) [91, 92].

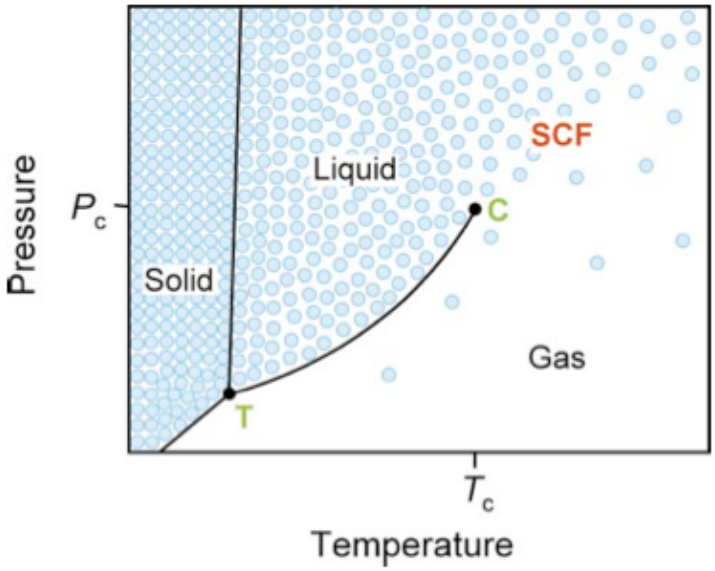


Figure 1.9 – Representation of the pressure *vs* temperature phase diagram for a pure substance (adapted from reference [93]). The triple point (T) and the critical point (C) are indicated. The blue circles give a schematic depiction of the change in density of the system at different conditions. The solid lines indicate the boundaries, at which phase transitions occur.

At the triple point (T) the three phases (vapour, liquid and solid) coexist and are in equilibrium. At the critical point (C), *i.e.* above the p_c and T_c, the phase boundary between the liquid and vapour phase does no longer exist: the substance becomes a single phase, namely a SCF. In this state, the liquid and the gas phases have the same density and become indistinguishable (Figure 1.10) [10, 91].

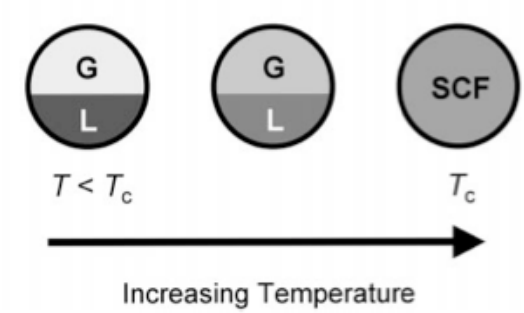


Figure 1.10 – Schematic depiction of the change from gas-liquid (G-L) equilibrium at $T<T_c$ to SCF at $T \geq T_c$ when a substance is heated at a pressure in excess of p_c [91].

For this reason, a SCF is characterised by unique properties that fall in between those typical of liquids and those of gases (Table 1.1). For instance, the density of a SCF can be relatively high (*i.e.* liquid-like), so that it can dissolve certain solids and liquids, while exhibiting gas-like properties such as high diffusivity and low viscosity.

Table 1.1 – A comparison of the typical values for physical properties of gases, SCFs and liquids (adapted from reference [94]). SCFs have properties in between those expected for classical gases and liquids.

Property	Gas	SCF	Liquid
Density (g mL^{-1})	10^{-3}	0.2-0.9	0.8-1.0
Diffusivity (cm^2 s^{-1})	10^{-2}-1	0.1-3.3 × 10^{-4}	0.5-2.0 × 10^{-5}
Viscosity (Pa s)	0.5-3.5 × 10^{-5}	0.2-1.0 × 10^{-4}	0.3-2.4 × 10^{-3}

In addition to this, SCFs are highly compressible and their densities can be effectively tuned by varying pressure and/or temperature (Figure 1.11) [91]. Hence, the solvent properties of a SCF can be changed by choosing carefully the pressure and temperature values [10, 94, 95].

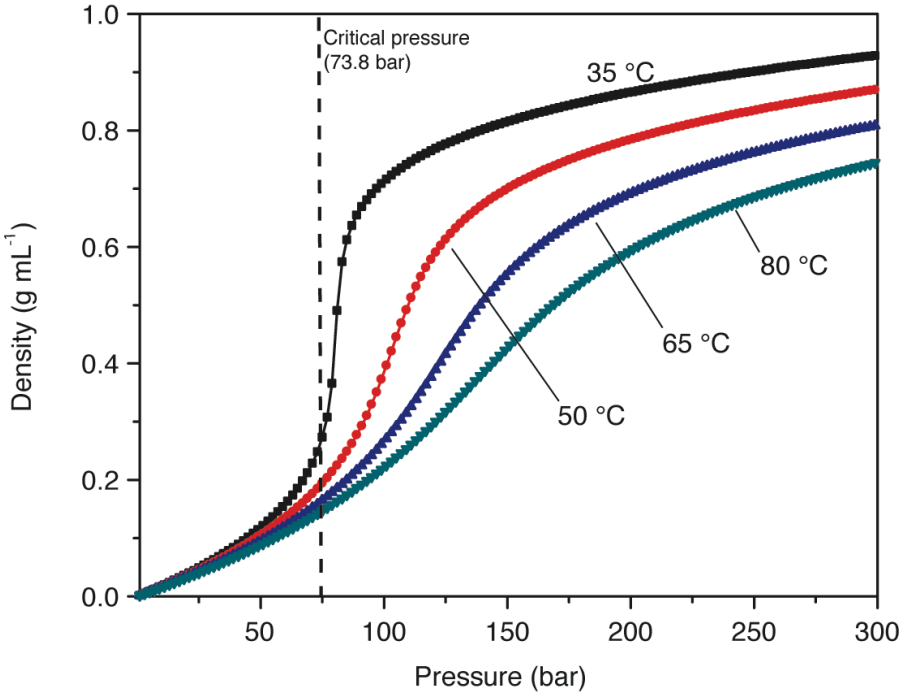


Figure 1.11 – Isothermal change in density with increasing pressure for carbon dioxide at four different temperatures above the T_c. Chart prepared using data taken from the National Institute of Standards and Technology (NIST) "Chemistry - Thermophysical Properties of Fluid Systems" WebBook [96].

1.4.1 Supercritical carbon dioxide

Supercritical carbon dioxide ($scCO_2$) is one of the most promising and exploited SCFs, and it is continuously attracting attention as a green solvent and potential replacement for conventional organic solvents [10, 95, 97, 98].

CO_2 is relatively cheap, non-toxic, non-flammable and inert towards reactive compounds. Furthermore, CO_2 has an easily accessible critical point (31.1 °C, 73.8 bar), when compared to other substances. For example, water has much higher T_c and p_c (374.2 °C, 221 bar), thus its use is more energy intensive and expensive when compared to $scCO_2$.

Also, CO_2 can be obtained from other industrial processes where it is produced as a by-product, in fact an important focus of modern science is on CO_2 capture [99]. This means that carbon dioxide is a very widely available resource that scientists

need to carefully plan to utilise and, since CO_2-assisted synthesis and processing reuse gas that is produced from other industrial processes, the net emission in the atmosphere is not increased [10].

Moreover, with the appropriate system design, the used CO_2 can be separated and recycled at the end of the process, thus potentially making the overall system highly commercially sustainable and viable, as currently done for CO_2-assisted extraction processes [95].

Carbon dioxide in its supercritical condition is characterised by low viscosity, high diffusivity and a tunable liquid-like density. For these reasons, $scCO_2$ can be an effective alternative to organic solvents in a wide range of applications.

The main industrial application in which $scCO_2$ finds purpose is in extraction processes, such as the extraction of caffeine from coffee beans or the extraction of essential oils from seeds [95, 100-104].

In recent years, new possible applications for $scCO_2$ have been investigated. For instance, CO_2 has been used for the synthesis of inorganic nanoparticles [105] and for biodiesel production [106]. Furthermore, the interest in employing $scCO_2$ as a medium for synthesis and processing of polymers has been constantly growing in the last two decades [10, 85, 91, 97, 98, 107-111].

1.4.1.1 Interaction of $scCO_2$ with polymers

In general, $scCO_2$ is a poor solvent for most polymers, with rare exceptions including fluoropolymers, silicones and few vinyl ester polymers and copolymers [97, 112, 113]. Nevertheless, CO_2 is very effective at penetrating and dissolving into polymeric materials, plasticising and effectively liquefying many polymers at temperatures well below their normal ambient pressure glass transition (T_g) and melting point (T_m) [91, 98, 107, 114, 115].

Below the T_g the chains in the amorphous regions of a polymer are locked into a rigid structure, whilst above the T_g they have enough thermal energy to move past each other when an external force is applied [116]. For this reason, polymers are typically processed at a temperature their T_g (or T_m when semicrystalline) [117-119]. However, the melt viscosity of polymers can be quite high; therefore, either considerably high temperatures or organic solvents are often required to facilitate their synthesis, processing and modification [120, 121].

Through addition of pressurised CO_2, the processing temperatures of many polymers can be lowered as the CO_2 molecules embed themselves between the polymer chains. This increases the spacing and the free volume fraction (v_f) allowing the polymer chains to slide past each other at a lower temperature; therefore, the CO_2 molecules act as a classic low molecular weight plasticiser [98, 107, 115, 122]. Moreover, the addition of CO_2 can also dramatically reduce the viscosity of polymer melts [120, 123, 124].

Finally, it is important to remark that CO_2 is also very different from classic plasticisers as its concentration (and hence the extent of the plasticisation) can be effectively tuned by controlling the applied pressure (Figure 1.12) [125].

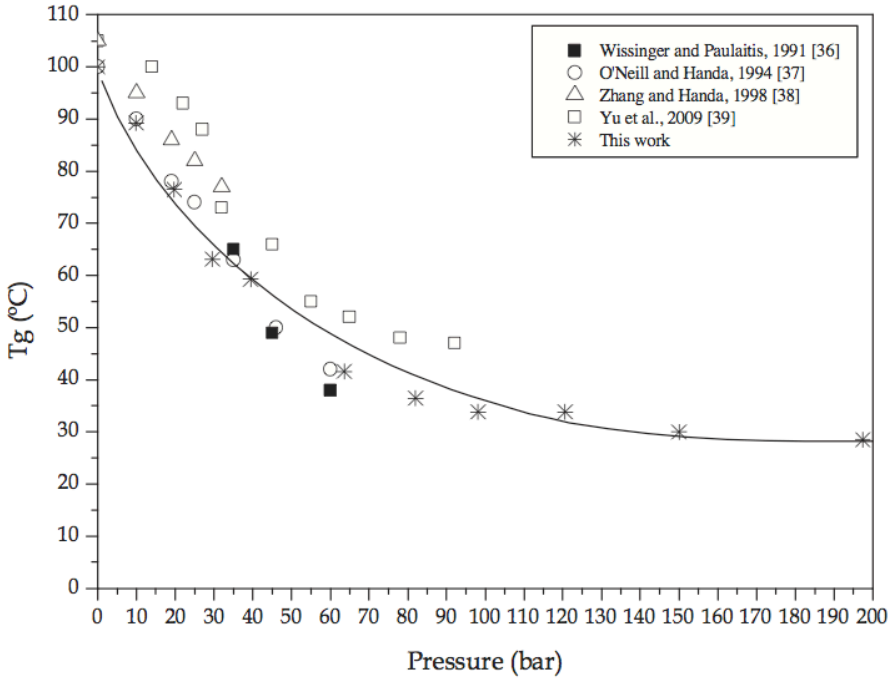


Figure 1.12 – Depression of the T_g for poly(styrene) with increasing CO_2 pressure. The graph is reproduced from reference [125].

A more in-depth description of the effects of high-pressure CO_2 on the rheological and mechanical properties of polymers and additional references on this subject are given in the introduction to Chapter 3.

1.5 Research aims

Modern polymer chemistry is characterised by several challenges. As previously stated, the research trends have been pushed towards the investigations of more environmentally friendly alternative materials and alternative synthetic procedures. One of the primary tasks is the expansion of the range of polymers derived from renewable sources. Similarly, the interest in finding greener replacements to traditional catalytic methods and designing novel synthetic approaches is becoming more and more important. This would allow synthesis to be conducted in a more environmentally friendly manner, avoiding harsh reaction conditions and diminishing (or completely eliminating) the utilisation of volatile organic compounds (VOCs).

This introductory chapter has outlined the background and fundamental chemistry upon which the research work presented in this thesis will be based on. Enzymes and CO_2 have been anticipated as suitable candidates for the design of novel synthetic procedures that can lead to the preparation of bio-based polymers through energetically and environmentally sustainable routes.

Therefore, this research aims to provide a route to sustainable and green polymer synthesis by combining $scCO_2$, a commercially available lipase (Novozym 435) and the use of renewable monomers.

Chapter 2 provides a detailed description of the high-pressure equipment used for synthesis and characterisation throughout this thesis. The standard operating procedures are also included.

Chapter 3 presents the high-pressure rheological analyses conducted on two PCL samples with different molecular weights. Shear moduli and shear viscosity studies performed over a range of pressures and temperatures are shown. The results are correlated to visual observations using a high-pressure fixed volume view cell. Besides, the effects of pressurised CO_2 are compared to those of high temperatures and those obtained through the use of a non-plasticising gas.

Chapter 4 aims to answer the question whether the combined use of CO_2 and Novozym 435 could be used to synthesise telechelic semi-crystalline bio-based polyesters directly from the diacid (*i.e.* without preliminary esterification) through

a solvent-free/low-temperature approach. Chains with varied DP are targeted and different functional end-cappers are used. Comparisons with high temperature melt polymerisations are shown to highlight the advantages obtained by using $scCO_2$.

Finally, Chapter 5 describes the attempt of extending this approach to the synthesis of amphiphilic block copolymers, opening up the possibility of preparing bio-based surfactants for detergents, and nano-carriers for medical applications.

1.6 References

[1] Plastics Europe, *Plastics – the Facts 2015. An analysis of European plastics production, demand and waste data* **2015**

[2] C.B. Frech, *Journal of Chemical Education*, 79, **2002**, p. 1072

[3] F.W. Lichtenthaler, *Carbohydrates as Organic Raw Materials*, Ullmann's Encyclopedia of Industrial Chemistry, Wiley-VCH Verlag GmbH & Co. KGaA, **2000**.

[4] M.N. Belgacem, A. Gandini, *Monomers, Polymers and Composites from Renewable Resources*, Elsevier Science, **2011**

[5] P.B. Smith, R.B. Gross, *Biobased Monomers, Polymers, and Materials*, OUP USA, **2013**

[6] J.H. Clark, *Nature Chemistry*, 1, **2009**, p. 12

[7] M. Poliakoff, P. Licence, *Nature*, 450, **2007**, p. 810

[8] EPA United States Enviromental Protection Agency, *Basics of Green Chemistry*, http://www.epa.gov/greenchemistry/basics-green-chemistry - definition, Last Access: 05/04/2016

[9] P.T. Anastas, J.C. Warner, *Green chemistry: theory and practice*, Oxford university press, New York, **1998**

[10] M.F. Kemmere, T. Meyer, *Supercritical carbon dioxide in polymer reaction engineering / edited by Maartje F. Kemmere and Thierry Meyer*, Wiley-VCH, **2005**

[11] N. Cordeiro, N.M. Belgacem, A. Gandini, C. Pascoal Neto, *Bioresource Technology*, 63, **1998**, p. 153

[12] M.A. Bernards, *Canadian Journal of Botany*, 80, **2002**, p. 227

[13] A. Gandini, C. Pascoal Neto, A.J.D. Silvestre, *Progress in Polymer Science*, 31, **2006**, p. 878

[14] A. Olsson, M. Lindström, T. Iversen, *Biomacromolecules*, 8, **2007**, p. 757

[15] B.D. Ulery, L.S. Nair, C.T. Laurencin, *Journal of Polymer Science Part B: Polymer physics*, 49, **2011**, p. 832

[16] Y. Jiang, A.J. Woortman, G.O. van Ekenstein, K. Loos, *Biomolecules*, 3, **2013**, p. 461

[17] S. Tsubaki, S. Sakumoto, N. Uemura, J. Azuma, *Food Chemistry*, 138, **2013**, p. 286

[18] S.N. Vouyiouka, E. Topakas, A. Katsini, C.D. Papaspyrides, P. Christakopoulos, *Macromolecular Materials and Engineering*, 298, **2013**, p. 679

[19] A.R.A. Palmans, A. Heise, *Enzymatic Polymerisation*, Springer Berlin Heidelberg, Berlin, **2010**

[20] *Renewable Bio Based Polymers* http://www.dupont.com/products-and-services/plastics-polymers-resins/bio-based-polymers.html, Last Access: 25/06/2015

[21] E. Rudnik, *Compostable Polymer Materials*, Elsevier Science, **2010**

[22] I. Vroman, L. Tighzert, *Materials*, 2, **2009**, p. 307

[23] M.A. Woodruff, D.W. Hutmacher, *Progress in Polymer Science*, 35, **2010**, p. 1217

[24] R. Marchal, E. Nicolau, J.P. Ballaguet, F. Bertoncini, *International Biodeterioration & Biodegradation*, 62, **2008**, p. 384

[25] R. Ooms, M. Dusselier, J.A. Geboers, B. Op de Beeck, R. Verhaeven, E. Gobechiya, J.A. Martens, A. Redl, B.F. Sels, *Green Chemistry*, 16, **2014**, p. 695
[26] J. Pang, M. Zheng, R. Sun, A. Wang, X. Wang, T. Zhang, *Green Chemistry*, 18, **2016**, p. 342
[27] Grand View Research, *Polyethylene Glycol (PEG) Market Analysis By Application (Medical, Personal Care, Industrial) And Segment Forecasts To 2020*, http://www.grandviewresearch.com/industry-analysis/polyethylene-glycol-peg-market, Last Access: 11/04/2016
[28] Green Chemicals Blog, *Europe explores creation of Bio-based products standards*, http://greenchemicalsblog.com/2015/03/16/europe-explores-creation-of-bio-based-products-standards/, Last Access: 11/04/2016
[29] H.J. Arpe, *Ullmann's Encyclopedia of Industrial Chemistry, Ullmann's Encyclopedia of Industrial Chemistry: Set: Printed Fifth Edition plus Sixth Edition Electronic Release*, Wiley, **1999**
[30] Y. Watanabe, N. Hamada, M. Morita, Y. Tsujisaka, *Archives of Biochemistry and Biophysics*, 174, **1976**, p. 575
[31] E. Chiellini, A. Corti, S. D'Antone, R. Solaro, *Progress in Polymer Science*, 28, **2003**, p. 963
[32] L. Yu, K. Dean, L. Li, *Progress in Polymer Science*, 31, **2006**, p. 576
[33] M. Watanabe, F. Kawai, S. Tsuboi, S. Nakatsu, H. Ohara, *Macromolecular Theory and Simulations*, 16, **2007**, p. 619
[34] G. Kale, *Biodegradation of Commercially Available Biodegradable Packages in Real and Simulated Composting Conditions*, Michigan State University, **2007**
[35] Y. Tokiwa, B.P. Calabia, C.U. Ugwu, S. Aiba, *International Journal of Molecular Sciences*, 10, **2009**, p. 3722
[36] F. Ylmaz, *Polymer Science*, InTech, **2013**
[37] M.P. Stevens, *Polymer Chemistry: An Introduction*, Oxford University Press, **1999**
[38] P. Dubois, O. Coulembier, J.M. Raquez, *Handbook of Ring-Opening Polymerization*, Wiley, **2009**
[39] V. Siracusa, P. Rocculi, S. Romani, M.D. Rosa, *Trends in Food Science & Technology*, 19, **2008**, p. 634
[40] T. Kijchavengkul, R. Auras, M. Rubino, S. Selke, M. Ngouajio, R.T. Fernandez, *Polymer Degradation and Stability*, 95, **2010**, p. 2641
[41] X.A. Peixiang Xing, Lisong Dong, and Zhiliu Feng, *Macromolecules*, 31, **1998**, p. 6898
[42] L. Urbanczyk, C. Calberg, F. Stassin, M. Alexandre, R. Jérôme, C. Jérôme, C. Detrembleur, *Polymer*, 49, **2008**, p. 3979
[43] L. Urbanczyk, F. Ngoundjo, M. Alexandre, C. Jérôme, C. Detrembleur, C. Calberg, *European Polymer Journal*, 45, **2009**, p. 643
[44] K. Suthapakti, R. Molloy, W. Punyodom, K. Nalampang, T. Leejarkpai, P.D. Topham, B.J. Tighe, *Macromolecular Symposia*, 354, **2015**, p. 299
[45] S. Ruengdechawiwat, J. Siripitayananon, R. Molloy, R. Somsunan, P.D. Topham, B.J. Tighe, *International Journal of Polymeric Materials and Polymeric Biomaterials*, 65, **2016**, p. 277
[46] S. Ruengdechawiwat, R. Molloy, J. Siripitayananon, R. Somsunan, P.D. Topham, B.J. Tighe, *Macromolecular Symposia*, 354, **2015**, p. 347
[47] D.W. Hutmacher, *Biomaterials*, 21, **2000**, p. 2529

[48] P.J. Ginty, J.J.A. Barry, L.J. White, S.M. Howdle, K.M. Shakesheff, *European Journal of Pharmaceutics and Biopharmaceutics*, 68, **2008**, p. 82
[49] O.R. Davies, A.L. Lewis, M.J. Whitaker, H. Tai, K.M. Shakesheff, S.M. Howdle, *Advanced Drug Delivery Reviews*, 60, **2008**, p. 373
[50] C. Gualandi, L.J. White, L. Chen, R.A. Gross, K.M. Shakesheff, S.M. Howdle, M. Scandola, *Acta Biomaterialia*, 6, **2010**, p. 130
[51] L. Mandelkern, *Crystallization of Polymers: Volume 1, Equilibrium Concepts*, Cambridge University Press, **2002**
[52] P. Nalam, J. Clasohm, A. Mashaghi, N. Spencer, *Tribology Letters*, 37, **2010**, p. 541
[53] K. Friedrich, U. Breuer, *Multifunctionality of Polymer Composites: Challenges and New Solutions*, Elsevier Science, **2015**
[54] R.B. Borgens, D. Bohnert, *Journal of Neuroscience Research*, 66, **2001**, p. 1179
[55] S. Rameez, H. Alosta, A.F. Palmer, *Bioconjugate Chemistry*, 19, **2008**, p. 1025
[56] F. Kawai, *Applied Microbiology and Biotechnology*, 58, **2002**, p. 30
[57] A. Zgoła-Grześkowiak, T. Grześkowiak, J. Zembrzuska, Z. Łukaszewski, *Chemosphere*, 64, **2006**, p. 803
[58] Y. Doi, K. Fukuda, *Biodegradable Plastics and Polymers: Proceedings of the Third International Scientific Workshop on Biodegradable Plastics and Polymers, Osaka, Japan, November 9-11, 1993*, Elsevier Science, **2013**
[59] J. Tamada, R. Langer, *Journal of Biomaterials Science, Polymer Edition*, 3, **1992**, p. 315
[60] N. Kumar, R.S. Langer, A.J. Domb, *Advanced Drug Delivery Reviews*, 54, **2002**, p. 889
[61] B.M. Vogel, S.K. Mallapragada, *Biomaterials*, 26, **2005**, p. 721
[62] N. Paredes, A. Rodríguez-Galán, J. Puiggalí, *Journal of Polymer Science Part A: Polymer Chemistry*, 36, **1998**, p. 1271
[63] D.J. Walton, J.P. Lorimer, *Polymers*, Oxford University Press, Oxford, **2000**
[64] M. Ash, I. Ash, *Handbook of Green Chemicals*, Synapse Information Resources, **2004**
[65] M.E. Rogers, T.E. Long, *Synthetic Methods in Step-Growth Polymers*, Wiley, **2003**
[66] G. Holden, H.R. Kricheldorf, R.P. Quirk, *Thermoplastic Elastomers*, Hanser, **2004**
[67] S. Torron, M. Johansson, *Journal of Polymer Science Part A: Polymer Chemistry*, 53, **2015**, p. 2258
[68] X. Kong, H. Qi, J.M. Curtis, *Journal of Applied Polymer Science*, 131, **2014**, p. 1
[69] M. Eriksson, *PhD Thesis*, School of Biotechnology, KTH Royal Insitute of Technology, Stockholm, **2010**
[70] T. Maharana, B. Mohanty, Y.S. Negi, *Progress in Polymer Science*, 34, **2009**, p. 99
[71] M. Eriksson, K. Hult, E. Malmström, M. Johansson, S.M. Trey, M. Martinelle, *Polymer Chemistry*, 2, **2011**, p. 714
[72] A. Rüdiger, P. Hendil-Forssell, C. Hedfors, M. Martinelle, S. Trey, M. Johansson, *Journal of Renewable Materials*, 1, **2013**, p. 16
[73] S. Semlitsch, S. Torron, M. Johansson, M. Martinelle, *Green Chemistry*, **2016**, p.

[74] A. Lv, Z.-L. Li, F.-S. Du, Z.-C. Li, *Macromolecules*, 47, **2014**, p. 7707
[75] L. Gustini, B.A.J. Noordover, C. Gehrels, C. Dietz, C.E. Koning, *European Polymer Journal*, 67, **2015**, p. 459
[76] C. Japu, A. Martinez de Ilarduya, A. Alla, Y. Jiang, K. Loos, S. Munoz-Guerra, *Biomacromolecules*, 16, **2015**, p. 868
[77] S. Torron, S. Semlitsch, M. Martinelle, M. Johansson, *Macromolecular Chemistry and Physics*, 215, **2014**, p. 2198
[78] R.A. Gross, M. Ganesh, W. Lu, *Trends in Biotechnology*, 28, **2010**, p. 435
[79] S. Kobayashi, H. Uyama, S. Kimura, *Chemical Reviews*, 101, **2001**, p. 3793
[80] J. Zhang, H. Shi, D. Wu, Z. Xing, A. Zhang, Y. Yang, Q. Li, *Process Biochemistry*, 49, **2014**, p. 797
[81] T. Kulschewski, F. Sasso, F. Secundo, M. Lotti, J. Pleiss, *Journal of Biotechnology*, 168, **2013**, p. 462
[82] Novozymes Biopharma DK A/S, *Enzymes for biocatalysis for smarter chemical synthesis: Immobilized Lipases*, **2014**
[83] Y. Poojari, S.J. Clarson, *Biocatalysis and Agricultural Biotechnology*, 2, **2013**, p. 7
[84] J. Scheirs, T.E. Long, *Modern Polyesters: Chemistry and Technology of Polyesters and Copolyesters*, Wiley, **2005**
[85] S.M. Howdle, M.S. Watson, M.J. Whitaker, M.C. Davies, K.M. Shakesheff, V.K. Popov, F.S. Mandel, J.D. Wang, *Chemical Communications*, **2001**, p. 109
[86] J. Zhou, W. Wang, S. Villarroya, K.J. Thurecht, S.M. Howdle, *Chemical Communications*, **2008**, p. 5806
[87] C. Jérôme, P. Lecomte, *Advanced Drug Delivery Reviews*, 60, **2008**, p. 1056
[88] A.-C. Albertsson, I.K. Varma, *Biomacromolecules*, 4, **2003**, p. 1466
[89] R.C. Pratt, B.G.G. Lohmeijer, D.A. Long, R.M. Waymouth, J.L. Hedrick, *Journal of the American Chemical Society*, 128, **2006**, p. 4556
[90] M. Eriksson, L. Fogelström, K. Hult, E. Malmström, M. Johansson, S. Trey, M. Martinelle, *Biomacromolecules*, 10, **2009**, p. 3108
[91] A.I. Cooper, *Journal of Materials Chemistry*, 10, **2000**, p. 207
[92] J.A. Darr, M. Poliakoff, *Chemical Reviews*, 99, **1999**, p. 495
[93] F. Cansell, B. Chevalier, A. Demourgues, J. Etourneau, C. Even, V. Pessey, S. Petit, A. Tressaud, F. Weill, *Journal of Materials Chemistry*, 9, **1999**, p. 67
[94] V. Goodship, E.O. Ogur, *Polymer Processing with Supercritical Fluids*, Rapra Technology Limited, **2004**
[95] M. McHugh, V. Krukonis, H. Brenner, *Supercritical Fluid Extraction: Principles and Practice*, Elsevier Science, **2013**
[96] National Institute of Standards and Technology (NIST), *Chemistry WebBook-Thermophysical Properties of Fluid Systems* http://webbook.nist.gov/chemistry/fluid/, Last Access: 20/04/2016
[97] F. Picchioni, *Polymer International*, 63, **2014**, p. 1364
[98] E. Kiran, *The Journal of Supercritical Fluids*, 110, **2016**, p. 126
[99] A. Bandyopadhyay, *Carbon Capture and Storage: CO2 Management Technologies*, Apple Academic Press, **2014**
[100] J.M.D. Valle, J.C. De La Fuente, *Critical Reviews in Food Science and Nutrition*, 46, **2006**, p. 131
[101] W.-J. Kim, J.-D. Kim, J. Kim, S.-G. Oh, Y.-W. Lee, *Journal of Food Engineering*, 89, **2008**, p. 303
[102] C.L. Ye, Y.F. Lai, *Chemical Engineering & Technology*, 35, **2012**, p. 646

[103] C. Da Porto, A. Natolino, D. Decorti, *Journal of Food Science and Technology*, 52, **2015**, p. 1748
[104] L. Jaime, E. Vázquez, T. Fornari, M.d.C. López-Hazas, M.R. García-Risco, S. Santoyo, G. Reglero, *Journal of the Science of Food and Agriculture*, 95, **2015**, p. 722
[105] E.P. Da Silva, M.R. Guilherme, E.T. Tenório-Neto, A.F. Rubira, M.H. Kunita, L. Cardozo-Filho, C.G. Alonso, *Materials Letters*, 136, **2014**, p. 133
[106] P. Lozano, E. García-Verdugo, J.M. Bernal, D.F. Izquierdo, M.I. Burguete, G. Sánchez-Gómez, S.V. Luis, *ChemSusChem*, 5, **2012**, p. 790
[107] S.G. Kazarian, *Polymer Science Series C*, 42, **2000**, p. 78
[108] S.Y. Lee, P. Valtchev, F. Dehghani, *Green Chemistry*, 14, **2012**, p. 1357
[109] D. Markovic, S. Milovanovic, M. Radetic, B. Jokic, I. Zizovic, *The Journal of Supercritical Fluids*, 101, **2015**, p. 215
[110] L. Monnereau, L. Urbanczyk, J.-M. Thomassin, T. Pardoen, C. Bailly, I. Huynen, C. Jérôme, C. Detrembleur, *Polymer*, 59, **2015**, p. 117
[111] J.L. Kendall, D.A. Canelas, J.L. Young, J.M. DeSimone, *Chemical Reviews*, 99, **1999**, p. 543
[112] N.A. Birkin, N.J. Arrowsmith, E.J. Park, A.P. Richez, S.M. Howdle, *Polymer Chemistry*, 2, **2011**, p. 1293
[113] L. Du, J.Y. Kelly, G.W. Roberts, J.M. DeSimone, *The Journal of Supercritical Fluids*, 47, **2009**, p. 447
[114] Z. Zhang, Y.P. Handa, *Macromolecules*, 30, **1997**, p. 8505
[115] A. Bos, I.G.M. Pünt, M. Wessling, H. Strathmann, *Journal of Membrane Science*, 155, **1999**, p. 67
[116] G.M. Swallowe, *Mechanical properties and testing of polymers : an A-Z reference / edited by G.M. Swallowe*, Kluwer Academic, **1999**
[117] T.A. Osswald, *Polymer Processing Fundamentals*, Hanser, **1998**
[118] C.I. Chung, *Extrusion of Polymers: Theory and Practice*, Hanser Gardner Publications, **2000**
[119] C.A. Kelly, S.H. Murphy, G.A. Leeke, S.M. Howdle, K.M. Shakesheff, M.J. Jenkins, *European Polymer Journal*, 49, **2013**, p. 464
[120] C.A. Kelly, S.M. Howdle, K.M. Shakesheff, M.J. Jenkins, G.A. Leeke, *Journal of Polymer Science Part B: Polymer Physics*, 50, **2012**, p. 1383
[121] C.A. Kelly, A. Naylor, L. Illum, K.M. Shakesheff, S.M. Howdle, *Advanced Functional Materials*, 22, **2012**, p. 1684
[122] S.P. Nalawade, F. Picchioni, L.P.B.M. Janssen, *Progress in Polymer Science*, 31, **2006**, p. 19
[123] D. Gourgouillon, H.M.N.T. Avelino, J.M.N.A. Fareleira, M. Nunes da Ponte, *The Journal of Supercritical Fluids*, 13, **1998**, p. 177
[124] M. Iguchi, Y. Hiraga, K. Kasuya, T.M. Aida, M. Watanabe, Y. Sato, R.L. Smith, *The Journal of Supercritical Fluids*, 97, **2015**, p. 63
[125] C. Gutiérrez, J.F. Rodríguez, I. Gracia, A. de Lucas, M.T. García, *The Journal of Supercritical Fluids*, 76, **2013**, p. 126

2 Experimental: high-pressure techniques

This chapter describes in detail the experimental high-pressure apparatus employed throughout the project. First, the general high-pressure setup is depicted and then additional information on the specific equipment used to carry out polymerisations and characterisations under pressure is given, *i.e.*:

1. The in-house built clamp-sealed stainless steel autoclave utilised for the high-pressure polymerisations;
2. The in-house built stainless steel view cell equipped with sapphire windows to study the behaviour of samples in CO_2;
3. The commercial high-pressure rheometer used for the rheometric studies under pressure.

Experimental practises are summarised covering the standard operating procedure for all the apparatus.
Specific additional details related to reactants, solvents, reaction conditions and particular characterisation of products (structural, thermal *etc.*) can be found in the experimental part of the individual following chapters.

2.1 General high-pressure setup

In their most general description, the high-pressure systems consisted of a means of supplying the desired pressure to the systems (*i.e.* a pump), high-pressure Swagelok® tubing and fittings, a stainless steel vessel (for reactions or characterisations) and monitoring equipment necessary to check continuously the pressure and temperature values.

The standard system to supply pressure to the reaction vessels is depicted in schematic form (Figure 2.1).

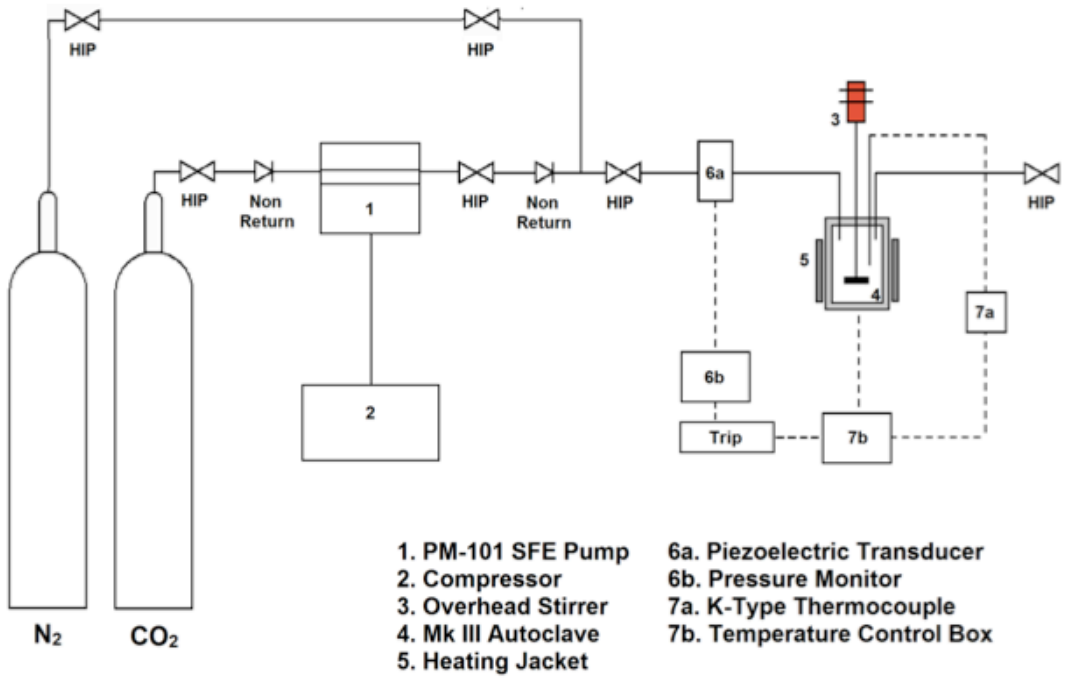


Figure 2.1 - Schematic diagram of a general high-pressure setup. Non return valves (NRV) are placed before and after the Pickel pump to prevent backflows.

A PM-101 SFE Pickel pump (New Ways of Analytics, Germany) was used to deliver compressed CO_2 to the autoclaves. The pump is composed of a gas input, a refrigerator unit for gas liquefaction and an outlet. The pump draws gaseous CO_2 from the cylinder (at a pressure of 55 bar), and the gas is condensed into a liquid by the pump refrigerator. Compressed air at 3-5 bar (supplied by an external compressor) is needed to compress the liquid CO_2 and achieve the

desired output pressure (typically 275-280 bar), which can be set *via* an external knob on the pump.

High-pressure stainless steel tubing supplied by Swagelok® were used to transport the compressed CO_2 to the reaction rigs. Manual HiP valves (High Pressure Equipment Company, USA) were employed to control the CO_2 inlet and outlet flows when filling the autoclaves and at the end of the reactions to vent the system. Non-return valves (NRV) were also employed before each autoclave, to prevent backflow and hence avoid contamination in the CO_2 supply line and into the pump. An optional N_2 cylinder could be integrated in the line, *via* a Swagelok® T-piece, to allow for pressurisation with a non-plasticising gas if needed.

2.1.1 MK III Clamp sealed autoclaves

The reaction autoclaves used to conduct the polymerisations consisted of 20 mL or 60 mL stainless steel 316 vessels designed in-house at the University of Nottingham. These are described in detail elsewhere [1, 2].

In general, the autoclave consists of a stainless steel base and a head, which is attached to the base with a stainless steel clamp (Figure 2.2). The maximum working pressure of this stainless steel vessel is 300 bar at 300 °C.

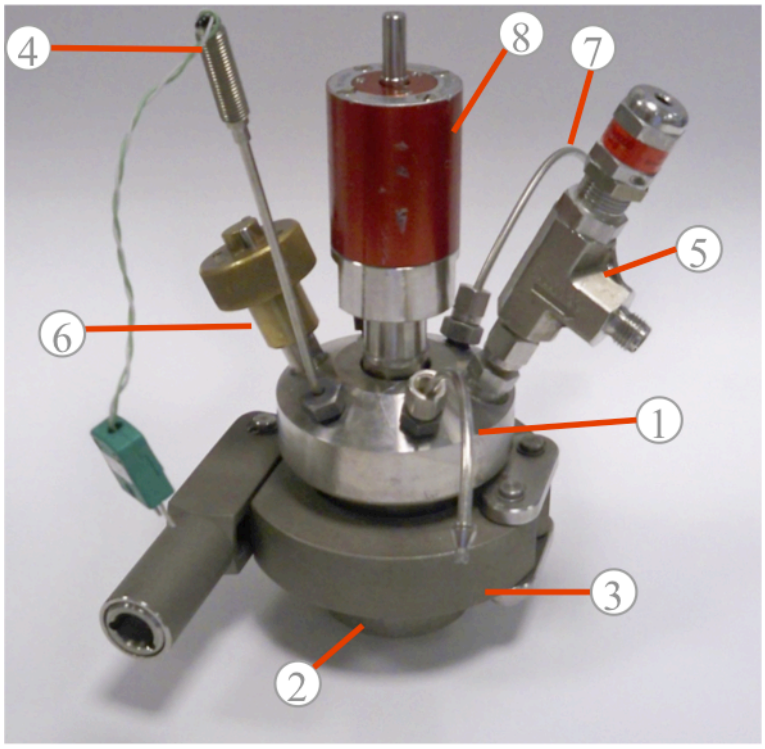


Figure 2.2 – MK III clamp sealed autoclave equipped with a 20 mL base.

The autoclave is composed of:

1. Inlet pipe
2. Base (20 mL or 60 mL)
3. Clamp
4. Thermocouple
5. Spring release valve
6. Safety key
7. Outlet pipe
8. Magnetically coupled stirrer

For clarity, the autoclave is shown in graphic form (Figure 2.3). An ethylene propylene diene monomer rubber (EPDM) O-ring is used to seal the clamped base and head. The use of EPDM O-rings limits the pressure and temperature range to 300 bar at 150 °C. The minimum service temperature is around -50 °C.

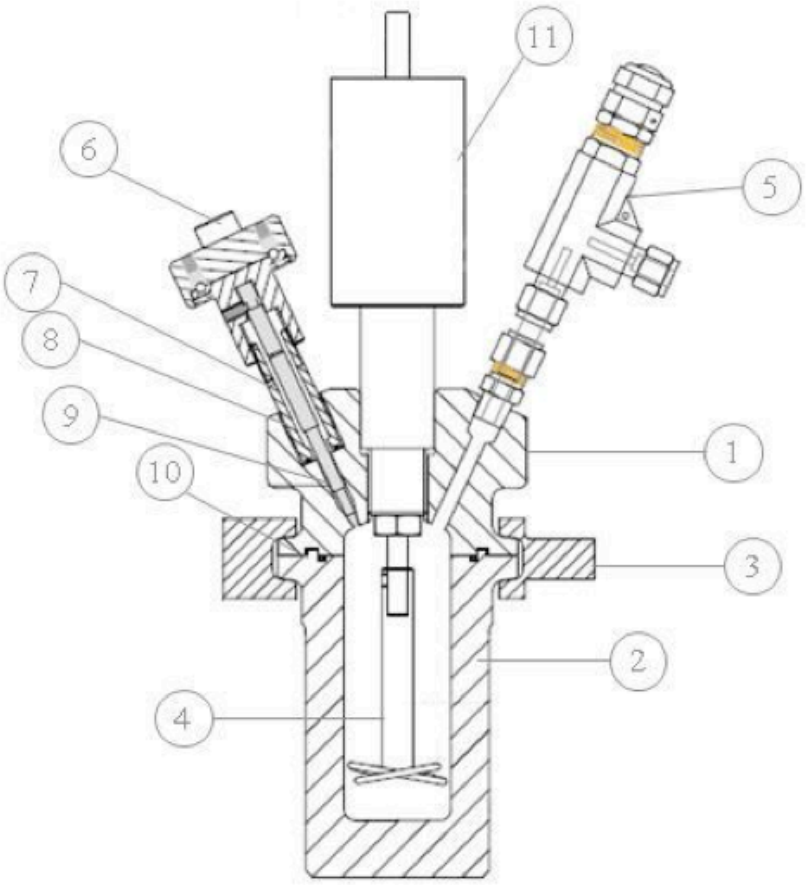


Figure 2.3 – Schematic diagram of a 60 mL MKIII autoclave: (1) head, (2) body, (3) clamp, (4) stirrer, (5) spring-release valve, (6) knob, (7) screw insert, (8) access hole, (9) safety needle, (10) EPDM O-ring and (11) magnetically coupled stirrer.

The head of the reactor is equipped with a magnetically coupled stirrer column, inlet and outlet high-pressure pipes, an internal thermocouple, a spring-release valve (which releases pressures at above 345 bar).

A safety key insert is also present on the head. The safety key is composed of a safety needle and a knob. The safety needle fits in the insert, thus finally sealing the system. If the safety needle is loosened slightly when the system is under pressure, the pressure is slowly and safely released through the insert. Therefore, since the knob has a unique shape that is necessary to close and open the autoclave clamp (Figure 2.4), this guarantees that it is not possible to open the vessel with residual pressure in it.

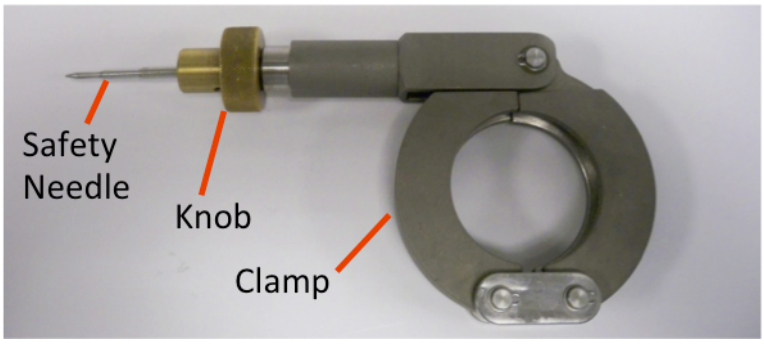


Figure 2.4 – Safety key and clamp to seal the autoclave. To ensure the complete release of pressure before opening the vessel, each clamp has a unique fitted safety key.

In order to allow for constant monitoring of the system pressure, the inlet pipe is connected to pressure transducer. Piezoelectric transducers were used in all the rigs. These devices use the piezoelectric effect to monitor the pressure through conversion of the strain experienced under pressure by a quartz crystal to an electrical output, which can be read on a display. A calibration performed by the manufacturer allows for precise and reproducible readouts.

A stainless steel heating jacket (Watlow, UK) that fits on the base provided efficient heating during the experiments. The heating jacket and the thermocouple Type-K (chromel-alumel) (RS Components, UK) are connected to a CAL-3300 digital heating controller (CAL Controls, USA). This allows the temperature to be fine-tuned as required.

Stirring of the reaction is achieved through an overhead stirring motor (IKA Works GmbH, Germany) magnetically connected to the internal autoclave stirrer. Two different lengths of the shaft are available and chosen depending on the size of the base. Stirring rate between 50 and 2000 revolutions per minute (rpm) can be achieved. Normally, 100 rpm were used.

Finally, a trip switch is incorporated in the rig. This is connected to the pressure controller and supplies energy to the heating system. In this way, if the pressure exceeds the set upper limit (in this case 300 bar), the power supply to the heating jacket will be disabled and the pressure will decrease as a consequence of the temperature drop.

2.1.1.1 Standard operating procedure (SOP) for MK III clamp sealed polymerisations autoclave

In order to minimise risks and increase safety of the high-pressure polymerisations, the following SOP was adhered to:

1. The autoclave was fully assembled by placing an EPDM o-ring between the head and body of the autoclave. The two parts were then clamped together. The clamp was tightened using the safety key, which was then screwed into the head. The inlet and outlet pipes were connected and the Swagelok® fittings tightened, then the heating jacket was secured around the body.
2. The thermocouple was connected to the control box to monitor the internal autoclave temperature.
3. The setup was leak tested by pressurising to ~40bar (with CO_2 or N_2) at room temperature. All fittings were checked for leaks using Snoop® liquid leak detector.
4. If required, the autoclave was vented to ambient pressure through the outlet HiP tap and any leaking fittings adjusted. Fittings were never tightened under pressure.
5. Steps 3 and 4 were repeated until no leaks remained.
6. Residual pressure from the leak test was vented until the autoclave was at atmospheric pressure. The vessel was opened and the appropriate amount of reactants, catalyst and molecular sieves was added to the bottom part of the autoclave.
7. The autoclave was once again clamped together and purged with a flow of CO_2 (at 2 bar) to flush out residual air from the system (keeping the safety key unscrewed) for 5 minutes.
8. After this time the safety key was screwed into the head to finally seal the vessel.
9. The stirrer was switched on, set to 100 rpm, and the vessel pressurised to around 50 bar.
10. The heating jacket was connected to the control box and the temperature set to the desired value with the pressure monitored throughout.

11. The autoclave was allowed to reach its final temperature and the pressure increased to 275 bar by slow addition of CO_2.
12. After the desired reaction time, the reactions were stopped by switching off and removing the heating jacket from the body, and placing the vessel in a water/ice bath (0 °C).
13. When the pressure was around or below 20 bar, the CO_2 was vented into the fumehood by opening the outlet HiP tap. Generally this was over a 20-30 minute period.
14. Once at ambient temperature and pressure, the safety key was removed and the Swagelok® fittings undone.
15. Finally, the clamp was opened and the product collected.

2.1.2 High-pressure fixed volume view cell

In order to study the behaviour of polymers and reagents under high-pressure CO_2, a fixed volume (100 mL) view cell was used (Figure 2.5).

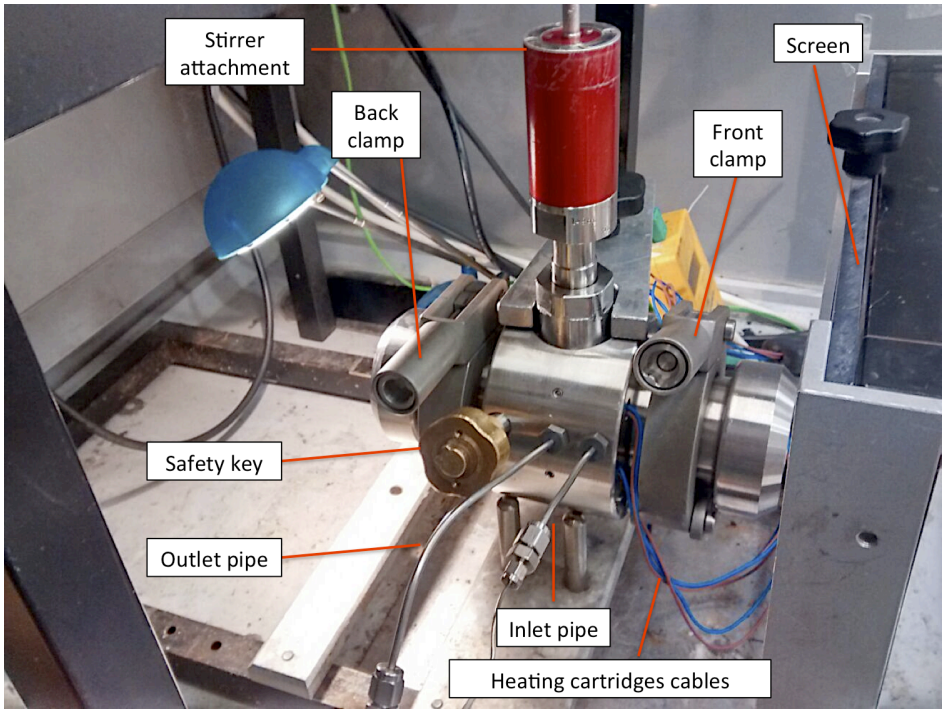


Figure 2.5 - Side view of the high-pressure view cell (fully assembled). An external lamp was positioned at the back of the autoclave to increase the light and the visibility inside of the cell.

This view cell was manufactured in-house at the University of Nottingham and its basic design is similar to the MKIII autoclave, consisting of a cylindrical body heated by internal cartridges (Watlow, UK) and kept horizontally in the fumehood. Two heads containing sapphire windows are clamped to the two ends of the body with the same safety key/clamp system. The view cell body houses the inlet and outlet pipes. The internal and the body temperature were monitored by two thermocouples Type-K (chromel-alumel) (RS Components, UK) connected to a CAL-3300 digital heating controller (CAL Controls, USA). The need for two different thermocouples (internal and external) is given by the increased thickness of the wall of this autoclave.

Similarly to the reaction autoclaves, the inlet pipe is connected to pressure transducer in order to allow for constant monitoring of the system pressure. A trip switch connected to the pressure box and temperature monitor was also included for safety. A stirrer is attached on top of the body, but this was not used for the investigations described in this thesis.

For increased clarity, the view cell is shown also in its schematic form (Figure 2.6).

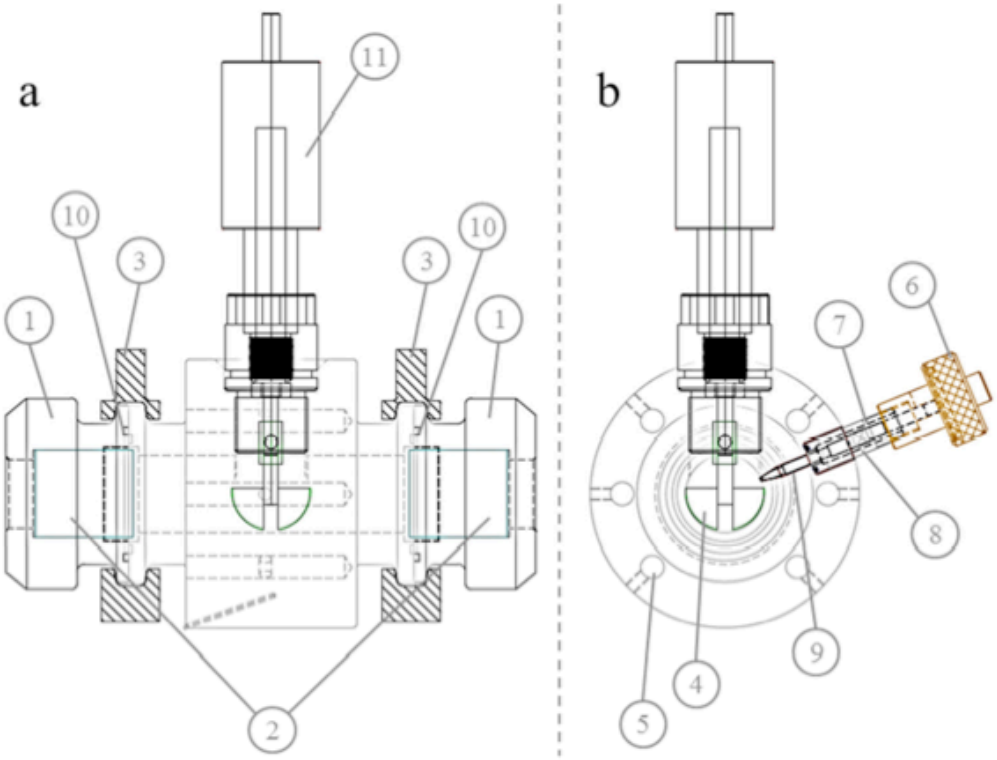


Figure 2.6 – Scheme of the 100 mL fixed volume view cell: (1) heads, (2) sapphire windows, (3) clamps, (4) stirrer, (5) heating cartridges holes, (6) safety key, (7) vent hole, (8) screw insert, (9) safety needle, (10) o-ring gap, (11) overhead stirrer attachment.

2.1.2.1 Standard operating procedure for clamp-sealed 100 mL view cell

The SOP for the usage of this autoclave was as follow:

1. The view cell was fully assembled:
    a. EPDM o-rings were fitted around the sapphire windows (one for each window);
    b. Teflon spacers were put between the windows and the relative heads (to ensure pressure of the sapphires against a soft surface);
    c. The head was laid onto a level surface and the sapphire windows fully inserted in the heads;
    d. An EPDM o-ring was placed in the body at the rear end, then the back head and body clamped together (tightening the clamp with the safety key). The body was positioned on a purpose-built stand

and secured in place in the fumehood. The inlet and outlet pipes were attached and the Swagelok® fittings tightened;

e. The heating cartridges were inserted into the body, then an EPDM o-ring was placed in the front end of the body and then the front head clamped to the body. The clamp was tightened using the safety key, which was then screwed into the body.

2. The internal and external thermocouples were connected to the control box.
3. A polycarbonate safety screen was positioned in front of the window, removing it only when at ambient pressure.
4. The setup was leak tested by pressurising to ~40 bar (using CO_2). All fittings were checked for leaks with Snoop® liquid leak detector.
5. If required, the autoclave was vented to ambient pressure through the outlet HIP tap and any leaking fittings adjusted.
6. Steps 4 and 5 were repeated until no leaks remained.
7. Residual pressure from the leak test was vented until the autoclave was at atmospheric pressure. The key was removed and the front end opened. Then, solid materials (polymers or monomer) contained in an open glass vial (kept in place in the autoclave by using Blu-Tack) were placed inside. The front end was then re-sealed.
8. The safety screen was positioned again in front of the window.
9. The pressure was raised to 50 bar.
10. The heating cartridges were connected to the control box and set to the desired temperature with the pressure monitored throughout. Typically, a lag (2-3 °C) was observed between the internal and external thermocouple due to the increased wall thickness relative to the MKIII autoclave.
11. When the temperature reached the set value, the pressure was increased to the experimental desired value by slow addition of CO_2.
12. Once complete, the heating cartridges were switched off to cool the autoclave, allowing the temperature to drop to ambient.
13. The CO_2 was vented into the fume hood by opening outlet HiP tap. This was done slowly (over a 45 minute period) to avoid excessive foaming and stress on the windows.
14. Once at ambient temperature and pressure, the safety key was removed, and the front end clamp opened

15. Finally, the vial containing the sample was collected.

2.1.3 High-pressure rheometer

A Physica MCR301 rheometer (Anton Paar, Austria) equipped with a 150 bar high-pressure cell, a Peltier temperature controller and parallel plate geometry of diameter 20 mm and fixed gap of 1 mm (PP20/Pr) was used for the oscillatory rheometric studies. A different rheometer, Physica MCR103 (Anton Paar, Austria) with the same PP20/Pr geometry and an electrically heated 400 bar high-pressure cell was used for the rotational viscosity studies. Thanks to the Peltier unit the MCR301 rheometer afforded a controlled cooling rate, and hence a controlled crystallisation of the samples, which is a fundamental requirement when analysing the melting point of materials. This could not be achieved with the electrically heated 400 bar cell of the MCR103 (hence, this rheometer was used only for viscosity studies at a fixed temperature at higher pressures).

However, in both cases the rheometer is essentially a high-pressure autoclave held together by a screw thread and sealed with an EPDM o-ring. Previous studies have shown that this apparatus can be used to measure viscosities with a precision of 0.25 Pa.s [3].

The lower part of the rheometer contains a removable stainless steel cup that houses the inlet/outlet pipe and a burst disc (*i.e.* a pressure relief device) (Figure 2.7).

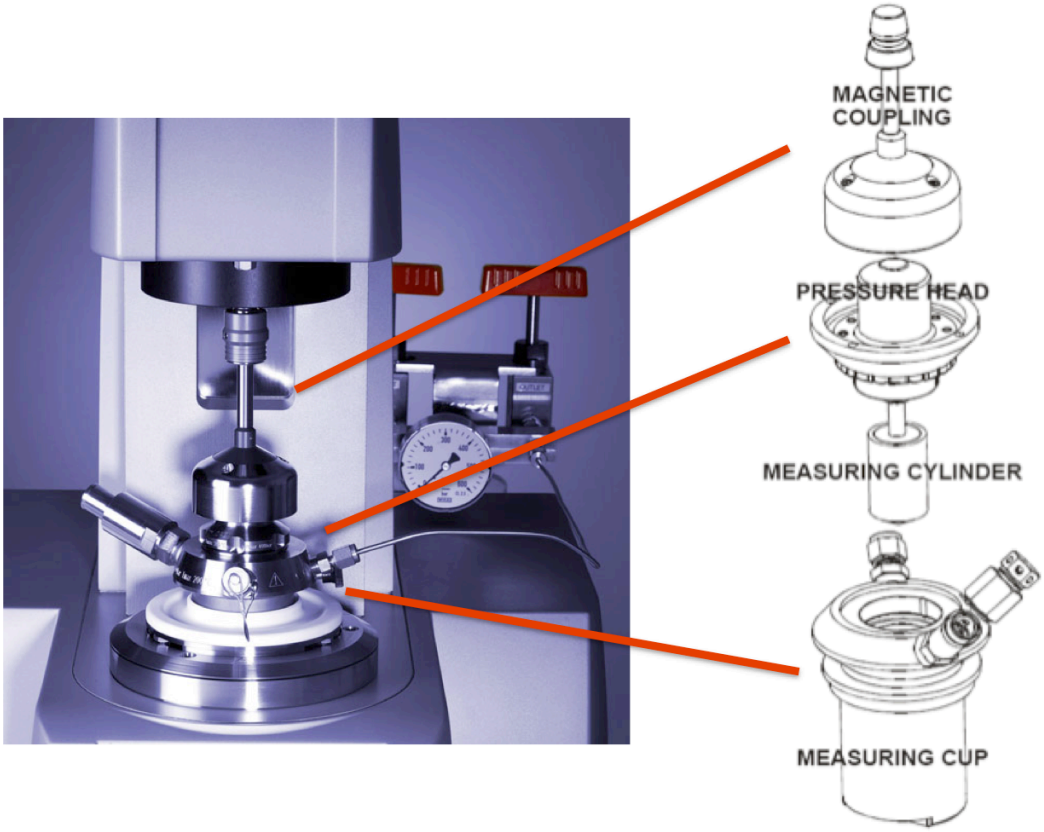


Figure 2.7 – Picture of the rheometer and schematic diagram of the pressure cell supplied by Anton Paar. The cylindrical burst disc can be seen in the picture on the left of the pressure cell.

The head of the cell has the PP20/Pr geometry attached and is combined to the rotating spindle of the rheometer though a magnetic coupling. Two ball bearings in the pressure head ensure minimal friction. However, a "motor-adjustment" performed without sample is always needed before carrying out any experiments to take in account the (small but still present) internal friction of the system. Besides, an "air-check" is typically conducted before each rheology session, in order to test the bearings (controlling if replacements are needed).

The CO_2 is added *via* a 260D syringe pump (Teledyne ISCO, USA) using a high-pressure line composed of HiP taps and Swagelok® tubing and fittings. The syringe pump keeps the pressure constant to the set value (by appropriate displacement of a piston) and hence it can counteract any leaks that may occur within the system and also ensure that the pressure remains constant during temperature scans or fluctuations.

An optional N_2 cylinder can be connected to the rheometer inlet through a HiP tap and excluding the syringe pump from the line.

In addition to the usual piezoelectric pressure transducer, the rheometer has also a Bourdon-tube gauge integrated by the supplier on the inlet line.
Since this rig is slightly different from the general high-pressure setup, the scheme of the full high-pressure rheometer rig is shown (Figure 2.8).

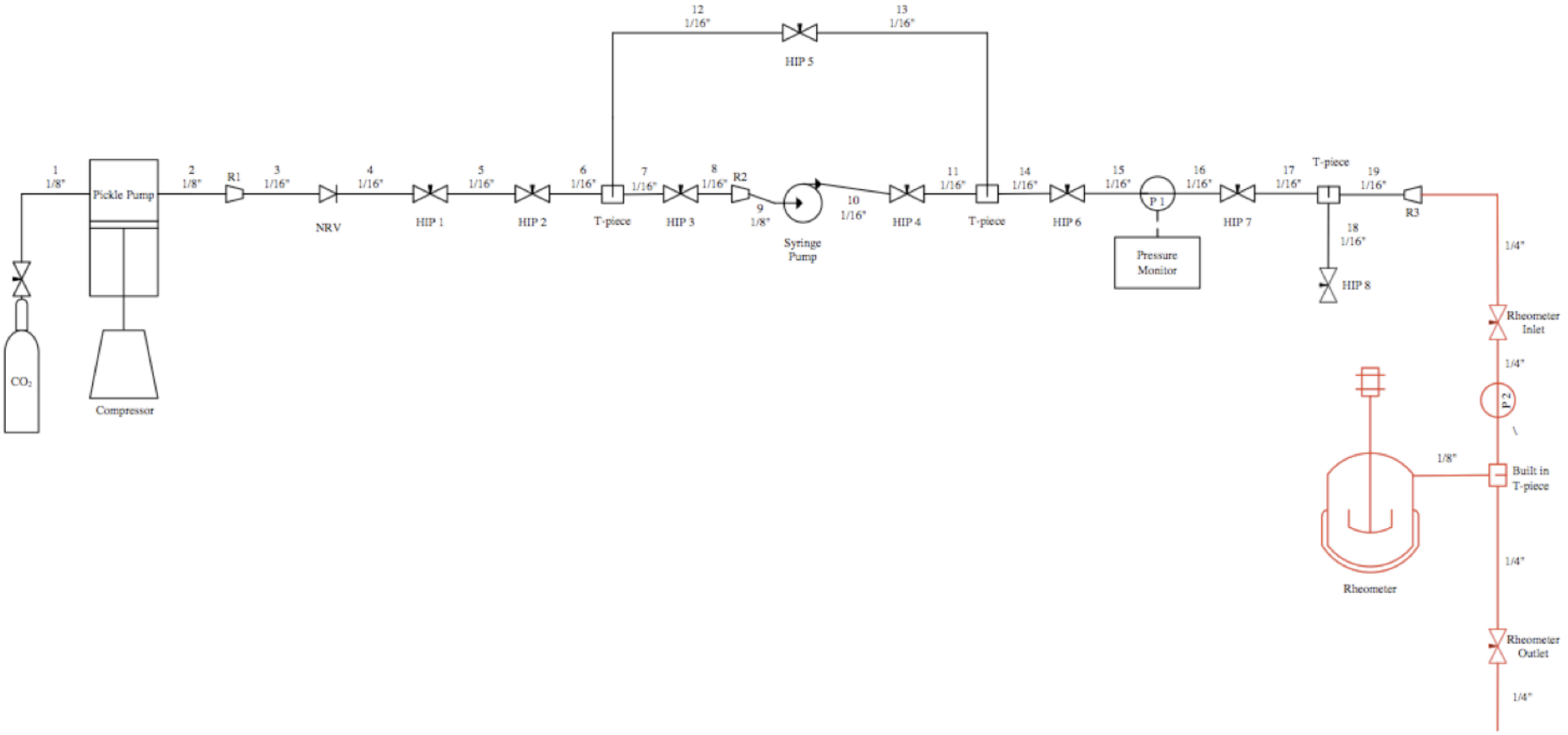


Figure 2.8 – High-pressure rheometer rig schematic: a N_2 cylinder could be attached to the HiP tap 6; the line was equipped with a piezoelectric pressure transducer (P1) and a Bourdon-tube gauge (P2). The HiP taps 3 and 4 allowed for exclusion of the syringe pump and direct filling of the cell from the CO_2 cylinder.

2.1.3.1 Standard operating procedure for high-pressure rheometric studies

Details on the specific settings used for the viscosity and mechanical studies under high-pressure can be found in Chapter 3. However, the general SOP for the usage of this piece of equipment was as follow:

1. The high-pressure cell was fully assembled:
    a. An EPDM o-ring was fitted around the pressure head;
    b. The pressure head was screwed tightly on the measuring cup by using the appropriate spanner provided by Anton Paar;
    c. The inlet pipe was connected to the measuring cup and the fitting tightened;
    d. A polycarbonate shield was put in in front of the rheometer whenever pressure was used in the system.
2. The setup was leak tested by pressurising to ~40 bar (using CO_2). All fittings were checked for leaks with Snoop® liquid leak detector.
3. If required, the cell was vented to ambient pressure through the outlet tap and any leaking fittings adjusted.
4. Steps 2 and 3 were repeated until no leaks remained.
5. Residual pressure from the leak test was vented until the autoclave was at atmospheric pressure. A “motor-adjustment” and an “air-check” were run at ambient pressure to warm-up the rheometer, record the internal friction of the system and check whether the bearings in the pressure-head needed replacement or not.
6. If needed, the pressure-head bearings were replaced and an “air-check” run again to ensure the internal friction of the system was minimal. A “motor-adjustment” was run each time the bearings were changed and before each “air-check”.
7. When the “air-check” afforded a positive result, the cell was opened and the sample inserted in the measuring cup.
8. The sample was molten and the pressure head was once again screwed in to create a polymer disk: this ensured an even sample was being measured and the thermal history of the sample deleted.

9. The desired temperature and analysis settings (*e.g.* oscillation/rotation, frequency/shear rate *etc.*) were set.
    a. If pressure was needed, CO_2 was loaded through the syringe pump (ensuring the syringe pump had enough CO_2 in it);
    b. If the syringe pump needed refilling, this was done by opening the HiP taps between the CO_2 cylinder and the syringe pump (set on "REFILL");
    c. The was left for the appropriate soaking time (see Chapter 3 for details);
    d. The HiP taps on the inlet line where left open to ensure a constant pressure throughout temperature sweeps.
10. The pressure was constantly monitored from the readings on the pressure box, Bourdon-tube gauge and syringe pump display.
11. Once complete, the heating was switched off to cool the autoclave, allowing the temperature to drop to ambient. For the MCR103 a water circulator was used to speed up this process.
12. The CO_2 was vented into from outlet tap. This was done slowly (typically over a 35 minute period) to avoid excessive foaming of the polymers.
13. Once at ambient temperature and pressure, the pressure-head was unscrewed and the measuring cup removed and cleaned.

N.B. Whenever N_2 pressure was needed, the gas was supplied directly from a cylinder (200 bar) by manual control of the inlet flow through HiP taps.

2.2 References

[1] H.M. Woods, *PhD Thesis*, School of Chemistry, The University of Nottingham, Nottingham, **2005**
[2] H. Tai, *PhD Thesis*, School of Chemistry, The University of Nottingham, Nottingham, **2005**
[3] C.A. Kelly, *PhD Thesis*, School of Chemistry, The University of Nottingham, Nottingham, **2009**

3 High-pressure rheological analysis of CO_2-induced melting point depression and viscosity reduction of poly(ε-caprolactone)

Thermoplastic polymers are normally processed in the molten state. Typical melt processes employed on the industrial scale are extrusion and injection moulding. Both of them involve steps such as: (a) heating and melting of the polymer, (b) driving the polymer into the shaping unit, (c) shaping the melt and (d) final cooling and solidification [1, 2].

In general, high viscosity characterises polymer melts thus rendering melt processes energy intensive and, sometimes, problematic [3, 4]. Hence, understanding and quantifying the effects of compressed CO_2 on the mechanical and rheological properties of polymers are basic requirements in order to develop CO_2-assisted melt processes.

In the current literature much information is available on the effects of $scCO_2$ on amorphous polymers [5-10]. However, there is a lack of any direct study of the loss and storage moduli as a function of temperature and pressure for the detection of the melting point depression of semicrystalline polymers under pressure.

This chapter describes the use of high-pressure rheology to assess the effects of supercritical carbon dioxide ($scCO_2$) on the melting point (T_m) and viscosity of poly(ε-caprolactone) (PCL), a semicrystalline polyester, over a range of temperatures and pressures up to 300 bar over a wide range of shear rates. The author hypothesised that plots of the storage and loss moduli against temperature could be used to obtain important information on the T_m of the polymer in the presence of CO_2, therefore giving a rheological viewpoint to the T_m depression.

Furthermore, since only few shear viscosity data over a narrow shear rate range are available for PCL in the presence of $scCO_2$, in-depth viscosity studies will be presented. Experimental viscosity data will be fitted to the Carreau model to quantify the extent of the plasticising effects on the zero-shear viscosity and relaxation time under different conditions. Similar analyses will be conducted under high-pressure nitrogen and at high temperature, to compare the effects of

pressurised CO_2 to those obtained in the presence of a non-plasticising gas and to high-temperature processes. Furthermore, the rheology results will be corroborated with visual observations by using a fixed volume high-pressure view cell.

The results of this chapter are published in the paper:

S. Curia, D.S.A. De Focatiis and S.M. Howdle, "High-pressure rheological analysis of CO_2-induced melting point depression and viscosity reduction of poly(ε-caprolactone)", *Polymer* (69), **2015**, 17-24

3.1 Introduction

In recent years there has been increasing interest in the use of high-pressure CO_2 as a reaction medium or plasticiser for polymer synthesis and processing [11-16]. CO_2 has been exploited as a solvent for polymerisations [17, 18], as a foaming agent [11, 19-23], for precipitation/separation [24], particle formation [25, 26] and encapsulation [27].

As described in Chapter 1 (Section 1.4.1.1, page 23), CO_2 acts like a typical low molecular weight (MW) plasticiser for a variety of polymers, but it is also very different because the concentration can be selectively tailored by controlling the pressure [6, 8, 9, 12, 26, 28-34]. Hence, the extent of polymer softening can be easily controlled.

This phenomenon is known as *CO_2-induced plasticisation*. This allows an initially glassy polymer to demonstrate the flexible properties associated with a rubbery or liquid-like state when exposed to pressurised CO_2.

By lowering the glass transition temperature (T_g) and reducing viscosity, new processing routes might be available for the plasticised polymer melts that could not only reduce energy costs associated with the process, but also improve the overall efficiency. In fact, this phenomenon opens up opportunities for novel processes and incorporation of thermally labile molecules [27, 35].

CO_2-induced plasticisation mimics the effect of heating the polymer and it is characterised by an increased segmental and chain mobility [36].

Due to their linear structure and symmetry, CO_2 molecules do not have a dipole moment. Nonetheless, they exhibit significant specific interactions with many polymers, owing to their large quadrupole moment and Lewis acidity [15, 37]. Fourier Transform Infrared spectroscopy (FTIR) has been used to confirm and study these interactions in depth [38, 39].

Examples of chemical moieties found in polymers that can show weak interactions with CO_2 are carbonyl, ether and aromatic groups (Figure 3.1). CO_2 has been proven to act as an electron acceptor for polymers containing lone electron pairs (*e.g.* carbonyl groups in polyesters) and to interact electrostatically

with π-systems (*e.g.* the phenyl rings in poly(styrene)) [38, 40]. These interactions can significantly enhance CO_2 sorption levels relative to polymers with no distinctive functional groups, such as poly(ethylene) [38].

In addition to this, the free volume fraction (v_f) of the polymer has an influence on the CO_2 sorption [41]. For example, even though carbon dioxide has a very low solubility in a non-polar polymer such as poly(ethylene) it has high solubility in a non-polar polymer like poly(dimethyl siloxane) (PDMS). This difference is thought to be due to the high chain flexibility and larger v_f of PDMS [41].

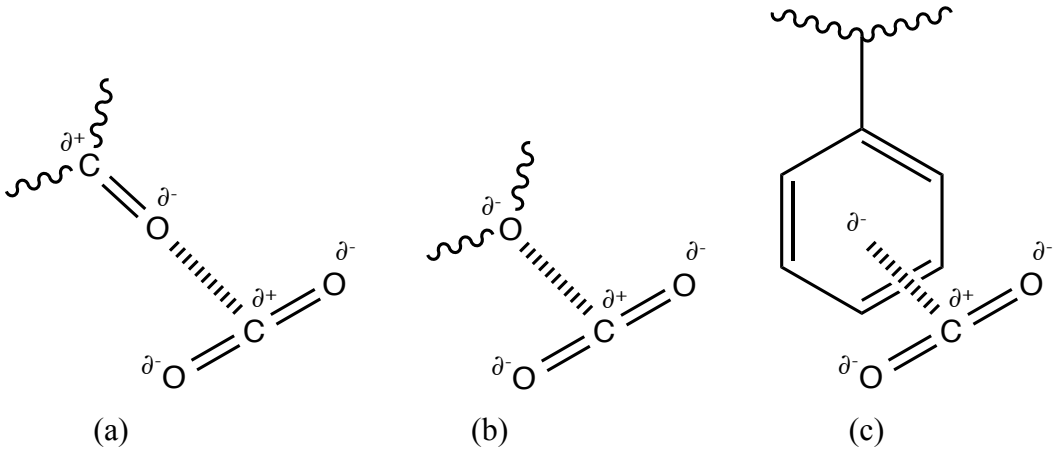


Figure 3.1 – Weak interactions of CO_2 with different chemical groups that can be found in polymer backbones: (a) carbonyl, (b) ether and (c) aromatic rings.

The interactions between the chemical groups found in the backbone of polymers and the CO_2 molecules often result in high sorption levels that decrease the intermolecular bonding between the chains [10]. This causes an increase in the v_f of the polymer and therefore a higher mobility of the polymer chains, hence, leading to a decrease in viscosity with the CO_2 molecules acting as molecular lubricants [10, 26].

The CO_2 sorption levels for different polymers have been quantified by gravimetry [33], chromatography [40] and optical inspection [42]. For example, a suspension balance was used to quantify the CO_2 sorption for homo- and copolymers of lactide and glycolide indicating a weak effect of the MW and a more important role of the copolymer composition [33]. Both chromatographic investigations on poly(methyl methacrylate) [40] and optical inspection on PCL [42] showed that CO_2 sorption levels increase with pressure and decrease with increasing temperature.

Another important characteristic of the CO_2-induced plasticisation is that this phenomenon is reversible: upon depressurisation the supercritical solvent is removed and the polymer reverts to its initial physical state. For this reason, this use of CO_2 can be extremely valuable in the preparation of polymeric materials for food packaging and medical applications [26, 36, 43].

For instance, this effect can be exploited to produce porous materials based on biodegradable polyesters with T_g above ambient temperature, which can find applications in tissue engineering as scaffolds for cellular growth [23, 43, 44].

In these types of processes, during the depressurisation stage run at constant temperature, the pressure decreases and the CO_2 phase changes from supercritical, to liquid and then to gas. Consequently, nucleation and growth of gas bubbles occurs in the rubbery polymer, thus producing pores. Contemporaneously, the polymer T_g increases as a consequence of the resulting lower plasticiser concentration. Finally, the porous structure is fixed in the glassy state once the T_g approaches the ambient pressure value and the polymer becomes solid again at ambient temperature and pressure [19, 23, 45].

Furthermore, the CO_2 plasticisation can also induce crystallisation [46]. In some case the dissolved CO_2 can in fact reduce the T_g and enhance the chain mobility, thereby favouring the packing process of the macromolecules and thus increasing the degree of crystallinity of a polymer after depressurisation compared to its pristine state. This effect has been observed for several polymers such as poly(lactic acid) [47], *tert*-butyl poly(ether ether ketone) [48] and poly(ethylene terephthalate) [49].

The foaming process can be extended to different polymers to produce porous materials not only for medical applications, but also for a wide range of different uses. For example, nanocomposite polymeric foams based on poly(carbonate) (PC) containing carbon nanotubes (CNTs) find application in electromagnetic interference shielding devices (Figure 3.2) [21].

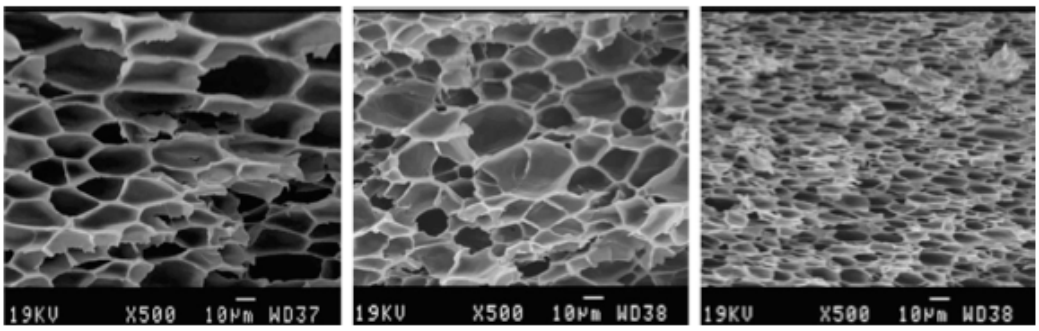


Figure 3.2 – PC based foams containing CNTs with different concentrations (0% left, 1% centre, 2% right) obtained CO_2 processing [21].

Furthermore, precise control of the depressurisation rate allows for control of the three-dimensional structure and, hence, of the pore size of the foamed materials (Figure 3.3) [23]. Finally, if a solid non-porous material has to be prepared, cooling of the polymer with dry ice before venting effectively prevents foaming [50].

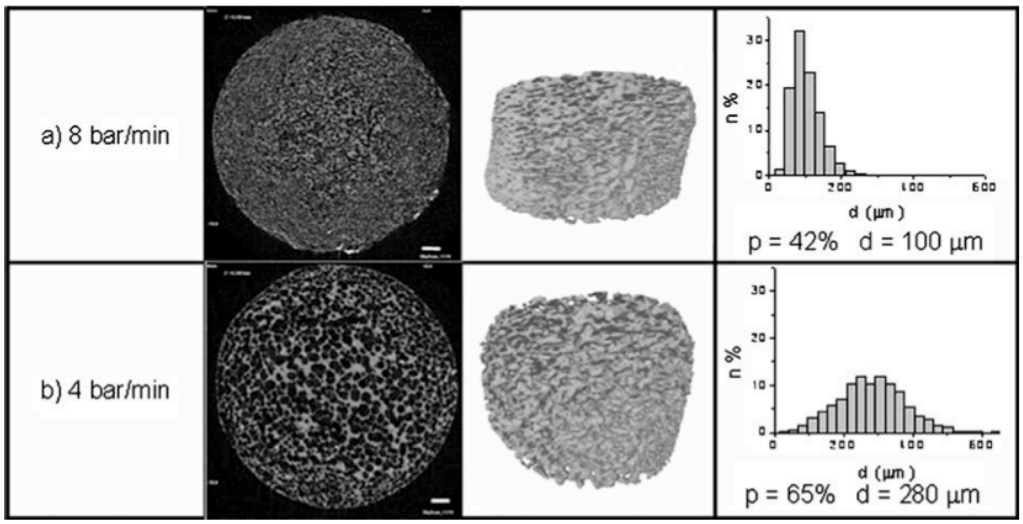


Figure 3.3 - Effect of depressurisation rate on poly(ω-pentadecalactone-*co*-ε-caprolactone) scaffold morphology, where *p* is the porosity and *d* the pore diameter. The pore size becomes bigger and with a broader distribution with lower flow rates [23].

To sum up, these effects together with the accessible critical point of CO_2 (31.1 °C and 73.8 bar) and its non-flammability, non-toxicity and low price, make CO_2 a valuable renewable alternative to conventional solvents for polymer synthesis and processing.

3.1.1 Melt processing in CO_2

High viscosity can be the major complication when processing polymers [2, 4, 51]. In order to overcome this issue the easiest option is to heat the polymer and decrease its viscosity. However, this solution can be rather energy intensive; for instance, melt processing of PCL requires temperatures around 140 °C to achieve a sufficiently low viscosity [52-54]. Moreover, at high temperatures the degradation of some polymers can become an important concern [4].

A second option is the use of organic solvents to prepare low viscosity polymer solutions. This allows for lower temperature processing; nonetheless, additional problems associated with the purification of the polymers and environmental concerns arise [4].

Furthermore, both of these options are far from being ideal when preparing polymeric materials for medical applications, since large amounts of solvents and high temperatures can easily inactivate bioactive molecules [55].

For these reasons, in the last twenty years increased attention has being given to CO_2-assisted processes in which the temporary CO_2-induced polymer plasticisation is exploited to achieve low temperature processing without the aid of solvents [6, 13, 27, 28, 37, 51].

As a consequence, experimental and theoretical studies on the rheological properties of polymer/CO_2 systems have generated much interest and are still topical in modern polymer science [4, 6, 10, 13, 26, 56].

3.1.1.1 Rheology of polymers in CO_2

Rheological studies are crucial to determine the effects that pressurised CO_2 has on polymers. Hence, not only they are needed to obtain information on the processability of polymers under pressure, but also to understand the advantages and the commercial feasibility of high-pressure processes from an industrial perspective.

Many shear viscosity studies that can be found in the literature have focussed on vinyl polymer such as poly(methyl methacrylate) [32], poly(propylene) [56],

poly(styrene) [16] and biodegradable polymers like poly(lactic acid) [10, 57] and poly(ethylene glycol) [25, 29, 34].

Typical data show the viscosity values *versus* shear rate at different pressures (Figure 3.4).

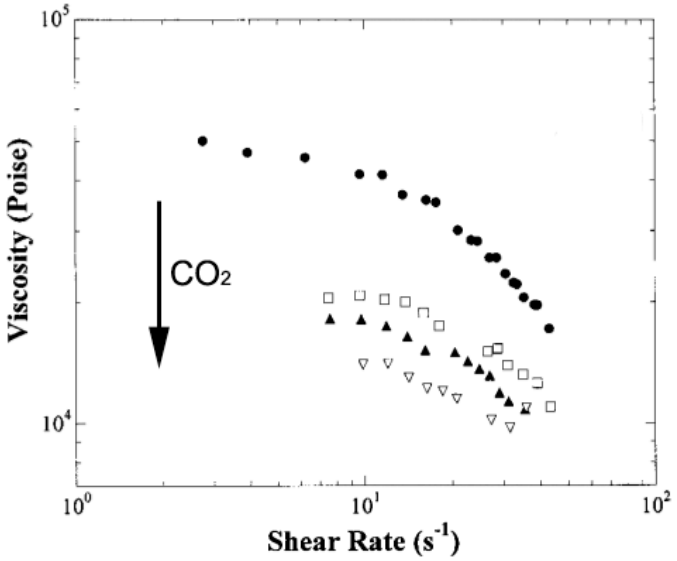


Figure 3.4 - Viscosity *vs* shear-rate for poly(methyl methacrylate) at various CO_2 pressures at 210 °C. Graph adapted from reference [32].

Several high-pressure studies are also available in the literature for some of these polymers dissolved in conventional [58, 59] and green solvents [12] when exposed to CO_2. Also in these cases a decrease in the viscosity was observed when increasing the CO_2 pressure, and the largest relative viscosity reduction was detected at the lowest temperature and the highest CO_2 pressure.

However, so far most of the research has strongly focussed on amorphous polymers and much less information is available for semicrystalline systems.

3.1.2 Poly(ε-caprolactone) and aims of the study

Poly(ε-caprolactone) (PCL) is a hydrophobic biodegradable polyester used in a wide range of applications such as food packaging, engineering materials, medical materials and adhesives [54, 60-65]. It is a semicrystalline polyester, with T_m ~55-70 °C (depending on the MW) and T_g ~-60 °C, that is generally synthesised through ring-opening polymerisation of ε-caprolactone (ε-CL) using metal-based

catalysts such as stannous octanoate ($Sn(Oct)_2$) or enzymes such as *Candida antarctica* Lipase B (CaLB) (Figure 3.5) [50, 66].

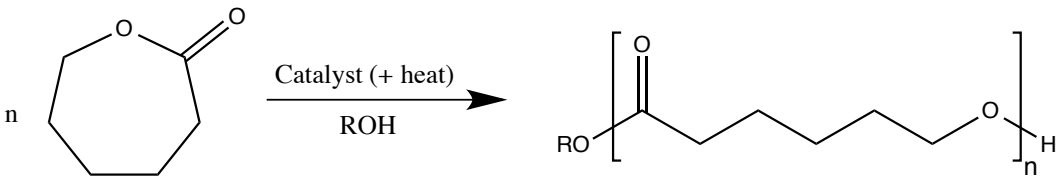


Figure 3.5 - Schematic synthesis of poly(ε-caprolactone) using a catalyst and a general initiator ROH (R= -H, $-CH_3$, $-(CH_2)_xCH_3$, $-C_6H_5$ etc.). This polymerisation can be carried out both in solvents (such as toluene), in the bulk and in $scCO_2$. Typically used catalysts are organometallic catalysts and enzymes [50, 66, 67].

The degradation of PCL occurs through the hydrolysis of its ester linkages under physiological conditions [66]. For this reason, PCL has also received much attention for use as an implantable, resorbable material and it is already used in many medical applications such as drug delivery, sutures, dentistry and tissue engineering [19, 22, 42, 45, 66].

Nonetheless, as mentioned previously, molten PCL requires the use of high temperatures (above 140 °C) in order to achieve suitably low viscosities for melt processing [52-54]. These conditions are not acceptable for most medical applications where bioactive molecules are incorporated into the polymer, since these can be easily damaged by the high temperature. As described in Section 3.1.1 (page 56), lower temperature processing can be achieved by use of organic solvents, but this introduces unwelcome residues and can inactivate complex biomolecules [55]. In addition, the use of solvents imposes the need for an often challenging purification step for their removal after processing, thus making the overall process longer and more expensive.

The ability of CO_2 to be absorbed into PCL has been previously shown [68]. A change in the morphology of the polymer under CO_2 was also observed through FTIR analysis by monitoring the carbonyl peak at 1720 cm^{-1} [69], and a decrease in the reptation time in the presence of high-pressure CO_2 was also found by the same group [53]. The plasticisation of this polymer under CO_2 was also studied optically [70, 71] and through high-pressure calorimetry [72].

In addition, the diffusivity, solubility and specific volume of PCL/CO_2 solutions have been recently studied by coupling gravimetric and spectroscopic techniques

[73, 74]. Thus, there is no doubt that high-pressure studies for the development and optimisation of CO_2–assisted polymer processing techniques are relevant and timely [13].

However, in the current literature there is a lack of any direct study of the loss and storage moduli as a function of temperature and pressure, and hence of the T_m of PCL in CO_2 through high-pressure rheological analysis. Therefore, we have investigated the use of high-pressure rheology to detect the melting point of PCL under CO_2 (1-120 bar) by conducting an oscillatory rheometric study under high-pressure conditions.

Furthermore, to the best knowledge of the author, very little shear viscosity data over a very narrow shear rate range are available for PCL in the presence of $scCO_2$ [75]. Hence, the aims of this study are to measure the T_m depression of PCL through direct monitoring of the polymer viscoelasticity under CO_2, and to study the effects of compressed CO_2 and N_2 on the shear viscosities of two grades of PCL of different molar mass (10 kg mol^{-1} and 80 kg mol^{-1}) under various temperature and pressure conditions, over a wide range of shear rates. These data will contribute to the understanding of the structural state of semicrystalline polyesters in the presence of $scCO_2$, and will aid the development of lower temperature melt processes of such polymers.

3.2 Experimental

3.2.1 Materials

PCL flakes (PCL10) with a density of 1.15 g mL^{-1} at 25 °C, M_n ~10 kg mol^{-1} and M_w ~14 kg mol^{-1} (by GPC declared from the supplier) and PCL beads (PCL80) with a density of 1.15 g mL^{-1} at 25 °C, M_n ~80 kg mol^{-1} and M_w ~94 kg mol^{-1} (by GPC declared from the supplier) were purchased from Sigma Aldrich (UK). The polymers were ground to obtain a granular-powdery sample (particle size 0.5-1 mm) before use. Supercritical Fluid Chromatography (SFC) grade 4.0 CO_2 (minimum purity 99.99%) and N_2 (99%) were purchased from BOC Special Gases (UK) and used as received.

3.2.2 Methods

3.2.2.1 T_m depression analysis

The effect of CO_2 on the T_m of PCL10 was studied using an Anton Paar Physica MCR301 rheometer equipped with Peltier temperature controller and a high-pressure cell (parallel plate geometry with 20 mm diameter and a 1 mm gap disc; PP20/Pr) with an upper operating pressure of 150 bar at room temperature and a maximum temperature of 300 °C (although this upper limit is considerably lowered depending on the type of rubber o-ring used). In a typical experiment 700 mg of polymer powder were added to the cup of the rheometer. A preliminary temperature ramp to 80 °C at 10 °C min^{-1}, followed by 5 minutes isothermal, was carried out to obtain a solid polymer disk upon cooling to 20 °C at 10 °C min^{-1}.
Three preliminary strain amplitude sweeps at 1 Hz at ambient pressure were performed on the PCL10 disk to identify a strain value within the linear viscoelastic region (LVR). From these measurements, a strain amplitude of 1% was identified as suitable and well within the LVR.

The cell was then sealed and CO_2 was added using a Teledyne Isco 260D syringe pump. After pressurisation, the polymer was left to soak at 20 °C for 50 minutes to allow for CO_2 diffusion. A time study showed that longer times did not result in significant further drops in the T_m, see Section 3.3.2.1 (page 67). The temperature of the cell was increased at a rate of 5 °C min^{-1} whilst imposing an oscillating strain of 1% to the sample at 1 Hz. Throughout the temperature scans the syringe remained connected to the cell to maintain the required pressure during heating. The shear storage modulus, G', and the loss modulus, G'', were recorded as a function of temperature. The T_m was taken as the temperature at which G'' is a maximum. All the experiments were repeated three times to give data confidence.

3.2.2.2 Shear viscosity high-pressure analyses

High-pressure rotational rheometric studies (continuous shearing with increasing shear rate) were carried out on PCL10 and PCL80 using an Anton Paar MCR 102 rheometer equipped with a Teledyne Isco 260D syringe pump and with a 400 bar cell electrically heated (parallel plate geometry, PP20/Pr). The electric heating system does not allow for control of the cooling rate, which is a crucial requirement for T_m analysis in order to guarantee that the sample is subjected always to the same thermal history. For this reason, T_m analyses could not be conducted with this piece of equipment. The instrument was calibrated with mineral oils of standard viscosity supplied by Anton Paar.

The polymer sample was inserted in the cup and a preliminary temperature sequence was performed to melt the polymer. Then, the sample was allowed to equilibrate at 80 °C and the system sealed and pressurised at the desired pressure. Samples were left for 50 minutes at pressure to soak. The rotational experiments were performed at constant temperature with logarithmically increasing the shear rate over a 2 minutes period from 10^{-3} to 10^{3} s^{-1} for PCL80, and from 1 to 10^{3} s^{-1} for PCL10. The duration of each measuring point was set to 10 s. This value was considered as appropriate since no significant start-up effects were observed at low shear rates with this duration [76]. Due to the structural limits given by the ball-bearings in the pressure cell, the minimum torque that could be applied with our system was 200 μN m. When applying the minimum torque to two different

liquids, the resulting minimum shear rate will be lower in the higher viscosity material. For this reason, measurements carried out on low viscosity materials start at higher shear rates.

A matching set of experiments were carried out under N_2 at 60, 120 and 180 bar, by connecting a cylinder directly to the rheometer inlet through high-pressure Swagelok® tubing.

All rotational experiments were repeated at least three times; the mean values ± 1 standard deviation are shown in the figures.

3.2.2.3 Viscosity vs Temperature studies at ambient pressure and under high-pressure

Temperature studies at ambient pressure and under CO_2 (at 120 bar) were conducted on PCL10 ($\dot{\gamma}$ =12.0 s^{-1}) and PCL80 ($\dot{\gamma}$=0.1 s^{-1}) by increasing the temperature from 80 to 180 °C in 20 °C steps at 5 °C/min. The shear rate values were chosen in order to analyse the viscosity in the Newtonian plateau (zero-shear viscosity).

After each ramp, a period of 10 minutes was imposed in order for the sample to reach thermal equilibrium before the collection of 5 measurements, and then ramping to the next temperature. The data are reported as the mean values ± 1 standard deviation.

3.2.2.4 Transient shear experiment studies

Transient shear experiment studies (time-dependent viscosity at constant applied shear rates, ranging from 0.25 s^{-1} to 5 s^{-1}) were conducted on PCL80 at ambient pressure (80 and 120 °C) and under CO_2 (80 °C, 120 bar) to investigate whether any phase separation and/or changes of solubility arise during shearing. Measurements of viscosity are plotted against time. The measuring point duration was changed from 0.3 s to 1 s on with a logarithmic increase. With this setting, a significant number of data points could be collected at the beginning of each test.

Due to the low viscosity and the equipment low torque limit, the same analysis could not be carried out on PCL10.

3.2.2.5 View cell plasticisation study

In order to observe visually the effect of CO_2 on the physical state of PCL10, a fixed volume view cell (100 mL) was used [77]. This view cell was manufactured in-house from 316-stainless steel with two thick sapphire windows located at the two ends of the cylindrical body which houses the inlet and outlet pipes.
In a typical experiment, 200 mg of sample were added in a glass vial and inserted in the view cell. The windows were sealed and clamped to the body, and CO_2 was added up to 50 bar. The temperature was raised to the desired value. When the temperature was stable, the CO_2 pressure was increased to the required value.

3.2.2.6 Differential Scanning Calorimetry (DSC)

DSC analyses on PCL10 were performed using a TA Instruments TA-Q2000 DSC calibrated with sapphire and indium standards. In a standard experiment, the sample (6.00 ± 0.10 mg) was melted with a first heating scan up to 80 °C and cooled down to 20 °C (10 °C/min). A second heating scan, with the same temperature ramp settings of the oscillatory rheological analyses (80 °C; 5 °C/min), was then carried out. Between each ramp a 5-minute isotherm was imposed.
The T_m was determined from the maximum of the endothermic peak and the degree of crystallinity (X_c) was calculated from Equation (3.1):

$$X_c = \frac{\Delta H_f(T_m)}{\Delta H_f^0(T_m^0)} \qquad (3.1)$$

where $\Delta H_f(T_m)$ is the measured enthalpy of fusion and $\Delta H_f^0(T_m^0)$ is the enthalpy of fusion of fully crystalline PCL, taken as 135.44 J g^{-1} [78-81].

The T_m as measured from DSC analysis is 64.6 ± 0.2 °C, whilst the X_c is 51.7 ± 0.5 %.

3.3 Results

3.3.1 T_m of PCL10 at ambient pressure

Before carrying out oscillatory experiments, it is important to identify the linear viscoelastic region (LVR) of the polymer. The LVR is the region in which the strain applied to the sample is never large enough to destroy the elastic structure of the material. Therefore, in the LVR the properties of the sample are not affected by the test itself (the material response is independent of the deformation and the structure of the sample shows no significant changes at these low deformations) [76].

Three strain amplitude sweeps at 1 Hz at ambient pressure were performed on the PCL10 disk to identify a strain value within the LVR, and mean values are shown in Figure 3.6. From these data, a strain amplitude of 1% was identified as suitable and well within the LVR.

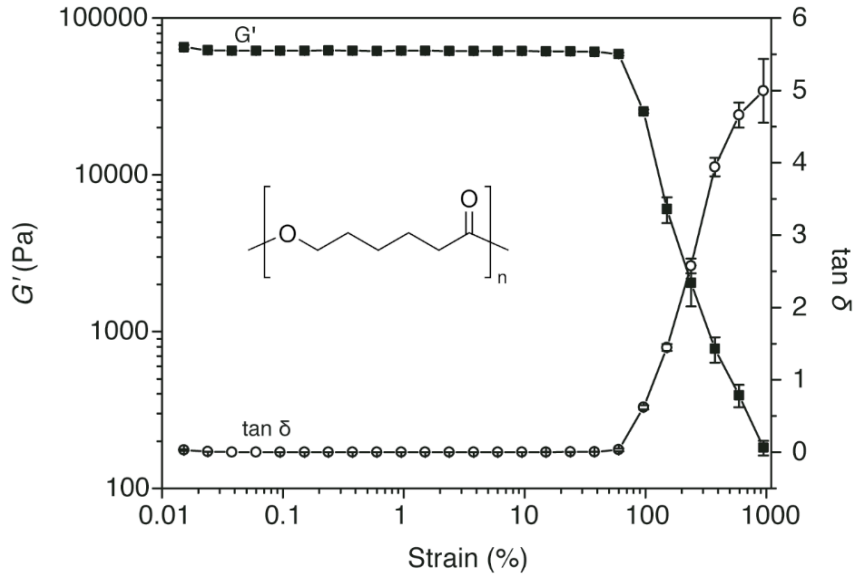


Figure 3.6 - Strain amplitude sweep showing the storage modulus, *G′*, and loss tangent, tan *δ*, as a function of strain for PCL10 at ambient pressure and 20 °C at 1 Hz. The point at which the *G′* and tan *δ* start to deviate from the plateau values indicates departure from linear viscoelastic behaviour. For this reason, the oscillatory tests were conducted at 1 Hz with a strain amplitude of 1%. The polymer structure is shown (inset).

Using these settings (1 Hz frequency, 1% strain), typical oscillatory rheometric data obtained for PCL10 at ambient pressure show two distinct regions (Figure 3.7): at lower temperatures G' has a value of ~60 kPa, typical of PCL above its T_g but below its T_m [82]. With increasing temperature there is a steep drop in the value of G' to ~2 kPa, as the material undergoes a thermal transition to a viscous fluid. Concurrently, there is an associated peak in G'' at the same temperature. This transition is associated with the melting of crystal spherulites in the polymer.

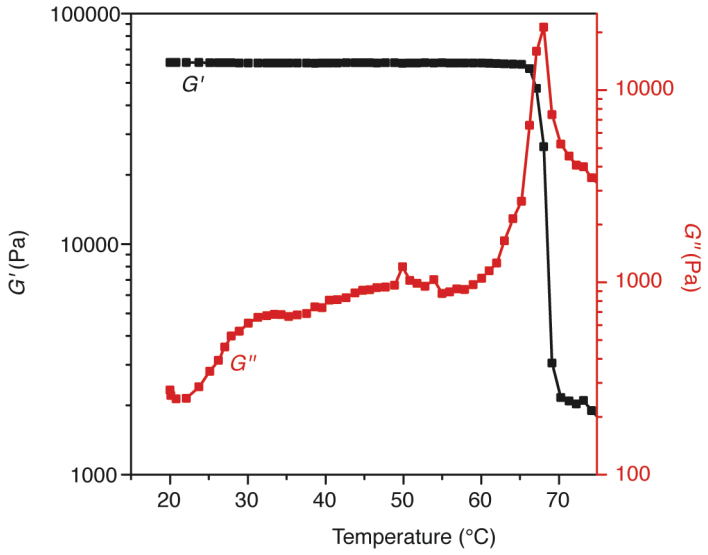


Figure 3.7 - Oscillatory rheometric measurements of G' and G'' as a function of temperature for PCL10 at ambient pressure. The dramatic changes in G' and G'' are produced by the melting of the polymer crystals. The average T_m obtained from the peak in G'' is 68.1 ± 0.6 °C.

The T_m at atmospheric pressure, as measured by rheology, is therefore 68.1 ± 0.6 °C, in good agreement with the T_m reported elsewhere in the literature (typically comprised between 60-65 °C) [53, 66] and with the value measured by DSC, which is around 65 °C (Figure 3.8).

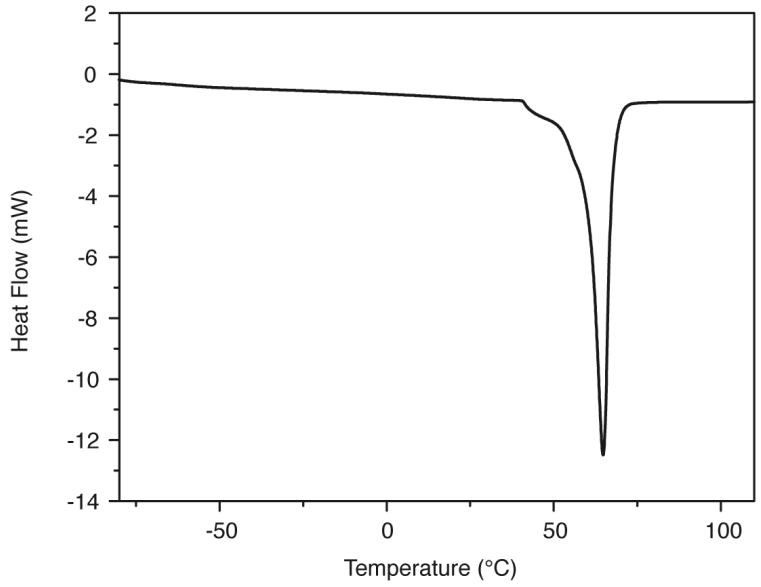


Figure 3.8 – DSC scan for PCL10 at ambient pressure. The melting point calculated from the maximum of the endothermic peak is 64.6 ± 0.2 °C (N=3).

Furthermore, integration of the endothermic peak obtained from the DSC analysis, revealed an enthalpy of fusion of around 70.0 J g^{-1}. This value is indicative of a semicrystalline polymer where the crystalline regions represent around 52% of the sample.

3.3.2 Effect of pressure on T_m of PCL10

3.3.2.1 Soaking time study

The *G'* drop and *G''* peak are expected to be shifted when the polymer is exposed to pressurised CO_2 due to the plasticising effects of CO_2 and the consequent T_m depression. An important parameter to consider when studying the plasticisation of a polymer in CO_2 is the soaking time needed for full sorption of the gas into the polymer. This will change depending on the affinity between the CO_2 and the polymer and the extent of the diffusivity of the gas into the polymer structure.
For these reasons, preliminary soaking time studies were conducted in order to investigate the amount of time required for the CO_2 to penetrate completely into

the polymer. These data allow for determination of the waiting time needed to acquire stable and repeatable results upon pressurisation of the sample.

Oscillatory rheometric data showed that the T_m of PCL10 was shifted to lower temperatures already after 15 minutes in subcritical CO_2 at 70 bar. Nonetheless, repeating the experiment at a later time (50 minutes) a lower T_m value was registered (Figure 3.9). Thus, showing that 15 minutes did not allow for a full penetration and diffusion of the CO_2 in the polymer.

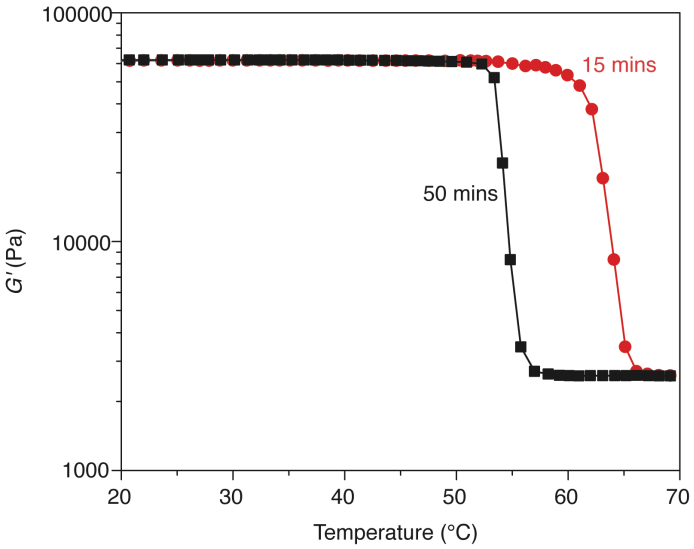


Figure 3.9 – *G'* analysis on PCL10 over a range of temperatures at 70 bar and different soaking times: 15 minutes (red) and 50 minutes (black).

Experiments at longer soaking times (up to 70 minutes) showed that the results acquired after 50 minutes were reproducible, within the error (T_m = 53.6 ± 1.0 °C), since no further decreases were detected at longer times (Figure 3.10). Hence, 50 minutes can be considered as an appropriate soaking time.

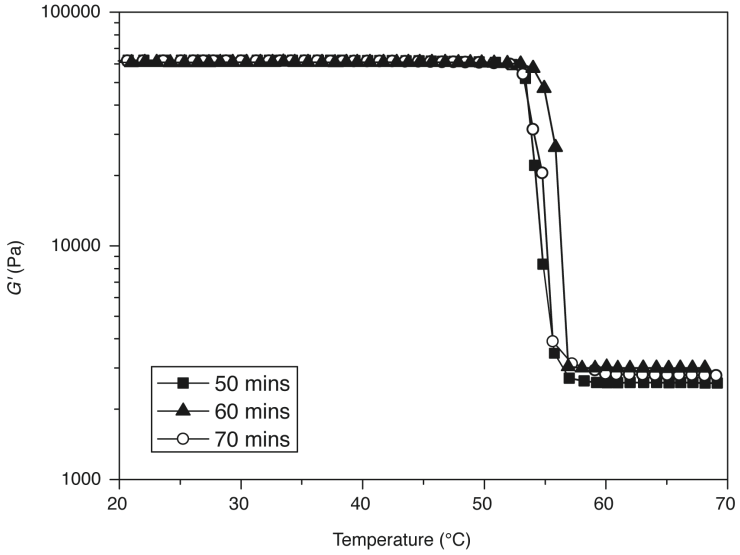


Figure 3.10 – *G'* analysis on PCL10 over a range of temperatures at 70 bar and different soaking times: 50 minutes, 60 minutes and 70 minutes. These results show that a stable T_m value was obtained after 50 minutes (53.6 ± 1.0 °C).

The same experiments were repeated at 100 bar to check the validity of this result also in $scCO_2$. Also in this case, 15 minutes did not allow for a full diffusion of the CO_2 into the polymer (Figure 3.11).

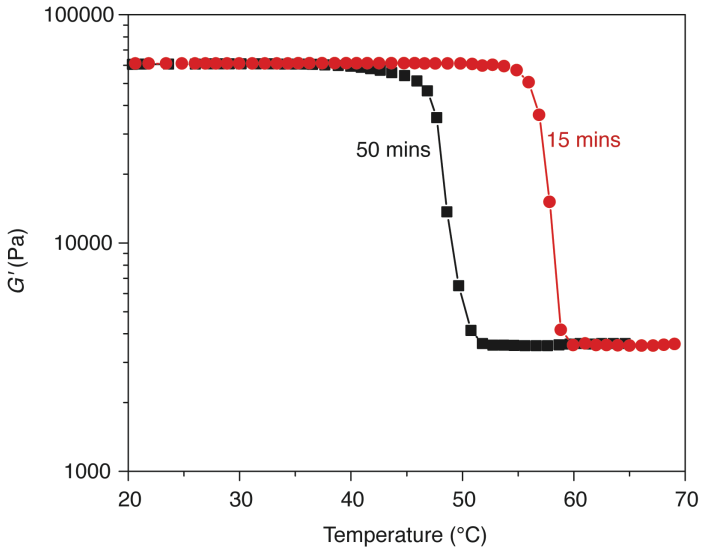


Figure 3.11 - *G'* analysis on PCL10 over a range of temperatures at 100 bar and different soaking times: 15 minutes (red) and 50 minutes (black).

Similar to the results obtained at 70 bar, soaking times longer than 50 minutes did not show any additional drop in the T_m value and the error on the average value is within the error range (47.2 ± 0.8 °C) (Figure 3.12).

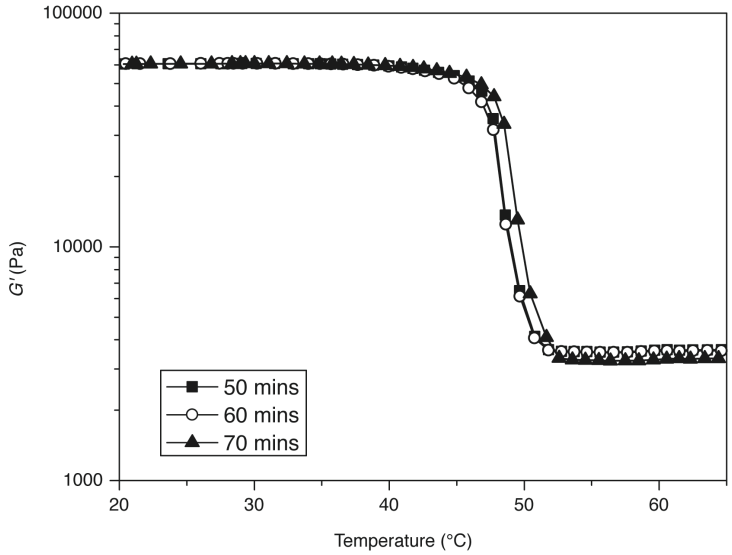


Figure 3.12 - *G'* analysis on PCL10 over a range of temperatures at 100 bar and different soaking times: 50 minutes, 60 minutes and 70 minutes. These results show that a stable T_m value was obtained after 50 minutes (47.2 ± 0.8 °C).

A view cell study was conducted to visually inspect the CO_2-induced polymer plasticisation and to corroborate the rheometric studies.

Images of this study carried out under subcritical CO2 (55°C and 70 bar, Figure 3.13) clearly show that PCL10 initially appeared as a granular sample (a), but in the presence of CO_2 at 55 °C and 70 bar was gradually plasticised (b-e). The view cell also confirmed the need for a long soaking time: after 25 minutes the sample was not fully plasticised (b), after 35 and 45 minutes some solid bits were still visible (c and d respectively), whilst after 48 minutes no solid residue could be observed anymore (e).

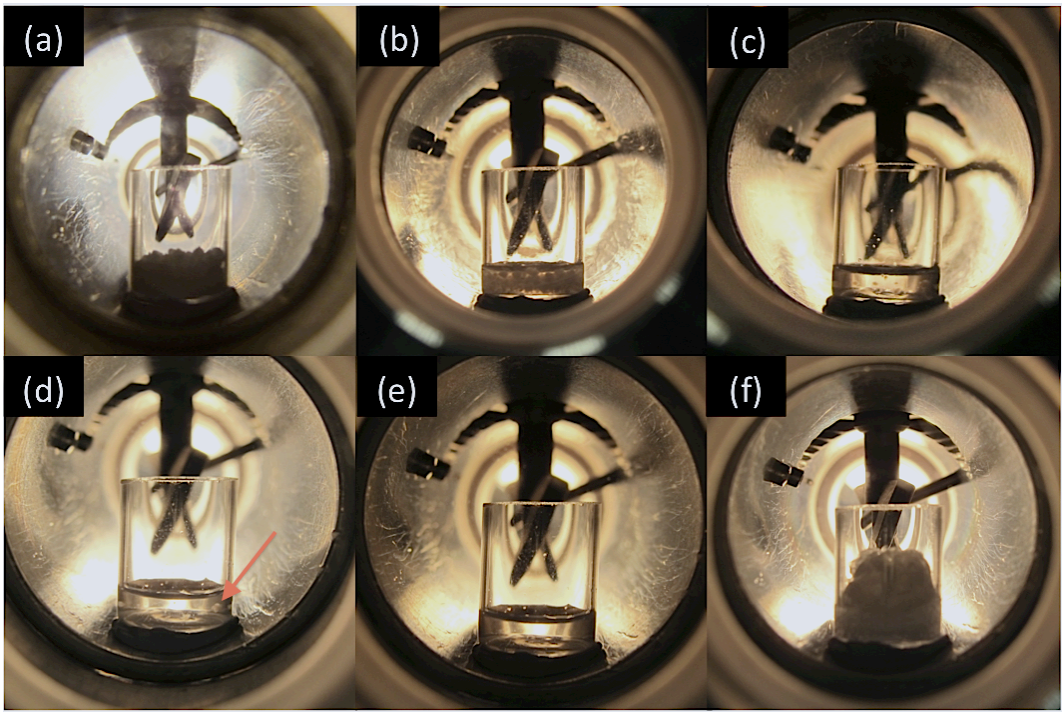


Figure 3.13 - Transitions observed for PCL10 in the view cell under subcritical CO_2 (55 °C, 70 bar): (a) initial polymer in a granular form; (b) sample not fully plasticised after 25 minutes; (c) sample almost fully plasticised after 35 minutes; (d) sample after 45 minutes: few solid bits are still visible (red arrow); (e) after 48 minutes the sample is completely liquefied; (f) polymer foamed upon CO_2 removal. Although the mechanical stirrer is visible in the images, the sample was not stirred during the experiments

An additional view cell experiment carried out in supercritical conditions can be found in the next section (Section 3.3.2.2, page 75, Figure 3.18). Here again, the need for a 50-minute soaking time needed to achieve the complete plasticisation of the polymer is shown.

This rather long soaking time is most probably due to the high crystallinity of PCL10 (around 52% by DSC, see Section 3.3.1, page 65). It is indeed well known that CO_2 is able to diffuse and dissolve only in the amorphous regions of polymers [15, 28, 83], and that the T_m depression is given by both polymer-CO_2 interactions in the amorphous regions and crystallite characteristics (*e.g.* lamellar thickness and heat of fusion per unit of volume); hence, different effects will be expected for different levels of amorphous fractions [28, 83].

3.3.2.2 T_m depression in CO_2

Having found the appropriate soaking time, oscillatory rheometric investigations were carried out over a range of pressures to evaluate the effect of high-pressure CO_2 on the T_m of PCL10. Both of the moduli, G' (Figure 3.14) and G'' (Figure 3.15), show a strong dependence upon temperature and CO_2 pressures. As expected, the shapes of the curves are similar to those obtained at ambient pressure (see Figure 3.7). However, a comparison between the curves shows that the G' drop and G'' peak, and hence the T_m, are shifted to lower temperatures in the presence of pressurised CO_2.

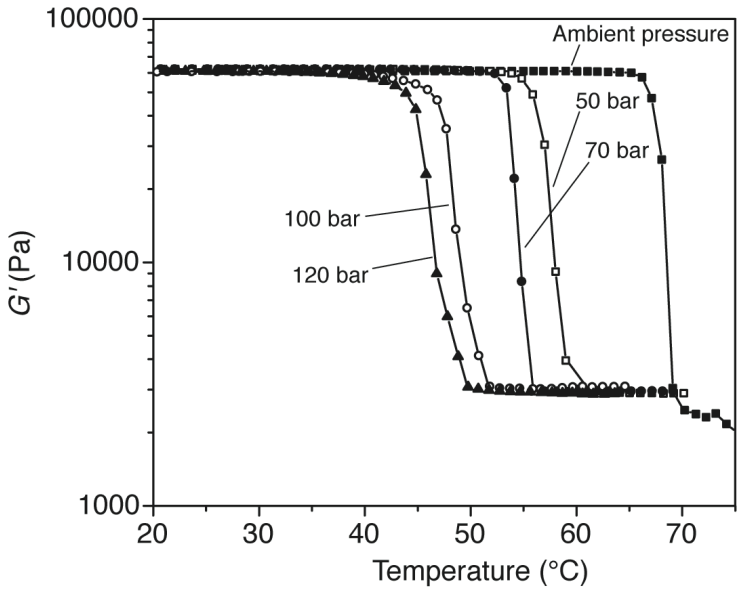


Figure 3.14 - Oscillatory rheometric measurements of G' as a function of temperature for PCL10 at a range of CO_2 pressures. The rapid decrease in G' is indicative of the polymer melting. Under high-pressure CO_2 the drop is shifted to lower temperatures, thus indicating a significant reduction in the T_m of the polymer (from 68 °C to 46 °C).

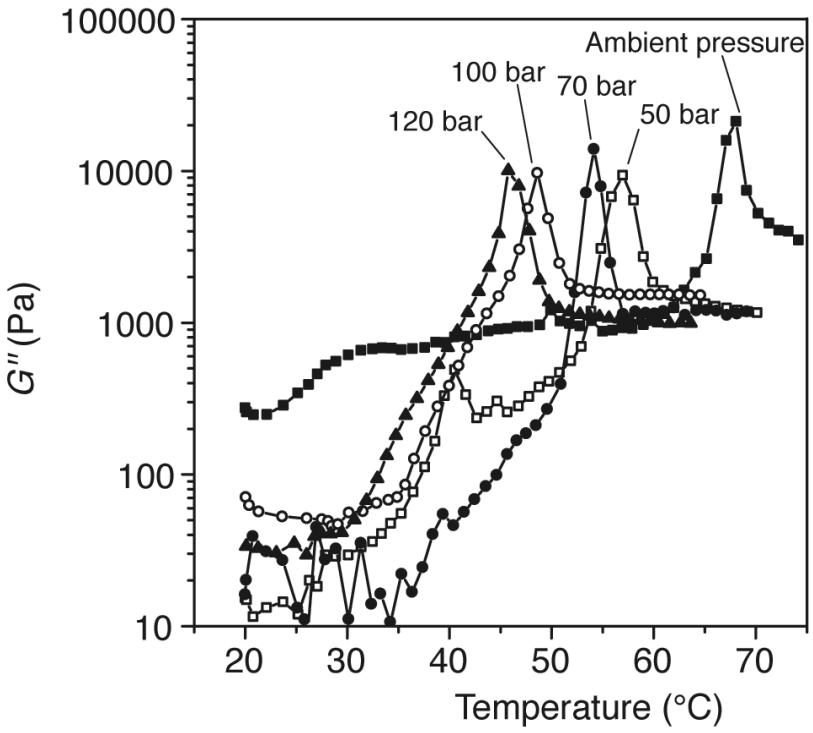


Figure 3.15 - Oscillatory rheometric measurements of *G´´* as a function of temperature for PCL10 at a range of CO_2 pressures. The peak in *G´´* is indicative of the polymer melting. Under CO_2 a significant reduction in the T_m of the polymer is observed.

It can be noted also that the *G'* plateau after the T_m at ambient pressure has a lower value compared to that obtained in CO_2 (Figure 3.14) and this result was reproducible (each experiment was run in triplicate). An unquestionable reason for this effect could not be found. The author believes that an augmented friction in the bearings of the pressure-cell (due to the pressure in the system) could cause the increased values in the plateau under CO_2. However, it must be also noted that the graph is plotted in a logarithmic scale, thus values in the low-value range are emphasised. In fact, the relative reduction in *G'* above the T_m is very similar both at ambient pressure and in CO_2 (around 97% at ambient pressure and 95% in CO_2). Besides, the most important piece of information acquired from a *G' vs T* plot is the temperature at which the dramatic change in the storage modulus occurs, which indicates the temperature at which the thermal transition is happening.

Therefore, this is a powerful demonstration of the ability of CO_2 to act as a temporary plasticiser for PCL, by diffusing into the polymer and interacting

through Lewis acid/base interactions with the carbonyl groups of the backbone (Figure 3.16). As a result, the intermolecular interactions are weakened and the polymer can melt at temperatures much lower than the ambient pressure melting point.

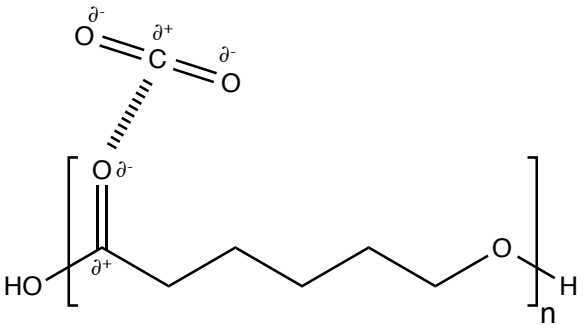


Figure 3.16 - Schematic depiction of the interaction between CO_2 and the carbonyl group of PCL.

The melting point reduction measured from the peaks in *G´´* under high-pressure CO_2 has been plotted as a function of pressure and compared to two literature studies measuring the drop in T_m by DSC [72] and FTIR [69] (Figure 3.17). The data are consistent with the results obtained in those previous studies and show a high correlation (R^2>0.99) linear decrease with increasing pressure, moving from 68.1 °C at atmospheric conditions through to a significantly lower value of 45.8 °C under CO_2 at 120 bar.

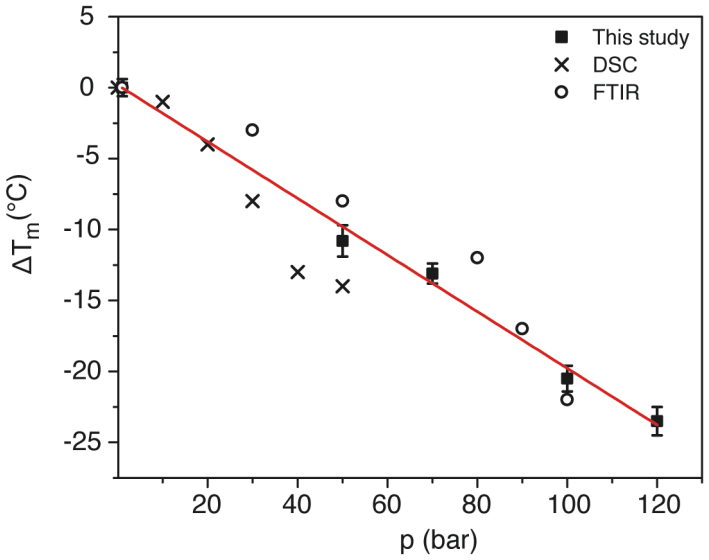


Figure 3.17 - Effect of CO_2 pressure on the change in T_m relative to atmospheric conditions, of PCL10 measured from the peak in G''. The results of this study follow a linear trend with high correlation ($R^2 > 0.99$). The data are in good agreement with the results obtained by other research groups through DSC [72] and FTIR [69].

Images from a view cell study carried out at the highest pressure investigated in the oscillatory rheometric study clearly show that PCL10 initially appeared as a white granular-powdery sample (a), but in presence of CO_2 at 45 °C and 120 bar was gradually plasticised (b) and became a completely colourless liquid after around 50 minutes (c) (Figure 3.18). Therefore, the visual observation corroborates the rheological study.

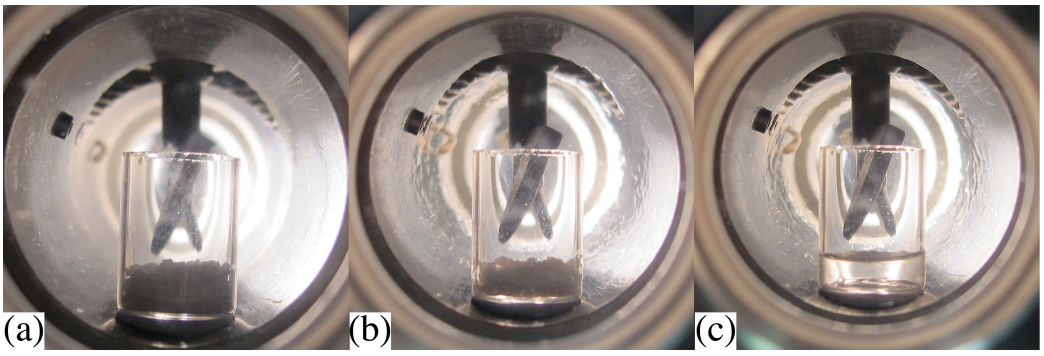


Figure 3.18 - Transitions observed for PCL10 in the view cell experiment at 45 °C: (a) initial polymer in the form of white granules (room temperature and pressure); (b) sample not completely plasticised after 15 minutes (45 °C, 120 bar); (c) polymer fully plasticised after 50 minutes (45 °C, 120 bar). Although the mechanical stirrer is visible in the images, the sample was not stirred during the experiments.

3.3.3 Effect of pressure and MW on the viscosity of PCL

When melt processing of a polymer is needed, the most important parameter to consider is clearly the viscosity of the melt. High viscosities can hinder the possibility of melt processing and can make the overall process energy intensive and not commercially sustainable [4].

It is well known that for linear polymers the T_m is an increasing function of the chain length only at small MW values, while it plateaus at higher MWs [84]. This behaviour was confirmed also for PCL. For this polymer the T_m was found to increase significantly with the mass average molecular weight (M_w) until about 9000 g mol^{-1} [85].

In more detail, the T_m was about 45 °C for a M_w value around 1000 g mol^{-1}. It increased dramatically to 60 °C and 63 °C for M_w around 3500 and 4500 g mol^{-1} respectively. Finally, PCL samples with M_w above 9000 g mol^{-1} were characterised by a T_m comprised between 64 and 67 °C (Figure 3.19).

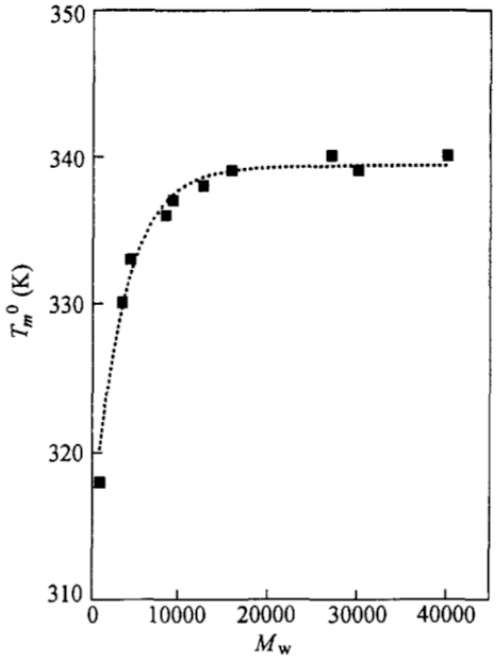


Figure 3.19 – T_m of PCL as a function of the mass average MW. A plateau value is observed above about 9000 g mol^{-1} [85].

Furthermore, the degree of crystallinity of PCL is known to decrease with increasing MW [86]. This has been explained in terms of chain folding, which is more significant with longer chains and impedes the formation of bigger spherulites.

On the contrary, the viscosity of a polymer in the molten state will strongly increase with increasing MW. Longer chains will result in more entanglement and, hence, higher viscosity [1, 2, 87]. As expected, this applies also to PCL [88].

For these reasons, investigations on the effects of pressure on the viscosity of PCL samples with different MW are crucial to understand the flow properties. This will give an insight to the possibility of using high-pressure processing for semicrystalline polymers with varied chain length.

3.3.3.1 Viscosity of PCL10 and PCL80 under CO_2

Rotational rheometric experiments were performed at 80 °C on two PCL samples with different MW, PCL10 and PCL80 (M_n ~10 kg mol^{-1} and ~80 kg mol^{-1} respectively) at a range of CO_2 pressures after 50 minutes soaking. This soaking time was chosen in accordance with the results obtained for the oscillatory measurements (Section 3.3.2.1).

Data in the shear rate region between 10^{-3}-10^{3} s^{-1} were obtained for PCL80. For PCL10, which is of lower MW, and hence of lower viscosity, such low shear rates could not be investigated due to experimental limitations.

The measurements of viscosity as a function of shear rate at 80 °C at a range of CO_2 pressures for PCL10 show that the sample exhibits Newtonian behaviour at low shear rates, followed by a shear-thinning region at shear rates above 300 s^{-1} (Figure 3.20). The zero-shear viscosity is dramatically decreased under CO_2, in agreement with results obtained on other polymers such as amorphous poly(lactic acid) [10], poly(ethylene glycol) [29], and poly(dimethylsiloxane) [89].

At pressures above 120 bar the shear-thinning region was less detectable in this shear rate range. This is due to a decrease in the relaxation time of the polymer (higher chain mobility), which results in an extended Newtonian plateau [10]. The critical shear rate at which the shear-thinning behaviour starts ($\dot{\gamma}_{cr}$) is, in fact, inversely proportional to the relaxation time [2, 87, 90, 91].

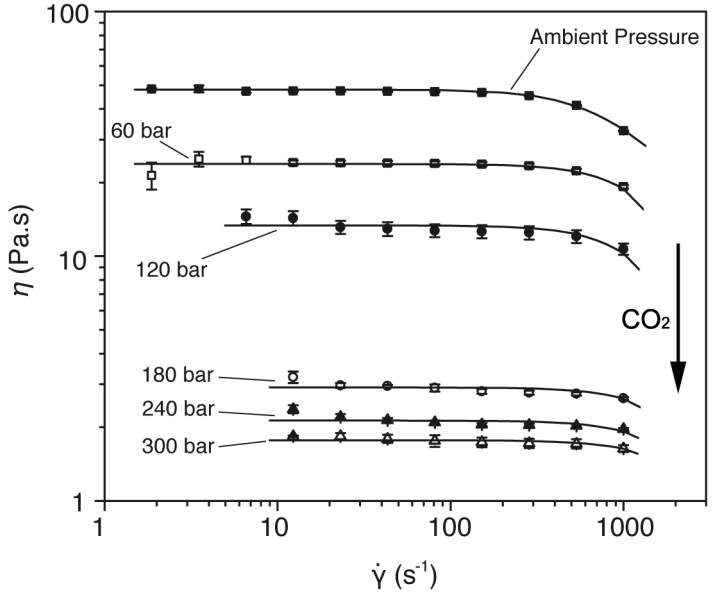


Figure 3.20 - Measurements of shear viscosity of PCL10 (T = 80 °C) at ambient pressure and under increasing CO_2 pressures. A significant reduction in the viscosity is observed with rising CO_2 pressure. The Carreau model (solid lines) is fitted to the data ($R^2 > 0.99$ for all the fits).

The viscosity data were fitted to the Carreau model (Equation 3.2) to enable quantitative determination of the relaxation time (see Section 3.3.3.3, page 86) and of the zero-shear viscosity (*i.e.* the viscosity at low shear rate). The model is given by:

$$\eta(\dot{\gamma}) = \eta_0[1 + (\lambda\dot{\gamma})^2]^{-P} \qquad (3.2)$$

where $\eta(\dot{\gamma})$ (Pa s) is the viscosity at a given shear rate $\dot{\gamma}$ (s^{-1}), η_0 (Pa s) is the zero-shear viscosity, λ (s) is the relaxation time of the polymer and P is the Carreau exponent [10, 92].

The ability of $scCO_2$ to plasticise higher MW PCL was confirmed by viscosity studies carried out on PCL80 (Figure 3.21). The measurements of viscosity as a function of shear rate at 80 °C at a range of CO_2 pressures for PCL80 clearly show that this polymer has a much higher viscosity than PCL10, as expected from the higher degree of chain entanglement [90, 93, 94]. Also, $\dot{\gamma}_{cr}$ is considerably reduced. This is due to the longer relaxation time given by the increased chain length [2, 87, 90, 91].

Nonetheless, a dramatic effect of the pressurised CO_2 on the viscosity was observed also for this higher MW polymer.

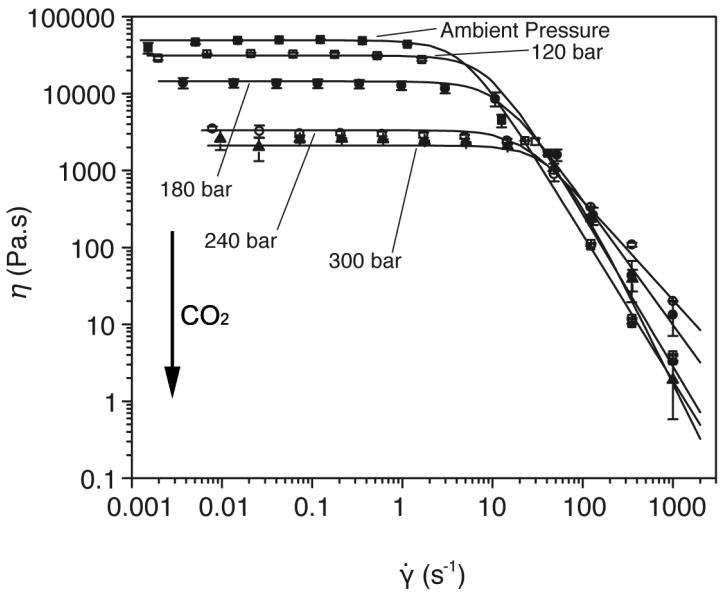


Figure 3.21 - Measurements of shear viscosity of PCL80 (T = 80 °C) at ambient pressure and under increasing CO_2 pressures. A significant reduction in the viscosity is observed with rising pressure. The Carreau model (solid lines) is fitted to the data (R^2 > 0.99 for all the fittings).

The zero-shear viscosity is again significantly reduced with increasing CO_2 pressure, and the viscosity reduction is particularly significant in the shear rate region typical of traditional polymer extrusion processes (between 1 and 5 s^{-1}, *i.e.* 60-300 rpm) [1, 2, 95, 96]. As expected, increasing CO_2 pressure results in higher $\dot{\gamma}_{cr}$ values and, therefore, in reduced relaxation times.

Furthermore, it can be noticed how at very high shear rates (above 10 s^{-1}) a clear trend viscosity *vs* pressure could not be identified. Similar results have been observed also on poly(lactic acid) under varied CO_2 pressures [10]. Also in this case, at high shear rate values curves recorded at higher pressures crossed the lower pressure ones and showed higher viscosities without a clear trend. This effect has not been fully understood nor analysed in the literature and it could be partially attributed to a combined effect of the extension of the Newtonian plateau under pressure (reduced relaxation time in CO_2), to compressive pressure effects and to the high shear applied to the polymer, which could perturbate the system.

However, all the lines show shear-thinning behaviour at high shear rates and the viscosity is significantly reduced with increasing pressure within the Newtonian plateau (*i.e.* below 10 s^{-1} for this polymer).

Table 3.1 shows a comparison of the viscosities of the two polymers at representative shear rates in the Newtonian plateau at ambient pressure, η_0^{amb}, and when plasticised by 300 bar CO_2, $\eta_0^{300\,bar\,CO_2}$.

Viscosities are reduced by around 95% for both polymers as a result of the plasticising effect. This shows that the effects are significant and comparable for both of the polymers and, hence that CO_2 is able to act as an effective plasticiser for PCL samples with medium-low and high MW.

Table 3.1 - High-pressure CO_2-induced maximum viscosity reduction of PCL10 and PCL80 in the Newtonian plateau at 80 °C.

M_n (kg mol^{-1})	$\dot{\gamma}$ (s^{-1})	η_0^{amb} (Pa s)	$\eta_0^{300\,bar\,CO_2}$ (Pa s)	η_0 reduction (%)
10	12.0	47.37 ± 0.40	1.84 ± 0.01	96.1
80	0.1	50000 ± 430	2590 ± 280	94.8

3.3.3.1 CO_2 effect vs temperature and activation energy for viscous flow (E_a) in CO_2

Without a doubt, as shown in the previous section the viscosity reduction achieved exposing PCL10 and PCL80 to high-pressure CO_2 is quite significant. Nonetheless, if the same (or comparable) results can be obtained by heating the polymer at a temperature slightly higher than 80 °C the use of CO_2 would be not commercially justifiable and viable.

For this reason, an additional set of experiments was conducted at ambient pressure over a temperature range of 80 to 180 °C in order to correlate the CO_2-induced viscosity depression (showed in Section 3.2.2.2, page 61) to the temperature-induced reduction.

The same temperature ramp was performed under CO_2 (at 120 bar) to allow also for determination of the activation energy (E_a) with and without pressurised CO_2 (Table 3.2). Higher pressures could not be investigated for safety reasons, according to the temperature-pressure rating of the equipment taking into consideration the rubber o-ring used to seal the pressure cell.

The zero-shear viscosities of PCL10 ($\dot{\gamma}$=12.0 s^{-1}) and PCL80 ($\dot{\gamma}$=0.1 s^{-1}) are shown as a function of temperature in an Arrhenius plot (Figure 3.22).

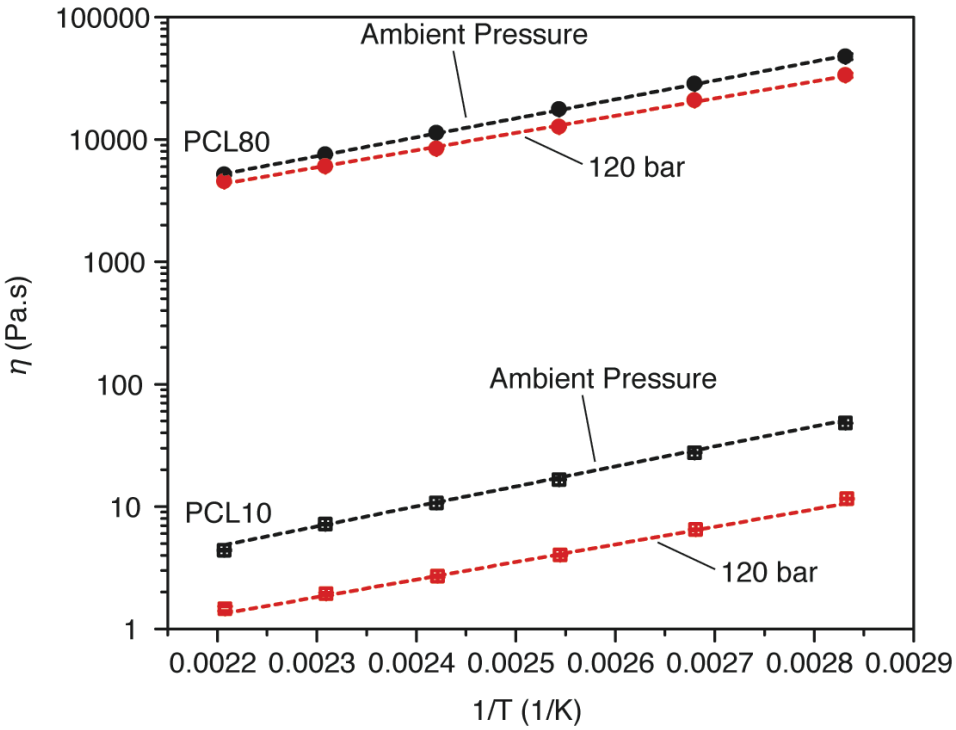


Figure 3.22 - Arrhenius plot of zero-shear viscosity as a function of temperature for PCL10 and PCL80 at ambient pressure and under CO_2 (120 bar). In PCL10, a 91% reduction in the viscosity is obtained between 80 °C and 180 °C, whilst an 88% reduction is observed for PCL80 in the same temperature range. The data were collected from 80 °C (right) to 180 °C (left) with 20 °C steps. The data were fitted to an Arrhenius equation with very high correlation ($R^2 > 0.99$).

First of all, the data plotted in Figure 3.22 show the dramatic effect of processing with CO_2. For example, comparing Figure 3.20 and Figure 3.22, processing at 240 bar of CO_2 at 80 °C of PCL10 results in a viscosity (~3 Pa s) which is equivalent to processing at 180 °C at ambient pressure conditions.

For PCL80, comparing Figure 3.21 and Figure 3.22, exposure to 240 bar of CO_2 at 80 °C produces a viscosity (~3 kPa s) which is even lower than the ambient pressure viscosity obtained at 180 °C (~6 kPa s). In fact, extending the data fitting, a temperature around 250 °C would be needed in order to achieve a viscosity equal to the viscosity value under 300 bar of CO_2 at 80 °C (~2 kPa s).

Therefore, these measurements demonstrate the significant opportunities that high-pressure CO_2 processing of polymers could deliver in terms of energy saving and processing of thermally labile materials [27].

Furthermore, the data points in Figure 3.22 have been fitted to an Arrhenius equation with very high correlation (R^2>0.99 for both of the datasets). An approximation model for kinetic activity in chemistry was developed in its general form in 1899 by Svante Arrhenius [97]. Arrhenius introduced the concepts of an activation energy required to start a chemical process.

The Arrhenius model can be used to effectively model the change in viscosity of a polymer for both increasing and decreasing temperatures [76]. The relation is given by the Equation (3.3):

$$\eta(T) = Ae^{\frac{E_a}{RT}} \qquad (3.3)$$

where A is the pre-exponential factor (Pa s) (which can be approximated to the infinite-temperature viscosity [98]), T is the temperature in Kelvin, R is the universal gas constant (~$8.31 \cdot 10^{-3}$ kJ K^{-1} mol^{-1}) and E_a is the activation energy for viscous flow (kJ mol^{-1}).

In this case, the E_a value characterises the energy required in order to set in motion the polymer chains against the frictional forces of the other adjacent chains, which is clearly a crucial parameter to consider when processing a polymer in the molten state.

As expected, the fittings show that the E_a for both of the polymers is reduced under CO_2 (Table 3.2). Thus, the energy requirement to start the macromolecular motions is lowered under high-pressure CO_2.

Table 3.2 - E_a reduction for PCL under CO_2. The E_a values are reduced under $scCO_2$ for both polymers, meaning that less energy is required to set in motion the polymer chains.

MW	E_a (kJ/mol)		Reduction
(kg mol^{-1})	Ambient	120 bar	(%)
80	29.59 ± 0.20	26.96 ± 0.18	8.9
10	31.27 ± 0.67	27.50 ± 0.35	12.1

These values are in good agreement with results obtained from the frequency sweeps (reptation time analysis) carried out on PCL (M_n ~120 kg mol^{-1}) by Kelly *et al.* [53] and confirm that the v_f increase reduces the energy required for the polymer chains to move and, therefore, the polymer to flow. This can lead to a more cost-effective process and diminish the probability of degradation in the case of thermally-labile materials incorporation.

3.3.3.2 Viscosity of PCL10 and PCL80 under N_2

The viscosity depression under CO_2 is due to the interactions between the CO_2 molecules and the polymer chains. Hence, a polymer melt exposed to a high-pressure non-plasticising gas should show a viscosity increase rather than a decrease since the polymer chains will be compressed and the amount of v_f within the structure will decrease. Hence, the macromolecules will be more and more limited in their mobility [76].

For this reason, rotational rheometric experiments were also repeated under N_2, a non-plasticising gas, up to 180 bar (higher pressures were not investigated since for these studies a N_2 cylinder was directly attached to the rheometer inlet), to prove this and gain a better understanding of plasticisation and compression effects.

Measurements of viscosity as a function of shear rate at 80 °C at a range of N_2 pressures for PCL10 display a small but noticeable increase in viscosity with pressure (Figure 3.23). Also, no significant changes in the extent of the zero-shear plateau (hence, in $\dot{\gamma}_{cr}$) were observed, and shear-thinning behaviour was always clearly observed within the shear rate range.

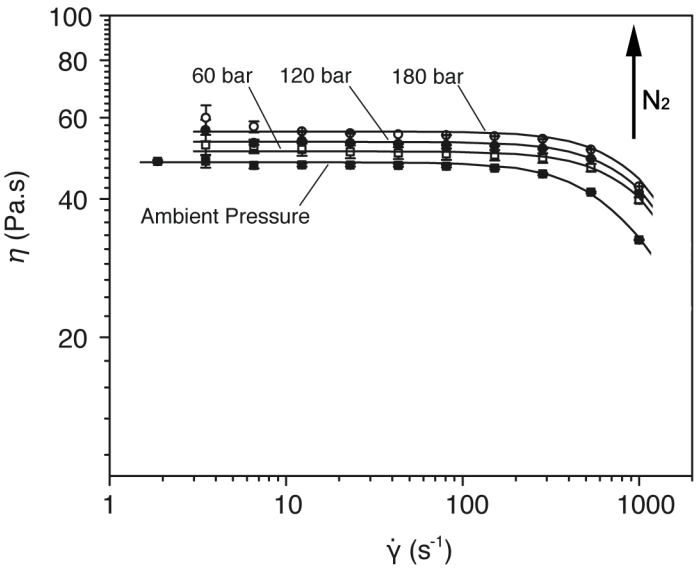


Figure 3.23 - Measurements of shear viscosity of PCL10 (T = 80 °C) at ambient pressure and under increasing N_2 pressures. A small increase in the viscosity is observed with increasing N_2 pressure. The Carreau model (solid lines) is fitted to the data ($R^2 > 0.99$ for all the sets of data).

Rotational rheological studies were carried out also for PCL80 in the presence of high-pressure N_2 (Figure 3.24). Here again no viscosity decrease or changes in the extent of the Newtonian plateau could be observed. The zero-shear viscosity increases with increasing pressure, although the effect is small (zoomed in region).

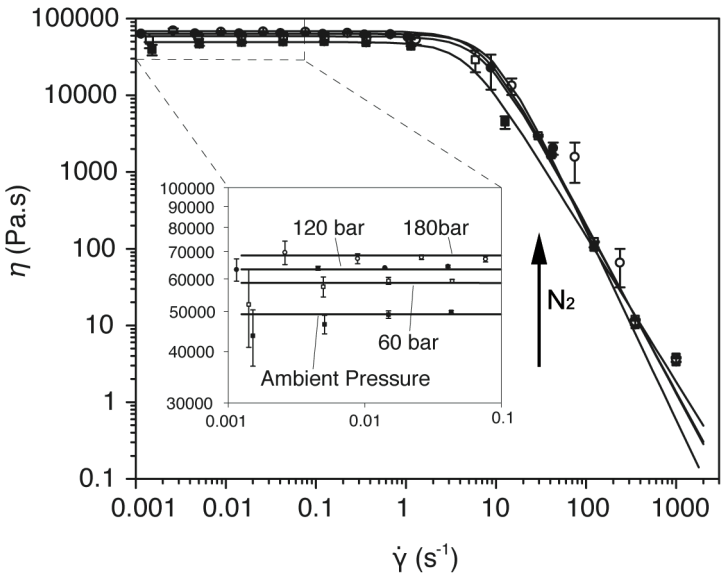


Figure 3.24 - Measurements of shear viscosity of PCL80 (T = 80 °C) at ambient pressure and under increasing N_2 pressures. A small increase in the zero-shear viscosity is observed with rising pressure (zoomed in region). The Carreau model (solid lines) is fitted to the data (R^2>0.99 for all the fittings).

The zero-shear viscosities, calculated from fittings of the Carreau model for both polymers under CO_2 and N_2, have been plotted as a function of pressure (Figure 3.25). A trend of increasing zero-shear viscosity with pressure is found under N_2, and of decreasing viscosity with pressure under CO_2. These data show that the pressure effects in the presence of N_2 give a viscosity increase, in good agreement with the Barus law, Equation (3.4):

$$\eta_0(p) = \eta_0^{\text{atm}} e^{ap} \qquad (3.4)$$

where $\eta_0(p)$ (Pa s) is the viscosity at pressure p (Pa), η_o^{atm} (Pa s) is the viscosity at atmospheric pressure and a (Pa^{-1}) is a pressure-viscosity coefficient [99]. The viscosity reduction with CO_2 pressure would require a negative pressure-viscosity coefficient in order to fit the Barus equation, but the quality of fit would be vastly reduced as the reduction in log viscosity is not linear. For this reason, the data obtained in CO_2 are connected with a solid line as a guide to the eye.

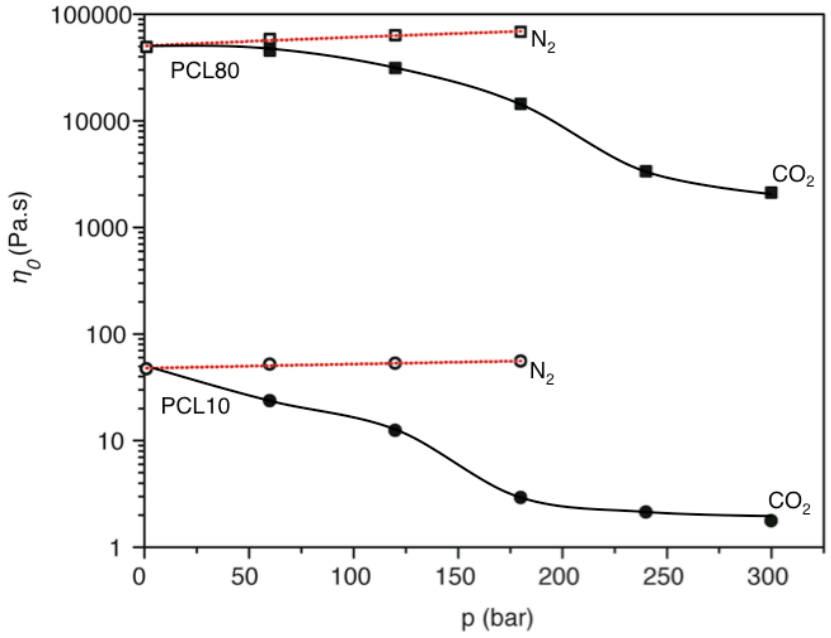


Figure 3.25 - Zero-shear viscosity of PCL10 and PCL80 (T=80 °C) under CO_2 and N_2. A small increase in the zero-shear viscosity is observed on raising the N_2 pressure (empty symbols), whilst a decrease is seen under CO_2 (black symbols). The data collected under N_2 were fitted to the Barus equation (red dotted lines) with high correlation (R^2>0.99 for all the fittings). The black solid lines connecting the CO_2 data have been drawn as a guide to the eye.

3.3.3.3 Relaxation time analysis

The relaxation time of a polymer (λ) is an important parameter that can be obtained from Carreau model fits. This physical quantity can be used to give an indication of the time scale associated with the viscoelastic response in a polymer. In more detail, the relaxation time of a polymer indicates the time it takes for the polymer chains to return to the equilibrium state after a perturbation (*e.g.* shear stress). Hence, this quantity is indicative of the viscosity of the polymer and it is intrinsically related to the length and entanglement of the polymeric chains [3].

As stated before (Section 3.3.3.1, page 78), CO_2 plasticisation also results in a change in the relaxation time of the polymer, which is caused by the higher chain mobility.

In PCL80 a linear decrease ($R^2 > 0.96$) in relaxation time with CO_2 pressure was recorded (Figure 3.26). On the contrary, in PCL10 a decrease with a clear trend could not be observed. For this polymer, the relaxation time was 0.0015 s at

ambient pressure and it decreased to around 0.0005 s under CO_2, independently of the applied pressure. It is postulated that in PCL10 the chains are not sufficiently entangled because of their low MW. Therefore, the effect of CO_2 plasticisation at different pressures on the relaxation time on this polymer may be less noticeable, since the chains are already amply mobile due to the thermal energy and their short length.

A similar result has been obtained with increasing temperature for poly(lactic acid) by Kelly *et al.* who observed that at sufficiently high temperatures (T_{exp}=140 °C; T_g=55 °C; M_n=155 kg mol^{-1}) no changes in relaxation time could be observed upon the addition of CO_2 [10]. In this case the absence of a clear trend in the relaxation time values as a function of the CO_2 pressure was attributed to the high thermal energy (*i.e.* high temperature). This made the effects of the absorbed CO_2 on the relaxation time negligible.

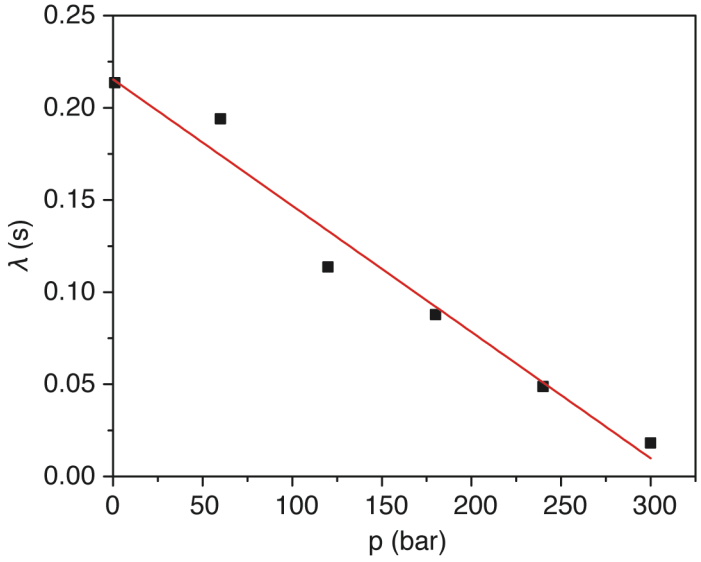


Figure 3.26 - Relaxation time as a function of CO_2 pressure obtained from Carreau model fits for PCL80 at T = 80 °C. A linear decrease (R^2 > 0.96) is observed.

3.3.3.4 Transient shear viscosity analyses: is the CO_2 solubility changing while shearing?

One challenge when analysing the properties of polymers in CO_2 is that the gas concentration is not fixed *a priori*. It is well known that the amount of CO_2

absorbed in a polymer is a function of temperature and pressure; as described in many papers dealing with the quantification of the carbon dioxide sorption levels in polymers [33, 42, 73].

In addition to these variables, the shear rate must be considered when analysing the flow behaviour of a polymer. In fact, the equilibrium might be changed whilst shearing the sample: as a result, the solubility may increase or decrease during shear sweep experiments. This could lead to changes in the plasticisation effects, phase separation and/or formation of bubbles in the molten polymer.

For these reasons, it is important to investigate whether or not the shear sweeps represent a perturbation of the equilibrium and, hence, if the CO_2 plasticisation is affected by the measurements or not. This is a challenging problem that, to the best of the author's knowledge, has not been investigated in literature and is difficult to probe experimentally giving definitive answer. Although rheometers are now available that have an endoscopic camera at the parallel-plate, devising such device for use in $scCO_2$ would be challenging and is beyond the scope of this work.

In order to investigate more in-depth upon this, the author hypothesised that transient shear measurements could give additional information on the solubility during shearing. This is the first time that these type of studies have been carried out in CO_2. In these tests the data were collected at low shear rates with a short measuring point duration (0.3-1 s with a logarithmic increment) to allow for collection of transient shear viscosity data [76]. In this case, start-up effects (or time dependent transition effects) are obtained, since the viscosity data are collected before the system reaches a steady state situation. Therefore, the viscosity will be a function of both shear rate and time.

Typically, a linear increasing regime is expected at the beginning and then a plateau is observed at lower shear rates, whilst an overshoot can be detected at higher shear rate values [100, 101]. These effects have been explained in terms of initial elastic response of the entangled polymer network, and disentanglement at high stresses. Hence, any unexpected behaviour observed under high-pressure CO_2 could be assigned to solubility change and/or phase separation while shearing.

Carrying out an experiment at ambient pressure on PCL80 at 80 °C and 120 °C the expected behaviour was observed (Figure 3.27). It can be noted how, the most important effect of the temperature increase is a shift to lower values in the

viscosity. In particular, at the two different temperatures, the order of the lines towards the end of the experiment remains the same with the viscosity clearly decreasing with increasing frequency.

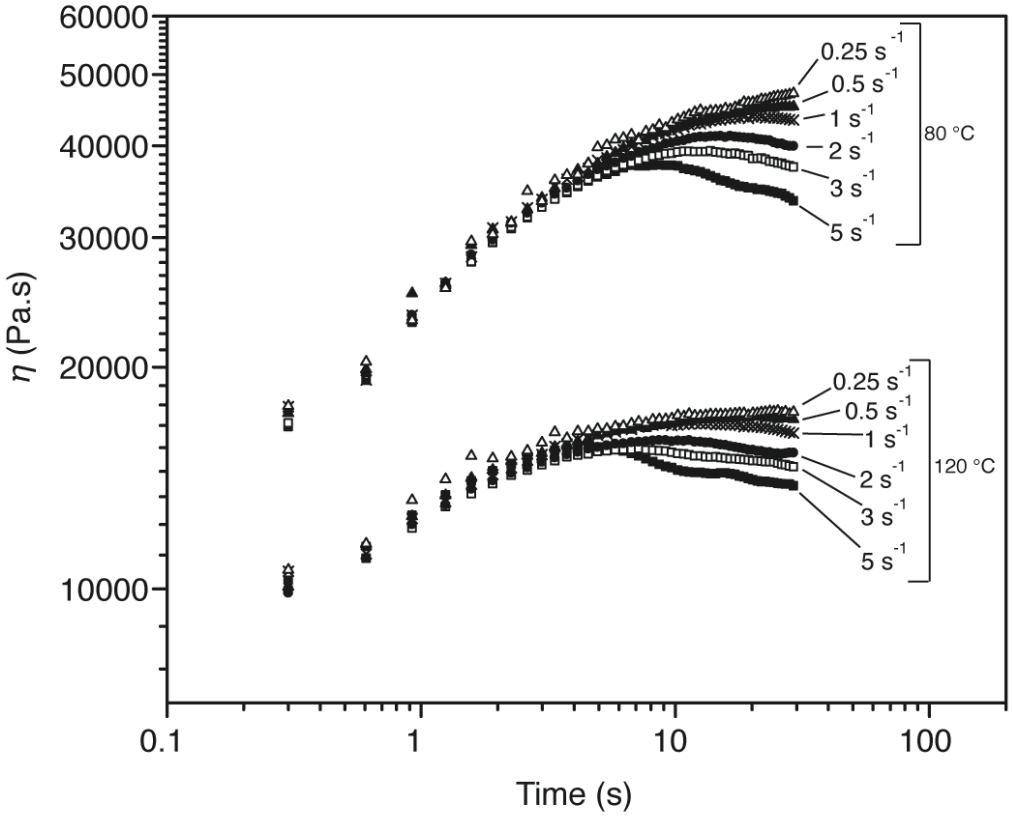


Figure 3.27 – Transient shear viscosity *vs* time for PCL 80 °C and 120 °C at ambient pressure. The time dependent transition effects show the same trend obtained in scCO$_2$ (see Figure 3.28).

Transient shear viscosity data at the same shear rates under CO_2 (120 bar, 80 °C) show again that the CO_2-induced plasticisation mimics the temperature effects (Figure 3.28).

Here again, the linear increase is observed at the beginning of the test and then a plateau is detected. Similarly, the overshoot at high shear rates (>2 s^{-1}) was observed too. The most pronounced difference between the curves collected at 80 °C with and without CO_2 is a reduced viscosity under pressure: also in this case the final part of the curve for each frequency could in principle be overlapped with the application of an appropriate shift factor. If it were the case

that solubility was changing with shearing (with a shear rate dependency), one might have expected an additional change in viscosity appearing as a function of the applied shear. On the contrary, the same trend, which is decreasing viscosity with increasing frequency, is always observed. The lack of any effects beyond the expected stress overshoots at high rates and linear viscoelasticity at low rates, together with the high reproducibility and quality of these and all the viscosity data previously shown, suggest that phase separation, solubility changes during shearing or bubble formation are unlikely to be taking place during the experiments.

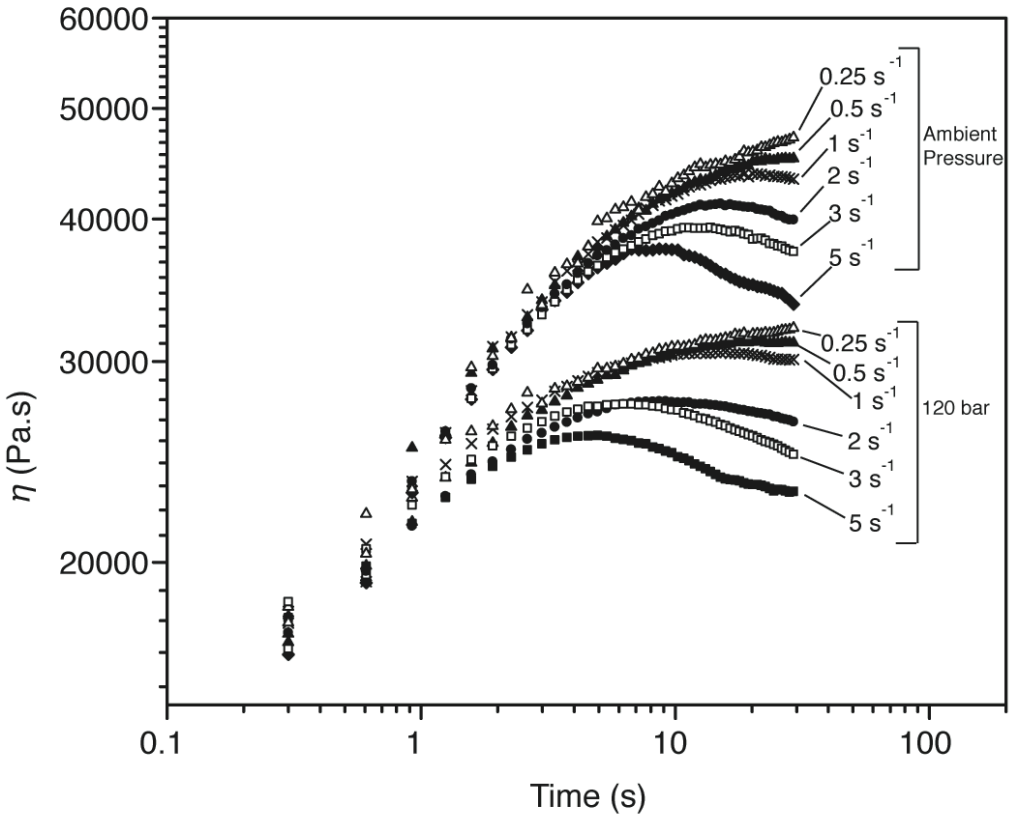


Figure 3.28 – Transient shear viscosity *vs* time for PCL80 at 80 °C at ambient pressure and under CO_2 (120 bar).

Due to the low viscosity and the equipment torque limitations, the same analysis could not be carried out on PCL10 (the initial linear regime could not be observed, a clear separation of the curves at each frequency could not be achieved and,

because of the short measuring point duration, the influence of the bearings on the data was quite significant).

3.4 Conclusions

High-pressure rheology was employed to demonstrate clearly the ability of CO_2 to plasticise PCL at supercritical and even sub-critical (60 bar) conditions at 80 °C. For the first time, interpretation of the viscoelastic moduli with temperature plots have been used to show that by adding CO_2 it is possible to lower the melting point of PCL by more than 20 °C (from 68 to 46 °C). This provides a rheological viewpoint to the CO_2-induced T_m depression of this polymer that correlates well with previous studies using DSC and FTIR spectroscopy, and a linear drop in T_m with increasing CO_2 pressure was observed. Therefore, a new methodology to assess the T_m depression of semicrystalline polymers in CO_2 has been designed.

The viscosity of PCLs of different MWs decreased significantly when pressurised CO_2 was added. The reductions observed at 80 °C and 180 bar are comparable to those achieved at 180 °C at ambient pressure. At 300 bar 96% decrease in viscosity relative to ambient pressure was achieved for the 10 kg mol^{-1} polymer, whilst a 95% reduction was obtained for the 80 kg mol^{-1} polymer.

The Carreau model was employed for determination of the zero-shear viscosity and the relaxation time, both of which decreased with increasing CO_2 pressure. By contrast, the effect of a non-plasticising gas, N_2, was to increase the zero-shear viscosity. In addition to this, efforts were made to prove that shearing did not induce changes in the CO_2 solubility by carrying out transient shear experiments under pressure.

To sum up, this chapter demonstrated the use of a high-pressure rheometer to detect the T_m depression of polymers under CO_2, highlighting the ability of CO_2 to act as a green and efficient temporary plasticiser that allows for processing of semicrystalline degradable polymers at significantly lower temperatures. In more detail, CO_2 gives the opportunity for significantly lower temperature processing (*i.e.* 80 °C rather than 250 °C for PCL80).

Therefore, these results emphasise the significant prospects that high-pressure CO_2 processing of semicrystalline polymers could deliver in terms of energy saving and processing of thermally labile materials. This learning has been the

base for the development of the next two chapters where it will be used to design novel green lower temperature synthetic routes.

3.5 References

[1] T.A. Osswald, *Polymer Processing Fundamentals*, Hanser, **1998**
[2] C.I. Chung, *Extrusion of Polymers: Theory and Practice*, Hanser Gardner Publications, **2000**
[3] H.F. Brinson, L.C. Brinson, *Polymer Engineering Science and Viscoelasticity: An Introduction*, Springer US, **2015**
[4] S.P. Nalawade, F. Picchioni, L.P.B.M. Janssen, *Progress in Polymer Science*, 31, **2006**, p. 19
[5] R.G. Wissinger, M.E. Paulaitis, *Journal of Polymer Science Part B: Polymer Physics*, 29, **1991**, p. 631
[6] M. Lee, C. Tzoganakis, C.B. Park, *Polymer Engineering & Science*, 38, **1998**, p. 1112
[7] A. Bos, I.G.M. Pünt, M. Wessling, H. Strathmann, *Journal of Membrane Science*, 155, **1999**, p. 67
[8] P. Alessi, A. Cortesi, I. Kikic, F. Vecchione, *Journal of Applied Polymer Science*, 88, **2002**, p. 2189
[9] L. Yu, H. Liu, L. Chen, *Polymer Engineering & Science*, 49, **2009**, p. 1800
[10] C.A. Kelly, S.M. Howdle, K.M. Shakesheff, M.J. Jenkins, G.A. Leeke, *Journal of Polymer Science Part B: Polymer Physics*, 50, **2012**, p. 1383
[11] C. Tsioptsias, M.K. Paraskevopoulos, D. Christofilos, P. Andrieux, C. Panayiotou, *Polymer*, 52, **2011**, p. 2819
[12] C. Gutiérrez, M.T. Garcia, S. Curia, S.M. Howdle, J.F. Rodriguez, *The Journal of Supercritical Fluids*, 88, **2014**, p. 26
[13] F. Picchioni, *Polymer International*, 63, **2014**, p. 1364
[14] J. Jennings, M. Beija, J.T. Kennon, H. Willcock, R.K. O'Reilly, S. Rimmer, S.M. Howdle, *Macromolecules*, 46, **2013**, p. 6843
[15] O.R. Davies, A.L. Lewis, M.J. Whitaker, H. Tai, K.M. Shakesheff, S.M. Howdle, *Advanced Drug Delivery Reviews*, 60, **2008**, p. 373
[16] F. Yang, M. Manitiu, R. Kriegel, R.M. Kannan, *Polymer*, 55, **2014**, p. 3915
[17] L. Du, J.Y. Kelly, G.W. Roberts, J.M. DeSimone, *The Journal of Supercritical Fluids*, 47, **2009**, p. 447
[18] J. Jennings, M. Beija, A.P. Richez, S.D. Cooper, P.E. Mignot, K.J. Thurecht, K.S. Jack, S.M. Howdle, *Journal of the American Chemical Society*, 134, **2012**, p. 4772
[19] I. Tsivintzelis, E. Pavlidou, C. Panayiotou, *The Journal of Supercritical Fluids*, 42, **2007**, p. 265
[20] L. Monnereau, L. Urbanczyk, J.-M. Thomassin, T. Pardoen, C. Bailly, I. Huynen, C. Jérôme, C. Detrembleur, *Polymer*, 59, **2015**, p. 117
[21] L. Monnereau, L. Urbanczyk, J.-M. Thomassin, M. Alexandre, C. Jérôme, I. Huynen, C. Bailly, C. Detrembleur, *Polymer*, 55, **2014**, p. 2422
[22] M.J. Jenkins, K.L. Harrison, M.M.C.G. Silva, M.J. Whitaker, K.M. Shakesheff, S.M. Howdle, *European Polymer Journal*, 42, **2006**, p. 3145
[23] C. Gualandi, L.J. White, L. Chen, R.A. Gross, K.M. Shakesheff, S.M. Howdle, M. Scandola, *Acta Biomaterialia*, 6, **2010**, p. 130
[24] B. Bungert, G. Sadowski, W. Arlt, *Fluid Phase Equilibria*, 139, **1997**, p. 349
[25] S.P. Nalawade, F. Picchioni, L.P.B.M. Janssen, *Chemical Engineering Science*, 62, **2007**, p. 1712

[26] C.A. Kelly, A. Naylor, L. Illum, K.M. Shakesheff, S.M. Howdle, *Advanced Functional Materials*, 22, **2012**, p. 1684
[27] S.M. Howdle, M.S. Watson, M.J. Whitaker, M.C. Davies, K.M. Shakesheff, V.K. Popov, F.S. Mandel, J.D. Wang, *Chemical Communications*, **2001**, p. 109
[28] Z. Zhang, Y.P. Handa, *Macromolecules*, 30, **1997**, p. 8505
[29] D. Gourgouillon, H.M.N.T. Avelino, J.M.N.A. Fareleira, M. Nunes da Ponte, *The Journal of Supercritical Fluids*, 13, **1998**, p. 177
[30] S.A.E. Boyer, J.P.E. Grolier, *Pure and Applied Chemistry*, 77, **2005**, p. 593
[31] Z. Zhang, Y.P. Handa, *Journal of Polymer Science Part B: Polymer Physics*, 36, **1998**, p. 977
[32] J.M.D. Joseph R. Royer, Saad A. Khan, *Journal of Polymer Science Part B: Polymer Physics*, 39, **2001**, p. 3055
[33] R. Pini, G. Storti, M. Mazzotti, H. Tai, K.M. Shakesheff, S.M. Howdle, *Journal of Polymer Science Part B: Polymer Physics*, 46, **2008**, p. 483
[34] M. Iguchi, Y. Hiraga, K. Kasuya, T.M. Aida, M. Watanabe, Y. Sato, R.L. Smith, *The Journal of Supercritical Fluids*, 97, **2015**, p. 63
[35] P.J. Ginty, J.J.A. Barry, L.J. White, S.M. Howdle, K.M. Shakesheff, *European Journal of Pharmaceutics and Biopharmaceutics*, 68, **2008**, p. 82
[36] S.G. Kazarian, *Polymer Science Series C*, 42, **2000**, p. 78
[37] A.I. Cooper, *Journal of Materials Chemistry*, 10, **2000**, p. 207
[38] S.G. Kazarian, M.F. Vincent, F.V. Bright, C.L. Liotta, C.A. Eckert, *Journal of the American Chemical Society*, 118, **1996**, p. 1729
[39] S.G. Kazarian, N.H. Brantley, B.L. West, M.F. Vincent, C.A. Eckert, *Applied Spectroscopy*, 51, **1997**, p. 491
[40] R.R. Edwards, Y. Tao, S. Xu, P.S. Wells, K.S. Yun, J.F. Parcher, *The Journal of Physical Chemistry B*, 102, **1998**, p. 1287
[41] F. Rindfleisch, T.P. DiNoia, M.A. McHugh, *The Journal of Physical Chemistry*, 100, **1996**, p. 15581
[42] M.A. Fanovich, P. Jaeger, *Materials Science and Engineering: C*, 32, **2012**, p. 961
[43] M. Tang, M. Purcell, J.A.M. Steele, K.-Y. Lee, S. McCullen, K.M. Shakesheff, A. Bismarck, M.M. Stevens, S.M. Howdle, C.K. Williams, *Macromolecules*, 46, **2013**, p. 8136
[44] D.W. Hutmacher, *Biomaterials*, 21, **2000**, p. 2529
[45] Q. Xu, X. Ren, Y. Chang, J. Wang, L. Yu, K. Dean, *Journal of Applied Polymer Science*, 94, **2004**, p. 593
[46] J.S. Chiou, J.W. Barlow, D.R. Paul, *Journal of Applied Polymer Science*, 30, **1985**, p. 3911
[47] X. Liao, A.V. Nawaby, P.S. Whitfield, *Polymer International*, 59, **2010**, p. 1709
[48] Y.P. Handa, Z. Zhang, J. Roovers, *Journal of Polymer Science Part B: Polymer Physics*, 39, **2001**, p. 1505
[49] K. Mizoguchi, T. Hirose, Y. Naito, Y. Kamiya, *Polymer*, 28, **1987**, p. 1298
[50] F.C. Loeker, C.J. Duxbury, R. Kumar, W. Gao, R.A. Gross, S.M. Howdle, *Macromolecules*, 37, **2004**, p. 2450
[51] M.F. Kemmere, T. Meyer, *Supercritical carbon dioxide in polymer reaction engineering / edited by Maartje F. Kemmere and Thierry Meyer*, Wiley-VCH, **2005**
[52] B. Kapoor, M. Bhattacharya, *Polymer Engineering & Science*, 39, **1999**, p. 676

[53] C.A. Kelly, S.H. Murphy, G.A. Leeke, S.M. Howdle, K.M. Shakesheff, M.J. Jenkins, *European Polymer Journal*, 49, **2013**, p. 464
[54] A. Munoz-Bonilla, M.L. Cerrada, M. Fernandez-Garcia, A. Kubacka, M. Ferrer, M. Fernandez-Garcia, *Internationl Journal of Molecular Sciences*, 14, **2013**, p. 9249
[55] K. Fu, A.M. Klibanov, R. Langer, *Nature Biotechnology*, 18, **2000**, p. 24
[56] J.H.H. Sang Myung Lee, Kyung Yl Kim, Young Joon Ahn and Jae Wook Lee, *Korea-Australia Rheology Journal*, 18, **2006**, p. 83
[57] H. Tai, C.E. Upton, L.J. White, R. Pini, G. Storti, M. Mazzotti, K.M. Shakesheff, S.M. Howdle, *Polymer*, 51, **2010**, p. 1425
[58] E.K. Sang-Do Yeo, *Journal of Supercritical Fluids*, 15, **1999**, p. 261
[59] E.K. Sang-Do Yeo, *Journal of Applied Polymer Science*, 75, **1999**, p. 306
[60] M.F. Koenig, S.J. Huang, *Polymer*, 36, **1995**, p. 1877
[61] S. Mecham, A. Sentman, M. Sambasivam, *Journal of Applied Polymer Science*, 116, **2010**, p. 3265
[62] S. Ebnesajjad, *Plastic Films in Food Packaging: Materials, Technology and Applications*, Elsevier Science, **2012**
[63] S. Alix, A. Mahieu, C. Terrie, J. Soulestin, E. Gerault, M.G.J. Feuilloley, R. Gattin, V. Edon, T. Ait-Younes, N. Leblanc, *European Polymer Journal*, 49, **2013**, p. 1234
[64] S. Ruengdechawiwat, R. Molloy, J. Siripitayananon, R. Somsunan, P.D. Topham, B.J. Tighe, *Macromolecular Symposia*, 354, **2015**, p. 347
[65] S. Ruengdechawiwat, J. Siripitayananon, R. Molloy, R. Somsunan, P.D. Topham, B.J. Tighe, *International Journal of Polymeric Materials and Polymeric Biomaterials*, 65, **2016**, p. 277
[66] M.A. Woodruff, D.W. Hutmacher, *Progress in Polymer Science*, 35, **2010**, p. 1217
[67] P. Dubois, O. Coulembier, J.M. Raquez, *Handbook of Ring-Opening Polymerization*, Wiley, **2009**
[68] J.C. Gary Leeke, Mike Jenkins, *Journal of Chemical & Engineering Data*, 51, **2006**, p. 1877
[69] C.A. Kelly, K.L. Harrison, G.A. Leeke, M.J. Jenkins, *Polymer Journal*, 45, **2013**, p. 188
[70] Z. Lian, S.A. Epstein, C.W. Blenk, A.D. Shine, *The Journal of Supercritical Fluids*, 39, **2006**, p. 107
[71] Z. Lian, A.D. Shine, *Polymeric Materials: Science & Engineering*, 93, **2005**, p. 890
[72] S. Murphy, *MRes Thesis*, School of Engineering, Department of Metallurgy and Materials, University of Birmingham, **2011**
[73] M.G. Pastore Carbone, E. Di Maio, G. Scherillo, G. Mensitieri, S. Iannace, *The Journal of Supercritical Fluids*, 67, **2012**, p. 131
[74] M.G. Pastore Carbone, E. Di Maio, P. Musto, A. Braeuer, G. Mensitieri, *Polymer*, 56, **2015**, p. 252
[75] E. Di Maio, S. Iannace, G. Mensitieri, L. Nicolais, *Journal of Polymer Science Part B: Polymer Physics*, 44, **2006**, p. 1863
[76] T.G. Mezger, *The Rheology Handbook: For Users of Rotational and Oscillatory Rheometers*, Vincentz Network, **2014**
[77] P. Licence, M.P. Dellar, R.G.M. Wilson, P.A. Fields, D. Litchfield, H.M. Woods, M. Poliakoff, S.M. Howdle, *Review of Scientific Instruments*, 75, **2004**, p. 3233

[78] V. Crescenzi, G. Manzini, G. Calzolari, C. Borri, *European Polymer Journal*, 8, **1972**, p. 449
[79] F.B. Khambatta, F. Warner, T. Russell, R.S. Stein, *Journal of Polymer Science: Polymer Physics Edition*, 14, **1976**, p. 1391
[80] J. Wang, M.K. Cheung, Y. Mi, *Polymer*, 43, **2002**, p. 1357
[81] H. Ikeda, Y. Ohguma, S. Nojima, *Polymer Journal*, 40, **2008**, p. 241
[82] K.P. Menard, *Dynamic mechanical analysis : a practical introduction / Kevin P. Menard*, CRC Press, **2008**
[83] Y.P. Handa, Z. Zhiyi;, W. Betty, *Macromolecules*, 30, **1997**, p. 8499
[84] G. Natta, I. Pasquon, A. Zambelli, G. Gatti, *Die Makromolekulare Chemie*, 70, **1964**, p. 191
[85] Y. Huang, X. Xu, X. Luo, D. Ma, *Chinese Journal of Polymer Science*, 20, **2002**, p. 45
[86] M.J. Jenkins, K.L. Harrison, *Polymers for Advanced Technologies*, 17, **2006**, p. 474
[87] G.M. Swallowe, *Mechanical properties and testing of polymers : an A-Z reference / edited by G.M. Swallowe*, Kluwer Academic, **1999**
[88] A. Izuka, H.H. Winter, T. Hashimoto, *Macromolecules*, 25, **1992**, p. 2422
[89] L.J. Gerhardt, A. Garg, C.W. Manke, E. Gulari, *Journal of Polymer Science Part B: Polymer Physics*, 36, **1998**, p. 1911
[90] R.B. Bird, R.C. Armstrong, O. Hassager, *Dynamics of polymeric liquids. Vol. 1, 2nd Ed. : Fluid mechanics*, **1987**
[91] B.J. Anderson, *PhD Thesis*, Department of Chemical and Biomolecular Engineering, University of Illinois at Urbana-Champaign, Urbana and Champaign, **2008**
[92] P.J. Carreau, *Transactions of the Society of Rheology*, 16, **1972**, p. 99
[93] R.H. Colby, L.J. Fetters, W.W. Graessley, *Macromolecules*, 20, **1987**, p. 2226
[94] J.J. Cooper-White, M.E. Mackay, *Journal of Polymer Science Part B: Polymer Physics*, 37, **1999**, p. 1803
[95] C. Abeykoon, A.L. Kelly, J. Vera-Sorroche, E.C. Brown, P.D. Coates, J. Deng, K. Li, E. Harkin-Jones, M. Price, *Applied Energy*, 135, **2014**, p. 560
[96] P. Mitchell, S.M. Engineers, *Tool and Manufacturing Engineers Handbook: Plastic part manufacturing*, Society of Manufacturing Engineers, **1996**
[97] S. Arrhenius, *Über die Dissociationswärme und den Einfluss der Temperatur auf den Dissociationsgrad der Elektrolyte*, Wilhelm Engelmann, **1889**
[98] S. Giap, *Journal of Physical Science*, 21, **2010**, p. 29
[99] C. Barus, *Proceedings of the American Academy of Arts and Sciences*, 27, **1891**, p. 13
[100] M. Doi, S.F. Edwards, *Journal of the Chemical Society, Faraday Transactions 2: Molecular and Chemical Physics*, 75, **1979**, p. 38
[101] Y. Wang, S.-Q. Wang, *Journal of Rheology*, 53, **2009**, p. 1389

4 Green process for green materials: viable low temperature lipase-catalysed synthesis of renewable telechelics in supercritical CO_2

Traditionally, synthetic polymers have been prepared using fossil-based raw materials [1]. In the last few decades, several factors - such as resource depletion, poor degradability, environmental accumulation and customer awareness - have moved the research trends towards the investigation of more sustainable and environmentally friendly alternatives to be exploited as polymer precursors [2-5].

At the same time, interest towards greener alternatives to traditional catalysts and more environmentally friendly reaction systems has increased steeply. In this context, enzymes - because of their selectivity, remarkably high catalytic efficiency and intrinsic environmental sustainability and non-toxicity - are considered to be strong and competitive alternatives to metal-based catalysts [6, 7]. Finally, greener polymerisations, carried out to minimise the use of solvents and at milder conditions, have been arousing much interest in modern polymer science [8-11].

This chapter focuses upon new systems that try to address all of these issues. In particular, can the combination of supercritical CO_2 ($scCO_2$) and a catalytic enzyme open the possibility for a green, solvent-free polycondensation route to bio-based functional materials? By exploiting the initial partial solubility of the polymer precursors in the supercritical medium and then the plasticising effects of CO_2 on the polymer, we will probe if the polycondensation of bio-based monomers could be carried out at a mild temperature without the need for monomer pre-modification (which is typically necessary to lower the melting point and/or afford solubility in organic solvents). This, together with that selectivity enzymes bring, could ensure minimal side reactions and introduce the possibility of inserting specific functionalities, which could useful for cross-linking, further functionalisation or chain extension reactions.

Moreover, the use of mild reaction conditions could afford the possibility of retaining the enzyme activity and, hence, of efficiently recycling the catalyst. Thus, imparting an added value to the process.

Therefore, this chapter explores the possibility of a novel low temperature enzymatic approach to synthesise telechelic renewable polyesters by exploiting the unique properties of $scCO_2$.

The functionalised polymer products will be characterised by ^{1}H-NMR, MALDI-TOF, GPC and DSC in order to carefully assess their properties and the efficiency of the synthetic route.

Moreover, enzyme recycling tests will be carried out to investigate the commercial sustainability of this process, and preliminary studies to test the utility of these new materials will be presented.

The results of this chapter have been published in the primary literature:

S. Curia, A.F. Barclay, S. Torron, M. Johansson and S.M Howdle, "Green process for green materials: viable low temperature lipase-catalysed synthesis of renewable telechelics in supercritical CO_2", *Philosophical Transactions of the Royal Society A: Mathematical, Physical and Engineering Sciences* (373), **2015**, 1-16

4.1 Introduction

4.1.1 Green functional polymers

The use of green monomers to replace non-renewable and fossil-based raw materials is an important research focus of modern polymer science, both in academia and industry [4, 12-14]. Biodegradable and renewable plastics are being developed to limit the use of plastics derived from petroleum that at the end of their life cycle are usually incinerated or disposed of in landfills, thus representing a potentially serious future environmental issue [15].

Applications of green plastics range from food packaging [16], medical and tissue engineering [17], through to fabrics and coatings [4], to name just a few. Recently, great importance has been given to low molecular weight (comprised between 1000 and 4000 g mol^{-1}) telechelic polyesters [18-21]. These are functional polymers that carry the same functional group at both ends [22] and are used as cross-linkers, chain extenders, and building blocks for macromolecular structures (*e.g.* star, hyperbranched or dendritic polymers) [23]. The possible applications range from surface modification [18, 19], to medical materials [24], block copolymer formation [25], cross-linked networks [20, 26] *etc*.

Telechelic polyesters are typically synthesised by polycondensations of diacids (or diesters) with diols, or by ring-opening polymerisation of lactone monomers.

To produce telechelic polyesters through polycondensation, acid or alcohol end-cappers can be used in the synthesis [27]. The synthesised polyester backbone will be structured as an alternating copolymer with the functional end-capper attached to both ends of the polymer chain (Figure 4.1).

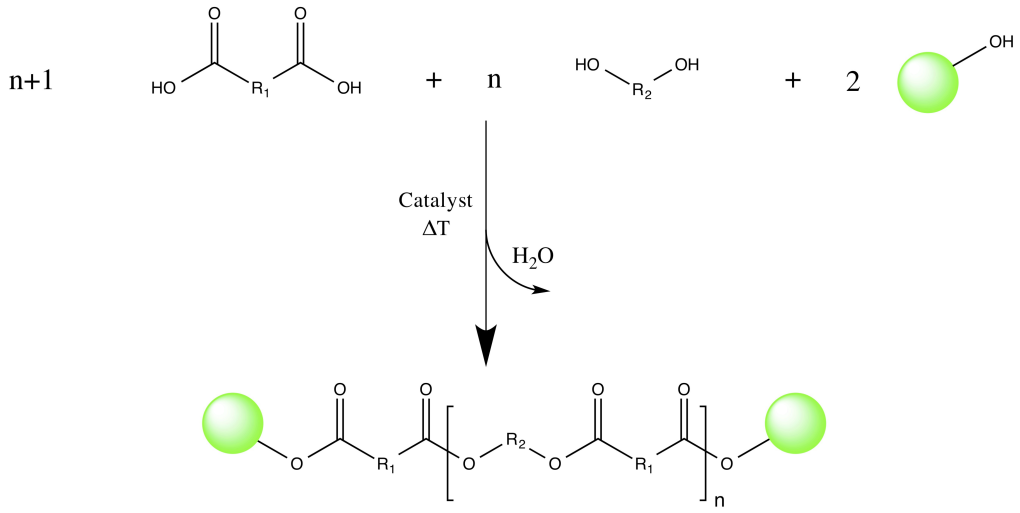


Figure 4.1 - Schematic representation of a generic polycondensation for the synthesis of a telechelic polyester with an alcohol end-capper; R_1 and R_2 can be aliphatic or aromatic. The green spheres represent the end-capper moiety.

The other possible route is the ring-opening polymerisation of lactones initiated with difunctional co-initiators [28]. In this way HO-polyester-OH chains can be prepared and the terminal alcohol groups can then be used to bind acid end-cappers. For clarity, a potential reaction scheme for the preparation of telechelic poly(ε-caprolactone) is shown (Figure 4.2).

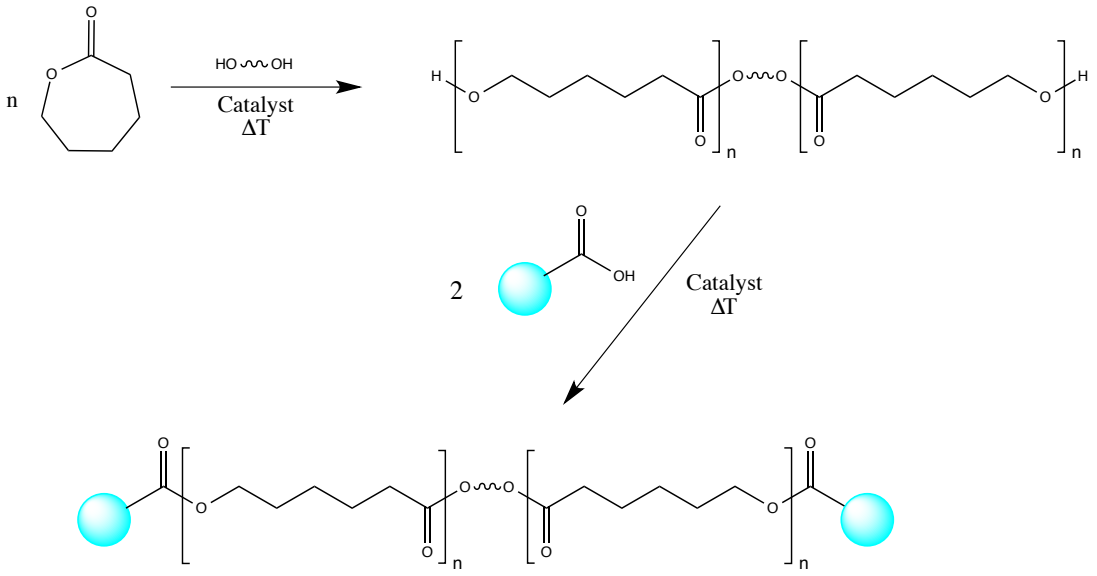


Figure 4.2 – Reaction scheme of the ring-opening polymerisation of ε-caprolactone with a generic diol and subsequent end-capping for the synthesis of telechelic poly(ε-caprolactone). The pale blue spheres represent the end-capper moiety.

Recently, the preparation of telechelics by self-polymerisation of naturally occurring ω-hydroxy-fatty acids has been described [20, 21, 29]. In this case, an additional diacid/diester must be used as a linker (or a diol, depending on the moiety of the end-capper available for condensation) (Figure 4.3).

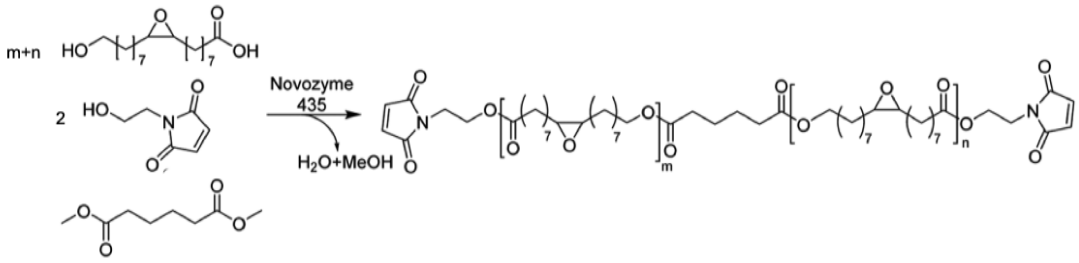


Figure 4.3 - Preparation of a telechelic polymer starting from a naturally occurring ω-hydroxy-fatty acid (figure adapted from reference [30]). The reaction is carried out at high temperature (85 °C) to melt the monomer. In this case, dimethyl adipate was used as a linker. If end-cappers with unsaturated moieties are used, the reaction must be carried out in toluene at a lower temperature (60 °C) in order to avoid premature radical cross-linking during the synthesis [20, 30].

Generally, low molecular weights are desirable in order to obtain low-viscosity materials and, hence, good filmability [18, 20, 21]. Furthermore, if a cross-linkable system is the desired product, low molecular weight between the reactive moieties is necessary in order to achieve a high cross-link density and therefore a tougher network [18, 20, 26].

4.1.2 Lipase-catalysed polymerisations

To achieve a fully green process, enzymes have been exploited as substitutes for metal-based catalysts that are potentially toxic [31-34], expensive, and require high temperatures (normally greater than 160 °C for polycondensations) to work effectively [35-39]. By employing enzymes, polymeric materials have been synthesised through ring-opening and condensation polymerisations [19, 40, 41]. Furthermore, the specificity of enzymes allows for preservation of particular functional groups, which can be exploited subsequently for further reaction

processing [34, 42]. For this reason, enzymes are important alternatives to metal catalysts for the synthesis of functional polymers.

As explained in Chapter 1, *Candida antarctica* Lipase B (CaLB) is the most studied enzyme used in polymer synthesis [34, 43, 44]. This lipase is responsible for the hydrolysis of fatty esters in nature, however in anhydrous conditions it can be active in the reverse reaction. Hence, by combining di-acyl donors (*e.g.* dicarboxylic acids or diesters) with di-nucleophiles (*e.g.* diols) in anhydrous media, polyesters can be produced enzymatically [34]. Moreover, CaLB can also catalyse the ring-opening polymerisation of cyclic esters [18, 26]. In order to increase the enzyme stability and optimise its characteristics in organic solvents, immobilisation on cross-linked synthetic supports is widely exploited [34]. This allows also for easier handling and separation of the enzyme from the final products: at the end of the reaction the products are dissolved in a solvent and the enzyme beads are separated by simple filtration [27].

Enzymatic polycondensations are normally carried out in the bulk or, when possible, in apolar solvents (*e.g.* toluene) [20, 34, 41]. Unfortunately, owing to the high melting point (>100 °C) of most naturally occurring diacids, the melt processes are limited since at temperatures higher than 100 °C the activity of CaLB is vastly reduced [11, 45]. Hence, high-temperature processes are not commercially sustainable in the long term due to the impossibility of retaining the initial enzyme activity and, thus, of recycling efficiently the expensive catalyst.

Moreover, most of the diacids are not usually soluble in apolar media, and polar solvents (*e.g.* methanol) cannot be used because they would prevent effective polycondensation (usually leading to diesters).

A common work-around is to introduce an extra step, to esterify the diacids and to work from the diesters, which are typically characterised by a lower melting point and increased solubility [19, 29, 43, 46]. Unfortunately, this is not always desirable and introducing extra steps can impact dramatically upon the viability of a commercial process.

In addition to this, one key drawback when synthesising functional telechelics is that higher temperatures can introduce side reactions of the terminal chemical groups; thus leading to undesired branching and cross-linking during the polymerisation [41, 47].

4.1.3 $ScCO_2$ as a polymerisation medium, azelaic acid and 1,6-hexanediol as building blocks: aims of the study

High-pressure CO_2 is a good solvent for many small molecules and it is very effective at plasticising and effectively liquefying many polymers at temperatures below their glass transition temperature (T_g) and melting point (T_m) [48-59], therefore opening up new opportunities for polymer synthesis and modification. As shown in the previous chapter, the effects of CO_2 are significant also on semicrystalline polyesters, with both the viscosity and the T_m being significantly reduced under pressure.

Different types of polymers have been synthesised in CO_2: for instance, radical controlled polymerisations of vinyl monomers [60] and tin-catalysed ring-opening polymerisations of lactones [61, 62] have been successfully conducted.

Furthermore, immobilised CaLB has been shown to be stable and to retain its catalytic activity under pressurised CO_2 and, hence, it has been used for ring-opening polymerisations [40] and for the production of biodiesel [63] in $scCO_2$.

This chapter describes the attempt to extend this methodology and test whether polycondensation syntheses normally carried out at high temperature can be carried out in CO_2 at milder conditions using CaLB as a catalyst. Hence, the lipase-catalysed synthesis of novel green telechelics based on azelaic acid and 1,6-hexanediol in $scCO_2$ will be investigated.

Azelaic acid is a naturally occurring saturated dicarboxylic acid with T_m ~110 °C (Figure 4.4), slightly soluble in $scCO_2$ [64], which is found in wheat, rye and barley [65]. It can also be produced in significant quantity through ozonolysis of oleic acid [1, 64]. In addition to this, azelaic acid is commonly used in cream formulations for its body-compatibility, and anti-septic/antibacterial properties: hence, it can be an interesting building block to exploit for polymer synthesis. However, this diacid is not soluble in apolar solvents and the only polymerisations shown in the literature were performed in the bulk with the aid of metal catalysts at temperatures as high as 230 °C [66, 67], which are required to melt the diacid and activate the catalyst.

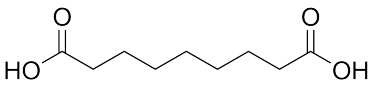


Figure 4.4 – Azelaic acid is a saturated diacid with T_m ~110 °C naturally occurring in wheat, rye and barley.

The co-monomer chosen for the production of polyesters is 1,6-hexanediol. This monomer is a polar diol that can be synthesised from renewable resources [11, 68-70]. Therefore, a final polymer containing azelaic acid and 1,6-hexanediol will have a fully bio-based backbone.

These two monomers are not plasticised by the $scCO_2$. Nonetheless, it has been reported that azelaic acid displays a small degree of solubility in this supercritical medium [64]. To the best of the author's knowledge, the solubility of 1,6-hexanediol in pressurised CO_2 has never been investigated. On the contrary, the solubility of its isomer 1,2-hexanediol and of 1-hexanol have both been described [71]. Furthermore, the acid-catalysed etherification of 1,6-hexanediol with methanol in pressurised CO_2 has been carried out; however, this process was performed at a rather high temperature (*i.e.* 150 °C) [72].

Taking all this into account, this chapter seeks to test the hypothesis that if the monomer 1,6-hexanediol does indeed have some solubility in $scCO_2$, it could react in solution with azelaic acid. Under these conditions dimers and low molecular weight oligomers would be formed that would likely be insoluble in CO_2, but highly plasticised (as shown for poly(ε-caprolactone) in the previous chapter) after precipitating out from the supercritical phase. This plasticised-molten phase would provide an ideal environment for further polymerisation/end-capping and the reaction could then proceed in a melt system with the $scCO_2$ acting as a plasticiser that reduces significantly the viscosity. Therefore, the approach is to use $scCO_2$ as the reaction medium for the production of a variety of telechelic polyesters based on azelaic acid, to demonstrate that it is possible to exploit a low temperature enzymatic route to synthesise functional poly(hexylene azelate)s (PHAzs) without pre-modification of the monomer and in a solvent-free system.

For the purpose of producing polymers with tailored functionalities, it is important to carry out selective polymerisation, hence a low temperature will be of great significance. This is particularly important for all those applications where thermally

labile chemical groups (*e.g.* unsaturated ones) or bioactive molecules must be incorporated into the polymer.

The reactions were carried out in CO_2 (275 bar) at 35 °C targeting the molecular weight of the chains by using functional end-cappers. Namely, sorbic alcohol (SA), 12-hydroxy stearic acid (HSA), 2-hydroxyethyl methacrylate (HEMA) and trimethylolpropane oxetane (TMPO) were used (Figure 4.5).

These molecules contain one moiety able to undergo condensation and another one useful for further reaction (*e.g.* cross-linking or chain extension). In more detail, SA is a diene that can undergo Diels-Alder addition, thiol-ene click chemistry and radical reactions, HSA contains a secondary hydroxyl group that can be cross-linked with isocyanates, HEMA is characterised by a double bond that can be radically reacted, finally TMPO is an oxetane derivative that can be ring-opened by using a Lewis acid.

Furthermore, SA is a naturally occurring molecule and HSA is produced through hydrogenation of castor oil; hence, the bio-content of the polymers obtained with these two functionalisers is 100%.

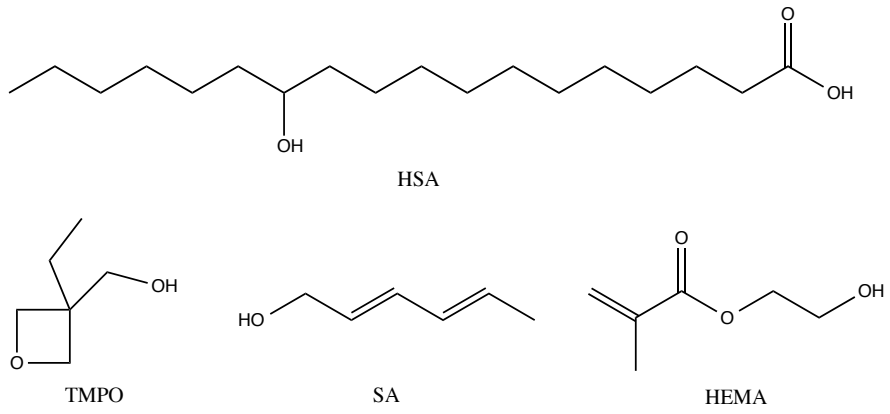


Figure 4.5 - The functional end-cappers used in this study: sorbic alcohol (SA), 12-hydroxy stearic acid (HSA), 2-hydroxyethyl methacrylate (HEMA) and trimethylolpropane oxetane (TMPO).

Combined use of CaLB, $scCO_2$ and consequent mild temperature, should ensure minimal side reactions, thus preserving the functionality of the end-cappers. Furthermore, another aim is to show that the enzyme can be re-used without loss of activity.

Therefore, the objective of this chapter is to demonstrate that by using $scCO_2$ it is possible to prepare a range of green functional materials with targeted degree of polymerisation (DP) through enzymatic syntheses at near-room-temperature conditions and without pre-modification of the monomers. This route could be particularly valuable for applications where the incorporation of thermally labile functional groups or additives (*e.g.* proteins, drugs, hormones *etc.*) is desired.

4.2 Experimental

4.2.1 Materials

Azelaic acid (98%) was purchased from Alfa Aesar (UK) and dried for 24 h under vacuum (100 mbar) at 50 °C before use. 1,6-hexanediol (98%) and HSA (99%) were purchased from Sigma Aldrich (UK) and dried for 24 h under vacuum (100 mbar) at room temperature (RT) before use. SA (>97%), TMPO (96%) and HEMA (97%) were purchased from Sigma Aldrich (UK) stored at -50 °C and used as received. Novozym 435 (CaLB immobilised on cross-linked acrylic resin beads) was kindly donated by Novozymes (Denmark) stored at 4 °C and dried for 24 h under vacuum (100 mbar) at RT before use. All the solvents were of analytical grade, or Chromasolv® were specified, purchased from Sigma Aldrich (UK) and used as received. Supercritical Fluid Chromatography (SFC) grade 4.0 CO_2 (minimum purity 99.99%) was purchased from BOC Special Gases (UK) and used as received. Photo-initiators Uva-Cure 1600 and Irgacure 651 were supplied by CYTEC and BASF, respectively, stored in the dark at RT and used as received.

4.2.2 Methods

4.2.2.1 Enzymatic synthesis of telechelic poly(hexylene azelate) (PHAz)

In a typical procedure the diacid (10.20 mmol), diol (DP6: 8.73 mmol; DP3: 7.65 mmol) and one end-capper chosen from SA, HEMA and TMPO (DP6: 2.91 mmol; DP3: 5.10 mmol) were added to the stainless steel reaction autoclave (60 mL) [60, 73], along with enzyme and fresh molecular sieves (3 Å, particle size 1.6-2.5 nm) (25% by weight of each relative to the total amount of monomers and end-cappers). The vessel was then sealed and pressurised up to 50 bar. Then, the temperature was raised to 35 °C, the pressure stabilised at 275 bar and the reaction left to run for 24 h while stirring at 100 rpm. To avoid polymer foaming and consequent tubing

blockages [40], the reactions were stopped by cooling the vessel in a water/ice bath (0 °C) and the CO_2 was vented when the pressure fell below 20 bar. Finally, the product was dissolved in 6 mL of toluene (gently heated at 40 °C, to melt the diol and retain information on conversion) and filtered to remove the enzyme and molecular sieves. Filtered solutions were dried at 40 °C under reduced pressure leaving solid polymeric products. Product yield was calculated by dividing the dry product mass by the theoretical mass. The enzyme beads were manually separated from the sieves and collected to recycle them and then to determine the residual activity.

When using HSA as an end-capper, an excess of diol was used in order to obtain OH-end-functional chains able to react with the hydroxy fatty acid. Accordingly, 10.20 mmol of diol and 8.73 mmol (DP6) or 7.65 mmol (DP3) of diacid were used. The reaction conditions and purification procedure were as described above.

The reactions were performed at least twice to check reproducibility. The nomenclature used in this chapter is detailed in Table 4.1.

Table 4.1 - Naming scheme of the telechelic poly(hexylene azelate)s (PHAzs) presented in this chapter.

Name	DP	Functionaliser
PHAz-SA3	3	Sorbic alcohol (SA)
PHAz-SA6	6	
PHAz-HSA3	3	12-hydroxy stearic acid (HSA)
PHAz-HSA6	6	
PHAz-TMPO3	3	Trimethylolpropane oxetane (TMPO)
PHAz-TMPO6	6	
PHAz-HEMA3	3	2-hydroxyethyl methacrylate (HEMA)
PHAz-HEMA6	6	

The reaction schemes are shown in Figure 4.6.

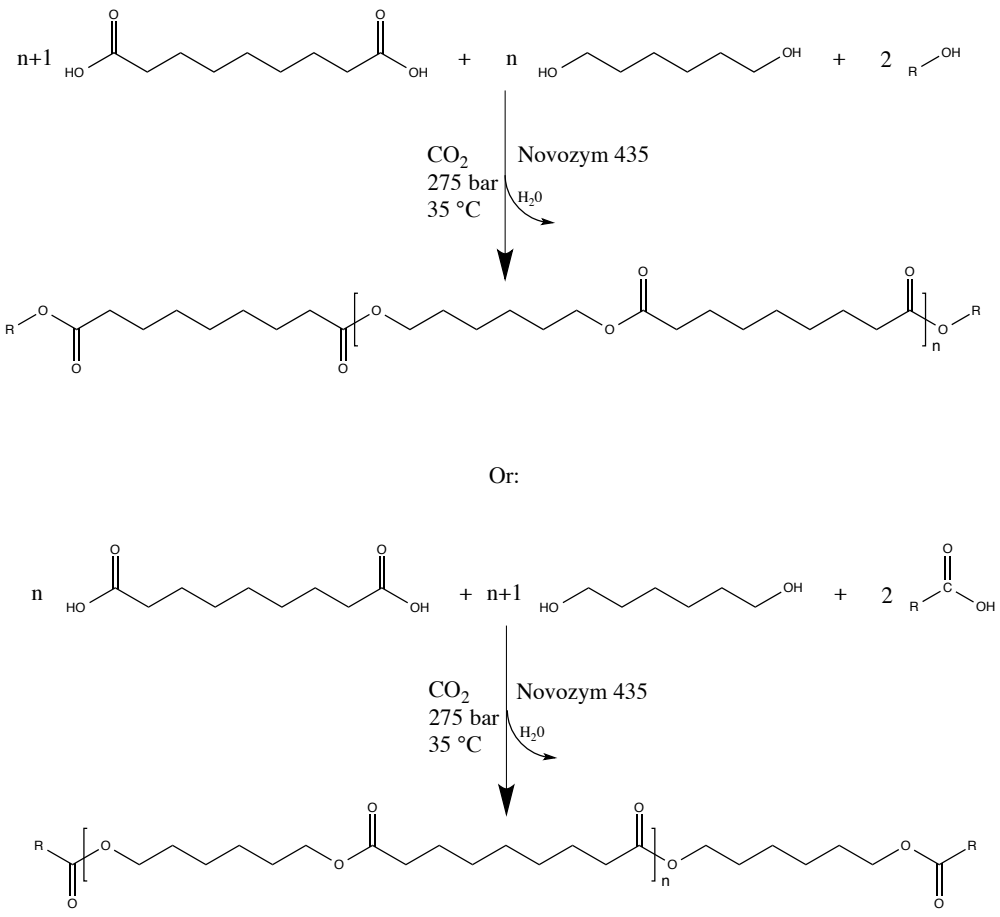


Figure 4.6 – Reaction schemes for the enzymatic syntheses of the green telechelics in scCO$_2$. An excess of diacid was used for alcohol end-cappers (SA, HEMA and TMPO), whilst an excess of diol was required in the case of the acid end-capper (HSA) (n=3 or 6). R-OH and R-COOH represent the end-cappers.

4.2.2.2 Cross-linking procedure

The telechelics functionalised with SA, HEMA and TMPO were cross-linked by selective reaction of the end-groups present in the polymers (using Irgacure 651 for radical cross-linking and Uva-Cure 1600 for cationic cross-linking). Typically, tin foil-covered vials were charged with 25 mg of polymer, 1 mg of initiator (4% by weight) and 100 mg of chloroform. After homogenisation of the mixture, the sample was cast onto a microscope glass slide and the solvent was left to evaporate before proceeding with the curing process. When the solvent was fully evaporated a second glass slide was put on the sample and cross-linking was performed by irradiation with a Black Ray B-100AP Hg ultraviolet (UV) lamp (100 W, λ = 365 nm, irradiance 21 mW cm^{-2}) for 5 minutes.

4.2.2.3 ^{1}H and ^{13}C-NMR analysis.

NMR analyses were conducted on a Bruker DPX300 spectrometer in $CDCl_3$ (concentration: 20 mg mL^{-1}). The number of scans was 16 for ^{1}H (300 MHz) and 4096 for ^{13}C (75 MHz). Conversion and chain length were analysed through monomer peak and end-group analysis respectively.

The intensities of the peaks assigned to the PHAz backbone were normalised with respect to the number of protons of the end-capper.

For increased clarity, the spectrum and the structure with labels for PHA-TMPO6 are shown (Figure 4.7).

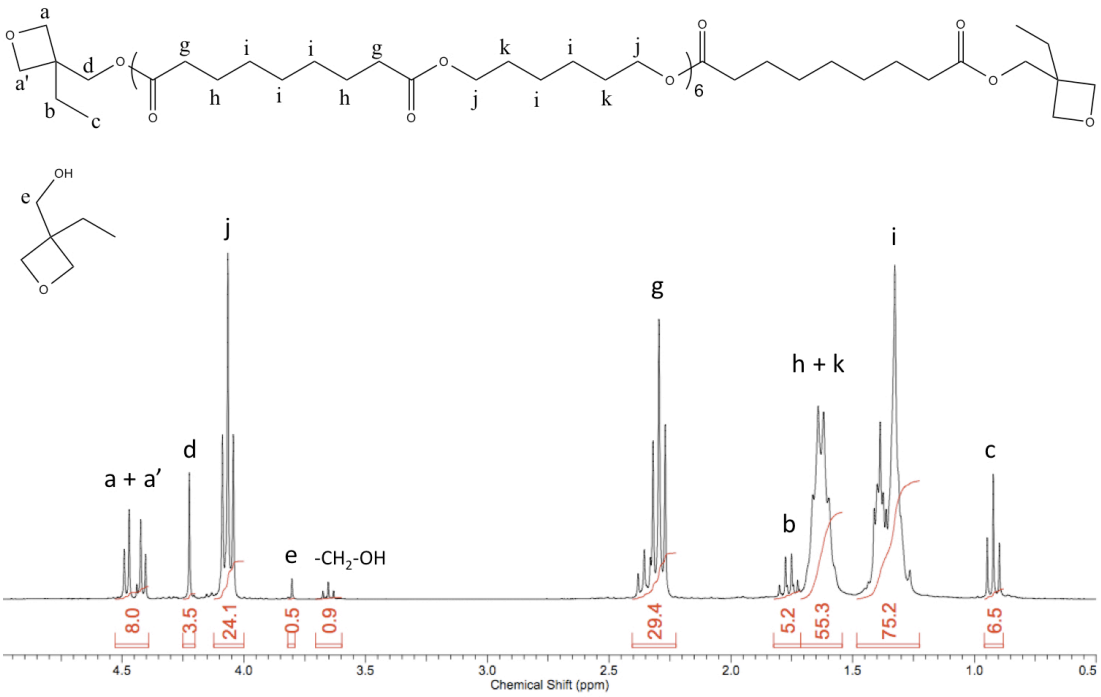


Figure 4.7 - ^{1}H-NMR of PHAz-TMPO6: the end-capper peaks are observed at around 4.50 ppm (a and a'), 1.75 ppm (b), 0.95 ppm (c) and 4.25 ppm (d), a peak assigned to unreacted TMPO (<13%) is observed at 3.81 ppm (e). The triplet around 3.65 ppm is assigned to –C$\underline{H_2}$-OH protons in 1,6-hexanediol and was used to estimate monomer conversion.

Equation (4.1) was used for the determination of the average M_n of the polymer chains functionalised with SA, TMPO and HEMA:

$$M_n^{NMR} = \frac{\left(\frac{I_i - 6}{10} + \frac{I_{h+k} - 4}{8} + \frac{I_g - 4}{4} + \frac{I_j}{4}\right)}{4} \times 270.4 + 154.2 + 2(MW_{EC}) \qquad (4.1)$$

Where I_x are the integrals of the peaks with the relative label (x=*i, h+k, g,* or *j*) and MW_{EC} is the molecular weight of the end-capper. The numbers subtracted from I_i, I_{h+k} and I_g take in account the azelaic acid unit which is not part of the repeating unit but gives a contribution to these peaks (this segment is accounted for through the additional "154.2" term in Equation (4.1)).

In the case of PHAz-HSA the equation is slightly different to take into account the different structure (additional 1,6-hexanediol unit instead of azelaic acid) and the protons of the end-capper which contribute to the integral of peaks *i*, *g* and *h*, Equation (4.2):

$$M_n^{NMR} = \frac{\left(\frac{I_i - 56}{10} + \frac{I_{h+k} - 8}{8} + \frac{I_g - 4}{4} + \frac{I_j - 4}{4}\right)}{4} \times 270.4 + 116.2 + 2(MW_{HSA}) \qquad (4.2)$$

Here again, I_x are the integrals of the peaks with the relative label (x = *i, h+k, g,* or *j*) and MW_{HSA} is the molecular weight of HSA. The values subtracted from I_g and I_j take into account the 1,6-hexanediol unit which is not part of the repeating unit but does give a contribute to these peaks (this segment accounted for through the additional term "116.2" in equation (2)). The value 56 is subtracted to I_i in order to take into account the protons of HSA (26×2 protons) and the protons of 1,6-hexanediol (4 protons), which contribute to the integral of this broad peak. Finally, the value 8 is subtracted from I_{h+k} in order to take into account the protons of HSA (2×2 protons) and those of 1,6-hexanediol (4 protons).

The spectrum of PHA-HSA6 is shown for added clarity (Figure 4.8).

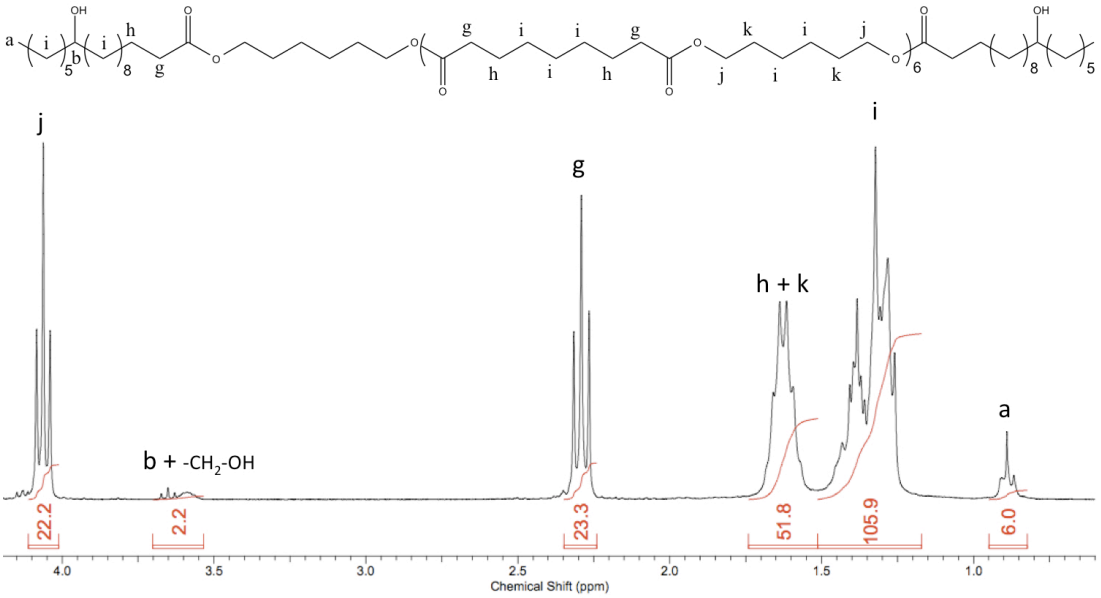


Figure 4.8 - ^{1}H-NMR of PHAz-HSA6: the end-capper peaks are observed at 0.90 ppm (a), 3.60 ppm (b) and in the broad peak at 1.45 ppm (i). An additional small triplet that is assigned to protons adjacent to an alcohol group (either in the 1,6-hexanediol monomer or in uncapped chains) is observed at 3.65 ppm. This peak was used to estimate the approximate conversion and extent of functionalisation.

The chemical shifts are reported in parts per million (ppm) with respect to residual solvent peaks (7.26 ppm for ^{1}H and 77.36 ppm for ^{13}C) [74].

4.2.2.4 Gel permeation chromatography (GPC)

The molecular weights of the samples were analysed using a Polymer Laboratories GPC 50 with a refractive index detector and calibrated with poly(styrene) standards in the range of 100 g mol^{-1} – 500 kg mol^{-1}. The machine was equipped with a PL PLgel guard (8 µm) column followed by two PL PLgel Mixed-D (8 µm) columns. The samples were run in $CHCl_3$ Chromasolv® (5 mg mL^{-1}) at a flow rate of 1 mL min^{-1}. Cirrus software was used for analysis.

4.2.2.5 Differential scanning calorimetry (DSC)

DSC analyses were performed using a TA-Q2000 DSC (TA Instruments, USA) calibrated with sapphire and indium standards. In a standard experiment, the sample

(2.00 ± 0.10 mg) was melted with a first heating scan up to 100 °C (10 °C min^{-1}) and cooled down to -90 °C (10 °C min^{-1}). A second heating scan up to 100 °C, with the same heating rate, was then carried out to detect the melting point. Isothermal 5-minute segments were performed at the conclusion of each ramp. The experiments were carried out under a N_2 flow (50 mL min^{-1}).
The T_m was taken as the maximum of the endothermic peak. Each experiment was repeated three times and the results are shown as the average ± 1 standard deviation.

4.2.2.6 Matrix-assisted laser desorption/ionisation-Time of flight mass spectrometry (MALDI-TOF)

MALDI-TOF analyses were performed using a Bruker UltraFlex III. DCTB (*trans*-2-[3-(4-*tert*-butylphenyl)-2-methyl-2-propenylidene]malononitrile) was used as a matrix with Na^+ and K^+ as cations. The analyses were performed in reflection mode. For the sample preparation, 20 μL of a solution of polymer in $CHCl_3$ (10 mg mL^{-1}) were mixed with 20 μL of a DCTB solution in acetonitrile (10 mg mL^{-1}) and 0.5 μL of sodium and potassium trifluoroacetate in acetonitrile (5 mg mL^{-1}); 1 μL of this mixture was spotted on the target plate and left to dry at room temperature.

4.2.2.7 Real time Fourier Transform Infrared (FTIR)

Real time FTIR analyses were carried out using a Perkin Elmer Spectrum 2000 FTIR instrument equipped with a Specac Golden Gate attenuated total reflection (ATR) unit and a Hamamatsu L5662 (Hg-Xe) UV light source (λ = 365 nm, irradiance 6 mW cm^{-2}) provided with optical fibres to direct the radiation towards the sample. In a typical analysis, the sample (25 mg polymer, 1 mg photo-initiator in 100 mg of $CHCl_3$) was left to dry on the ATR crystal and then covered with a glass slide. The spectrum was collected from 600 to 4000 cm^{-1} (16 scans) and the acquisition was stopped when no changes in the peaks could be detected anymore. The setup (schematic+photograph) is shown in Figure 4.9.

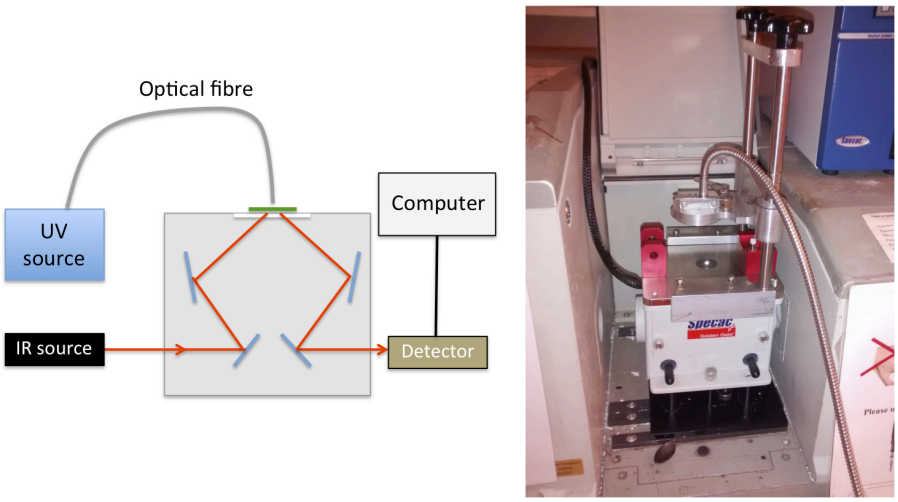


Figure 4.9 – Real time FTIR setup for photo-initiated cross-linking of the telechelics. Scheme (left) and picture (right) of the equipment are shown.

4.2.2.8 Melt (high-temperature) synthesis

For comparisons, the polymerisations were carried out also in the melt targeting DP3 using the same amount of monomers and end-cappers as before: 3.4 mmol of azelaic acid, 2.55 mmol of 1,6-hexanediol, 1.7 mmol of functionaliser (SA, TMPO and HEMA) and 25% by weight of Novozym 435 and molecular sieves (4Å). In the case of HSA 3.4 mmol of diol, 2.55 mmol of diacid and 1.7 mmol of HSA were used. The oil bath temperature was set to 115 °C in order to achieve 110 °C in the centre of the 20 mL round bottom flask (checked with an internal thermocouple) and the reaction was left to run for 24 hours. The product was dissolved in 2 mL of toluene to remove the enzyme and sieves (therefore collecting only the soluble fraction of the product). The enzyme beads were manually separated from the sieves and the insoluble fraction of the product in order to test their residual activity.

4.2.2.9 Enzyme recycling test

The activity of fresh enzyme was compared with the activity of the enzyme that had been used for up to five reactions in $scCO_2$ and for one reaction at 110 °C, by carrying out the esterification of 0.71 mmol of oleic acid (200.00 mg) with an equimolar amount of 1-propanol (42.67 mg) to form propyl oleate (Figure 4.10). The

reaction was performed at 50 °C in toluene (300 μL) with 25% wt of enzyme loading while stirring at 300 rpm.

The conversion of the reaction was monitored through ^{1}H-NMR analysis by comparing the peak at 3.65 ppm (a) and the peak at 4.10 ppm (b). Samples were taken after 1, 3, 5 and 24 hours.

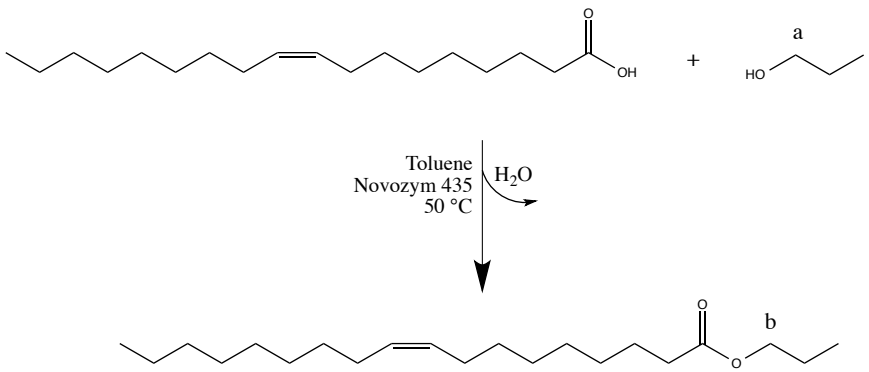


Figure 4.10 - Synthesis of propyl oleate. This reaction was used to monitor the enzyme activity after the high- pressure polycondensations. The reaction was monitored through ^{1}H-NMR by comparing the 1-propanol peak (a) at 3.65 ppm and the propyl oleate peak (b) at 4.05 ppm.

4.3 Results

4.3.1 Low temperature enzymatic route to telechelic PHAz in $scCO_2$

Two commercially available bio-based monomers have been exploited as building blocks for the backbone of the telechelics: azelaic acid and 1,6-hexanediol. As previously stated, these two monomers are not plasticised by the $scCO_2$; however, azelaic acid does display a small degree of solubility (~10^{-5} mole fraction) [64]. On the other hand, to the best of the author's knowledge the solubility of 1,6-hexanediol in CO_2 has not been investigated; whilst its isomer 1,2-hexanediol does show some solubility in CO_2 (~10^{-5} mole fraction) [71].
View cell investigations were carried out to observe if any clear hints of solubility could be observed (Figure 4.11).

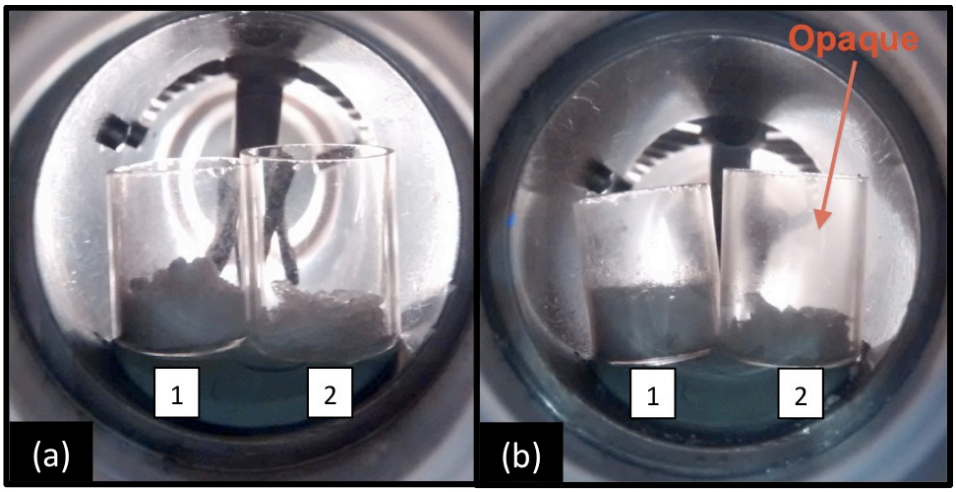


Figure 4.11 - Visual inspection of (1) azelaic acid and (2) 1,6-hexanediol: (a) in CO_2 (35 °C, 275 bar) and (b) upon removal of the supercritical fluid (after 7 hours under pressure). A quasi-foamed structure is observed for azelaic acid and possible monomer residues are seen on the surface of the vials and on the sapphire window. Although the mechanical stirrer is visible, the content of the autoclave was not stirred during the experiments.

This study was performed at 35 °C, since this temperature is just above the critical point for CO_2 and the reported solubility for azelaic acid is in this range of temperature [64]. The observations confirmed that the two monomers are not liquefied under these conditions (35 °C, 275 bar).

Unfortunately our system did not allow for quantitative solubility tests, nonetheless it did show a clear interaction between the CO_2 and azelaic acid, since a quasi-foamed structure was obtained upon venting of the autoclave. Furthermore, the opaqueness of the glass vials and sapphire windows upon venting might be attributed to azelaic acid and 1,6-hexanediol solubilised in the CO_2 and deposited there after depressurisation of the view cell.

The starting hypothesis is that, if 1,6-hexanediol is characterised indeed by a degree of solubility in $scCO_2$, the initial solubility of the two monomers in supercritical medium would allow for some dimers and trimers to form. These would then precipitate out from the supercritical phase and be plasticised by the $scCO_2$: thus, being a melt and a co-solvent for the remaining monomers and end-capper.

Preliminary polymerisation studies carried out in $scCO_2$ (35 °C, 275 bar) by synthesising non-end-capped chains (not shown) demonstrated that 24-hour reactions afforded the desired products, whilst shorter times were not sufficient to obtain the targeted structures [75]. As expected, reactions performed at the same temperature in the absence of CO_2 did not afford any polymer products. Hence, the presence of $scCO_2$ plays a crucial role in this process.

Accordingly, the reactions described in this chapter were carried out at 35 °C in CO_2 (275 bar) targeting specific degree of polymerisations (*i.e.* DP3 and DP6) by carefully controlling the monomer and end-capper feed ratios. Once the autoclave was vented, solid white homogeneous products were collected. This immediately demonstrated a successful polymerisation, since the starting monomers are powders characterised by very different appearances. After separation of the enzyme/molecular sieves and drying, light yellow/white solid polymers were obtained. As a visual example, the PHAzs with DP equal to 3 are shown (Figure 4.12).

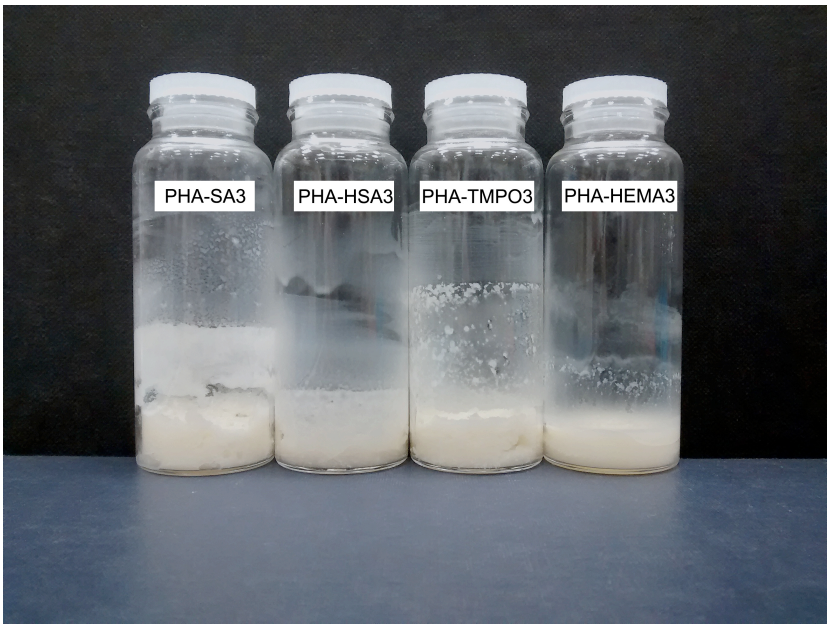


Figure 4.12 – Functional PHAzs (DP3) synthesised in this study. Light yellow/white solid materials were obtained. The polymers with DP6 showed similar appearance (not shown).

All the reactions provided products in good yields and almost quantitative conversions (Table 4.2).

Table 4.2 – Novozym 435-catalysed functional PHAzs synthesised in $scCO_2$. Molecular weight from ^{1}H-NMR and GPC, thermal properties and extent of functionalisation and conversion for each polymer are reported.

Product	M_n^{th} (g mol^{-1})[a]	M_n^{NMR} (g mol^{-1})[b]	M_n^{GPC} (g mol^{-1})[c]	$Đ^c$	T_m (°C)	ΔH_f (J g^{-1})	Yield (%)[d]	Di-end-functional (%)[e]	Conversion (%)[f]
PHAz-SA3	1160	1500	2400	1.96	38.6 ± 0.9	65.5 ± 1.0	86	94	>98
PHAz-SA6	1971	3000	3700	2.02	45.7 ± 0.2	88.8 ± 1.8	79	86	>99
PHAz-HSA3	1493	1400	2400	1.83	46.0 ± 0.2	81.2 ± 3.5	88	>95	>99
PHAz-HSA6	2303	2200	3200	2.19	47.4 ± 0.5	86.9 ± 2.7	80	>95	>99
PHAz-TMPO3	1196	1100	1500	1.73	29.1 ± 0.2	50.4 ± 0.8	87	88	>96
PHAz-TMPO6	2007	2100	2200	2.36	38.4 ± 0.4	67.9 ± 0.5	84	88	>96
PHAz-HEMA3	1230	1500	1700	2.18	31.0 ± 0.4	48.4 ± 0.5	78	96	>98
PHAz-HEMA6	2040	2200	2200	2.32	36.5 ± 0.5	66.3 ± 0.6	88	90	>96

[a]Calculated according to the reagents ratios; [b]Determined through ^{1}H-NMR from the integrals of the peaks of the polymer backbone and the end-group peak; [c]Against poly(styrene) in $CHCl_3$; [d]Yield= weight of collected product/theoretical weight×100; [e]Determined through ^{1}H-NMR from the peaks of the end-cappers linked to the polymeric chains and/or the peak assigned to non-end-capped chains; [f]Determined through ^{1}H-NMR from the ratio of the 1,6-hexanediol peak at 3.65 ppm and the polyester peak at 4.10 ppm.

The conversion of each reaction was analysed by monitoring the peaks relative to 1,6-hexanediol in its monomeric form (protons adjacent to the alcohol group) and when incorporated into the polymer backbone (protons adjacent to the ester group). All the reactions showed high conversion (≥96%) but it is worth pointing out that any polymers terminating with an alcohol group do also give a peak at 3.65 ppm and this does lead to a small underestimation of the conversion. MALDI-TOF data do show that there is a component of AB-type polymer that is alcohol terminated in PHAz-TMPO (see Figure 4.25).

4.3.2 Thermal properties

DSC analyses allowed for the determination of the thermal properties of the telechelics. The T_m and the enthalpy of fusion (ΔH_f) of the products with DP3 can be seen to change significantly when varying the end-capper (Figure 4.13).

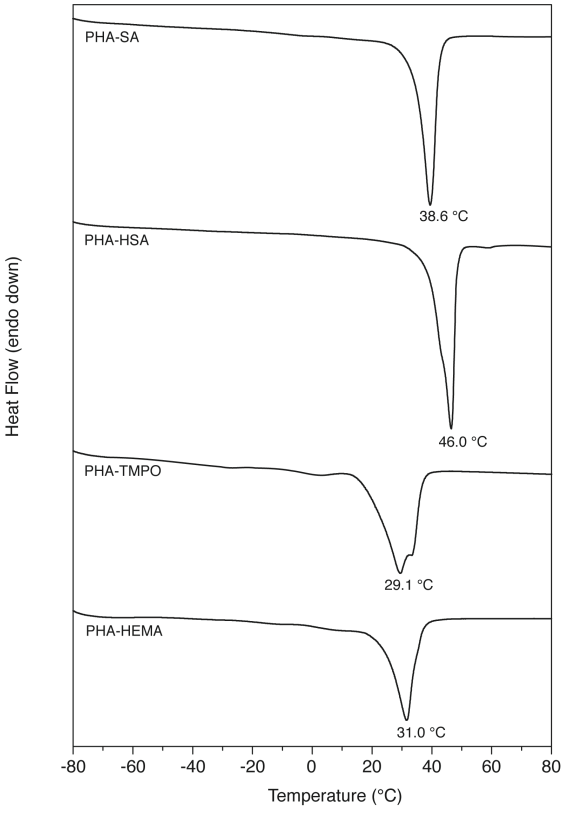


Figure 4.13 – DSC traces of PHAz (DP3) with different end-functionalisation. PHAz-HSA3 displays the highest T_m (46.0 °C), whilst PHAz-TMPO3 shows the lowest (29.1 °C).

It is well known that the thermal properties of low molecular weight polymers can be strongly influenced by the end-groups [76, 77]. Different end-groups can result in different crystallisation behaviour, therefore resulting in varied ΔH_f and T_m [78]. In more detail, the sharpest and largest endothermic peaks are shown by the HSA and SA functional PHAzs, whilst PHAz-TMPO3 and PHAz-HEMA3 exhibit the lowest T_m and ΔH_f. This is due to the bulkier structure of the latter end-cappers that results in a more significant alteration of the crystalline structure. A similar effect has been observed on phenoxyl and acetoxyl terminated low molecular weight poly(ethylene oxide) (1000-3000 g mol^{-1}**)** when compared to hydroxyl, methoxyl and ethoxyl terminated chains [79, 80].

In addition, PHAz-TMPO3 exhibits a bimodal melting endotherm. It is well known that in semicrystalline polyesters multiple endothermic peaks, or multimodal melting points, can be detected. This can arise from the melting of crystallites with different stability and size, or from reorganisation of the crystals [81].

Finally, it was not possible to clearly identify the T_g of the telechelics through DSC because of the low temperature operating capabilities of the apparatus. However, the T_g should be expected to be below -60 °C as has been observed by others for similar polyesters, such as poly(butylene azelate) [81].

Polymers with a longer PHAz backbone (DP6) displayed higher T_m and ΔH_f values (Figure 4.14) as expected result, and this can be attributed to larger crystallites that are formed when longer polymer chains pack. For instance, similar results were obtained on poly(ε-caprolactone) at low molecular weights by Huang *et al.*: in this case the T_m was found to increase significantly with the molar mass until about 9000 g mol^{-1}, after which it remained almost constant [82].

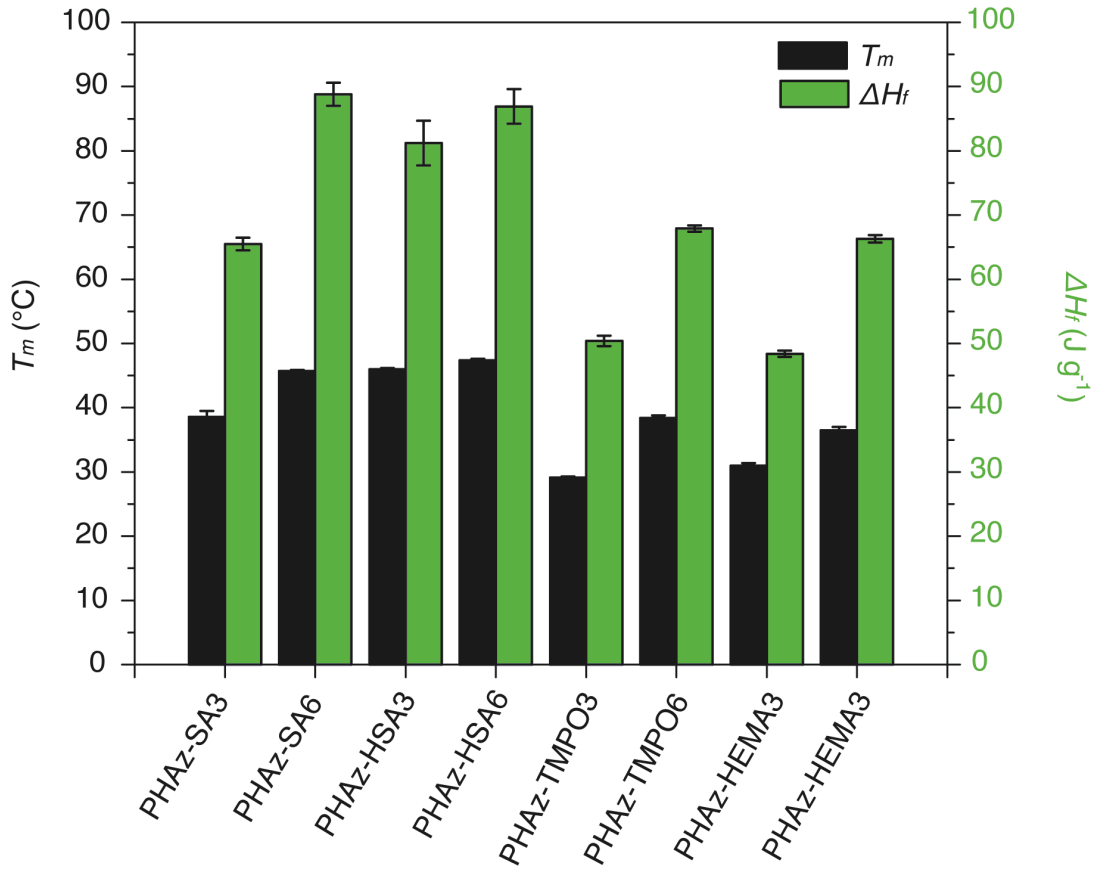


Figure 4.14 - T_m and ΔH_f values for PHAz with DP3 and DP6 and different end-functionalisation. Both of the quantities increased with the DP. The PHAz functionalised with SA and HSA were characterised by the highest T_m and ΔH_f.

4.3.3 Structural characterisation

4.3.3.1 NMR studies

Thorough ^{1}H-NMR investigations were performed to obtain information on chemical structure, molecular weight, functionalisation and monomer conversion. The M_n determined from ^{1}H-NMR (M_n^{NMR}) is in all the cases close to the theoretical value calculated from the diacid : diol : functionaliser ratios. Thus, this immediately demonstrates that the polymerisations yielded chains with DP within the desired range, suitable for coating applications and cross-linked networks [19, 20, 29]. The M_n calculation was performed by use of the integral values assigned to the peaks of

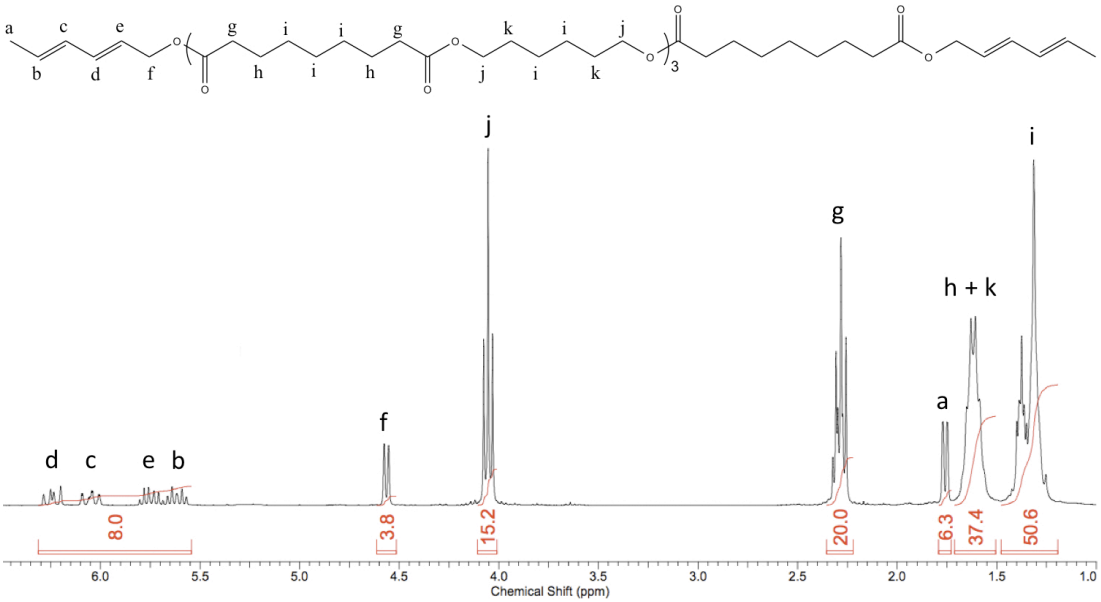
polymer backbone compared to those of end-group (using equation (4.1) and (4.2), as explained in the experimental section).

To confirm the results obtained from ^{1}H-NMR, GPC analyses were also used, and the numbers were always close to those calculated from ^{1}H-NMR (Table 4.2). However, there is clearly a slight overestimation in M_n^{GPC} for all the polymers. This is a consequence of the calibration performed with poly(styrene) (PSt) standards, which will always have hydrodynamic volumes different from the analysed polyesters. Similar differences have been encountered by other groups, when using GPC with PSt standards for polyester analysis [19, 21, 44]. Nevertheless, the agreement with ^{1}H-NMR is fairly good and the dispersity values are mostly around 2, which is a value typically expected for linear telechelics synthesised by polycondensations at high conversions and already found by other groups when synthesising low molecular weight telechelics [19, 26].

^{1}H-NMR (Figure 4.15-1,2 and Figure 4.17-1,2) and ^{13}C-NMR (Figure 4.19 to Figure 4.22) analyses for the polymer with DP6 also confirm the chemical structure and incorporation of intact end-groups. The ^{1}H-NMR spectra of the polymer with DP equal to 6 are shown in the Appendix I (Figure A.1 to Figure A.4).

The ^{1}H-NMR spectra clearly show that the end-group functionalities are incorporated into the polymer chains and are unaffected during the synthesis mainly as a result of the low reaction temperature (35 °C) achieved by using $scCO_2$. For example, it is well known that at higher temperatures (>85 °C) side reactions involving acrylate, methacrylate and oxetane moieties do occur [47, 83]. In addition, it is known that the selectivity of CaLB towards primary alcohol is significantly reduced at temperatures above 100 °C; thus leading to branching when monomers or end-cappers with secondary -OH groups are exploited [44]. Therefore, lower temperature approaches are without a doubt highly desirable when using CaLB.

(1)



(2)

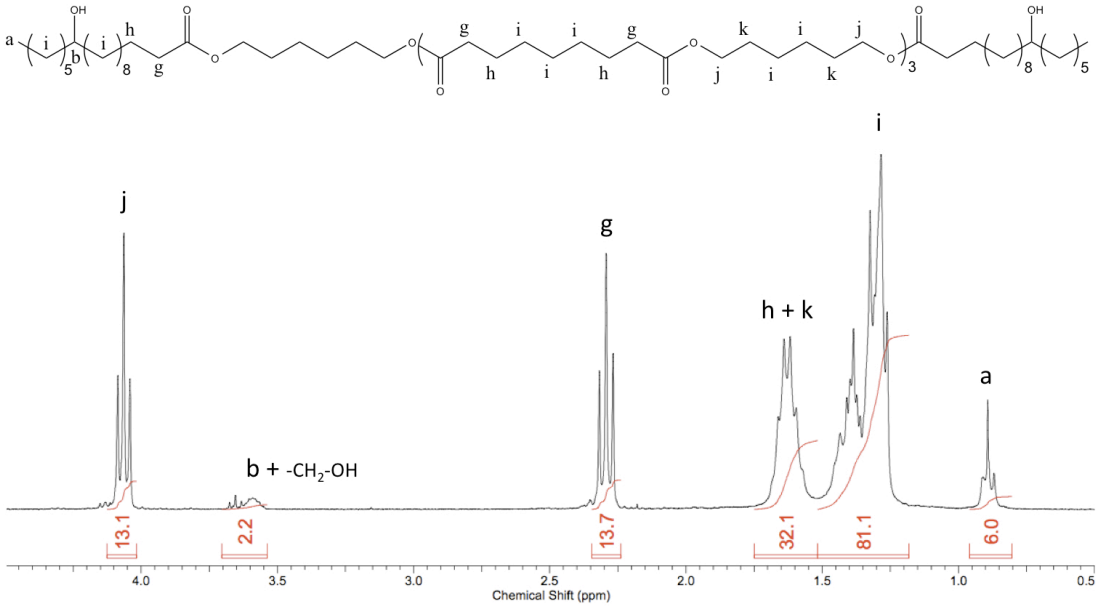


Figure 4.15 - ^{1}H-NMR of: (1) PHAz-SA3: the end-capper peaks are clearly observed at around 1.75 ppm (a), 4.52 ppm (f) and between 5.50 and 6.55 ppm (b-e); (2) PHAz-HSA3: the end-capper peaks are observed at 0.90 ppm (a), 3.60 ppm (b) and in the peak at 1.45 ppm (i). An additional small triplet that is assigned to protons adjacent to an alcohol group (either in the 1,6-hexanediol or uncapped chains) is observed at 3.65 ppm in PHAz-HSA.

In more detail, the spectrum of PHAz-SA3 (Figure 4.15-1) clearly shows the resonances attributed to the protons of the end-capper (*b-e*; between 5.5-6.5 ppm) and the integral of peak *f* (4.6 ppm) has been used to calculate the fraction of SA linked to the polymer chains (and hence the extent of di-functionalisation).

The spectrum of PHAz-HSA3 (Figure 4.15-2) shows that the peak assigned to the alkyl proton adjacent to the secondary –OH (at 3.6 ppm) is still present, thus showing the preservation of this functionality. In this case, the resonances of the end-capper did not explicitly demonstrate if HSA was attached to the chain: hence, the minimum amount of di-functional chains (shown in Table 4.2) was back-calculated using the full value of the integral of the overlapping peaks at 3.65 ppm (Figure 4.16). This integral has contributions from the alkyl protons adjacent to the secondary alcohol in HSA (broad peak, red dashed lines) and any alkyl protons adjacent to –OH groups in 1,6-hexanediol and OH-terminated chains (triplet, blue solid lines).

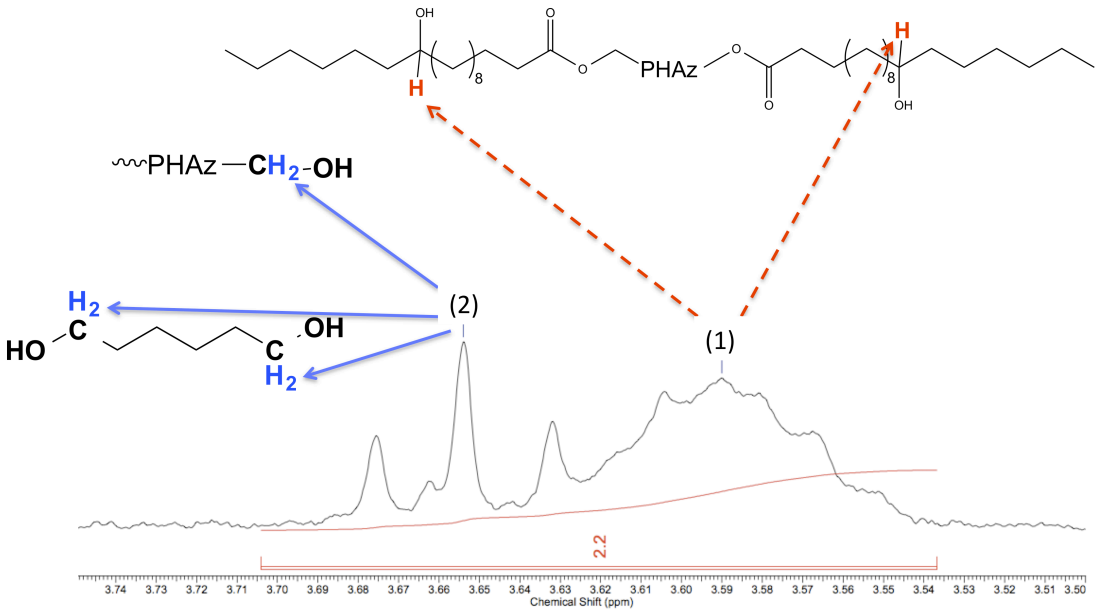


Figure 4.16 - The integral of the overlapped peaks around 3.65 ppm was used to calculate the amount of di-functional chains assuming 100% conversion. This integral has contributions from: (1) the broad peak (3.59 ppm) assigned to the protons adjacent to the secondary alcohol in the HSA end-capper (red dashed arrows); and (2) the triplet attributed to the hydrogens adjacent to –OH groups in 1,6-hexanediol and OH-terminated chains (*i.e.* non-functional chains). The wavy line represents the remainder of the PHAz backbone.

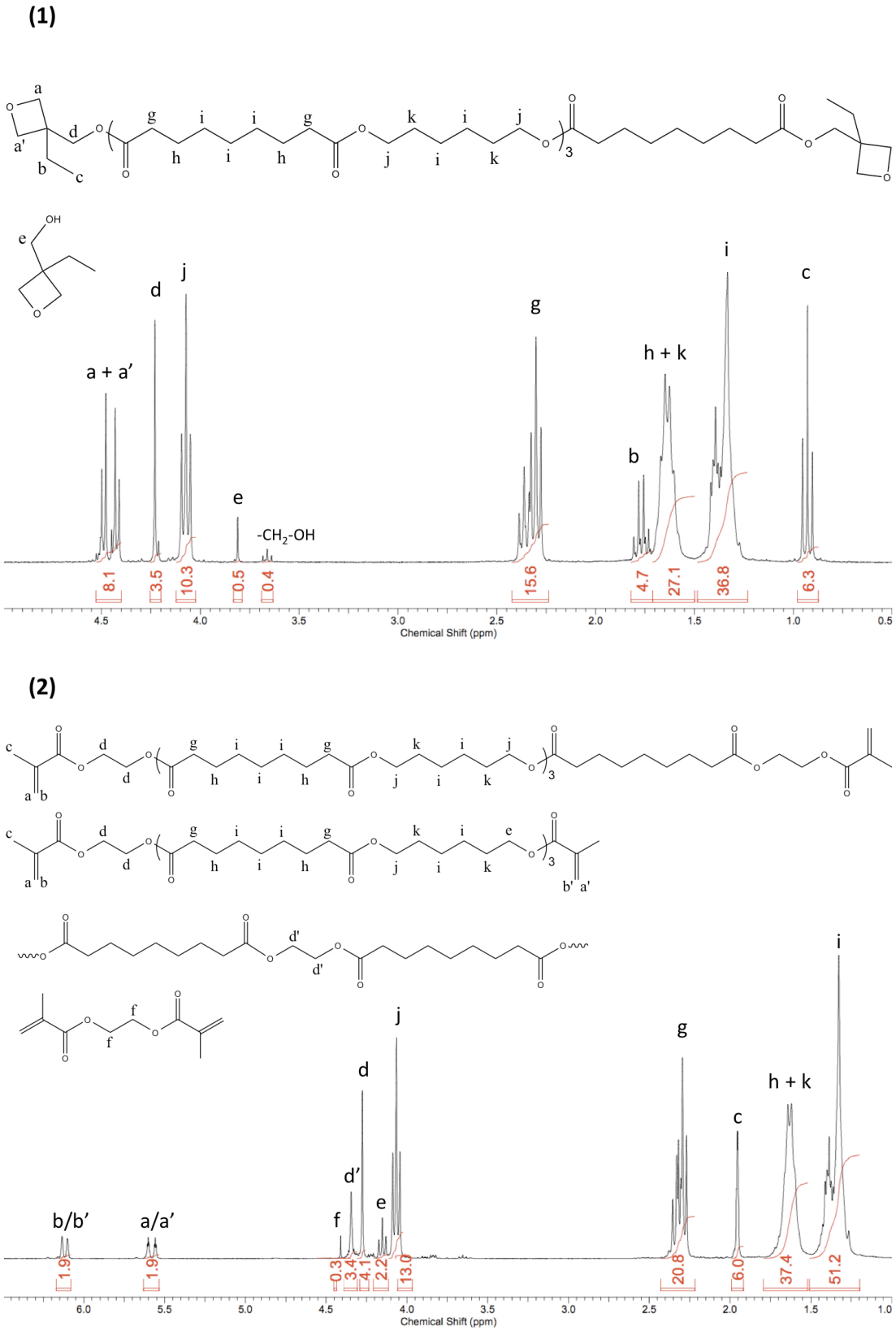


Figure 4.17 - ^{1}H-NMR of: (1) PHAz-TMPO3: the end-capper peaks are observed at around 4.50 ppm (a and a'), 1.75 ppm (b), 0.95 ppm (c) and 4.25 ppm (d), a peak assigned to unreacted TMPO (<13%) is observed at 3.81 ppm (e); (2) PHAz-HEMA3: the end-capper signals are seen at 5.55 ppm (a and a'), 6.65 ppm (b and b'), 1.98 ppm (c) and 4.28 (d).

In the case of PHAz-TMPO3 (Figure 4.17-1), the protons of the oxetane ring are observed around 4.5 ppm (*a*+*a'*). The integrals of *d* (4.25 ppm) and *e* (3.81 ppm) could be used to calculate the amount of TMPO attached to the polymer chains. The peak at 3.65 ppm (alkyl protons close to a primary –OH group) could be used to provide an estimation of the minimum conversion.

Furthermore, it is clear that in the spectrum of PHAz-HEMA3, in addition to the expected peaks, additional features can be assigned to different species (Figure 4.17-2). As expected, during the synthesis there are acyl transfer reactions going on between all the species (monomers, oligomers and end-capper) present in the system (see Chapter 1, Section 1.3.1.1, page 14 for more details on the reaction mechanism of CaLB). Therefore, in addition to the interaction with the carbonyl group of azelaic acid (in its monomeric form or in the PHAz backbone), CaLB can interact with the carbonyl group of HEMA (Figure 4.18). Hence forming a tetrahedral intermediate with HEMA and then an acyl-enzyme complex with the methacryloyl group (**1**). Contemporaneously ethylene glycol (**2**) is released. This diol can subsequently attack, as a nucleophile, another acyl-enzyme complex formed with azelaic acid (monomeric or in a PHAz chain). Therefore, the polymerisation will proceed and ethylene glycol units will be inserted in the telechelic backbone (**3**) (as observed in the ^{1}H-NMR Figure 4.17-2, peak *d'*) rather than at the end of the polymer chain. Equally, 1,6-hexanediol-terminated PHAz chains can attack the acyl-enzyme complex with the methacrylate group and, therefore, the methacrylate group will then be attached directly at the end of the PHAz chain (**4**) (Figure 4.17-2, peak *e*) without ethylene glycol as a linker.

Finally, the same acyl-enzyme complex can react with HEMA forming the diester ethylene glycol dimethacrylate (**EGDMA**) (Figure 4.17-2, peak *f*), although less than 4% of this species is detected through ^{1}H-NMR.

This is a clear demonstration of the dynamic nature of lipase-catalysed reactions. CaLB is continuously cleaving ester linkages and creating new ones, thus causing the migration of ethylene glycol units throughout the polymer chains as shown in Figure 4.17-2 and Figure 4.18, and as already reported in the literature [19].

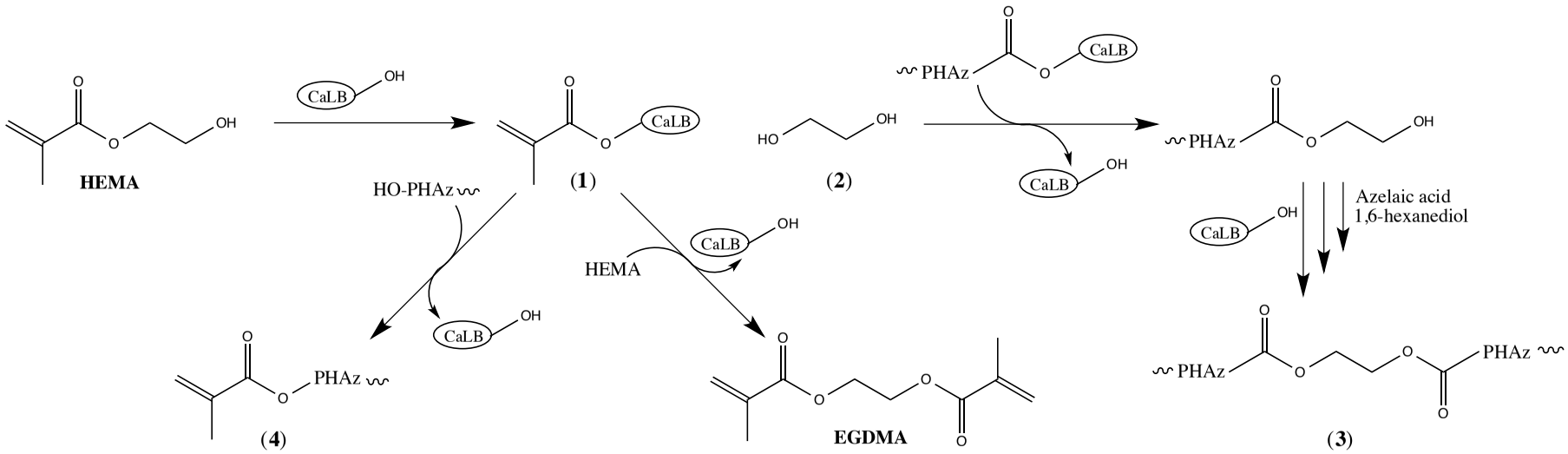


Figure 4.18 – Alternative reaction paths during the synthesis of PHAz-HEMA that lead to products different from that targeted. CaLB can interact with HEMA, hence: ethylene glycol units can be inserted in the telechelic backbone rather than at the end (3), methacryloyl groups can be attached directly to 1,6-hexanediol in the PHAz backbone without ethylene glycol as a linker (4), finally EGDMA can be produced. In this picture the wavy lines represent the remainder of the PHAz backbone.

The ^{13}C-NMR spectra of the same polymers showed again the achievement of successful polymerisations with addition of the end-cappers and preservation of the desired functional moieties (Figure 4.19 to Figure 4.22).

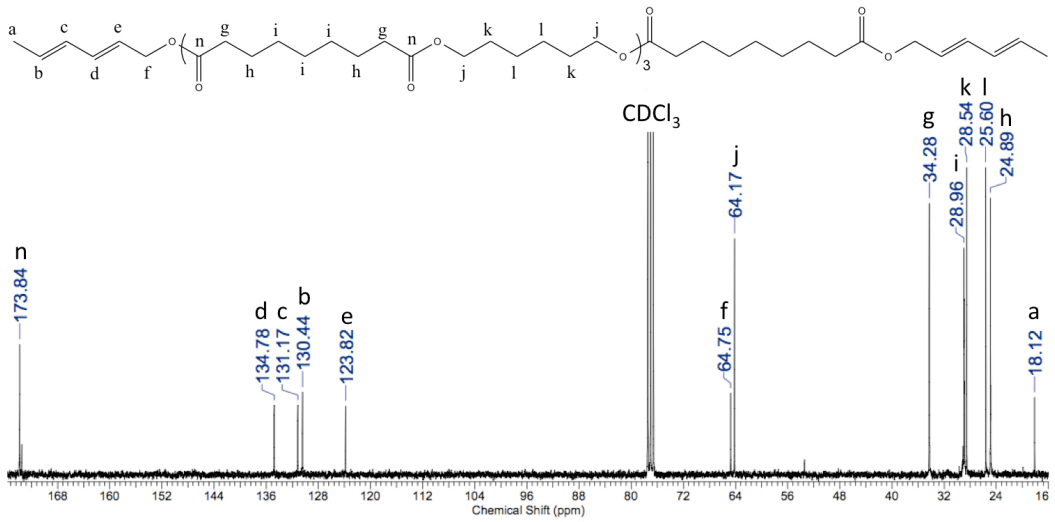


Figure 4.19 - ^{13}C-NMR spectrum of PHA-SA3. The PHAz alkyl backbone is observed at 24.9, 25.6, 28.5, 29.0, 34.3, 64.2 and 173.8 ppm, whilst the characteristic end group is observed between 120-136 ppm.

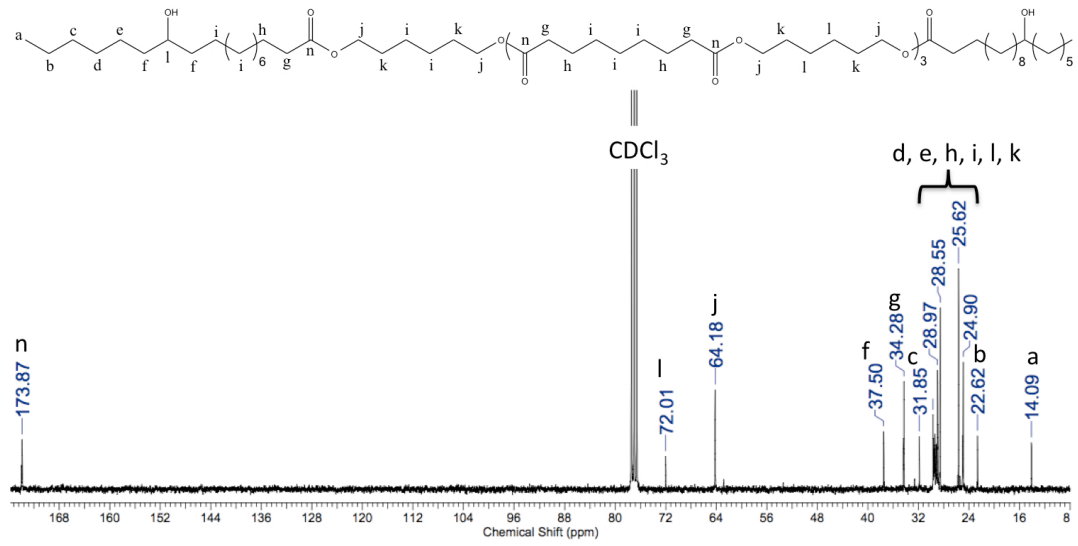


Figure 4.20 - ^{13}C-NMR spectrum of PHA-HSA3. The characteristic end group is observed at 72.0 ppm labelled "l" in the structure and on the spectrum.

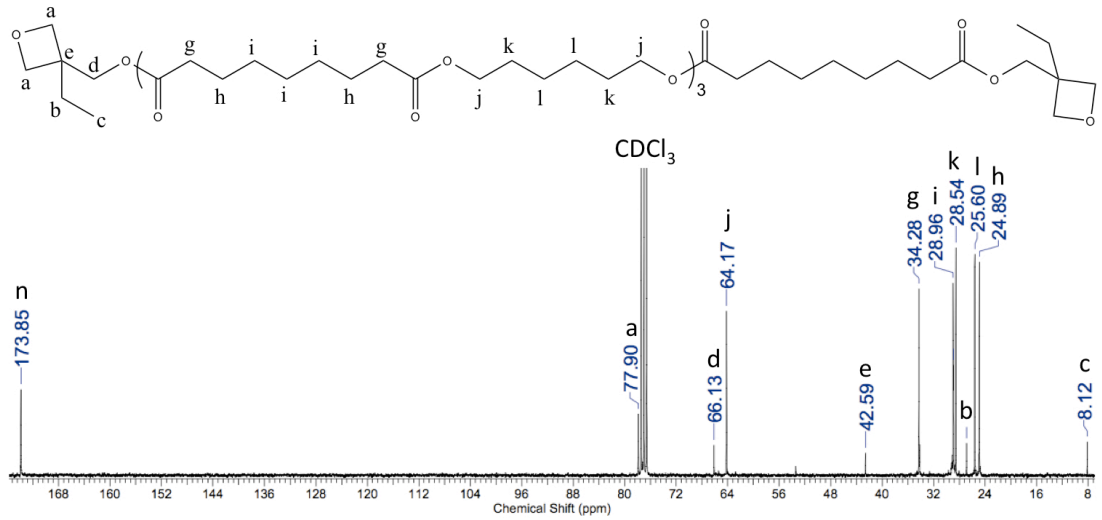


Figure 4.21 - ^{13}C-NMR spectrum of PHA-TMPO3. The characteristic end group is observed at 77.9 ppm (two identical carbons labelled "a").

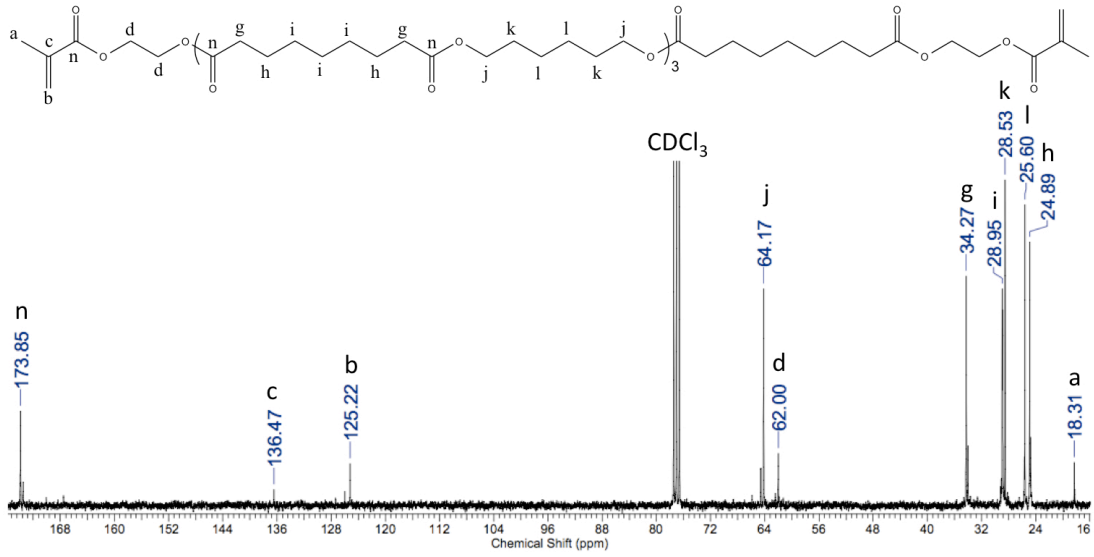


Figure 4.22 - ^{13}C-NMR spectrum of PHA-HEMA3. The characteristic end group is observed at 125.2 and 136.5 ppm with the olefinic carbon labelled "b" and "c".

As expected, the peaks assigned to the PHAz backbone (at 24.9, 25.6, 28.5, 29.0, 34.3, 64.2 and 173.8 ppm) were observed in all the polymers and, in addition to these, the resonances assigned to the specific moieties of the end-cappers were also detected (*i.e.* the unsaturated carbon resonances between 120-136 ppm for SA and HEMA, the carbon attached to a secondary alcohol at 72 ppm for HSA and the oxetane signal at 78 ppm for TMPO).

4.3.3.2 MALDI-TOF analyses

To obtain further verification and confirmation of the NMR results, the polymers with DP equal to 3 were studied by MALDI-TOF. These measurements confirmed successful enzymatic polymerisation and functionalisation. Several series of peaks with a repetitive pattern of 270.4 g mol^{-1} are detected for all the polymers (Figure 4.23 to Figure 4.26, light blue double-headed arrows), hence confirming the structure of the hexylene azelate repeating units.

In more detail, the spectrum of PHAz-SA3 clearly shows two main series that can be assigned to the di-functional polymer (series n) (Figure 4.23). Only one peak (m) with very low intensity assigned to a non-functional chain is detected. This, correlated with the ^{1}H-NMR results, confirms a high extent of functionalisation.

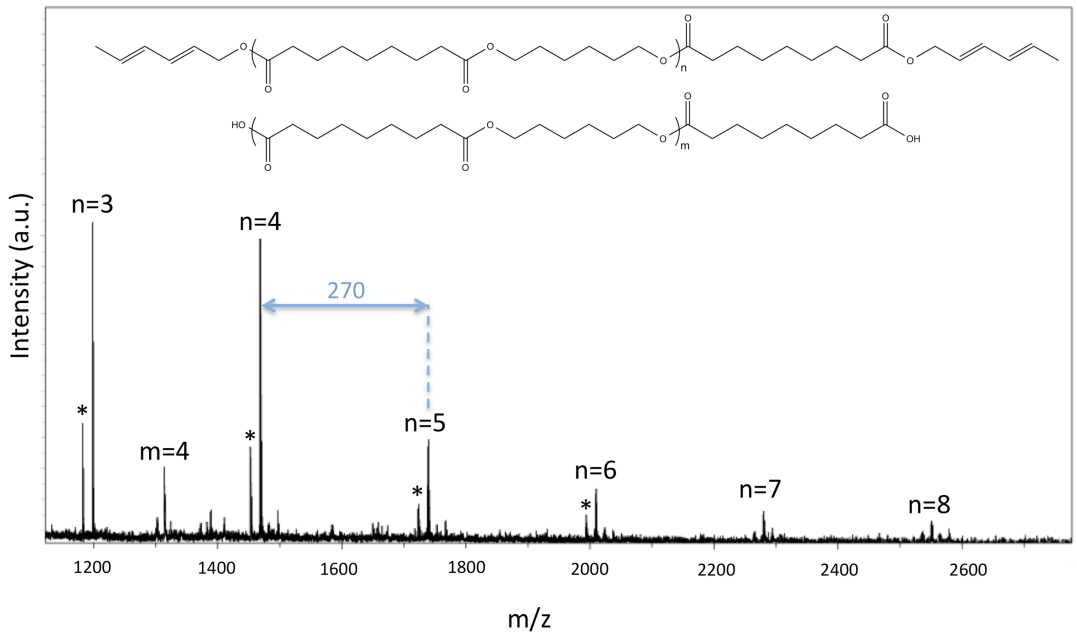


Figure 4.23 - MALDI-TOF spectrum of PHAz-SA3. The main series (n) is assigned to the telechelic chains ionised with K^{+}. Satellite signals at lower m/z (*) are given by chains with Na^{+} ions. The peak m can be assigned to a non-functional (AB)A-type chain with DP4.

The spectrum of PHAz-HSA3 shows only one series of peaks assigned to di-functional chains. No mono-functional or non-functional chains are detected (Figure 4.24).

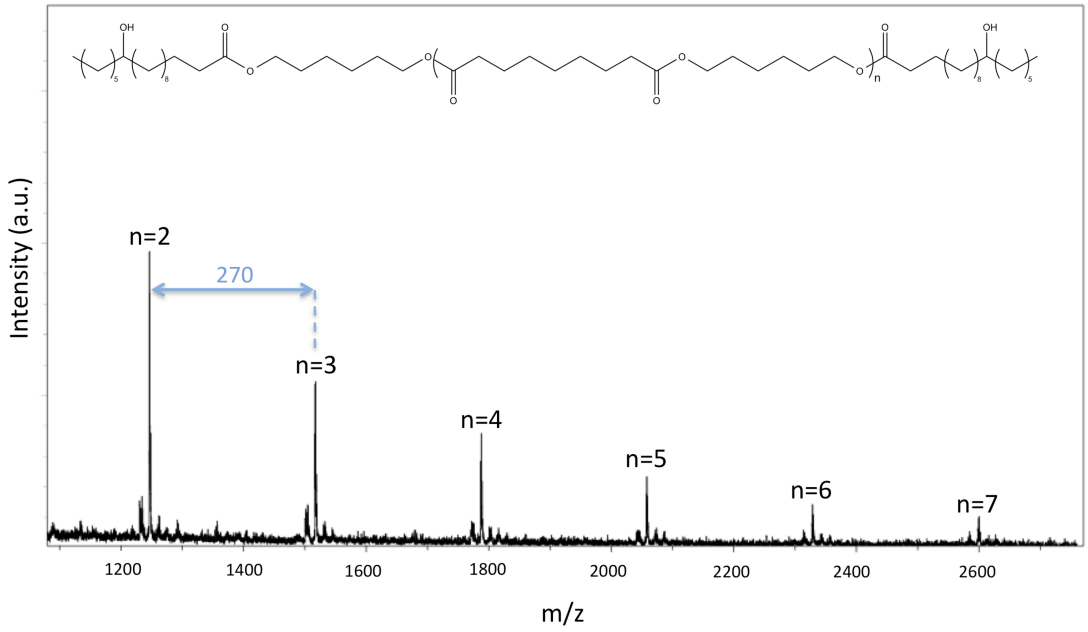


Figure 4.24 - MALDI-TOF spectrum of PHAz-HSA3. The main series (n) is given by the telechelic chains. No other species are detected. The mass difference between the peaks is 270, which corresponds precisely to the hexylene azelate repeating unit.

By contrast, the MALDI-TOF spectrum of PHAz-TMPO3 shows several different series (Figure 4.25). The main one (n) is given by the chains carrying oxetane moieties at both ends and, hence, the target telechelic. In addition to this, two other distributions are detected. Both of them are assigned to non-functional AB-type polymer chains; one terminating with an alcohol and a free acid end (m), the other (*) with an alcohol and a sodium carboxylate end-group formed in the MALDI-TOF sample preparation. Sodium carboxylate end-groups have been already observed in the mass spectrum of similar systems [19].

Although the intensity of the AB-type polymer peaks is quite high, it should be noted that this analysis is not quantitative, thus the size of the peaks does not indicate absolute quantities but only how effectively different fragments are ionised and fly down the MALDI-TOF [21, 84]. In fact, the non-functional AB-type chains represent around 13% of the product, as calculated from ^{1}H-NMR by analysis of the ratio between the peaks 4.20 ppm and at 3.65 ppm (Figure 4.17-1). Therefore, the targeted telechelic polyester represents more than 87% of the final product.

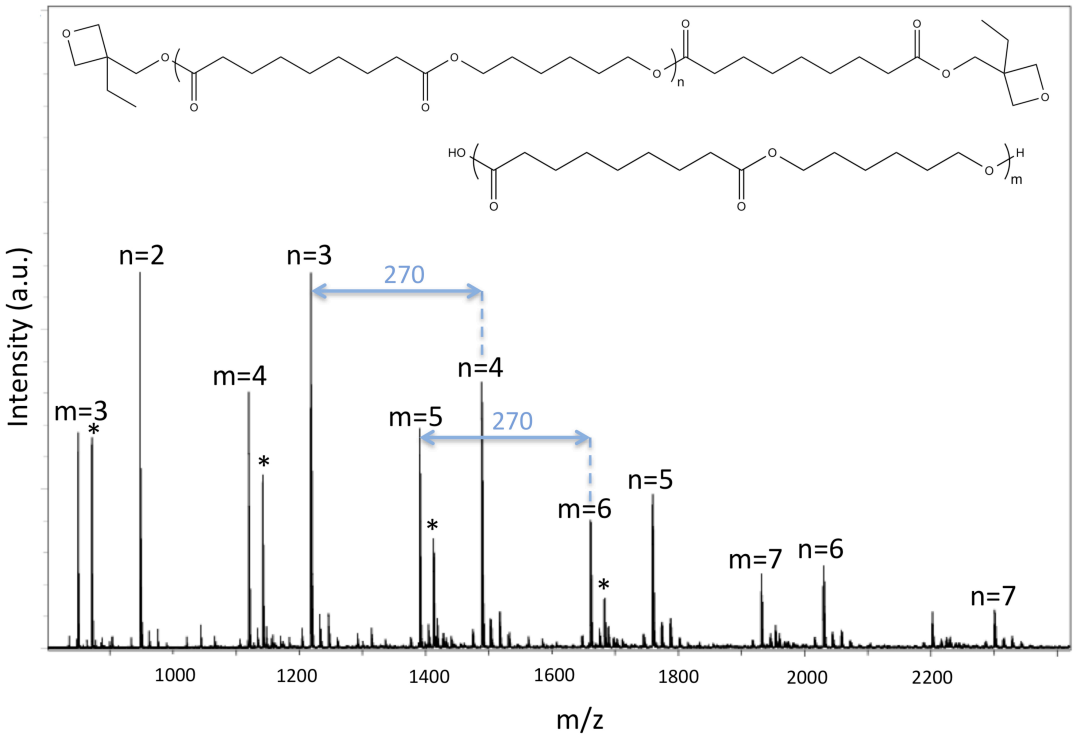


Figure 4.25 - MALDI-TOF spectrum of PHAz-TMPO3. (n) di-functional product; (m) AB-type chains with acid and alcohol end-group; (*) AB-type chains with a sodium carboxylate and an alcohol end. Note that the mass difference between the peaks of each series is 270, which corresponds to the hexylene azelate repeating unit

Finally, the spectrum of PHAz-HEMA shows once again the dynamic nature of lipase-catalysed polyesterifications (Figure 4.26). Five different species can be identified: three are di-functional and two mono-functional. These structures are differentiated by the presence or the absence of ethylene glycol units. Thus, confirming the ^{1}H-NMR results described previously and the dynamic nature of lipase-catalysed polycondensations (Figure 4.17-2 and Figure 4.18). Nonetheless, non-functionalised structures were not detected; therefore, all the polymer chains that are produced can participate in radical cross-linking reactions leading to useful functional materials.

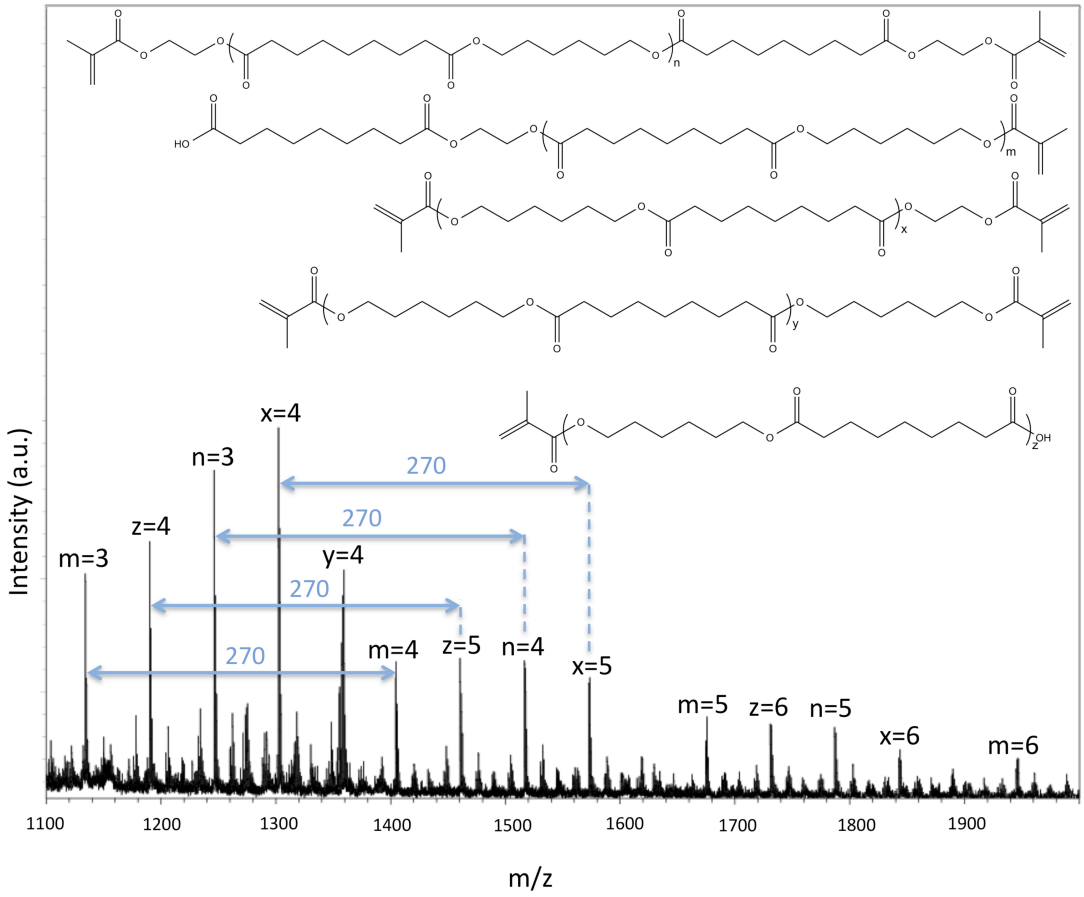


Figure 4.26 - MALDI-TOF spectrum of PHAz-HEMA3. Different species can be identified. (n), (x) and (y) are telechelic chains; (m) and (z) are mono-functional chains. All the series show the characteristic spacing of 270 between the peaks.

4.3.4 Effect of enzyme concentration

An important parameter to consider when carrying out an enzymatic reaction is the enzyme loading. In fact, the amount of enzyme can strongly affect the yield of the reaction and the commercial viability of the process (*i.e.* a high loading is detrimental from an industrial point of view because of the high cost in the long term). However, it is important to remark how in this case the weight of the catalyst is mainly given by the acrylic resin beads that support the enzyme: in fact, the lipase amount per entire catalyst (support+CaLB) weight in Novozym 435 is 10% [42].

Typical enzymatic polymerisations carried out using CaLB (immobilised on acrylic resin beads) require a supported enzyme amount comprised between 10 and 25% by weight (relative to the overall amount of reactants, which corresponds to 1 and 2.5%

by weight of lipase respectively) to obtain sufficiently high yields and conversions in a reasonable time (normally 24 hours) [11, 20, 29, 41, 44].

The reactions described so far were carried out using 25% by weight of Novozym 435 for 24 hours; hence, 2.5% by weight of lipase relative to the global amount of reactants were used for each reaction.

Further investigations were carried out to understand whether lowering the enzyme loading would have affected the reaction yield and conversion (always with a 24-hour reaction) or not. In fact, if comparable yields and end-capping efficiency could be achieved with lower enzyme loading this would make the process more commercially sustainable and interesting.

For this aim, the polymerisation with TMPO as an end-capper (targeting DP6) using 10% by weight of Novozym 435 was carried out. The reaction gave product with high yield (90%). Furthermore, the ^{1}H-NMR spectrum of the reaction product confirms the successful formation of a polymer with the targeted DP and, hence, M_n^{NMR} close to the theoretical value (M_n^{th} = 2100 g mol^{-1}; M_n^{NMR}= 2300 g mol^{-1}) (Figure 4.27).

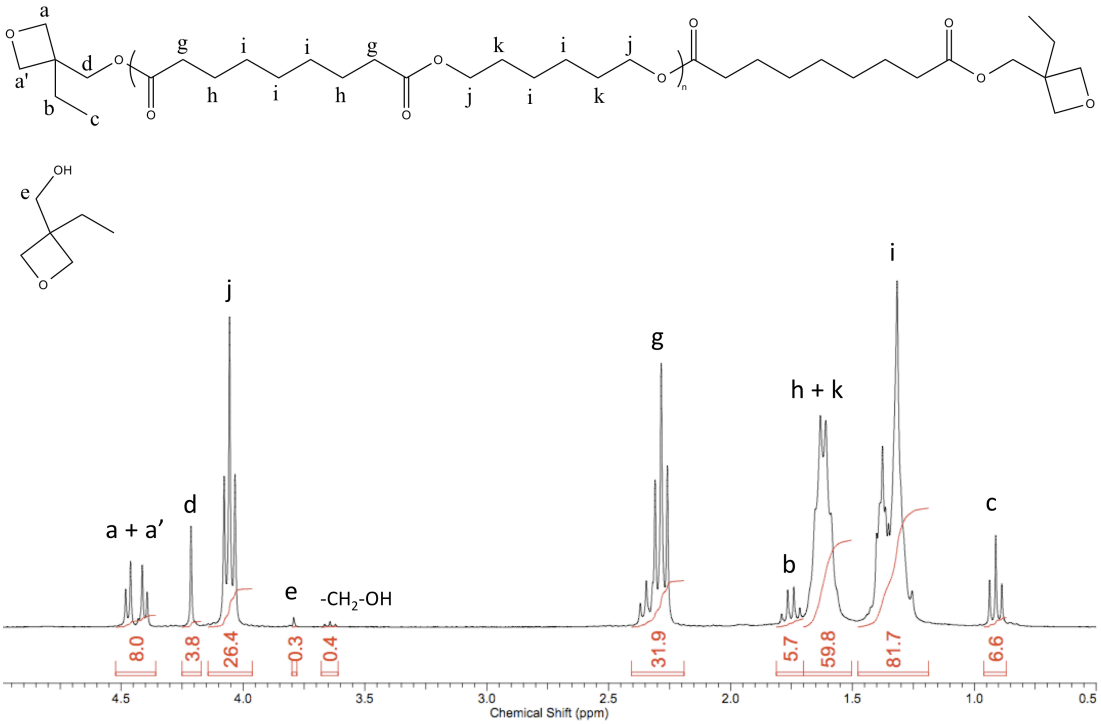


Figure 4.27 - ^{1}H-NMR of PHAz-TMPO6 synthesised by using 10% by weight of Novozym 435: the end-capper peaks are observed at around 4.50 ppm (a and a'), 1.75 ppm (b), 0.95 ppm (c) and 4.25 ppm (d), a peak assigned to unreacted TMPO (7%) is observed at 3.81 ppm (e).

Additionally, this spectrum shows also that when using 10% by weight of Novozym 435 the amount of difunctional chains is higher than that obtained when using 25% by weight of immobilised enzyme (93% as opposed to 88% respectively), whilst showing the same monomer conversion (around 98%). Therefore, not only is the yield of the reaction not affected by a lower enzyme loading, but also the functionalisation efficiency is slightly higher. A similar effect was observed elsewhere when preparing telechelics using divinyl adipate and 1,4-butanediol, where this was attributed to the increased hydrolysis of the end groups when the enzyme concentration was increased and sometimes no vinyl end-groups were found at all [85]. In fact, it is important to emphasise once again that lipase-catalysed polycondensations are dynamic reactions where the enzyme is continuously cleaving and forming new ester bonds. After the initial steps (when only monomers and end-cappers are present), several reaction intermediates and the propagating polyester chain itself can function as acyl donors. Therefore, the enzyme catalyst can also attack the ester bonds within the polymer chain and, hence, cleave the backbone [27]. An additional reaction was carried out lowering further the Novozym 435 loading to 5% by weight. In this case, the reaction yield was still remarkably high (85%) but the end-capping efficiency was much lower (70%) (Figure 4.28). Hence, this low amount of enzyme is not sufficient to catalyse efficiently the reaction and probably more than 24 hours would be needed to achieve good end-capping.

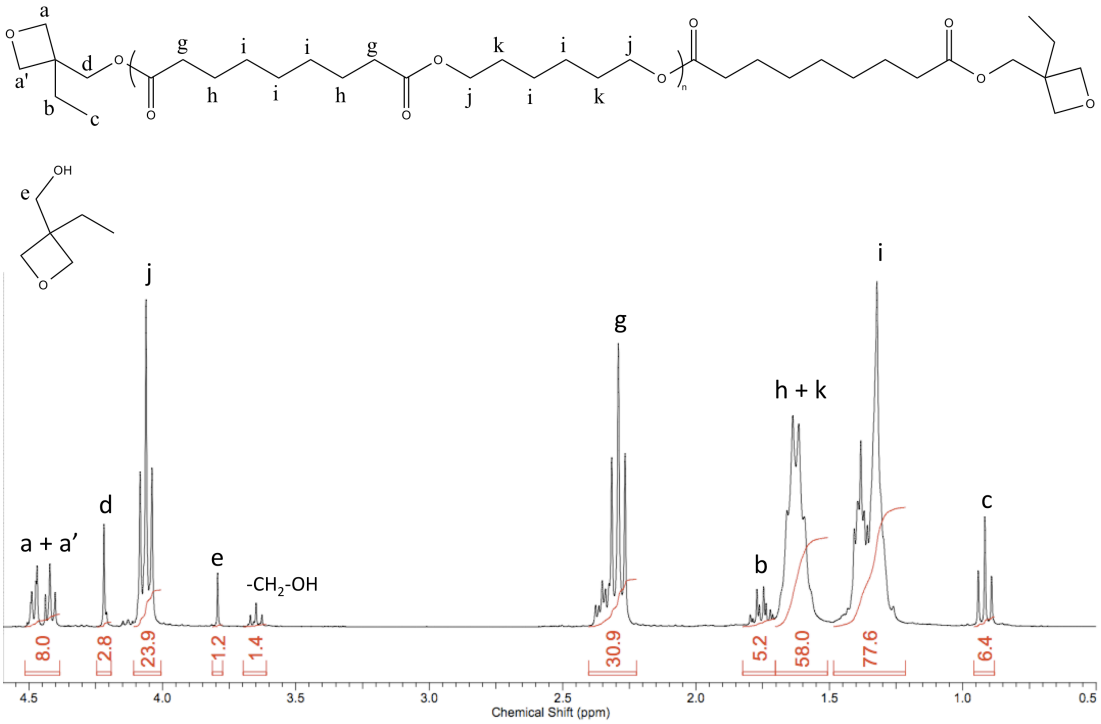


Figure 4.28 - ^{1}H-NMR of PHAz-TMPO6 synthesised by using 5% by weight of Novozym 435: the end-capper peaks are observed at around 4.50 ppm (a and a'), 1.75 ppm (b), 0.95 ppm (c) and 4.25 ppm (d), a peak with significant intensity assigned to unreacted TMPO (30%) is observed at 3.81 ppm (e).

4.3.5 Enzyme recycling

The results shown so far in the previous sections are undoubtedly significant and interesting. In a nutshell, it has been shown that condensation polymerisations of azelaic acid and 1,6-hexanediol and end-capping with functional molecules can be carried out at 35 °C, directly from the diacid and using an immobilised naturally occurring enzyme as a catalyst.

An additional hypothesis was that the low temperature of the reaction could provide the possibility of reusing the enzyme without significant loss of activity over a number of cycles. This would enhance the value of this novel approach in $scCO_2$. In fact, when designing enzymatic processes from an industrial point of view, successful recycling of the enzyme catalyst for several cycles is a crucial requirement [86].

To further emphasise this advantage, this novel low temperature approach was compared to reactions carried out in the molten state at high temperature. For these reasons, the polymerisations of azelaic acid and 1,6-hexanediol with the four different end-cappers were conducted in the melt targeting DP3, by using a normal oil-bath set up. In order to obtain a homogeneous molten phase, the internal temperature of the glass flask was set to 110 °C.

As expected, the first finding was that these polymerisations afforded products with much lower yields (Table 4.3).

Table 4.3 – Yields of the Novozym 435-catalysed polymerisation in the melt (110 °C).

Product	Yield (%)[a]
PHAz-SA3	40
PHAz-HSA3	72
PHAz-TMPO3	61
PHAz-HEMA3	60

[a]Yield= weight of collected product/theoretical weight×100;

It is clear that the yields of these high-temperature polymerisations were generally quite low (between 40 and 70%). It is postulated that this might be caused by a lower catalytic efficiency of CaLB at 110 °C (the optimum temperature window declared by the supplier is 30-60 °C [87]) and/or possible cross-linking reactions between the end-capped polymer chains that might also have led to insoluble products. The latter reason could also explain the erratic results obtained from ^{1}H-NMR analyses (see Appendix I, Figure A.6 to Figure A.8), which could not be used to obtain a sensible estimation of the average molecular weight (M_n^{NMR}). Integrals of the peaks assigned to the end-cappers showed values that did not match with the values expected for the intact structures. This can be attributed to side reactions involving the end-group moieties that likely occurred when carrying out the polymerisation in the melt at 110 °C, however in-depth investigations of these side reactions and identification of the products obtained are beyond the focus of this research.

In fact, these high temperature reactions were carried out mainly to analyse the activity of the enzyme after these melt polymerisations and those in $scCO_2$.

Loeker *et al.* tested the residual activity of CaLB after the ring-opening polymerisation of ε-caprolactone in CO_2 (50 °C, 160 bar). They repeated the polymerisation using the same enzyme beads and observed no changes in the average targeted molecular weight [40]. Accordingly, we also ran the polymerisations in duplicate and reused the enzyme beads for up to five high-pressure reactions, and observed no reduction in the yield and/or significant changes in the average molecular weight. Additionally, the enzyme beads used for five polymerisations in CO_2 at 35 °C were collected and their activity was tested and compared to that of fresh CaLB and that of beads used in the high-temperature melt reactions (at 110 °C). The assays were performed by synthesising propyl oleate starting from oleic acid and 1-propanol and monitoring the conversion by ^{1}H-NMR (spectra shown in the Appendix I, Figure A.10 to Figure A.12). Samples were taken after 1, 3, 5 and 24 hours (Figure 4.29).

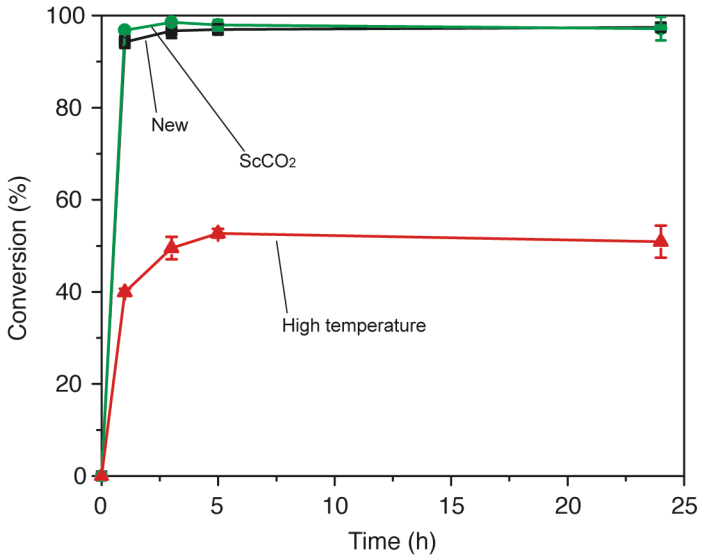


Figure 4.29 - Comparison between the conversion obtained in the propyl laureate synthesis when using fresh enzyme (black) and recycled beads: from the reactions in $scCO_2$ (green) and at high temperature in the melt (red). The points for the green plot are shown as the average between the data of five different measurements (after 1, 2, 3, 4 and 5 cycles in CO_2) ± one standard deviation. The data for the fresh sample and those recycled after the high temperature reactions are shown as the average of three different experiments ± one standard deviation.

The conversion values obtained using fresh Novozym 435 beads and those recycled from reactions in $scCO_2$ are essentially overlapping (within the error). Therefore,

these data show that no reductions in the enzyme activity were caused by the high-pressure reactions (up to five cycles, but possibly even more).
On the contrary, the polymerisations carried out at 110 °C resulted in a significant reduction in the activity (possibly due to enzyme denaturation/leaching and cross-linked insoluble polymer residues on the catalyst beads). Hence, this clearly shows that the melt polymerisations not only afforded low quality products with low yields, but also would not be commercially viable in the long term and on a large scale, because of the impossibility of recycling the enzyme efficiently. Conversely, the low-temperature supercritical route would be industrially more viable and sustainable.

4.3.6 Cross-linking tests

4.3.6.1 FTIR studies

As aforementioned, the synthesised telechelics can undergo further reactions (such as cross-linking, chain extension or a secondary functionalisation) by exploiting the reactivity of the end-cappers.
Preliminary real-time FTIR studies were conducted to understand if it might be possible to analyse the kinetics of the cross-linking reactions upon UV irradiation. These tests would confirm if any reaction happens at all and, if so, how long it takes for it to happen. Only the telechelics with DP3 were studied, since in these polymers the absorptions of the end-cappers would have been necessarily more easily detected than in polymers with a longer backbone (*i.e.* those with DP6); the intensity of an absorption band in an IR spectrum depends not only on the polarity of the bond but also on the number of the specific bonds present. Hence, the bands relative to the end-capper vibrations for a polymer with a lower DP should be more prominent, compared to those observed for a structure with a longer backbone.
These investigations were carried out in collaboration with the group of Professor Mats Johansson at the KTH Royal Institute of Technology (Stockholm), taking advantage of their expertise on radical and cationic cross-linking.

The cross-linking of HSA-functional polymers would require the use of isocyanates, and unfortunately the safety regulations of KTH did not allow for these experiments to be carried out. For these reasons, only the FTIR spectra of the telechelics end-capped with HEMA, SA and TMPO were analysed.

The success of the radical cross-linking for PHAz-HEMA3 could be monitored by complete disappearance of the small peak (a) at 1635 cm^{-1} (Figure 4.30). The wavenumber of this peak corresponds to that observed for the monomer methyl methacrylate [88, 89], and hence it can reasonably be assigned to the methacrylate double bound of the HEMA end-capper that is consumed during the radical cross-linking process.

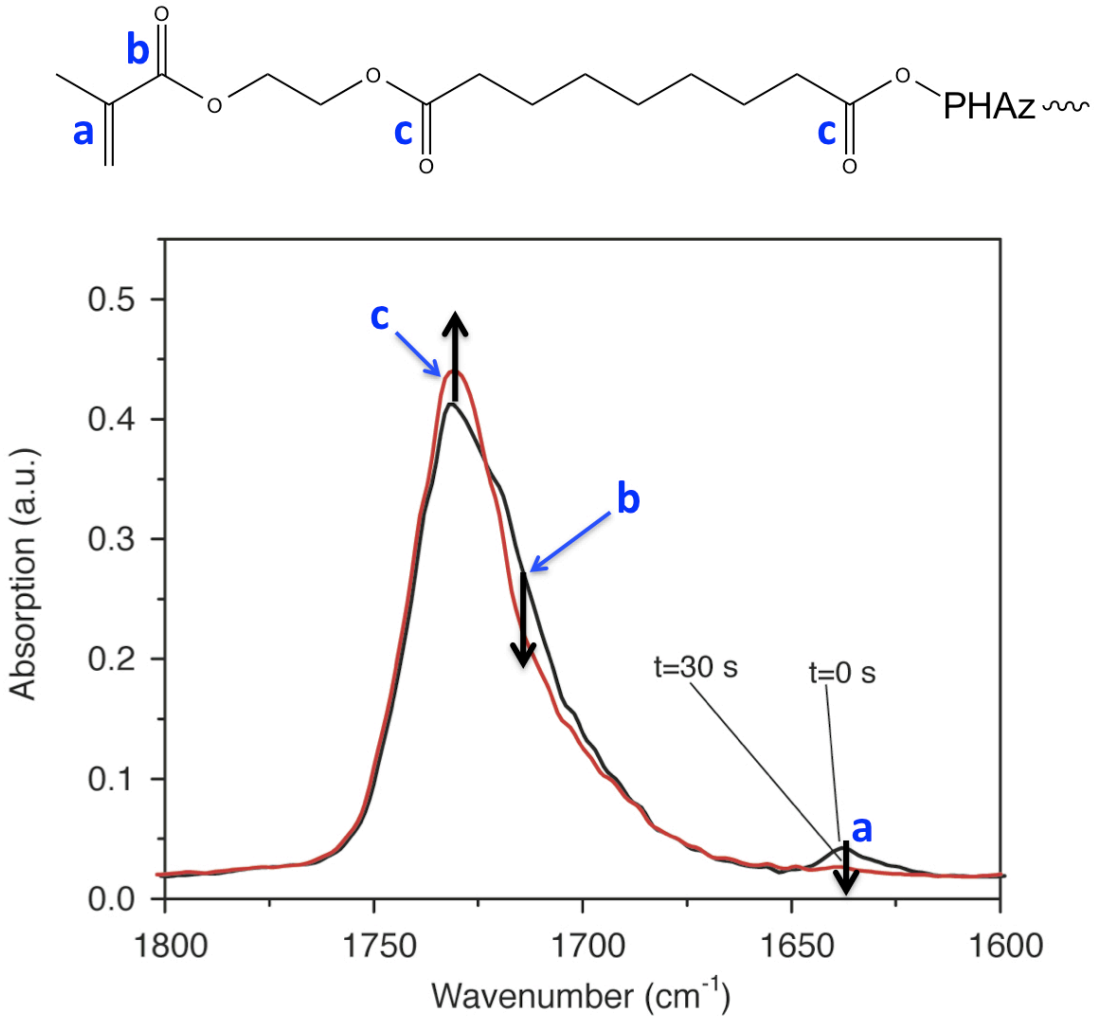


Figure 4.30 - Section of the FTIR spectrum of PHAz-HEMA3. As the cross-linking process is initiated, the peak at 1640 cm^{-1} rapidly depletes demonstrating loss of the C=C moieties. The black arrows show what peaks are decreasing or increasing in intensity over time. The wavy line in the upper structure represents the remaining of the PHAz backbone.

In addition, the small conjugated ester carbonyl shoulder at 1710 cm^{-1} (b) decreased with an overall increase of the carbonyl peak (c) at 1730 cm^{-1} (the conjugated ester carbonyls lose their conjugation upon reaction of the methacrylate double bound), as already observed for similar systems elsewhere [20]. These changes happened during the first 30 seconds, demonstrating a very rapid cross-linking process.

The analysis of the crosslinking process of PHAz-SA3 was more problematic. The C=C stretch around 1650 cm^{-1} was not strong enough to be monitored efficiently. In fact, not only are these bonds non-polar, but also they are internal and this is known to strongly decrease the intensity of an IR peak [90]. However, in the area between 1500 and 900 cm^{-1} several peaks disappeared and new ones appeared during UV exposure (Figure 4.31).

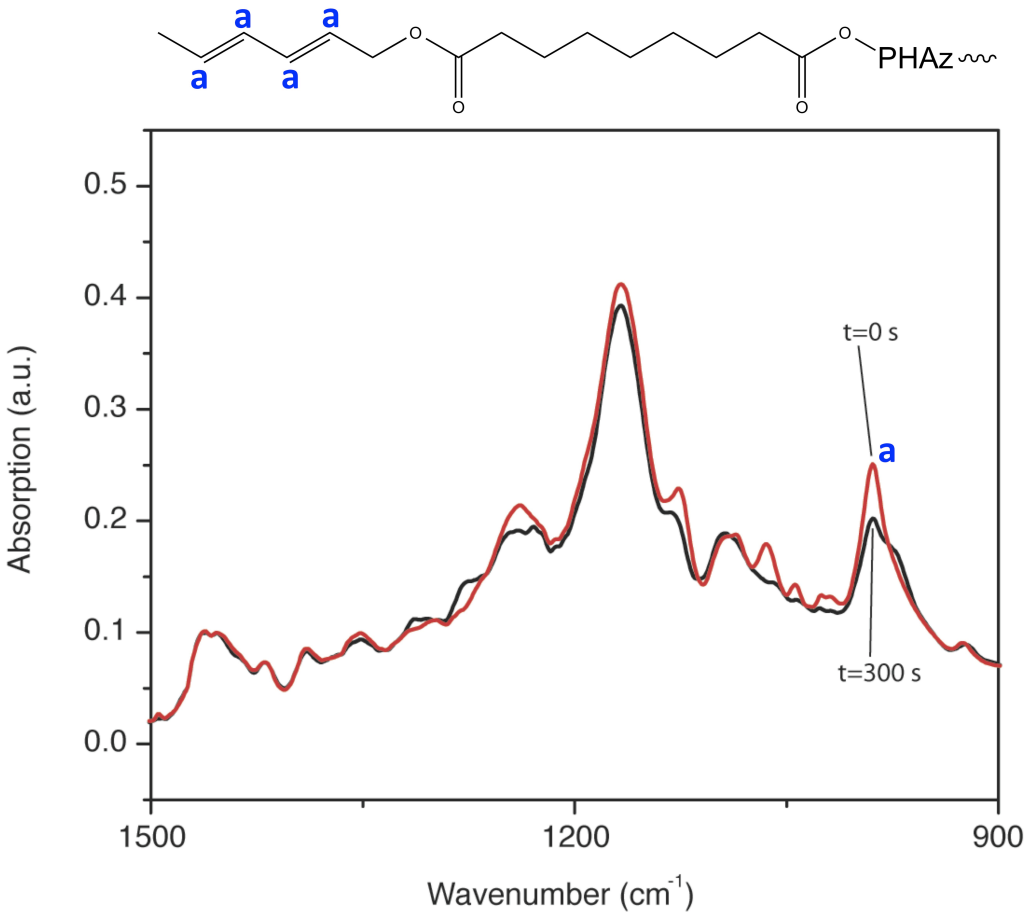


Figure 4.31 - Section of the FTIR spectrum of PHAz-SA3 radically cross-linked. Several peaks disappear over time (after 300 seconds). In particular, the peak (a) at 990 cm^{-1} decreases in intensity: this peak might be attributed to the C=C-H bend, thus indicating radical cross-linking (albeit not complete) of the SA conjugated double bonds. The wavy line in the upper structure represents the remaining of the PHAz backbone.

Unfortunately it was difficult to draw strong conclusions from this spectrum. However, a peak around 990 cm^{-1} (a), which could be assigned to the out-of-plane C=C-H bend, was examined over time. The intensity of this peak started to decrease after 2 minutes and reached its lowest intensity at 5 minutes. Monitoring this peak for additional 10 minutes showed no further changes in the intensity; thus, it is possible that some residual C=C bonds are still present after this time. Nonetheless, the film on the FTIR crystal became transparent and insoluble upon UV irradiation, hence the material certainly did cross-link in these conditions.

Finally, in the case of the telechelic cross-linked by cationic polymerisation (PHAz-TMPO3), significant variations in the spectrum were observed in the region between 1500 and 900 cm^{-1} (Figure 4.32). However, because of peak overlap the assignment and identification of the bands attributed to the vibration of the oxetane ring was challenging; as observed and reported elsewhere [29]. Nonetheless, the fact that we again obtained an insoluble transparent film upon UV irradiation was considered to be strong evidence of the cationic cross-linking.

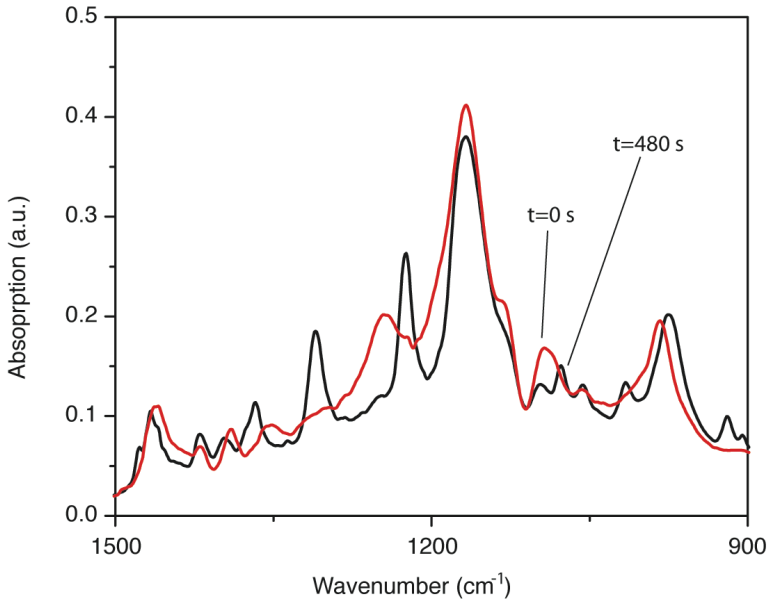


Figure 4.32 - Section of the FTIR spectrum of PHAz-TMPO3 radically cross-linked. Several peaks disappear over time (after 480 seconds). Significant changes happen around 1050 cm^{-1} and these might indicate the ring-opening of the oxetane ring.

Torron and Johansson reported that the ring-opening of oxetane-terminated telechelics could be monitored by observing the intensity of the peak assigned to the

cyclic oxetane (around 1107 cm^{-1}) and the formation of new peaks corresponding to the formation of aliphatic ethers (around 1080-1060 cm^{-1}) [29].

Zooming into the region between 1110 and 1040 cm^{-1} of the spectrum in Figure 4.32, the intensity of peak (a) (around 1100-1090 cm^{-1}) can be seen to diminish over time (Figure 4.33). This band can be attributed to the oxetane ring. Then, the subsequent appearance of new absorption bands around 1090-1050 cm^{-1} might be assigned to the formation of linear ether linkages by cationic ring-opening of the oxetane [29, 47].

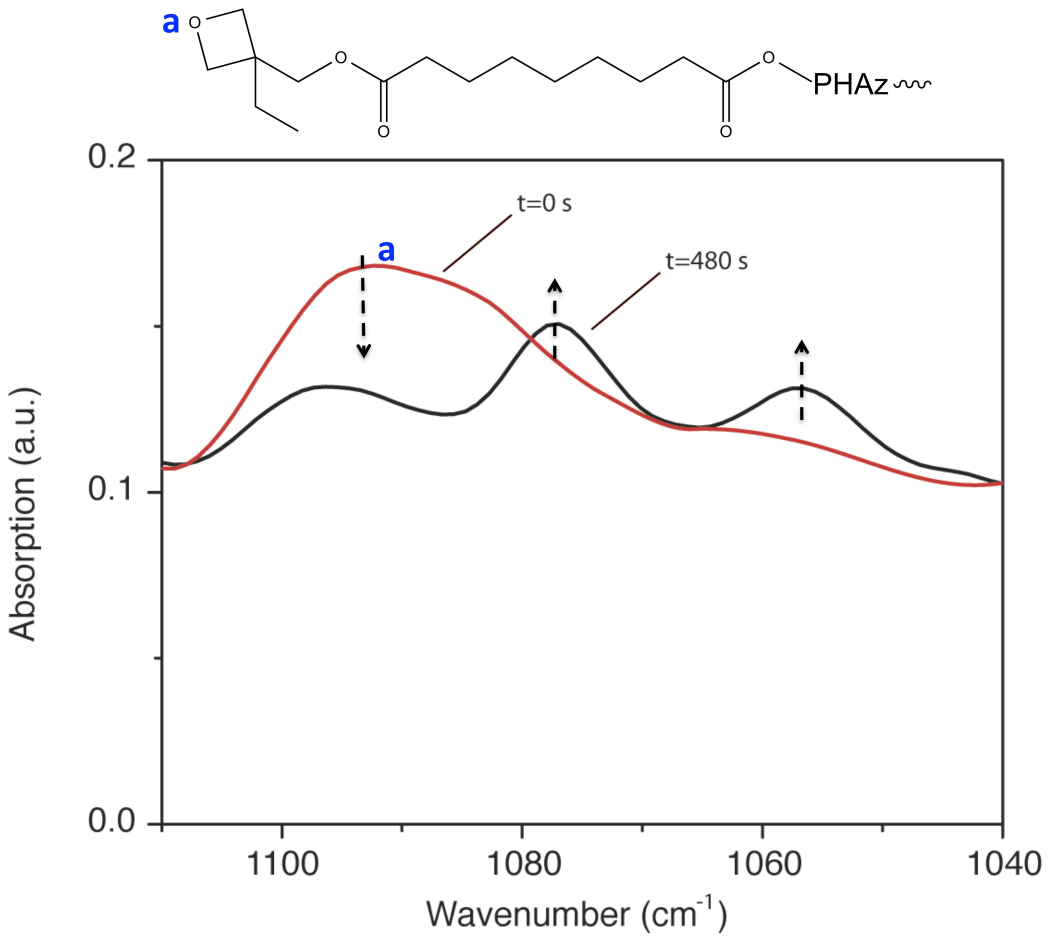


Figure 4.33 - Region between 1110 and 1040 cm^{-1} of the FTIR spectrum of PHAz-TMPO3 radically cross-linked. . The formation of new bands around 1090-1060 cm^{-1} has been assigned in literature to the formation of linear ether linkages upon ring-opening of the oxetane moieties [29].

These FTIR studies were preliminary investigations carried out to corroborate the ability of the three telechelics to react under appropriate conditions, thus confirming once again the successful synthesis of functional bio-based materials. More in-depth

studies would be required to understand this process fully, optimising the spectroscopic features and to follow the cross-linking process in more detail.

4.3.6.2 DSC studies on cross-linked samples

Small aliquots of the same samples used for the FTIR investigations (*i.e.* polymer and photo-initiator dissolved in $CHCl_3$) were cross-linked on microscope slides to obtain cured films. DSC measurements and solubility tests were performed on these films to determine the thermal transitions after curing and to emphasise any changes in solubility compared to the pristine status.

Through the formation of a network, the amorphous fraction of the system is expected to increase due to the motion restriction imposed by the cross-links, which typically would impede effective packing of the polymer chains. Accordingly, the enthalpy of fusion should decrease upon curing; as observed for other polyesters cross-linked by using isocyanates [44].

The data obtained from thermal analyses of the telechelics after UV irradiation are summarised in Table 4.4.

Table 4.4 – Thermal properties of the cured film through radical (SA and HEMA) and cationic (TMPO) cross-linking. Each sample was analysed in duplicates to ensure reproducibility.

Film	T_g (°C)[a]	T_m (°C)[a]	ΔH_f (J g^{-1})[a]	*Solubility (Y/N)*[b]
PHAz-SA3	-39.6 ± 0.4	30.6 ± 0.1	41.8 ± 0.6	N
PHAz-SA6	-34.2 ± 0.7	42.4 ± 0.1	62.4 ± 1.1	N
PHAz-TMPO3	-29.3 ± 1.8	36.1 ± 0.1	58.6 ± 0.9	N
PHAz-TMPO6	-22.7 ± 1.2	41.1 ± 0.2	69.0 ± 0.6	N
PHAz-HEMA3	-51.4 ± 0.3	20.2 ±0.6	28.1 ± 2.1	N
PHAz-HEMA6	-41.6 ± 0.6	33.1 ± 0.1	42.8 ± 0.5	N

[a]Second heating scan (10 °C min^{-1}); [b]Upon stirring in toluene and $CHCl_3$ (20 mg mL^{-1}, 300 rpm, RT) for 24 hours: the presence/absence of swollen lumps was optically inspected.

The first observation is that after curing all the telechelics become insoluble in organic solvents (toluene and chloroform), even after stirring 24 hours. Clear solutions were never obtained. This confirms the formation of a cross-linked insoluble network.

In addition, a T_g could be now identified for all the polymers. In the uncured state this transition was below -60 °C and could not be detected due to equipment limitations (this temperature range is where the machine stops to invert the temperature ramp, and this process gives a change in the heat flow that hides any weak transitions occurring at this range of temperature). On the contrary, after cross-linking the T_g is shifted towards higher temperatures (because of the motion restriction imposed by the cross-links) and the amorphous fraction increases. Hence, the T_g could be more easily detected by DSC.

Then, as expected, for the polymers functionalised with SA and HEMA the T_m and ΔH_f decreased significantly upon cross-linking (see also Table 4.2). In more detail, the crystallinity decreased by 36% for PHAz-SA3 and 30% for PHAz-SA6; whilst the decrease in crystallinity was 42% for PHAz-HEMA3 and 35% for PHAz-HEMA6.

On the other hand, a slight increase in the T_m and ΔH_f for the TMPO end-capped polymers was detected. This increase was around 15% for PHAz-TMPO3 and 2% for PHAz-TMPO6. Albeit small and maybe surprising at first glance, this effect (which was reproducible) might be explained in terms of formation of a linear polyether structure through cationic ring-opening of the oxetane end-groups, as observed through FTIR (previous section). It is known that the C-O-C linkage is more flexible compared to the C-C bond (rotation around the C-O bond does not bring H atoms into conflict with each other) [91, 92]. Hence, it can be postulated that this type of cross-linking is more flexible than the previous ones and, hence, it might preserve the ability of the polyester chains to pack effectively. Further investigations are undoubtedly needed to confirm and understand this fully.

In summary, these initial thermal analyses have confirmed the ability of the polymer chains to cross-link successfully affording cured networks with decreased crystallinity and chain mobility in the case of the SA and HEMA-functional telechelics. Additional studies are however needed to further confirm the hypothesis postulated for the cross-linking of the TMPO-functional polymers and to elaborate on details the formation cross-linked networks for each of the telechelics.

4.4 Conclusions

This chapter demonstrates a low temperature approach using $scCO_2$ that allows facile utilisation of Novozym 435 as a catalyst to synthesise different telechelics. Renewable monomers (azelaic acid and 1,6-hexanediol) were used as building blocks of the backbone and the reactions were carried out without pre-modification of the diacid in a solvent-free system.

The molecular weight of the polymers could be targeted efficiently by changing the feed ratio of the monomers and by end-capping the chains with functional molecules, namely: sorbic alcohol, 12-hydroxy stearic acid, 2-hydroxyethyl methacrylate and trimethylolpropane oxetane. The addition of these functional end-cappers afforded the preparation of telechelics, which could undergo further reaction (*e.g.* cross-linking or chain extension).

These polymerisations would have not been possible through conventional routes because of the high temperatures required to melt the monomer, which are simply not appropriate for lipase-catalysed syntheses of telechelics. Furthermore, suitable solvents for this polycondensation are not available because of the insolubility of the two monomers in apolar solvents.

By use of CO_2 and the enzyme we achieved remarkably high yields and monomer conversion at 35 °C. The combined use of CaLB and $scCO_2$ (and consequent mild temperature) also avoided competing side reactions involving the end-group functionalities.

The chemical structures have been confirmed by ^{1}H-NMR, ^{13}C-NMR and MALDI-TOF analyses, showing that all the products were successfully functionalised in a one pot-reaction and that no side-reactions involved the functional end-capper moieties, which were preserved.

For comparison, the same reactions were conducted in the melt without CO_2 and these resulted not only in much lower yields (likely due to undesired cross-linking reactions involving the end-groups), but also in a reduction in the activity of the enzyme which could not then be efficiently recycled.

By contrast, enzyme-recycling tests demonstrated that the lipase activity is not compromised during the high-pressure reactions and that the immobilised enzyme can be re-used without loss of activity for up to 5 cycles (and possibly even more).

Hence, this novel low-temperature route is certainly more commercially viable and sustainable.

The synthesised telechelics are valuable and can be exploited for further modification, such as cross-linking or chain extension processes, as shown by preliminary FTIR and DSC investigations. Therefore, we demonstrate that by exploiting the unique properties of $scCO_2$ it is possible to synthesise useful renewable materials without the need for high temperatures, large amounts of conventional solvents or pre-modification of the monomers. This route could be especially valuable for applications involving the incorporation of thermally labile functional groups and/or molecules (*e.g.* proteins, drugs *etc.*).

From a green perspective, the major drawback to the approach is the need to use an organic solvent (*e.g.* toluene), albeit in small amount, to separate the polymers from the enzyme beads. In principle this could be overcome by use of $scCO_2$ as a plasticiser, to effectively liquefy the polymer and accomplish the separation, as shown previously by our group [40].

This process could therefore lead towards a fully green, solvent-free, low-temperature route for the synthesis of renewable functional polyesters in $scCO_2$. Finally, it is interesting to note that the most significant energy expenditure in a large-scale polymerisation is for the heating, rather than for the compression costs needed for pressurisation (studies are being carried out in our group to prove this). Hence, dropping the typical working temperature from around 180-200 °C to 35 °C has a dramatic effect, and such high-pressure process would be more energetically sustainable than a conventional melt synthesis.

4.5 References

[1] H.J. Arpe, *Ullmann's Encyclopedia of Industrial Chemistry, Ullmann's Encyclopedia of Industrial Chemistry: Set: Printed Fifth Edition plus Sixth Edition Electronic Release*, Wiley, **1999**

[2] F.W. Lichtenthaler, *Carbohydrates as Organic Raw Materials*, Ullmann's Encyclopedia of Industrial Chemistry, Wiley-VCH Verlag GmbH & Co. KGaA, **2000**.

[3] C.B. Frech, *Journal of Chemical Education*, 79, **2002**, p. 1072

[4] M.N. Belgacem, A. Gandini, *Monomers, Polymers and Composites from Renewable Resources*, Elsevier Science, **2011**

[5] P.B. Smith, R.B. Gross, *Biobased Monomers, Polymers, and Materials*, OUP USA, **2013**

[6] A.R.A. Palmans, A. Heise, *Enzymatic Polymerisation*, Springer Berlin Heidelberg, Berlin, **2010**

[7] R.A. Gross, M. Ganesh, W. Lu, *Trends in Biotechnology*, 28, **2010**, p. 435

[8] M.F. Kemmere, T. Meyer, *Supercritical carbon dioxide in polymer reaction engineering / edited by Maartje F. Kemmere and Thierry Meyer*, Wiley-VCH, **2005**

[9] F. Picchioni, *Polymer International*, 63, **2014**, p. 1364

[10] E. Kiran, *The Journal of Supercritical Fluids*, 110, **2016**, p. 126

[11] A. Pellis, L. Corici, L. Sinigoi, N. D'Amelio, D. Fattor, V. Ferrario, C. Ebert, L. Gardossi, *Green Chemistry*, 17, **2015**, p. 1756

[12] N. Cordeiro, N.M. Belgacem, A. Gandini, C. Pascoal Neto, *Bioresource Technology*, 63, **1998**, p. 153

[13] A. Gandini, C. Pascoal Neto, A.J.D. Silvestre, *Progress in Polymer Science*, 31, **2006**, p. 878

[14] A. Gandini, *Macromolecules*, 41, **2008**, p. 9491

[15] T.R. Curlee, S. Das, U.S.E.P. Agency, *Plastic Wastes: Management, Control, Recycling, and Disposal*, Noyes Data Corporation, **1991**

[16] V. Siracusa, P. Rocculi, S. Romani, M.D. Rosa, *Trends in Food Science & Technology*, 19, **2008**, p. 634

[17] B.D. Ulery, L.S. Nair, C.T. Laurencin, *Journal of Polymer Science Part B: Polymer physics*, 49, **2011**, p. 832

[18] M. Eriksson, L. Fogelström, K. Hult, E. Malmström, M. Johansson, S. Trey, M. Martinelle, *Biomacromolecules*, 10, **2009**, p. 3108

[19] M. Eriksson, K. Hult, E. Malmström, M. Johansson, S.M. Trey, M. Martinelle, *Polymer Chemistry*, 2, **2011**, p. 714

[20] S. Torron, S. Semlitsch, M. Martinelle, M. Johansson, *Macromolecular Chemistry and Physics*, 215, **2014**, p. 2198

[21] A. Rüdiger, P. Hendil-Forssell, C. Hedfors, M. Martinelle, S. Trey, M. Johansson, *Journal of Renewable Materials*, 1, **2013**, p. 16

[22] A.D. McNaught, A. Wilkinson, *IUPAC. Compendium of Chemical Terminology, 2nd ed. (the "Gold Book)*, Blackwell Scientific Publications, Oxford, **1997**

[23] M.A. Tasdelen, M.U. Kahveci, Y. Yagci, *Progress in Polymer Science*, 36, **2011**, p. 455

[24] J. Ren, X. Hua, T. Zhang, Z. Zhang, Z. Ji, N. Gu, *Journal of Applied Polymer Science*, 121, **2011**, p. 210
[25] H. Keul, A. Neumann, B. Reining, H. Höcker, *Macromolecular Symposia*, 161, **2000**, p. 63
[26] N. Simpson, M. Takwa, K. Hult, M. Johansson, M. Martinelle, E. Malmström, *Macromolecules*, 41, **2008**, p. 3613
[27] M. Eriksson, *PhD Thesis*, School of Biotechnology, KTH Royal Insitute of Technology, Stockholm, **2010**
[28] A. Duda, *Macromolecules*, 27, **1994**, p. 576
[29] S. Torron, M. Johansson, *Journal of Polymer Science Part A: Polymer Chemistry*, 53, **2015**, p. 2258
[30] S. Semlitsch, S. Torron, M. Johansson, M. Martinelle, *Green Chemistry*, **2016**, p.
[31] F.J.C. Roe, E. Boyland, K. Millican, *Food and Cosmetics Toxicology*, 3, **1965**, p. 277
[32] A.P. de Groot, V.J. Feron, H.P. Til, *Food and Cosmetics Toxicology*, 11, **1973**, p. 19
[33] World Health Organization, *Tin and Inorganic Tin Compounds:* **2005**
[34] J. Zhang, H. Shi, D. Wu, Z. Xing, A. Zhang, Y. Yang, Q. Li, *Process Biochemistry*, 49, **2014**, p. 797
[35] P. Dubois, O. Coulembier, J.M. Raquez, *Handbook of Ring-Opening Polymerization*, Wiley, **2009**
[36] G. Montaudo, P. Rizzarelli, *Polymer Degradation and Stability*, 70, **2000**, p. 305
[37] D.N. Bikiaris, G.Z. Papageorgiou, D.S. Achilias, *Polymer Degradation and Stability*, 91, **2006**, p. 31
[38] G.Z. Papageorgiou, D.N. Bikiaris, *Biomacromolecules*, 8, **2007**, p. 2437
[39] G.Z. Papageorgiou, D.N. Bikiaris, D.S. Achilias, S. Nanaki, N. Karagiannidis, *Journal of Polymer Science Part B: Polymer Physics*, 48, **2010**, p. 672
[40] F.C. Loeker, C.J. Duxbury, R. Kumar, W. Gao, R.A. Gross, S.M. Howdle, *Macromolecules*, 37, **2004**, p. 2450
[41] A. Olsson, M. Lindström, T. Iversen, *Biomacromolecules*, 8, **2007**, p. 757
[42] J. Zhou, W. Wang, S. Villarroya, K.J. Thurecht, S.M. Howdle, *Chemical Communications*, **2008**, p. 5806
[43] Y. Jiang, A.J. Woortman, G.O. van Ekenstein, K. Loos, *Biomolecules*, 3, **2013**, p. 461
[44] L. Gustini, B.A.J. Noordover, C. Gehrels, C. Dietz, C.E. Koning, *European Polymer Journal*, 67, **2015**, p. 459
[45] Y. Poojari, S.J. Clarson, *Biocatalysis and Agricultural Biotechnology*, 2, **2013**, p. 7
[46] C. Japu, A. Martinez de Ilarduya, A. Alla, Y. Jiang, K. Loos, S. Munoz-Guerra, *Biomacromolecules*, 16, **2015**, p. 868
[47] F. Zhan, A. Asif, J. Liu, H. Wang, W. Shi, *Polymer*, 51, **2010**, p. 3402
[48] Z. Zhang, Y.P. Handa, *Macromolecules*, 30, **1997**, p. 8505
[49] D. Gourgouillon, H.M.N.T. Avelino, J.M.N.A. Fareleira, M. Nunes da Ponte, *The Journal of Supercritical Fluids*, 13, **1998**, p. 177
[50] P. Alessi, A. Cortesi, I. Kikic, F. Vecchione, *Journal of Applied Polymer Science*, 88, **2002**, p. 2189
[51] S.A.E. Boyer, J.P.E. Grolier, *Pure and Applied Chemistry*, 77, **2005**, p. 593

[52] C.A. Kelly, A. Naylor, L. Illum, K.M. Shakesheff, S.M. Howdle, *Advanced Functional Materials*, 22, **2012**, p. 1684
[53] M. Lee, C. Tzoganakis, C.B. Park, *Polymer Engineering & Science*, 38, **1998**, p. 1112
[54] Z. Zhang, Y.P. Handa, *Journal of Polymer Science Part B: Polymer Physics*, 36, **1998**, p. 977
[55] J.M.D. Joseph R. Royer, Saad A. Khan, *Journal of Polymer Science Part B: Polymer Physics*, 39, **2001**, p. 3055
[56] R. Pini, G. Storti, M. Mazzotti, H. Tai, K.M. Shakesheff, S.M. Howdle, *Journal of Polymer Science Part B: Polymer Physics*, 46, **2008**, p. 483
[57] L. Yu, H. Liu, L. Chen, *Polymer Engineering & Science*, 49, **2009**, p. 1800
[58] C. Gutiérrez, M.T. Garcia, S. Curia, S.M. Howdle, J.F. Rodriguez, *The Journal of Supercritical Fluids*, 88, **2014**, p. 26
[59] S. Curia, D.S.A. De Focatiis, S.M. Howdle, *Polymer*, 69, **2015**, p. 17
[60] J. Jennings, M. Beija, J.T. Kennon, H. Willcock, R.K. O'Reilly, S. Rimmer, S.M. Howdle, *Macromolecules*, 46, **2013**, p. 6843
[61] S.Y. Lee, P. Valtchev, F. Dehghani, *Green Chemistry*, 14, **2012**, p. 1357
[62] F. Stassin, O. Halleux, R. Jérôme, *Macromolecules*, 34, **2001**, p. 775
[63] P. Lozano, E. García-Verdugo, J.M. Bernal, D.F. Izquierdo, M.I. Burguete, G. Sánchez-Gómez, S.V. Luis, *ChemSusChem*, 5, **2012**, p. 790
[64] D.L. Sparks, R. Hernandez, L.A. Estévez, N. Meyer, T. French, *Journal of Chemical & Engineering Data*, 52, **2007**, p. 1246
[65] J. Sun Yu, A. Keun Kim, *Journal of Biomedical Science*, 17, **2010**, p. 1
[66] G.Z. Papageorgiou, D.N. Bikiaris, D.S. Achilias, N. Karagiannidis, *Macromolecular Chemistry and Physics*, 211, **2010**, p. 2585
[67] G.Z. Papageorgiou, D.N. Bikiaris, D.S. Achilias, E. Papastergiadis, A. Docoslis, *Thermochimica Acta*, 515, **2011**, p. 13
[68] A.M. Allgeier, N. DeSilva, E. Korovessi, C. Menning, J.C. Ritter, S.K. Sengupta, C.S. Stauffer, Patent *Process for preparing 1,6-hexanediol"*, **2013**
[69] J. Tuteja, H. Choudhary, S. Nishimura, K. Ebitani, *ChemSusChem*, 7, **2014**, p. 96
[70] V.J. Murphy, E.L. Dias, J.A.W. Shoemaker, Patent *Production of 1,6-hexanediol from adipic acid"*, **2015**
[71] K. Chyliński, J. Gregorowicz, *The Journal of Chemical Thermodynamics*, 30, **1998**, p. 1131
[72] P. Licence, W.K. Gray, M. Sokolova, M. Poliakoff, *Journal of the American Chemical Society*, 127, **2005**, p. 293
[73] J. Jennings, M. Beija, A.P. Richez, S.D. Cooper, P.E. Mignot, K.J. Thurecht, K.S. Jack, S.M. Howdle, *Journal of the American Chemical Society*, 134, **2012**, p. 4772
[74] H.E. Gottlieb, V. Kotlyar, A. Nudelman, *The Journal of Organic Chemistry*, 62, **1997**, p. 7512
[75] A. Barclay, *Master Thesis*, School of Chemistry, The University of Nottingham, Nottingham, **2015**
[76] T. Yamada, Y. Imamura, *Polymer Engineering & Science*, 28, **1988**, p. 381
[77] W.-C. Lai, W.-B. Liau, T.-T. Lin, *Polymer*, 45, **2004**, p. 3073
[78] L. Mandelkern, *Crystallization of Polymers: Volume 1, Equilibrium Concepts*, Cambridge University Press, **2002**
[79] P.C. Ashman, C. Booth, *Polymer*, 14, **1973**, p. 300
[80] M.J. Fraser, D.R. Cooper, C. Booth, *Polymer*, 18, **1977**, p. 852

[81] X. Kong, H. Qi, J.M. Curtis, *Journal of Applied Polymer Science*, 131, **2014**, p. 1
[82] Y. Huang, X. Xu, X. Luo, D. Ma, *Chinese Journal of Polymer Science*, 20, **2002**, p. 45
[83] J.L. Schuchardt, Patent US4970295 A,*"Preparation of oxetane polyether polyols using a bleaching earth catalyst"*, **1990**
[84] L. Li, *MALDI Mass Spectrometry for Synthetic Polymer Analysis*, Wiley, **2009**
[85] M. Castano, K.S. Seo, K. Guo, M.L. Becker, C. Wesdemiotis, J.E. Puskas, *Polymer Chemistry*, 6, **2015**, p. 1137
[86] R.A. Gross, A. Kumar, B. Kalra, *Chemical Reviews*, 101, **2001**, p. 2097
[87] Novozymes Biopharma DK A/S, *Enzymes for biocatalysis for smarter chemical synthesis: Immobilized Lipases*, **2014**
[88] E. Rubio, J. Almaral, R. Ramírez-Bon, V. Castaño, V. Rodríguez, *Optical Materials*, 27, **2005**, p. 1266
[89] J.C. Salamone, *Polymeric Materials Encyclopedia, Twelve Volume Set*, Taylor & Francis, **1996**
[90] A. Streitwieser, C.H. Heathcock, E.M. Kosower, *Introduction to Organic Chemistry*, Macmillan, **1992**
[91] M. Szycher, *High Performance Biomaterials: A Complete Guide to Medical and Pharmceutical Applications*, Taylor & Francis, **1991**
[92] M.E. Rogers, T.E. Long, *Synthetic Methods in Step-Growth Polymers*, Wiley, **2003**

5 Towards sustainable polymeric nano-carriers and surfactants: facile low temperature enzymatic synthesis of bio-based amphiphilic copolymers in $scCO_2$

In the last two decades, the research trends in the field of amphiphilic block copolymers have been shifted towards the use of renewable monomers, but only a few alternatives have so far been reported [1-3].

The author postulated that the low temperature enzymatic approach described in Chapter 4 could provide an innovative methodology for the production of valuable bio-based amphiphilic copolymers.

Therefore, this chapter demonstrates the preparation of renewable amphiphilic ABA copolymers composed of a semicrystalline hydrophobic segment based on azelaic acid and 1,6-hexanediol.

Azelaic acid and 1,6-hexanediol will be enzymatically polymerised to prepare polyester chains with targeted molecular weight and end-capped with methoxy poly(ethylene glycol) (MPEG) in a one-pot high pressure reaction.

The block copolymers will be characterised by ^{1}H-NMR, GPC and DSC in order to carefully assess their structural and thermal properties.

The self-assembly of these polymers in aqueous environment will be investigated through DLS, TEM and UV-Vis studies. Incorporation of highly hydrophobic Coumarin-6 will be used as a model to prove dispersion in water of lipophilic molecules.

In addition, maximum bubble pressure tests will be used to probe the reduction in surface tension of these polymers and comparisons will be made directly to commercial polymeric non-ionic surfactants.

The results presented in this chapter are summarised in the paper:

S. Curia and S.M. Howdle, "Towards sustainable polymeric nano-carriers and surfactants: facile low temperature enzymatic synthesis of bio-based amphiphilic copolymers in $scCO_2$", *Polymer Chemistry* (7), **2016**, 2130-2142

5.1 Introduction

5.1.1 Amphiphilic block copolymers: an overview

The large-scale production of amphiphilic block copolymers began in the 1950s, and these interesting macromolecules continue to attract considerable attention [3-7]. Amphiphilic block copolymers can self-assemble into different nanostructures in aqueous environment; *e.g.* micelles, wormlike micelles (also called cylindrical/rod-like micelles) and vesicles (known as polymersomes) [8]. The self-assembly of amphiphilic block copolymers in aqueous environment is based on hydrophobic interactions between the lipophilic segments of the polymer chains. This ensures minimal contact of the hydrophobic molecules with the polar medium [5].

Several parameters have an influence on the morphology and size of the structure formed upon aggregation. For instance, the mass (or volume) fraction of the hydrophilic block, the interaction parameter of the hydrophobic block with water and its degree of crystallinity are known to be critical parameters that can drive the self-assembly towards a particular structure and determine its size [5, 8-10]. Typically, the morphology of the aggregates can be predicted from the packing parameter p, Equation (5.1):

$$p = \frac{v}{a \times L} \qquad (5.1)$$

Where v is the hydrophobic volume, a is the cross-sectional area of the hydrophilic group and L is the length of the hydrophobic segment. In general, spherical micelles are observed for $p \approx 1/3$, cylindrical micelles for $p \approx 1/2$ and vesicles for $p \approx 1$.

Polymeric nanoparticles can find application as drug encapsulation and delivery systems and also in formulations as wetting agents, compatibilisers, emulsifiers and detergents [3-6, 8, 11-18]. For example, polymeric micelles are characterised

by a core-shell structure and have emerged as potential carriers for highly hydrophobic molecules because these can be encapsulated in the lipophilic core of the micelles (Figure 5.1) [4, 6, 16].

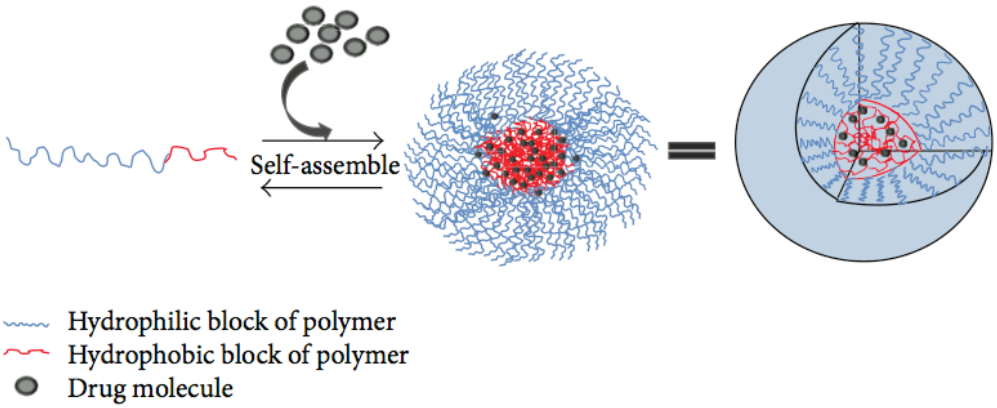


Figure 5.1 – Schematic of formation and drug loading of polymeric micelles by self-assembly of the chains in water [15].

Di-block, multi-block and graft amphiphilic copolymers are capable of forming micelles (Figure 5.2).

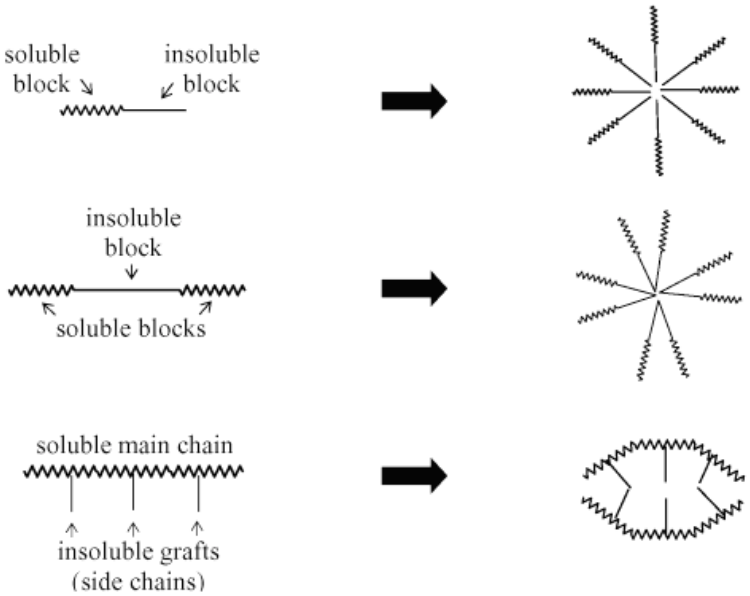


Figure 5.2 – Formation of micelles from di-block, multi-block and graft copolymers [19].

Polymeric vesicles (or polymersomes) are hollow spherical aggregates that contain an aqueous environment in the core surrounded by a bi-layer membrane

(Figure 5.3). The core of the polymersome can be utilised to encapsulate hydrophilic molecules, whilst the membrane can contain lipophilic molecules within its inner part [8].

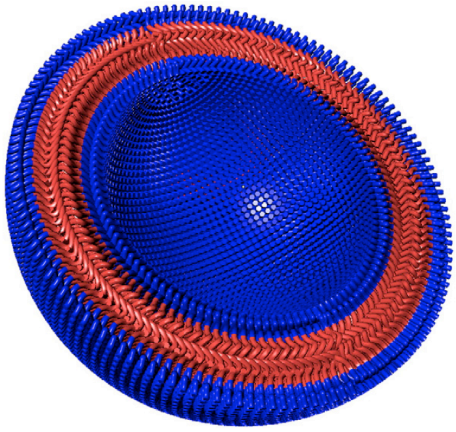


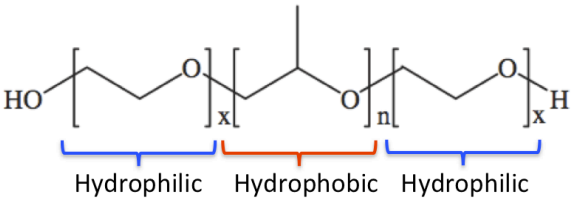
Figure 5.3 – Schematic depiction of a 3D cross-section of a polymersome bi-layer membrane based on a diblock copolymer. The hydrophilic portions (blue) form the internal and external part of the membrane; the lipophilic segment (red) constitutes the internal part of the membrane [8].

The hydrophilic segment of amphiphilic copolymers is responsible for stabilisation of the self-assembled nanostructures in aqueous environments and is normally made of poly(ethylene glycol) (PEG) [2-4, 7, 15], which has many advantages, such as high hydrophilicity, flexibility and biocompatibility [2].

In addition to this, recently the production of bio-based PEGs (or bio-PEGs) with varied molecular weights has been reported by Acme-Hardesty Co. (a US-based renewable chemicals distributor) [20, 21]. These PEGs are certified with the "United States Department of Agriculture (USDA) Biobased Product" label and are derived from sugarcane waste (*i.e.* bagasse). Thus, PEG can now be considered not only a safe and biocompatible material, but also a potentially green and sustainable choice. Furthermore, PEGs with molecular weight lower than 4000 g mol^{-1} were found to be biodegraded by many bacteria, so they do not accumulate in the environment [22].

The hydrophobic core of polymeric micelles is made of lipophilic polymers, such as poly(propylene glycol) (PPG). Multiblock ABA copolymers containing PPG and PEG (commercially known as Pluronic®, Figure 5.4) can spontaneously

organise into micelles and, hence, have been widely investigated for medical applications [6].



PEG-*b*-PPG-*b*-PEG

Figure 5.4 – Generic structure of a Pluronic: the central block (PPG) is lipophilic whilst the lateral ones (PEG) are hydrophilic.

Nonetheless, Pluronics display slow biodegradability under physiological conditions and they can accumulate in the body [23]. For this reason, an important prerequisite for a non-degradable or poorly degradable polymer, to be used as a drug carrier, is a molecular weight sufficiently low to allow for excretion *via* the renal route [24]. In more detail, all molecules with molecular weight greater than 10 kg mol^{-1} experience more and more restriction to renal filtration [25]; whereas, PEGs with molecular weight lower than 1 kg mol^{-1} are rapidly removed from the body [26]. However, Pluronics with a small PPG block are generally characterised by a fairly high (0.01-10% wt) critical aggregation concentration (CAC) due to the weak hydrophobicity of the PPG block: this means that the nanostructures are highly unstable and the micelles are likely to dissociate upon dilution (*i.e.* after injection in the body) [4, 23]. On the contrary, a low CAC ensures that the aggregated structure is retained in the bloodstream.

For these reasons, biodegradable polyesters such as poly(lactic acid) (PLA), poly(lactic-*co*-glycolic acid) (PLGA), and poly(caprolactone) (PCL) have been investigated extensively as hydrophobic segments in combination with PEG for the preparation of amphiphilic polymers that can be more easily eliminated from the body. These materials also show a higher CAC, as a result of the increased hydrophobicity of PLA and PCL compared to that of PPG [2, 7, 11, 14, 23]. Moreover, the incorporation of a hydrolytically degradable block in the structure automatically ensures a faster elimination from the body upon degradation of the polyester segment [23].

However, the synthesis of these polymers is typically carried out using high temperatures (normally ~80 °C for MPEG-PCL and ≥110 °C for MPEG-PLA copolymers) [2, 11], tin-based catalysts, and isocyanates as coupling molecules if a multi-block structure is desired (Figure 5.5) [1, 7, 13, 27]. All these factors are clearly far from being safe and ideal from a green chemistry point of view.

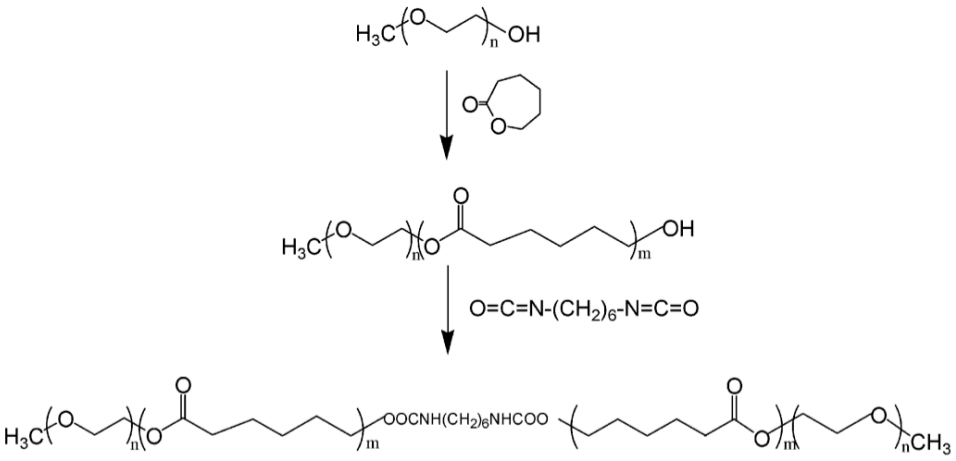


Figure 5.5 – Synthetic scheme showing a typical process employed for the synthesis of PEG-PCL-PEG copolymers [11]. Tin octanoate is normally used as a catalyst at a temperature of 80 °C (or higher) and hexamethylene diisocyanate is used as a coupling molecule. Hence, several factors of this kind of processes do not match with the commonly accepted green chemistry criteria.

To sum up, the ideal amphiphilic copolymer, to satisfy societal need for drug delivery and medical applications through to detergents and surfactants for home and personal care, must meet specific fundamental requirements. In particular, low toxicity, biodegradability and biocompatibility, whilst also having the desired amphiphilic characteristics and an appropriate CAC.

Accordingly, there has been an increasing focus on the use of renewable raw materials for the production of amphiphilic copolymers [2, 3, 28, 29]. This arises not only from future supply constraints for fossil-base resources, but also as a response to a strong market and customer demand to increase the overall sustainability of materials and processes and to lower the carbon footprint [3]. Naturally occurring and bio-derived molecules are fundamental resources that can be employed to achieve a more sustainable plastic industry and lead to polymers that are intrinsically biodegradable (*e.g.* polyesters) [30-32], which is a strong added value for medical materials.

Therefore, it is clear that the design of new sustainable synthetic routes, which can lead to the preparation of useful bio-based amphiphilic copolymers, could be an important step forward in modern polymer science.

5.1.1.1 Polymeric nanoparticles preparation

Depending on the properties of the block copolymer to be used, different procedures can be used to prepare empty and drug-loaded polymeric particles. Several papers and books describe these methodologies in-depth [5, 6, 15, 18, 33, 34], hence the present section will briefly outline the essential concepts and some more practical details.
Two different approaches can be identified:

a) Direct dissolution: this process involves the dissolution of the polymer (along with the drug when needed) in water and subsequent stirring for an appropriate amount of time. This methodology is normally used for highly hydrophilic copolymers, such as Pluronics with a fairly short PPG block [5]. A thermal treatment might be required to aid the self-assembly and help the initial dissolution.

b) Dissolution in a water-miscible organic solvent: this approach is more common and is normally used for all those amphiphilic copolymers that are not directly soluble in water. A water-miscible organic solvent (*i.e.* THF, acetone, DMF, DMSO *etc.*) is used to solubilise the polymer and the drug. Then, this solution can be either dialysed against water (dialysis) or dropped slowly into water whilst stirring (nano-precipitation). Complete solvent removal is ensured by several dialysis cycles (in the former case) or by gentle heating and application of reduced pressure (in the latter case) [5, 7].

Other methodologies can be employed (*e.g.* melting/sonication *etc.*) and can be more appropriate depending on the final application and the chemico-physical properties of the copolymer/drug system. In-depth description of these

methodologies is beyond the scope of this thesis and more detailed information can be found in the specific literature of the field [4, 14, 35].

5.1.1.2 Critical Aggregation concentration (CAC)

As aforementioned, the CAC - also known as Critical Micellar Concentration (CMC), if only micelles form upon aggregation - is an important characteristic of a surfactant.

For simplicity, the formation of micelles and the CMC will be described in more detail, but an equivalent description applies for the CAC and the formation of different aggregates, such as vesicles.

Below the CMC the surfactant molecules are first partitioned at the liquid-air interface and then, at higher concentration (when the surface is saturated and still below the CMC), some of them will be individually dispersed in the liquid phase. Eventually, upon reaching the CMC, the surfactants will aggregate in micelles and any further addition will result in an increased number of micelles (Figure 5.6).

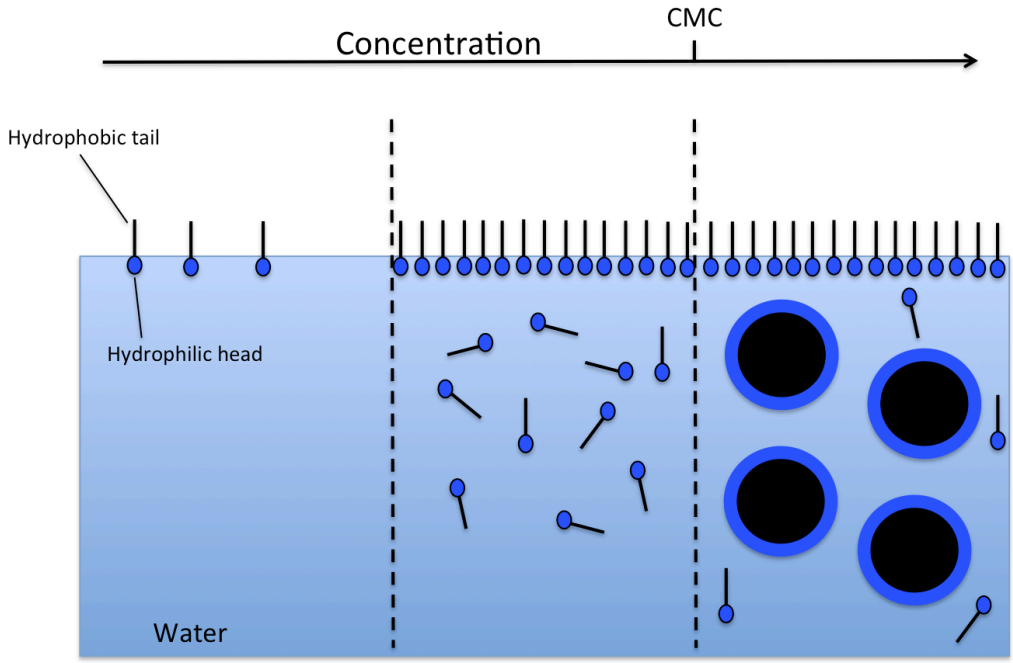


Figure 5.6 – Schematic illustration of micelle formation with increasing concentration. The formation of micelles does not exclude the presence of individual surfactants in solution. Note that this is just a depiction: micelles are dynamic species so they do not have a rigid structure with defined shape, although an average micellar shape can be defined and determined.

The CMC of classic low molecular weight surfactants is typically quite high (normally in the range from 10^{-3} to 10^{-4} M) and, hence, it can be determined easily by light scattering. In principle this technique is also applicable to block copolymers, however the much lower CAC/CMC of polymeric non-ionic surfactants (generally around 10^{-5} - 10^{-6} M) makes the application of light scattering more challenging and complicated (*i.e.* the CAC often falls below the sensitivity of the instruments) [6, 15].

For this reason, a preferred method involves the use of hydrophobic light emitting/absorbing probes that can be partitioned into the hydrophobic portions of the aggregated structures and change their optical properties depending on the environment [1, 4]. Examples are molecules like pyrene and 1,6-diphenyl-1,3,5-hexatriene (DPH) that are almost non-absorbing in water, but exhibit a strong emission/absorption when the self-assembled structures form, since they are partitioned in the hydrophobic regions [36]. The chemical structure of DPH is shown (Figure 5.7).

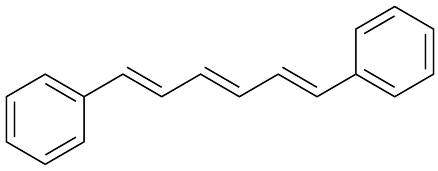


Figure 5.7 – Chemical structure of 1,6-diphenyl-1,3,5-hexatriene (DPH). This molecule is practically non-fluorescent/absorbing in water, whilst it shows a strong emission/absorption when intercalated into bi-layer membranes of vesicles or encapsulated in the hydrophobic core of micelles [36].

Fluorescence spectroscopy or ultraviolet-visible (UV-Vis) spectroscopy can be used to detect the abrupt increase in emission/absorption when increasing the polymer concentration at a fixed dye loading (normally extremely low, typically in the range of 10^{-7} - 10^{-6} M) and, hence, determine the CAC by extrapolation of the intensities at high and low polymer concentrations (Figure 5.8) [1, 6].

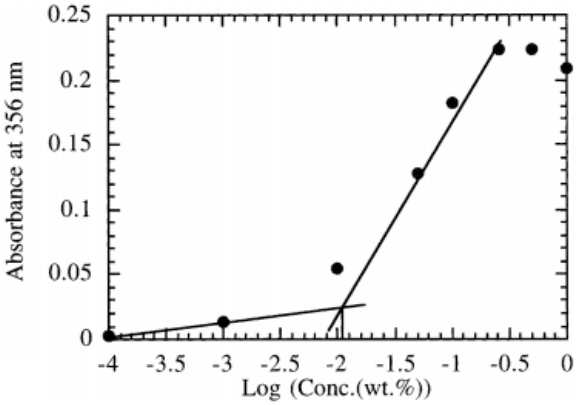


Figure 5.8 – Determination of CAC for a PEG-polyester-PEG copolymer by extrapolation method. The absorption of DPH was recorded when changing the polymer concentration at a fixed dye loading [1].

5.1.1.3 Characteristic size

The diameter of spherical polymeric micelles ranges from a few nm (2-3) up to 200 nm, and their small size is undoubtedly one of the most interesting features [6, 28, 33]. Not only does this afford high efficiency of penetration and diffusivity in the capillaries, but also it permits elimination of microorganisms by simple filtration of the formulation [4]. In fact, a micro-filter with pore size of 0.22 μm will effectively remove microorganisms (*e.g.* bacteria and fungi) [37], which typically have size ranging from 0.3 μm to few μm.

In general, micellar size depends on several factors, including polymer molecular weight, proportion of hydrophilic to hydrophobic chains, hydrophobicity of the apolar block, crystallinity *etc.* [4, 5, 38]. For instance, for a hydrophobic ratio ($M_n^{hydrophobic}/M_n^{hydrophilic}$) higher than 1, micelles with an amorphous hydrophobic core are generally characterised by a larger diameter (Figure 5.9). This was explained in terms of packing into tight crystalline regions in the case of semi-crystalline cores, which resulted in a smaller size [38]. Furthermore, the preparation methodology and the organic solvent used to dissolve the polymer can affect the micellar dimension as well [4].

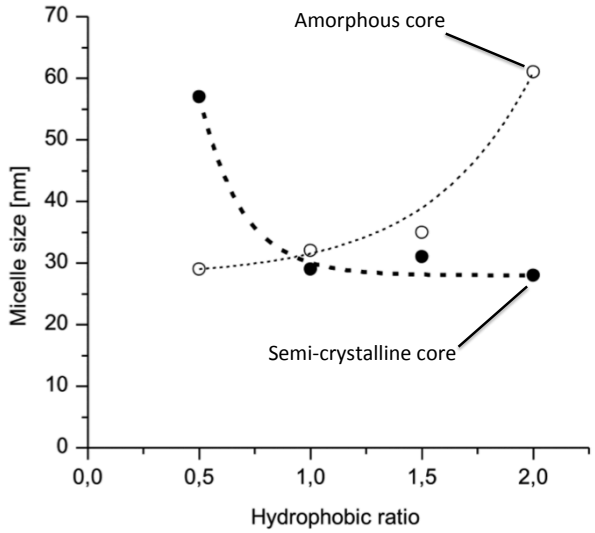


Figure 5.9 – Trends in micelles size observed for copolymers with a semi-crystalline core (filled circles) and amorphous core (empty circles) *vs* hydrophobic ratio. The size of the hydrophilic block was held constant and the hydrophobic one was varied. Graph adapted from reference [38].

On the contrary, polymersomes are typically much bigger aggregates. Depending on the characteristics of the copolymer and the technique employed for their preparation, the diameter of polymeric vesicles can range from 50 nm up to around 10-50 μm [8, 39].

Several methodologies can be employed to determine the size of polymeric nanoparticles with dynamic light scattering (DLS), atomic force microscopy (AFM) and transmission electron microscopy (TEM) the most widely used techniques for the analysis of particles with small diameters. Polymersomes with a diameter larger than 1 μm are also suitable for optical microscopy investigations [8].

However, it is important to emphasise how the use of only one technique does not give a thorough description of the real nature of the sample. In fact, light scattering gives information on the distribution of hydrated micelle but the intensity signal collected by the instrument is intrinsically dependent on size (although, mathematical data processing can be used to obtain volume and number distributions with the hypothesis of perfectly spherical particles); on the other hand, electron microscopies give a direct insight on aggregation, shape and size of single dry micelles, but these are not bulk techniques. Therefore, a

combination of scattering and microscopy must be used in order to obtain a detailed picture of the sample.

5.1.2 Low temperature enzymatic synthesis of bio-based amphiphilic copolymers: aims of the study

The previous chapter focussed on the utilisation of $scCO_2$ to prepare a range of green functional materials with targeted degree of polymerisation (DP) through enzymatic syntheses at near-room-temperature conditions and without pre-modification of the monomers (see Chapter 4 and reference [40]).

Here the aim is to extend this approach to the synthesis of novel green amphiphilic copolymers based on azelaic acid, 1,6-hexanediol and PEG in $scCO_2$.

As previously said, azelaic acid is a bio-based dicarboxylic acid with antibacterial and anti-inflammatory properties [41-45]. In addition, its high hydrophobicity and the crystallinity of the polyester chains obtained by copolymerising this diacid with 1,6-hexanediol could impart interesting properties for the preparation of amphiphilic copolymers for medical purposes and other applications.

Therefore, here we will focus on determining if the novel approach described in Chapter 4 can be used to obtain amphiphilic copolymers through low temperature enzymatic polycondensations, targeting the molecular weight of the chains by using end-cappers of methoxy poly(ethylene glycol) (MPEG) with two different molecular weight (350 and 550 g mol^{-1} respectively).

Amphiphilic copolymers will be prepared directly from the diacid/diol and characterised through ^{1}H and ^{13}C-NMR and differential scanning calorimetry (DSC) to assess the structural and thermal properties. Their self-assembly in water will be investigated through dynamic light scattering (DLS), transmission electron microscopy (TEM) and ultraviolet-visible spectroscopy (UV-Vis) to assess if the polymers can form useful nanostructured aggregates. Finally, maximum bubble pressure tests will be performed to examine the reduction in surface tension of these novel copolymers.

5.2 Experimental

5.2.1 Materials

Azelaic acid (98%) was purchased from Alfa Aesar (UK) and dried for 24 h under vacuum (100 mbar) at 50 °C before use; 1,6-hexanediol (97%) was purchased from Sigma Aldrich (UK) and dried at room temperature (RT) for 24 h under vacuum (100 mbar) before use. MPEG550 (M_n~550 g mol^{-1}) and MPEG350 (M_n~350 g mol^{-1}) were purchased from Sigma Aldrich (UK) and stored over fresh molecular sieves (4Å, particle size 1.6-2.5 mm) at RT. Tween® 20 (PEG sorbitan monolaurate, M_n~1200 g mol^{-1}) and Pluronic® L-121 (PEG-*b*-PPG-*b*-PEG, M_n~4500 g mol^{-1}) were used as received. Coumarin-6 (98%) and 1,6-diphenyl-1,3,5-hexatriene (98%) were purchased from Sigma Aldrich (UK) stored in the dark at RT and used as received. Novozym 435 (*Candida antarctica* Lipase B (CaLB) immobilised on cross-linked acrylic resin beads) was kindly donated by Novozymes (Denmark) stored at 4 °C and dried for 24 h under vacuum (100 mbar) at RT before use. All the solvents were of analytical grade, or Chromasolv® were specified, purchased from Sigma Aldrich (UK) and used as received. Millipore water (18.2 MΩ.cm, <5 ppb TOC) dispensed through a 0.22 μm filter was used for the preparation of all the polymer dispersions in water. Supercritical Fluid Chromatography (SFC) grade 4.0 CO_2 (minimum purity 99.99%) was purchased from BOC Special Gases (UK) and used as received.

5.2.2 Methods

5.2.2.1 Enzymatic synthesis MPEG-b-PHAz-b-MPEG

In a typical procedure the diacid (3.40 mmol), diol (DP6: 2.91 mmol; DP3: 2.55 mmol) and MPEG550 or MPEG350 (DP6: 0.97 mmol; DP3: 1.70 mmol) were

added to the stainless steel reaction autoclave (20 mL) [46, 47], along with enzyme and fresh molecular sieves (3 Å, particle size 1.6-2.5 nm) (10% by weight of enzyme beads and 25% of molecular sieves relative to the total amount of monomers and MPEG). An excess of diacid was used to ensure the synthesis of diacid terminated PHAz blocks (since the MPEG chains can react only with the carboxylic acid moieties).

The vessel was sealed and pressurised up to 50 bar. The temperature was then raised to 35 °C, the pressure stabilised at 275 bar and the reaction left to run for 24 h while stirring at 100 rpm. To avoid polymer foaming and consequent tubing blockages [48], the reactions were stopped by cooling the vessel in a water/ice bath (0 °C) and the CO_2 was vented when the pressure went below 20 bar. Finally, the product was dissolved in 6 mL of toluene (gently heating at 40 °C to melt any residual unreacted 1,6-hexanediol and, thus, retain information on conversion) and filtered to remove the enzyme and sieves. Filtered solutions were dried at 40 °C under reduced pressure leaving white solid-waxy polymeric products. Product yield was calculated by dividing the dry product mass by the theoretical mass (^{1}H-NMR analyses showed that the amount of unreacted species was negligible) [49-51].

The nomenclature used in this chapter is detailed in Table 5.1.

Table 5.1 - Nomenclature and letter scheme of the ABA copolymers presented in this study. The variables are the length of the MPEG block used for end-capping and the targeted molecular weight of the PHAz synthesised during the enzymatic polymerisation.

	Structure	M_n^{MPEG} (g mol^{-1})[a]	M_n^{PHAz} (g mol^{-1})[b]
(a)	$MPEG_{12}$-$PHAz_3$-$MPEG_{12}$	550	967
(b)	$MPEG_{12}$-$PHAz_6$-$MPEG_{12}$	550	1778
(c)	$MPEG_7$-$PHAz_3$-$MPEG_7$	350	967
(d)	$MPEG_7$-$PHAz_6$-$MPEG_7$	350	1778

[a]Declared by supplier; [b]Theoretical targeted M_n.

The reaction scheme is shown (Figure 5.10).

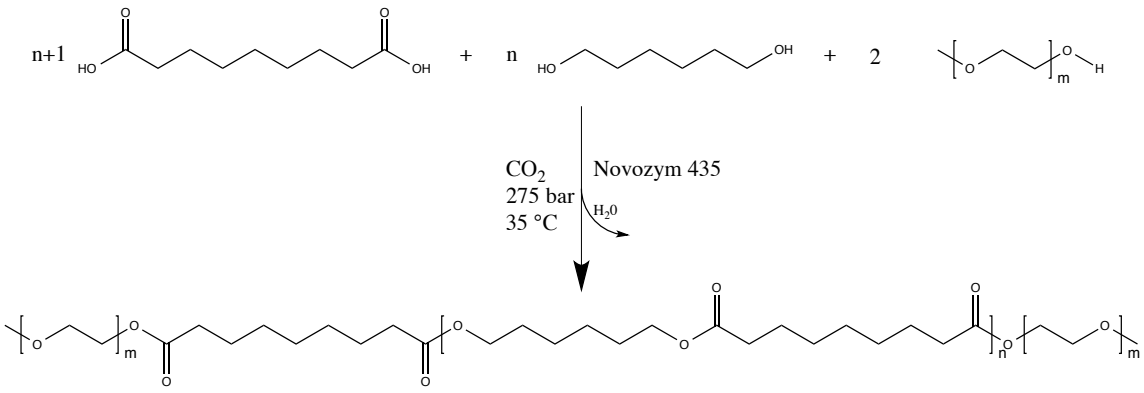


Figure 5.10 - Lipase-catalysed synthesis from azelaic acid, 1,6-hexandiol and MPEG to MPEG-*b*-PHAz-*b*-MPEG in scCO$_2$. An excess of azelaic acid was used in order to obtain an ABA-type block copolymer (azelaic acid used as a linker).

5.2.2.2 ^{1}H and ^{13}C-NMR analysis

NMR analyses were conducted on a Bruker Avance III 500 spectrometer in $CDCl_3$ or D_2O (20 mg mL^{-1}). The number of scans was 16 for ^{1}H (500 MHz) and 4096 for ^{13}C (125 MHz). The chemical shifts were reported in parts per million (ppm) with respect to residual solvent peaks (7.26 ppm for ^{1}H and 77.36 ppm for ^{13}C in $CDCl_3$, 4.80 ppm for ^{1}H in D_2O) [52]. Extent of functionalisation and chain length were analysed through end-group analysis.

For increased clarity, the ^{1}H-NMR and the structure (with labels) for polymer (b) $MPEG_{12}$-$PHAz_6$-$MPEG_{12}$ are displayed (Figure 5.11).

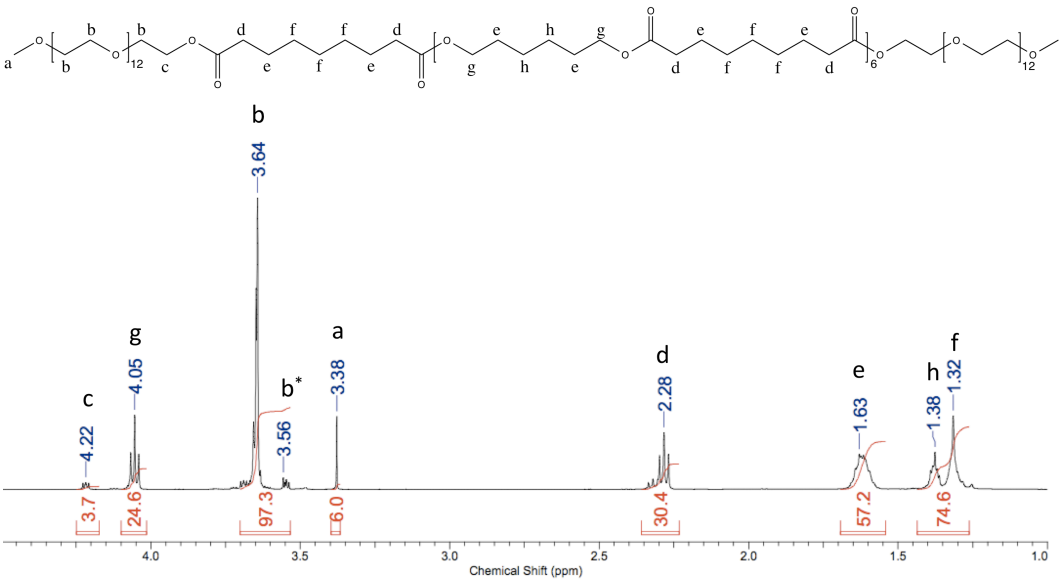


Figure 5.11 - ^{1}H-NMR and the structure with labels for polymer (b) $MPEG_{12}$-$PHAz_6$-$MPEG_{12}$. The value of the integrals are normalised to that of the peak (a) at 3.38 ppm (terminal methoxy group); hence, the peaks at (g) 4.05, (d) 2.28, (e) 1.63 and (f+h) 1.38-1.32 ppm (PHAz backbone) can be used to estimate the average molar mass of the polymer.

The average molecular weight (M_n^{NMR}) was calculated from the integrals assigned to the PHAz backbone (normalised to those of the methyl group of the MPEG end-capper) using Equation (5.2):

$$M_n^{NMR} = \frac{\left(\frac{I_{f+h}-6}{10}+\frac{I_e-4}{8}+\frac{I_d-4}{4}+\frac{I_g}{4}\right)}{4}\times 270.4+154.2+2(M_n^{MPEG}) \qquad (5.2)$$

Where the values I_x are the integrals of the peaks with the relative label (x = *d, e, f+h, g*), M_n^{MPEG} is the value of the molar mass of the MPEG used as an end-capper. The values subtracted to I_{f+h}, I_e, I_d, and I_g take in account the azelaic acid unit used as a linker (to react with the MPEG), which is not part of the repeating unit. The contribution of this segment to the final molecular weight is taken in account by the figure 154.2 in Equation (5.2).

The fraction of di-functional polymer (ABA structure) was calculated from Equation (5.3):

$$ABA(\%) = \frac{I_c/4}{I_a/6}\times 100 \qquad (5.3)$$

Where I_c is the integral of the peak attributed to the -C$\underline{H_2}$-O- of MPEG linked to the PHAz backbone and I_a is the integral of the terminal -O-C$\underline{H_3}$ group of MPEG (which does not shift when the MPEG block is linked to the chain or free). The integrals (I_c and I_a) have been normalised to the number of protons present in each group (2×2 and 2×3).

As explained later in the discussion, exact conversions could not be determined explicitly due to peak overlap but could be estimated for each polymer from the value expected for the peak (b) of the MPEG backbone (3.64 ppm, see Figure 5.11).

5.2.2.3 Gel permeation chromatography (GPC)

The molecular weight distributions of the samples were analysed using a Polymer Laboratories GPC 50 with a refractive index detector and calibrated with poly(styrene) standards in the range of 100 g mol^{-1} – 500 kg mol^{-1}. The machine was equipped with a PL PLgel guard (8 μm) column followed by two PLgel Mixed-D (8 μm) columns.

The samples were run in $CHCl_3$ Chromasolv® (5 mg mL^{-1}) at a flow rate of 1 mL min^{-1}. Cirrus software was used for analysis.

5.2.2.4 Differential scanning calorimetry (DSC)

DSC analyses were performed using a TA Instruments (USA) TA-Q2000 DSC calibrated with sapphire and indium standards. In a standard experiment, the sample (2.00 ± 0.10 mg) was melted with a first heating scan up to 100 °C (10 °C min^{-1}) and cooled down to -90 °C (10 °C min^{-1}). A second heating scan up to 100 °C, with the same heating rate, was then carried out to detect the melting point. Isothermal 5-minute segments were performed at the conclusion of each ramp. The experiments were carried out under a N_2 flow (50 mL min^{-1}).

The T_m was taken as the maximum of the endothermic peak. Each experiment was repeated three times (on three different portions of the sample) and the results are shown as the average ± 1 standard deviation.

5.2.2.5 Preparation of polymer nanoparticles

The polymeric nanostructures were prepared through nano-precipitation from THF Chromasolv®. The appropriate amount of polymer was dissolved in THF (1 mL) and this solution was added dropwise (100 µL, 30 seconds) to water (4 mL) whilst stirring at 1500 rpm. The THF was left to evaporate for 1 hour whilst stirring at ambient pressure, and then under reduced pressure (75 mbar) for 30 minutes at room temperature.

5.2.2.6 Dynamic light scattering (DLS)

DLS analyses were performed using a Malvern Zetasizer Nano ZS system in order to determine the hydrodynamic diameter of the polymeric particles in water. Polystyrene disposable cuvettes were used and the samples were not filtered to retain information on the possible presence of microscopic aggregates. The analyses were performed at 25 °C on a 1 mL sample collecting the scattered light at 173°. Typically, three separate experiments of 10-15 runs (chosen by the instrument depending on the optical quality of the dispersions) were performed for each sample to check upon data significance and reliability.
For the size-temperature study, 5 minutes were allowed after each temperature step in order for the sample to reach thermal equilibrium before collection of the data.

5.2.2.7 Transmission electron microscopy (TEM)

TEM analyses were carried out to obtain a visual observation of the nanostructures on a JEOL 2000-FX microscope. Typically, 30 µL of the polymer dispersions (0.10% in water) was dropped on holey carbon coated TEM grids (EMResolutions, UK). After drying of the water, 15 µL of 1% by weight aqueous uranyl acetate (UA) solution were added to each grid and dried with filter paper after 1 minute to obtain negative background staining. Before addition, the UA

solution was passed through a 0.22 μm filter to remove any UA acetate crystals from the solution.

5.2.2.8 Coumarin-6 (C6) incorporation

The incorporation of Coumarin-6 (C6, Figure 5.12) has been studied to test the ability of the polymers to act as nano-carriers for the encapsulation and stabilisation of hydrophobic molecules in water. To ensure the presence of one phase in the polymer/C6 solution, dichloromethane (DCM) was used as a solvent for the nano-precipitation. A stock solution of C6 dissolved in DCM (2.5% w/v) was prepared and 50 μL of this solution was added to 500 μL of a DCM 2% w/v polymer solution. This final solution (550 μL) was added dropwise (110 μL, 30 seconds) to 10 mL of water whilst stirring at 1500 rpm obtaining a final solution 0.1% wt of polymer in water. The DCM was left to evaporate for 1 hour while stirring at ambient pressure, and then under reduced pressure (75 mbar) for 30 minutes at room temperature. The dispersions were filtered through membrane syringe filter (0.22 μm, Millex.LG, Millipore Co., USA) to exclude larger aggregates and undissolved C6. Aliquots of the filtered formulations were used for UV-Vis analyses (at 25 °C) to quantify the amount of C6 dispersed by each polymer.

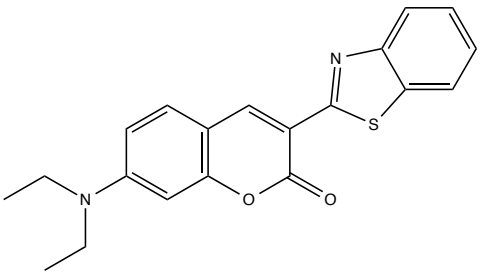


Figure 5.12 – Chemical structure of the dye Coumarin-6 (C6).

5.2.2.9 UV-Vis quantification of C6 incorporation

The ability of the synthesised polymers to act as systems to encapsulate C6 was determined through UV-Vis in THF using a Perkin Elmer Lambda 25

spectrometer with a matched pair of Hellma® 6030-UV quartz cuvettes (pathlength 10.00±0.05 mm). For a typical experiment, 0.3 mL of polymer dispersion in water with incorporated C6 (prepared as described previously) were added to 2.7 mL of THF. The absorption was recorded between 550 and 350 nm (480 nm min^{-1}, slit width 1 nm, data interval 1 nm).

The amount of dispersed C6 for each polymer sample was determined through comparison with the absorbance of standard solutions of C6 in 9:1 THF:water with known concentration considering the absorbance value at 452 nm. A calibration line was built (y=70.17x; R^2>0.99) (Figure 5.13).

Each UV-Vis experiment was run in duplicate to check upon reproducibility.

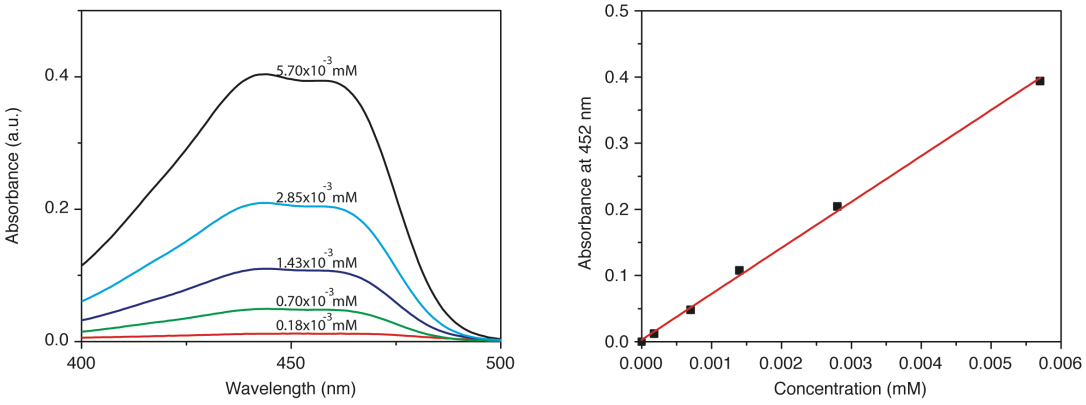


Figure 5.13 – UV-Vis spectra of C6 standards (in 9:1 THF:water) (a), and calibration line built by plotting the absorbance at 452 nm *vs* concentration (b).

5.2.2.10 Critical aggregation concentration (CAC) determination

The CAC of the synthesised polymers was determined through UV-Vis in water using a Perkin Elmer Lambda 25 spectrometer with a matched pair of Hellma® 6030-UV quartz cuvettes (pathlength 10.00 ± 0.05 mm) at 25 °C. Aqueous dispersions with different concentrations (typically from 0.1% to 0.0001% wt) were prepared for each polymer using the nano-precipitation methodology (from THF). A small aliquot of methanolic DPH (0.4 mM) was added to each polymer dispersion (10 µL of DPH 0.4 mM in 1 mL of polymer dispersion in water, final DPH concentration 0.004 mM) and equilibrated overnight on an orbital shaker

(400 rpm). The absorption spectra were recorded from 390 to 330 nm (480 nm min^{-1}, slit width 1 nm, data interval 1 nm). Dispersions with the same polymer concentration, but without DPH, were used as reference for each measure. Each experiment was run in duplicate to check reproducibility. Because of the cloudiness of some of the polymer dispersions, 0.05% wt was the highest analysed concentration, due to the lower light intensity passing through both the reference and the sample (consistent background absorption). The CAC was determined by the two extrapolated lines of the absorbance at 362 nm at low and high concentration regions [1].

5.2.2.11 Maximum bubble pressure test

The surface tension of the polymer dispersions in water (0.2% wt, 20 mL) was determined by using a SITA t100 Bubble Pressure tensiometer.

The working principles of this industrial methodology are briefly outlined: in this test a capillary with known radius (r_{kap}) is submerged into the liquid sample. Gas bubbles are produced and blown at a constant rate, whilst monitoring continuously the pressure inside the gas bubble. The maximum pressure value is reached when the bubble has its smallest radius (*i.e.* equal to that of the capillary) (Figure 5.14).

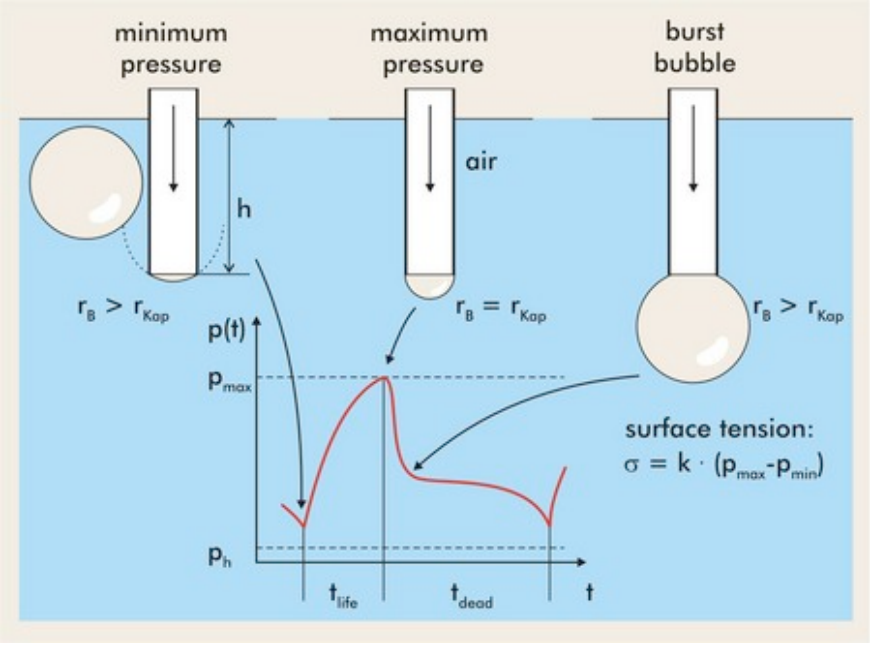


Figure 5.14 – Schematic of the maximum bubble pressure test working principles [53].

The surface tension σ (N m^{-1}) can be determined using Equation (5.4):

$$\sigma = k(p_{\max} - p_{\min}) \qquad (5.4)$$

Where k (m) is a calibration factor (typically equal to the radius of the capillary divided by 2), and p_{max} and p_{min} (N m^{-2}) are the maximum and minimum pressure values respectively.

The MPEG-PHAz-MPEG copolymers were compared to two commercial surfactants (Tween 20 and Pluronic L121). A sample containing only water was analysed as a control. The tests were run at 20 °C.

5.3 Results

5.3.1 Copolymers synthesis and structural characterisation

Azelaic acid, 1,6-hexanediol and MPEG have been exploited in this chapter for green polyester synthesis using an enzyme (immobilised CaLB) and $scCO_2$ at near-ambient temperature (35 °C). The polymers were prepared through a one-pot reaction by adding together the monomers and end-cappers, with enzyme supported on cross-linked acrylic beads into the reaction autoclave. Hence, the novel approach developed and described in Chapter 4 has been extended for the synthesis of a new range of bio-based amphiphatic copolymers.

The reactions targeted specific molecular weights by carefully controlling monomer and end-capper (*i.e.* MPEG) feed ratios.

Once the autoclave was vented, yellowish waxy products were collected. After separation of the enzyme/molecular sieves and drying, light yellow/white waxy polymers were obtained in very good yields (Table 5.2).

Table 5.2 - Molecular weight distribution (from NMR and GPC), isolated yield and conversion of the synthesised MPEG-PHAz-MPEG copolymers.

Product	M_n^{th} (g mol^{-1})[a]	M_n^{NMR} (g mol^{-1})[b]	M_n^{GPC} (g mol^{-1})[c]	$Đ$	ABA structure (%)[d]	Yield (%)[e]
(a) $MPEG_{12}$-$PHAz_3$-$MPEG_{12}$	2084	2500	2200	2.04	98	87
(b) $MPEG_{12}$-$PHAz_6$-$MPEG_{12}$	2896	3000	3200	2.24	93	84
(c) $MPEG_7$-$PHAz_3$-$MPEG_7$	1644	1800	1700	2.08	85	82
(d) $MPEG_7$-$PHAz_6$-$MPEG_7$	2455	2700	2400	1.88	93	91

[a]Calculated according to the reagents ratios; [b]Determined through ^{1}H-NMR from the ratio between the integrals of the peaks of the polymer backbone and the end-group peak using Equation (5.2); [c]In $CHCl_3$ against poly(styrene); [d]Percentage of polymer with ABA structure determined through ^{1}H-NMR analyses (peak at 4.22 ppm) using Equation (5.3); [e]Yield= weight of collected product/theoretical weight×100.

Exact conversions could not be estimated from ^{1}H-NMR, due to overlap of the peak assigned to the protons adjacent the alcohol group (3.65 ppm) in the 1,6-hexandiol monomer and the -(C$\underline{H_2}$)$_2$-O- peak of the MPEG backbone (3.64 ppm). However, from the value expected for the peak of the MPEG backbone (2×48.6 for MPEG550 and 2×30 for MPEG350 from ^{1}H-NMR analyses of the pure MPEG samples, see Appendix II Figure B.1 and Figure B.2), the conversion approached 90% for all the polymers. In more detail, the minimum conversion was 87% for (a) MPEG$_{12}$-PHAz$_3$-MPEG$_{12}$, 86% for (b) MPEG$_{12}$-PHAz$_6$-MPEG$_{12}$, 86% for (c) MPEG$_7$-PHAz$_3$-MPEG$_7$ and 91% for (d) MPEG$_7$-PHAz$_6$-MPEG$_7$.

As a general example, the ^{1}H-NMR spectrum of (a) MPEG$_{12}$-PHAz$_6$-MPEG$_{12}$ (Figure 5.15) shows integrals of the peaks at 3.38 ppm (terminal methoxy group in each of the MPEG blocks) and at 4.05, 2.28, 1.63 and 1.38-1.32 ppm (PHAz backbone protons) and these were used to calculate the number average molecular weight (M_n^{NMR}) by using equation (1).

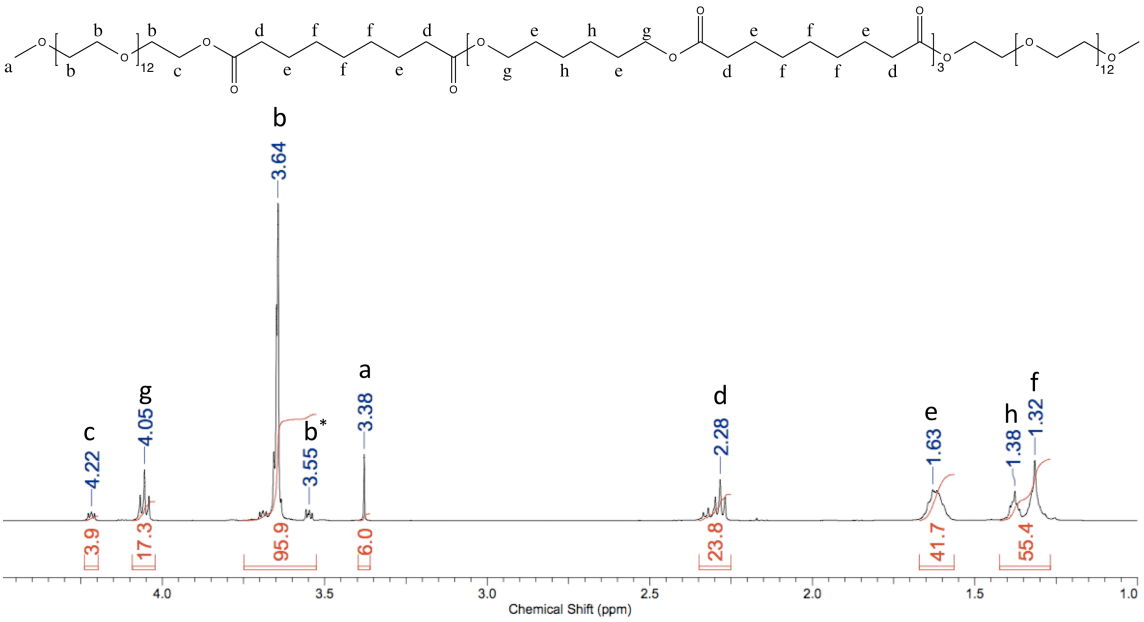


Figure 5.15 - ^{1}H-NMR of polymer (a) MPEG$_{12}$-PHAz$_3$-MPEG$_{12}$. Integrals of the peak at 3.38 ppm (terminal methoxy group) and 4.05, 2.28, 1.63 and 1.38-1.32 ppm (PHAz backbone) can be used to estimate the average molar mass of the polymer. The peak b (3.64 ppm) is assigned to the -CH$_2$- in the MPEG backbone, while the peak b* (3.55 ppm) is assigned to the -CH$_2$- protons directly attached to the terminal methoxy group (-O-CH$_3$) [13]. ^{1}H-NMR spectra for the other copolymers are available in the Appendix II.

The M_n^{NMR} calculated for all the copolymers show a very good agreement with expected molecular weights, thus indicating successful polymerisations that afforded the target structures (Table 5.2). Furthermore, the normalised ratio between the integrals of the peaks at 4.22 and 3.38 ppm indicates that 98% of the detected MPEG is attached to the PHAz backbone for this copolymer (see Equation (5.3)); similar results were obtained also for the other copolymers (see the respective ^{1}H-NMR spectra in the Appendix II, Figure B.3 to Figure B.5). This shows a high yield of end-capping and thus an efficient polymerisation to form ABA block copolymers *via* an enzymatic low temperature approach. It is important to emphasise that only for practical reasons, dissolution in toluene was used to physically separate the enzyme beads from the product at the end of the reaction. However, it is possible to completely avoid the use of conventional solvents by exploiting the plasticising effects of CO_2 to separate the enzyme beads from the polymer product [48]. Hence, a fully green solvent-free process can be potentially achieved by using $scCO_2$ both as a reaction medium (during the synthesis) and as a plasticiser for the separation (at the end of the reaction).

5.3.1.1 Thermal analyses

The thermal properties of the MPEG-PHAz-MPEG copolymers were studied through differential scanning calorimetry (DSC). The amphiphilic copolymers were semicrystalline with low T_m (Figure 5.16). A low melting point is a desirable feature for the preparation of self-assembled structures through melting/sonication, which is a novel methodology that can be used to prepare polymeric nanoparticles avoiding the use of organic solvents. Using this technique, polymer nanoparticles are prepared by exploiting ultrasonic frequencies (>20 kHz) at a temperature above the T_m of the polymer. Briefly, the polymer is added to water at a temperature above its T_m, to allow for copolymer melting. Then, the mixture is sonicated with a ultrasonic probe to achieve self-assembly of the polymer chains [35]. Hence, a low T_m is clearly a desirable feature.

Two melting points could be identified for the copolymers (a) and (b), this might be due to separate crystallisation of the polyester segment and the MPEG blocks

that in this case were most likely long enough (M_n^{MPEG}~550 g mol^{-1}) to crystallise [54, 55]. For example, a similar behaviour was observed also for PLA-*b*-PCL copolymers, which showed two separate endotherms attributed to the two different blocks when both of them were long enough to crystallise [56].

The higher T_m – attributed to the PHAz segment – was the bigger and sharper peak for all the polymers and this peak was clearly bimodal for polymers (a), (b) and (c). Typically, multiple and multimodal endothermic peaks are observed due to the melting of crystallites with different stability and size or to crystal reorganisation, as reported for other semicrystalline polyesters elsewhere [57]. Furthermore, the T_m of the PHAz block in polymer (b) $MPEG_{12}$-$PHAz_6$-$MPEG_{12}$ is significantly suppressed compared to that of a PHAz homopolymer with DP equal to 6 (38.6 ± 0.4 °C and 46.5 ± 0.8 °C respectively) [58]. This might suggest a partial miscibility of the MPEG and PHAz blocks, which allows MPEG to act as a macromolecular diluent for PHAz, as observed elsewhere for PCL-*b*-PLA systems [56].

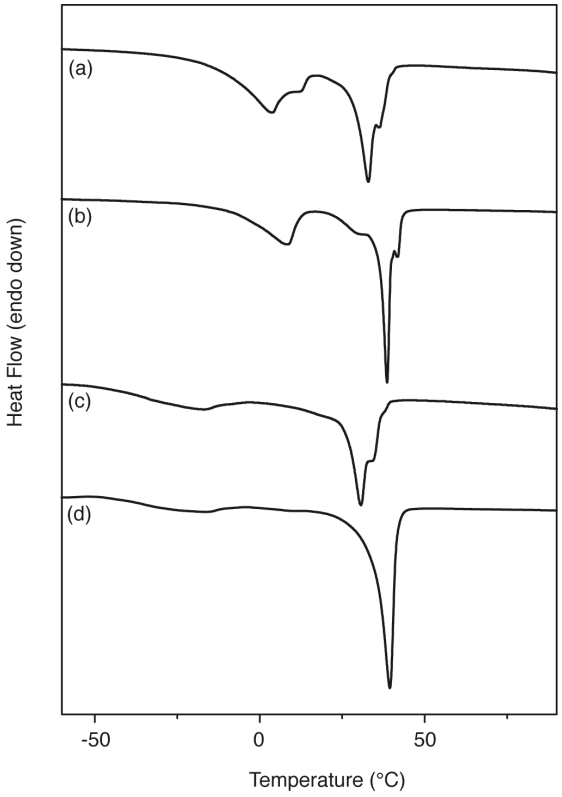


Figure 5.16 - DSC traces of the copolymers: (a) $MPEG_{12}$-$PHAz_3$-$MPEG_{12}$, (b) $MPEG_{12}$-$PHAz_6$-$MPEG_{12}$, (c) $MPEG_7$-$PHAz_3$-$MPEG_7$, (d) $MPEG_7$-$PHAz_3$-$MPEG_7$. Copolymers (b) and (d) display a higher T_m value. The 2nd heating scans are shown.

The T_m and enthalpy of fusion (ΔH_m) values are summed up in Table 5.3

Table 5.3 - Thermal properties of the ABA copolymers obtained from DSC analyses (2nd heating scan). The values are shown as the average between 3 different measurements ± 1 standard deviation.

Product	T_m[a] (°C)	ΔH_m (kJ mol^{-1})[b]
(a) $MPEG_{12}$-$PHAz_3$-$MPEG_{12}$	32.9 ± 1.1	33.3 ± 0.9
(b) $MPEG_{12}$-$PHAz_6$-$MPEG_{12}$	38.6 ± 0.4	55.8 ± 0.6
(c) $MPEG_7$-$PHAz_3$-$MPEG_7$	30.7 ± 0.9	40.2 ± 0.3
(d) $MPEG_7$-$PHAz_6$-$MPEG_7$	39.4 ± 0.6	68.6 ± 0.4

[a]Main T_m peak observed in the DSC trace.

It is clear how a longer PHAz backbone (polymer (b) and (d)) results in a higher T_m and ΔH_m. This behaviour is attributed to larger crystallites that can be formed when longer polymer chains pack, and it has been observed for other polyesters at small molecular weight values [59]. The T_g could not be detected due to equipment limitations and high crystallinity of the copolymers, but it is expected to be around -60 °C as observed previously for similar polyesters [57].

5.3.2 Aqueous self-assembly studies

5.3.2.1 NMR analyses

Effective aggregation in water with structure where the lipophilic block has restricted motion, was confirmed by comparison of ^{13}C-NMR spectra collected in D_2O and $CDCl_3$. Chloroform is a good solvent for the MPEG and PHAz blocks, while water is a good solvent only for PEG. For these reasons, in $CDCl_3$ the peaks of the MPEG and PHAz moieties are clearly observed, whereas in D_2O only the resonances attributed to PEG are detected (Figure 5.17). This implies that in $CDCl_3$ there is fast molecular motion of each block, while in D_2O the motion of

the PHAz segment is restricted and, consequently, its resonances are collapsed and broadened. The same observation has been made elsewhere for other similar systems containing PCL as a hydrophobic block [9, 12].

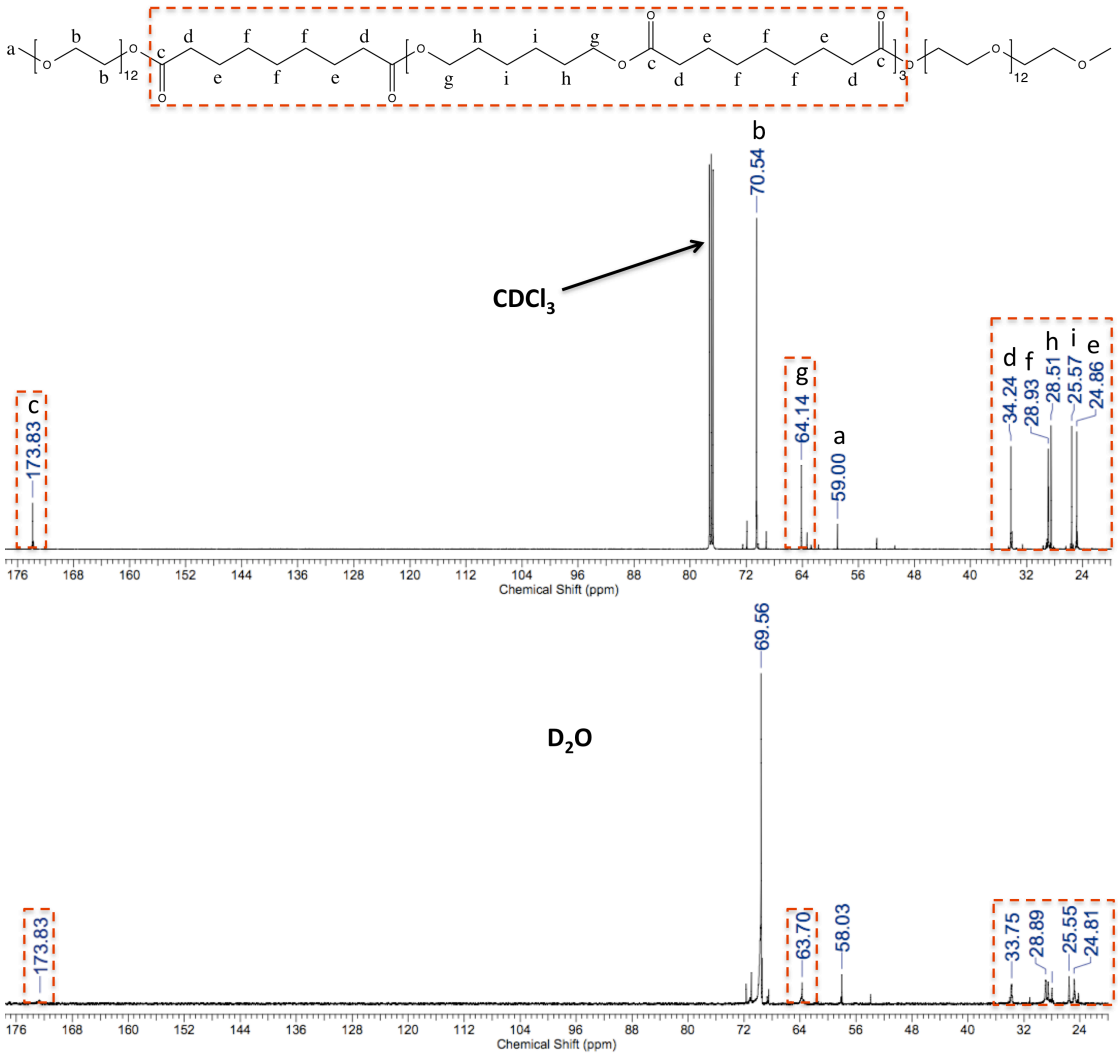


Figure 5.17 - ^{13}C-NMR spectra of (b) MPEG$_{12}$-PHAz$_6$-MPEG$_{12}$ in $CDCl_3$ (top) and D_2O (bottom) (20 mg mL^{-1}). All the peaks are clearly detected in chloroform, whilst the PHAz resonances (red dotted rectangles) are strongly suppressed in heavy water. In particular, the carbonyl peak (around 174 ppm) is almost undetectable in D_2O. This confirms the formation of aggregates with a rigid PHAz portion in aqueous environment.

As expected, an equivalent effect was also observed in the ^{1}H-NMR spectrum acquired in D_2O (see Appendix II, Figure B.6). Here again, the peaks attributed to the protons of the PHAz block are small and significantly broadened, clearly demonstrating that an aggregated structure with an external MPEG shell and an

internal PHAz portion with restricted motion is formed in water (*e.g.* micelles, vesicles) [24].

5.3.2.2 Size investigations: DLS and TEM

In order to use a copolymer as a drug delivery vehicle or as an effective micellar system, it is essential to investigate the nature of its self-assembly in aqueous environment and determine the characteristic size of the self-assembled structures. The nano-precipitation methodology has been previously shown as a successful and straightforward way to prepare empty and drug/dye loaded polymeric particles in a controlled manner [3, 5]. For this reason, we chose to use this method to prepare MPEG-PHAz-MPEG nanoparticles for DLS and TEM studies (since the polymers were not directly soluble in water).

The desired amount of copolymer was first dissolved in a non-selective solvent (*i.e.* THF) and this solution was added dropwise to an excess of water while stirring. To allow for THF evaporation and copolymer self-assembly the dispersion was left to stir for 1 hour (Figure 5.18). Complete removal of the organic solvent was achieved by applying reduced pressure (75 mbar) at room temperature, obtaining a final dispersion with a concentration of 0.1% wt in water.

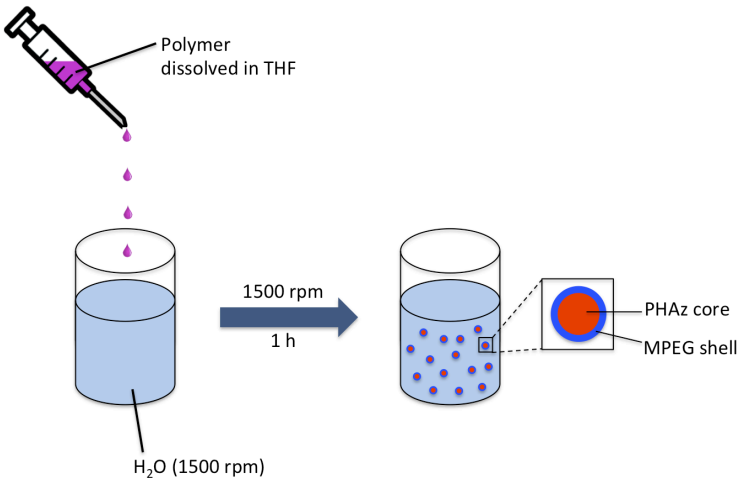


Figure 5.18 – Schematic representation of the nano-precipitation process for the preparation of MPEG-*b*-PHAz-*b*-MPEG self-assembled nanoparticles: the copolymer is dissolved in THF and added dropwise to H_2O whilst stirring at 1500 rpm. The dispersion is then left to stir for 1 h to allow for THF evaporation. Complete removal of the solvent is achieved by subsequent application of reduced pressure (75 mbar) at room temperature.

The diameter and size distribution of the structures formed was determined by DLS (Figure 5.19 upper). The DLS data for polymers (a), (c) and (d) displayed the presence of structures that are clearly quite large and likely indicate formation of aggregated structures or vesicles rather than spherical micelles.

To investigate this in more depth, TEM analyses (with negative background staining using uranyl acetate (UA)) were performed. The size determined through TEM analyses showed excellent agreement with the distribution by number obtained by DLS (Figure 5.19 lower). However, the DLS results were always slightly higher than the size observed in the TEM pictures, since they represent the hydrodynamic diameter of the solvated particles and those are necessarily bigger than the diameter of the dry aggregates observed through TEM. Furthermore, the intensity and size distribution obtained through DLS showed an overestimation of the dimension: because of the dependency on size of these type of distributions that leads to a size overestimation for non-monodisperse systems such as these polymeric nanoparticles (see Appendix II for all the DLS distribution plots, Figure B.7 to Figure B10).

The TEM analyses confirmed the presence of spherical micelles for polymer (b), whilst the micrographs of polymers (a), (c) and (d) showed the presence of diverse structures. In more detail, aggregated micelles and wormlike micelles could be identified for polymer (a) and (c), whilst aggregated micelles and possible vesicles were detected in polymer (d) (see Appendix II for additional TEM micrographs, Figure B.13), factors which may well also explain the larger sizes detected from DLS measurements.

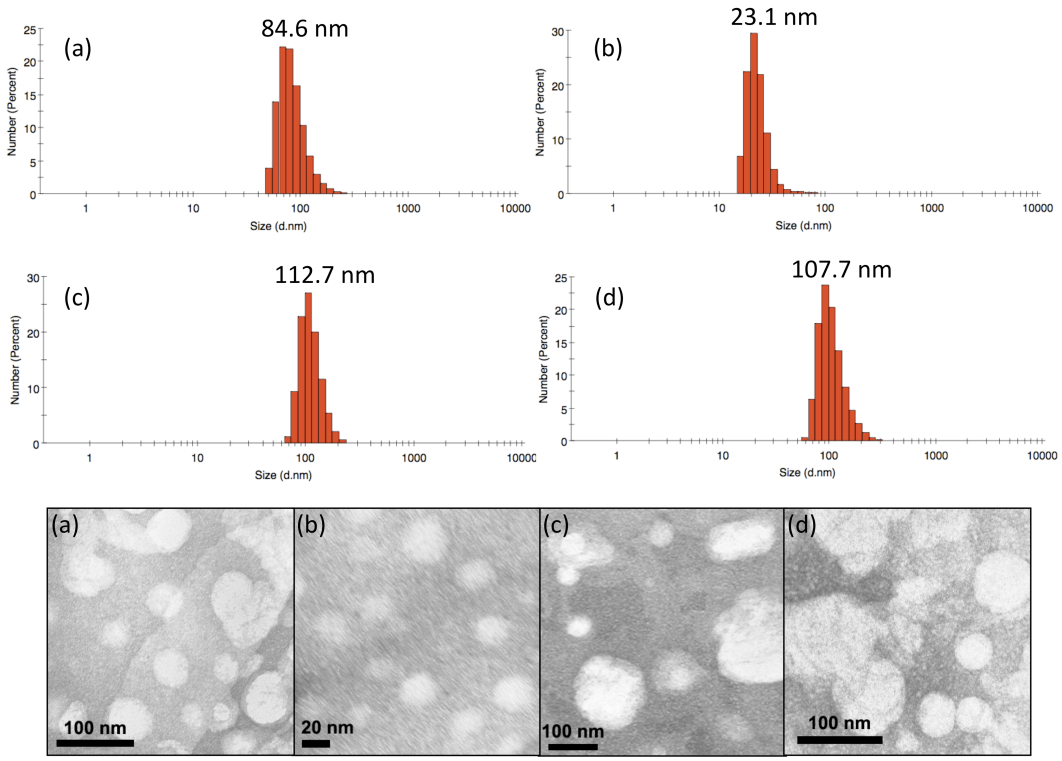


Figure 5.19 - Size distribution (by number) obtained through DLS analyses (25 °C) and TEM images of the copolymers (0.1% wt in water): (a) $MPEG_{12}$-$PHAz_3$-$MPEG_{12}$, (b) $MPEG_{12}$-$PHAz_6$-$MPEG_{12}$, (c) $MPEG_7$-$PHAz_3$-$MPEG_7$, (d) $MPEG_7$-$PHAz_3$-$MPEG_7$. Discrete spherical micelles are observed for polymer (b); whilst different structures are observed for the remaining copolymers. The peak size is shown in each DLS plot. Images were taken with UA negative background staining.

It is well known that several parameters (such as the ratio of the hydrophilic to the hydrophobic block, hydrophobicity of the apolar block, molecular weight *etc.*) influence the type and size of the nanostructure formed upon self-assembly. For instance, MPEG blocks with higher DP generally result in smaller micelles, as observed for other amphiphilic copolymers when increasing the size of the hydrophilic block [5, 9]. Whereas, short hydrophilic blocks can result in the formation of large structures upon hierarchical aggregation of smaller micelles [60].

Furthermore, the length and crystallinity of the hydrophobic block (in this case the PHAz) can also influence the micellar size. For example, for PEG-*b*-PCL micelles a smaller size was observed with increasing PCL molecular weight: this was attributed to the ability of the hydrophobic core to pack tightly in crystalline regions [38]. In addition, the degree of crystallinity of the core can also affect the

morphology of the aggregates [61]. For instance, for a given PCL length a change in the crystallinity of the core of PEG-PCL block copolymers has been observed to shift the morphology from rods to spherical micelles [10].

Therefore, in this case a particular balance between the PHAz core crystallinity and the PEG weight fraction might explain the formation of spherical micelles for polymer (b) and the different self-assembly/aggregation observed for the other copolymers. Further investigations are certainly required to understand thoroughly the self-assembly of these PHAz-based amphiphilic copolymers and reveal the role of the crystallinity, hydrophobic/hydrophilic ratio and interaction parameter of the PHAz block with water upon the aggregated nanostructures formed in aqueous environment.

Nonetheless, these preliminary studies showed that all the copolymers formed self-assembled aggregates with sizes suitable for drug delivery, since nanoparticles smaller than 200 nm can avoid recognition from the reticuloendothelial system (RES) (particles with diameter above 200 nm are readily cleared by the liver and the spleen) [38]. In addition, structures with characteristic dimension below 30 nm are highly desirable for pharmaceutical formulations, since these are characterised by a higher efficiency of penetration through blood vessel walls [5, 62, 63]. Hence, the copolymer (b) $MPEG_{12}$-$PHAz_6$-$MPEG_{12}$ is particularly interesting, since this formed micelles with average diameter around 20-25 nm. For this reason, the micellar size of this polymer was investigated further as a function of temperature (Figure 5.20).

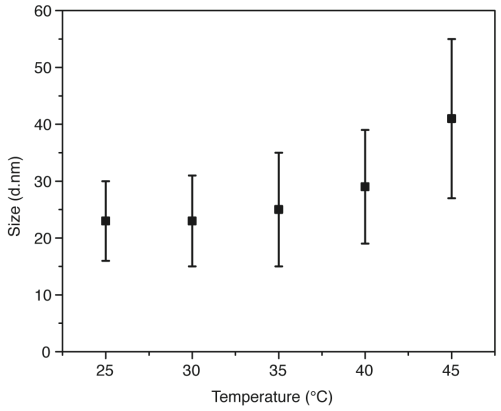


Figure 5.20 - Diameter of (b) $MPEG_{12}$-$PHAz_6$-$MPEG_{12}$ micelles *vs* temperature (0.1% wt in water). The size is stable between 25 and 35 °C. A significant increase is observed at 45 °C. The sizes shown are obtained from the peak value of the number distribution ± 1 standard deviation of the distribution (obtained from DLS).

The peak value of the distribution was almost constant in the temperature range between 25 and 35 °C, with a small increase at 40 °C and a more significant change (+78% compared to the starting value) at 45 °C. The standard deviation also increased, meaning that a broader particle distribution was obtained (see Appendix II for DLS plots, Figure B.11), indicating formation of micellar aggregates at higher temperatures [1]. However, these results do show that this polymer could prove to be an interesting drug delivery vehicle since the average micellar size is still below 30 nm at body temperatures.

5.3.3 UV-Vis studies

5.3.3.1 C6 incorporation

Coumarin-6 (C6) is a highly hydrophobic fluorescent dye that can be used to model the behaviour of lipophilic drugs for studies involving drug delivery and drug release [64]. For this reason, C6-loaded nanoparticles were prepared through nano-precipitation: DCM was used in this case to ensure the presence of a homogeneous solution (containing C6 and the copolymer) to use for the nano-precipiation process. DLS analyses showed that the size distribution of the $MPEG_{12}$-$PHAz_6$-$MPEG_{12}$ particles prepared from DCM was not significantly different from that of the micelles prepared from THF. Namely, the distribution was marginally broader and shifted towards slightly higher values. In more detail, the peak value of the number distribution was 30.2 ± 9.3 nm (see Appendix II for the DLS plot, Figure B.12). Therefore, although not miscible with water, DCM is still a fairly good solvent for the preparation of MPEG-PHAz-MPEG self-assembled structures.

The MPEG-PHAz-MPEG copolymers were compared to Tween 20 and Pluronic L121, two commercially available amphiphilic copolymers used for stabilisation and encapsulation of hydrophobic molecules [5, 65-69]. Visual observation of filtered C6-loaded nanoparticle dispersions (plus a control sample of water

without copolymer) gave a direct insight into the ability of some of the synthesised copolymers to encapsulate and stabilise C6 in water (Figure 5.21).

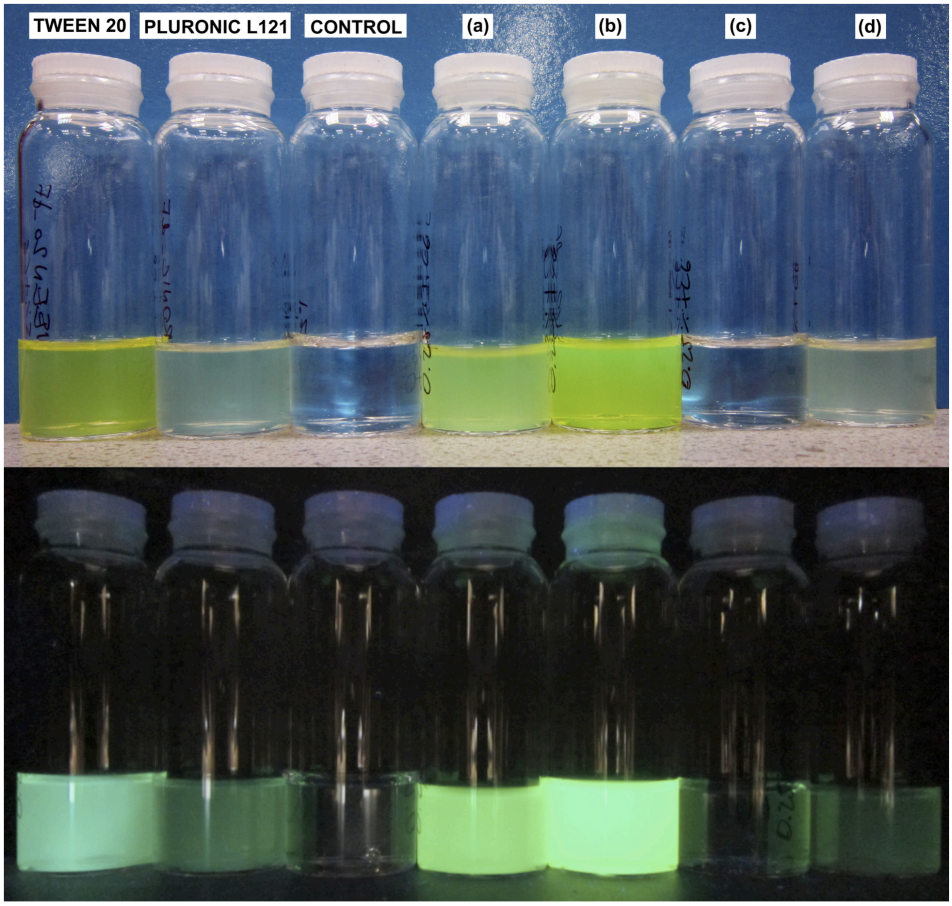


Figure 5.21 - Picture of the formulations for the synthesised copolymers (a) $MPEG_{12}$-$PHAz_3$-$MPEG_{12}$, (b) $MPEG_{12}$-$PHAz_6$-$MPEG_{12}$, (c) $MPEG_7$-$PHAz_3$-$MPEG_7$, (d) $MPEG_7$-$PHAz_3$-$MPEG_7$ compared to Tween 20 and Pluronic L121 under normal light (top) and UV light (bottom; λ=365 nm). No polymer was used in the control vial.

At first glance, it is clear that the MPEG-PHAz-MPEG polymers with longer hydrophilic segments (*i.e.* (a) $MPEG_{12}$-$PHAz_3$-$MPEG_{12}$ and (b) $MPEG_{12}$-$PHAz_6$-$MPEG_{12}$) were able to disperse the highest amount of C6 in the polar medium, with the latter displaying the strongest emission under UV light. The amount of C6 stabilised and dispersed in water was quantified through UV-Vis analyses, by diluting small aliquots of these aqueous dispersions in THF and comparing the results with known C6 concentrations (Figure 5.22).

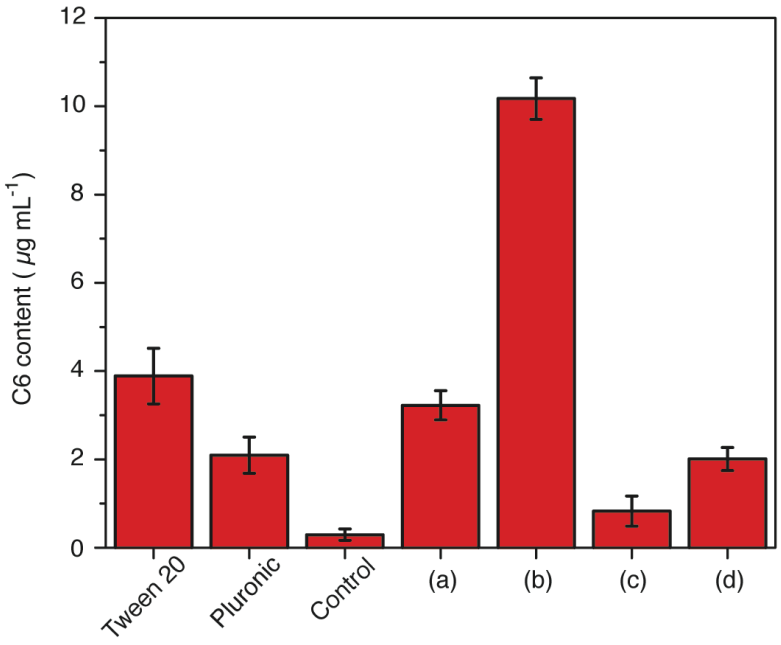


Figure 5.22 - C6 dispersed in the different formulations (μg of dye per mL of water). The synthesised copolymers (a) $MPEG_{12}$-$PHAz_3$-$MPEG_{12}$, (b) $MPEG_{12}$-$PHAz_6$-$MPEG_{12}$, (c) $MPEG_7$-$PHAz_3$-$MPEG_7$, (d) $MPEG_7$-$PHAz_3$-$MPEG_7$ are compared to Tween 20 and Pluronic L121. No polymer was used in the control sample. The copolymer (b) $MPEG_{12}$-$PHAz_6$-$MPEG_{12}$ showed the highest amount of C6 encapsulated and dispersed in water.

The UV-Vis results confirmed the visual observations and showed that the copolymer (a) had loading comparable to Tween 20 since around 3 μg mL^{-1} of dye were dispersed in water, whilst the copolymer (b) showed the highest loading with more than 10 μg mL^{-1} dispersed in water: three times higher than commercial Tween 20 and around 35 times the measured native solubility of C6 in H_2O (0.29 μg mL^{-1}). These data could be attributed to the different packing of the micellar core in the smaller micelles formed by this polymer. Furthermore, all of the dispersions were passed through 0.22 μm syringe filters to eliminate undissolved C6 and mimic the clearance by the RES [38], so it is possible that some of the particles in the other formulations could have been removed during this step.
However, these preliminary results clearly demonstrate the ability of amphiphilic copolymers based on azelaic acid and 1,6-hexanediol to act as potential drug delivery vehicles.

5.3.3.2 CAC determination

As aforesaid, another crucial parameter to determine, in order to understand the usefulness of polymers as nano-carriers, is the CAC. In fact, a low value ensures the formation of sufficiently stable nanostructures.

Incorporation of the hydrophobic dye 1,6-diphenyl-1,3,5-hexatriene (DPH) was used to obtain the CAC of the copolymers and to further confirm the micellar structure with a hydrophobic core. DPH is highly lipophilic and has a significantly lower intensity of absorption at 330-380 nm in water compared with that showed in a lipophilic environment. Thus as micelles and/or vesicles form, the dye is preferentially partitioned into the hydrophobic regions, leading to increased light absorption [1, 11]. The dramatic change in absorbance gives information on the assembly of the polymeric nanostructures and, hence, on the CAC. As an example, the UV-Vis spectra obtained for the copolymer (b) $MPEG_{12}$-$PHAz_6$-$MPEG_{12}$ at a fixed DPH concentration (0.004 mM) with increasing polymer concentration is shown (Figure 5.23).

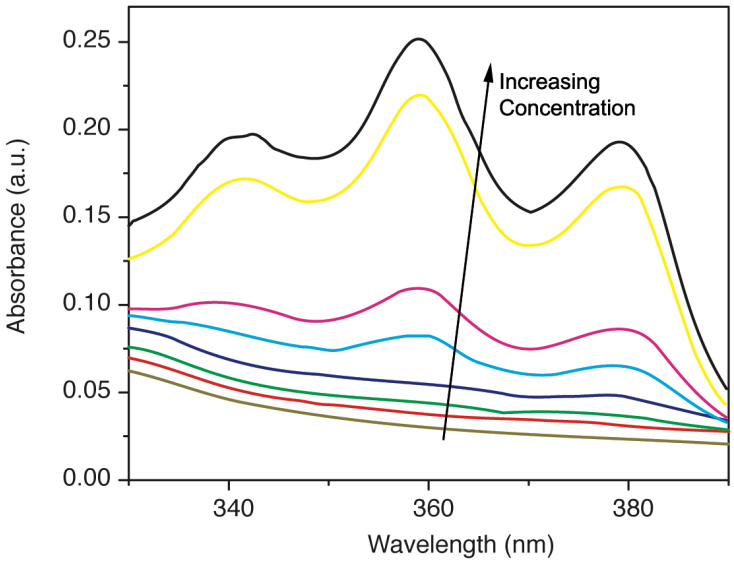


Figure 5.23 – UV-Vis spectra of copolymer (b) $MPEG_{12}$-$PHAz_6$-$MPEG_{12}$ at 25 °C. The absorbance between 330 and 390 nm increases dramatically with polymer concentration (0.00001, 0.0001, 0.0005, 0.001, 0.005, 0.01, 0.05, 0.1% wt) at a fixed DPH concentration (0.004 mM).

The CAC of this polymer was extrapolated from the absorbance recorded at 362 nm (Figure 5.24). The data were fitted with a logistic growth function (red solid line).

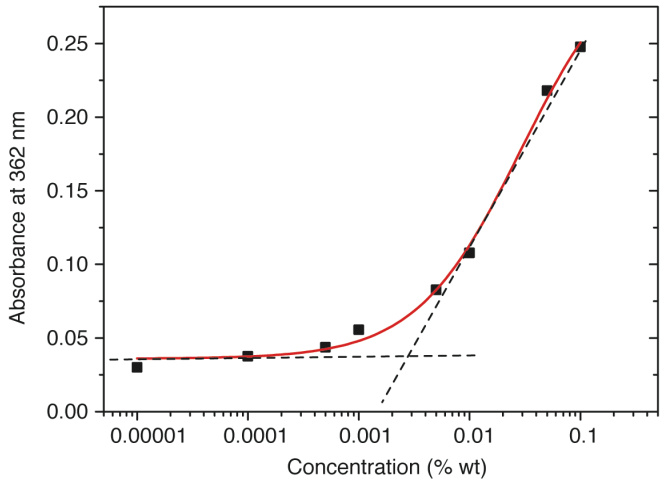


Figure 5.24 – Absorbance at 362 nm *vs* concentration (% wt) for polymer (b) $MPEG_{12}$-$PHAz_6$-$MPEG_{12}$ at 25 °C (DPH concentration fixed to 0.004 mM). The CAC was determined by extrapolated lines (black dotted lines at high and low concentrations) of the absorbance maximum at 362 nm (data were fitted to a logistic growth function, red solid line; R^2>0.98).

The CAC of copolymer (b) $MPEG_{12}$-$PHAz_6$-$MPEG_{12}$ was 0.0027% (27 µg mL^{-1}). The same analysis was conducted for the other copolymers to obtain their CAC (Table 5.4). Plots of the absorbance at 362 nm *vs* concentration for these copolymers are available in the Appendix II (Figure B.14 to Figure B.16).

Table 5.4 - CAC of the synthesised MPEG-PHAz-MPEG copolymers calculated from UV-Vis by the extrapolated lines of the absorbance maximum at 362 nm.

Product	*CAC*[a]		
	% wt	µg mL^{-1}	µM[b]
(a) $MPEG_{12}$-$PHAz_3$-$MPEG_{12}$	0.0047	47	18.8
(b) $MPEG_{12}$-$PHAz_6$-$MPEG_{12}$	0.0027	27	9.0
(c) $MPEG_7$-$PHAz_3$-$MPEG_7$	0.0021	21	11.7
(d) $MPEG_7$-$PHAz_6$-$MPEG_7$	0.0009	9	3.3

[a]The CAC error for each copolymer was less than 2% (experiments run in duplicate); [b]Calculated from M_n^{NMR}

As expected, the copolymers containing the smallest hydrophilic segments (*i.e.* polymers (c) and (d)) displayed the lowest CAC expressed in μg mL^{-1}. On the other hand, taking into account the molar mass of the copolymers, (b) and (d) displayed the lowest CAC expressed in μM (since these were characterised by the highest molecular weight). In more detail, for a given length of MPEG block the copolymers containing the larger PHAz segment displayed lower CAC values, as expected and already observed for similar systems elsewhere [9, 24]. It is well known that the hydrophobic length plays an important role and increased hydrophobicity shifts the CAC to lower values, since the aggregation starts at lower concentrations [6].

Moreover, the CAC values determined for the copolymers (b), (c) and (d) are comparable to those of other copolymers currently used for drug delivery (0.001 - 0.003% wt) [4, 15] and are much lower than the values observed for most of the Pluronics (typically around 0.1% wt, but even higher than 1% wt in some cases) [4, 6] and other PEG-polyester-PEG amphiphilic copolymers described in the literature (*e.g.* 0.005% for a PEG-PCL-PEG and 0.01 % wt for a PEG-PLGA-PEG copolymer) [1, 11]. This is likely a result of the higher hydrophobicity of the PHAz block in combination with the packing of the polymer chains into a crystalline core, which has also been shown to strongly influence the CAC value [38]. These data clearly show that copolymers with azelaic acid and 1,6-hexanediol based backbones could be promising candidates for a new generation of renewable nano-carriers.

5.3.4 Surface tension reduction

In addition to medical applications and drug delivery, such amphiphilic polymers can also find purpose in formulations for wetting agents, emulsifiers and detergents if there is a significant effect upon the surface tension [18]. For example, soaps and detergents include surfactants in order to reduce surface tension and achieve good contact between the liquid and the material to be cleaned. This allows lipophilic molecules and oily residues to be removed efficiently [17, 18].

For this reason, the reduction in surface tension was investigated through the maximum bubble pressure test and the values obtained were compared to surface tension reduction achieved with commercial Tween 20 and Pluronic L121, since these polymers are also commonly used as detergents and emulsifiers (Figure 5.25).

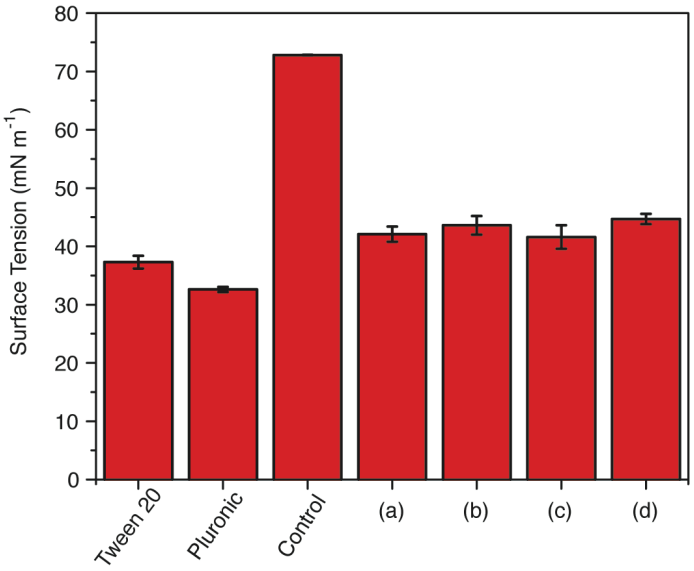


Figure 5.25 - Surface tension measured through maximum bubble pressure test. The synthesised copolymers (a) $MPEG_{12}$-$PHAz_3$-$MPEG_{12}$, (b) $MPEG_{12}$-$PHAz_6$-$MPEG_{12}$, (c) $MPEG_7$-$PHAz_3$-$MPEG_7$, (d) $MPEG_7$-$PHAz_3$-$MPEG_7$ are compared to Tween 20 and Pluronic L121 (0.2% wt in water). No polymer was used in the control sample. The MPEG-PHAz-MPEG copolymers showed a surface tension reduction comparable to those achieved by using commercial surfactants.

The surface tension of pure water at 20 °C is 72.8 mN m^{-1}, in current applications a molecule (or macromolecule) that is able to reduce the surface tension to below 60 mN m^{-1} is classed as a good surfactant [17, 18]. The results of the maximum bubble pressure test show that all the MPEG-PHAz-MPEG copolymers reduced the surface tension to around 40 mN m^{-1} and are comparable in their effects with Tween 20 and Pluronic L121. Therefore, this preliminary surface tension study demonstrates that these novel materials could certainly provide interesting opportunities for formulations where a green biodegradable surfactant is required.

5.4 Conclusions

The novel low temperature approach developed in Chapter 4 has been exploited here to develop new amphiphilic block copolymers based on azelaic acid and 1,6-hexanediol as building blocks of the hydrophobic backbone. The polymerisations were carried out in a solvent-free $scCO_2$ system, using natural enzyme CaLB as a catalyst at 35 °C and achieving remarkably high yields. The chains were end-capped with MPEG blocks of varied length that afforded hydrophilicity and control over the molecular weight (by tuning of the feed ratio). Such low temperature polymerisations would have not been possible without the aid of $scCO_2$ as a reaction medium and Novozym 435 as a catalyst.

The structural and physical properties of the novel polymers have been confirmed by NMR, DSC and GPC, showing that the synthetic route provides excellent control over the polymer molecular weight and properties.

DLS, TEM, NMR and UV-Vis studies were carried out to investigate the self-assembly of these polymers in water, obtaining promising preliminary data for nanostructure formation and encapsulation. All the polymers formed self-assembled structures characterised by an average characteristic size smaller than 200 nm. The size and type of aggregation changed depending on the MPEG and PHAz blocks length and micelles smaller than 25 nm could be obtained using polymer (b) $MPEG_{12}$-$PHAz_6$-$MPEG_{12}$. This is a remarkable result, since micelles of sizes lower than 30 nm have higher penetration efficiency into the capillaries.

Coumarin-6 loading tests demonstrated the ability of the polymers to disperse and stabilise lipophilic molecules in aqueous environment. The most promising example developed in this chapter is the polymer (b) $MPEG_{12}$-$PHAz_6$-$MPEG_{12}$, which could be used to disperse more than 10 $\mu g\ mL^{-1}$ of C6 in water affording a solubility three times higher than that obtained with a commercial amphiphilic copolymers currently used for drug encapsulation (Tween 20) and 35 times higher than the native solubility of C6 in water.

The CAC of these novel MPEG-PHAz-MPEG copolymers was determined by UV-Vis using 1,6-diphenyl-1,3,5-hexatriene as a probe to show high stability of the aggregated nanostructure: in particular the polymers (b) and (d) showed a

CAC of 9.0 and 3.3 μM respectively, which are comparable to those of other copolymers currently used for drug delivery and lower than those of most Pluronics.

Finally, the surface tension reduction achieved by dispersing these novel polymers in water was determined by maximum bubble pressure test and compared to those achieved for commercially available non-ionic polymeric surfactants (Tween 20 and Pluronic L121). The results showed a significant reduction, indicating that these new bio-based copolymers might find applications also as surfactants in detergents and body-care formulations.

To sum up, the green low temperature approach described in Chapter 4 has been successfully extended to the production of novel bio-based functional polymers that could be interesting candidates as nano-carriers and surfactants. Further analyses need to be done to investigate more in-depth the self-assembly of these copolymers in water, to assess their biodegradability and to evaluate their real potential in drug delivery and other formulations.

5.5 References

[1] B. Jeong, Y. Han Bae, S. Wan Kim, *Colloids and Surfaces B: Biointerfaces*, 16, **1999**, p. 185
[2] R.Z. Xiao, Z.W. Zeng, G.L. Zhou, J.J. Wang, F.Z. Li, A.M. Wang, *International Journal of Nanomedicine*, 5, **2010**, p. 1057
[3] K.K. Bansal, D. Kakde, L. Purdie, D.J. Irvine, S.M. Howdle, G. Mantovani, C. Alexander, *Polymer Chemistry*, 6, **2015**, p. 7196
[4] M.-C. Jones, J.-C. Leroux, *European Journal of Pharmaceutics and Biopharmaceutics*, 48, **1999**, p. 101
[5] G. Riess, *Progress in Polymer Science*, 28, **2003**, p. 1107
[6] Z. Ahmad, A. Shah, M. Siddiq, H.-B. Kraatz, *RSC Advances*, 4, **2014**, p. 17028
[7] S. Payyappilly, S. Dhara, S. Chattopadhyay, *Journal of Biomedical Materials Research A*, 102, **2014**, p. 1500
[8] J.S. Lee, J. Feijen, *Journal of Controlled Release*, 161, **2012**, p. 473
[9] Y.-C. Wang, L.-Y. Tang, T.-M. Sun, C.-H. Li, M.-H. Xiong, J. Wang, *Biomacromolecules*, 9, **2008**, p. 388
[10] S.C. Owen, D.P.Y. Chan, M.S. Shoichet, *Nano Today*, 7, **2012**, p. 53
[11] M.J. Hwang, J.M. Suh, Y.H. Bae, S.W. Kim, B. Jeong, *Biomacromolecules*, 6, **2005**, p. 885
[12] C. Gong, S. Shi, L. Wu, M. Gou, Q. Yin, Q. Guo, P. Dong, F. Zhang, F. Luo, X. Zhao, Y. Wei, Z. Qian, *Acta Biomaterialia*, 5, **2009**, p. 3358
[13] C.Y. Gong, P.W. Dong, S. Shi, S.Z. Fu, J.L. Yang, G. Guo, X. Zhao, Y.Q. Wei, Z.Y. Qian, *Journal of Pharmaceutical Science*, 98, **2009**, p. 3707
[14] Z.L. Tyrrell, Y. Shen, M. Radosz, *Progress in Polymer Science*, 35, **2010**, p. 1128
[15] W. Xu, P. Ling, T. Zhang, *Journal of Drug Delivery*, 2013, **2013**, p. 340
[16] G. Bonacucina, M. Cespi, G. Mencarelli, G. Giorgioni, G.F. Palmieri, *Polymers*, 3, **2011**, p. 779
[17] J. Texter, *Reactions And Synthesis In Surfactant Systems*, Taylor & Francis, **2001**
[18] R.J. Farn, *Chemistry and Technology of Surfactants*, Wiley, **2008**
[19] C.O. Rangel-Yagui, A. Pessoa Jr, L.C. Tavares, *Journal of Pharmacy & Pharmaceutical Sciences*, 8, **2005**, p. 147
[20] Green Chemicals Blog, *Europe explores creation of Bio-based products standards*, http://greenchemicalsblog.com/2015/03/16/europe-explores-creation-of-bio-based-products-standards/, Last Access: 11/04/2016
[21] Grand View Research, *Polyethylene Glycol (PEG) Market Analysis By Application (Medical, Personal Care, Industrial) And Segment Forecasts To 2020*, http://www.grandviewresearch.com/industry-analysis/polyethylene-glycol-peg-market, Last Access: 11/04/2016
[22] R. Marchal, E. Nicolau, J.P. Ballaguet, F. Bertoncini, *International Biodeterioration & Biodegradation*, 62, **2008**, p. 384
[23] C. Gong, S. Shi, P. Dong, B. Kan, M. Gou, X. Wang, X. Li, F. Luo, X. Zhao, Y. Wei, Z. Qian, *International Journal of Pharmaceutics*, 365, **2009**, p. 89
[24] L. Piao, Z. Dai, M. Deng, X. Chen, X. Jing, *Polymer*, 44, **2003**, p. 2025

[25] R.A. Rhoades, D.R. Bell, *Medical Phisiology: Principles for Clinical Medicine*, Wolters Kluwer Health, **2012**
[26] J.M. Harris, S. Zalipsky, A.C.S.D.o.P. Chemistry, A.C.S. Meeting, *Poly(ethylene Glycol): Chemistry and Biological Applications*, American Chemical Society, **1997**
[27] B. Jeong, Y.H. Bae, D.S. Lee, S.W. Kim, *Nature*, 388, **1997**, p. 860
[28] X. Zhao, Z. Poon, A.C. Engler, D.K. Bonner, P.T. Hammond, *Biomacromolecules*, 13, **2012**, p. 1315
[29] C. Gozlan, E. Deruer, M.-C. Duclos, V. Molinier, J.-M. Aubry, A. Redl, N. Duguet, M. Lemaire, *Green Chemistry*, **2016**, p.
[30] I. Vroman, L. Tighzert, *Materials*, 2, **2009**, p. 307
[31] M.N. Belgacem, A. Gandini, *Monomers, Polymers and Composites from Renewable Resources*, Elsevier Science, **2011**
[32] P.B. Smith, R.B. Gross, *Biobased Monomers, Polymers, and Materials*, OUP USA, **2013**
[33] G. Gaucher, M.H. Dufresne, V.P. Sant, N. Kang, D. Maysinger, J.C. Leroux, *Journal of Controlled Release*, 109, **2005**, p. 169
[34] R. Trivedi, U.B. Kompella, *Nanomedicine*, 5, **2010**, p. 485
[35] F. Ungaro, C. Conte, L. Ostacolo, G. Maglio, A. Barbieri, C. Arra, G. Misso, A. Abbruzzese, M. Caraglia, F. Quaglia, *Nanomedicine: Nanotechnology, Biology and Medicine*, 8, **2011**, p. 637
[36] The American Chemical Society (ACS), *Molecule of the Week: trans-trans-trans-1,6-Diphenyl-1,3,5-hexatriene*, http://www.acs.org/content/acs/en/molecule-of-the-week/archive/d/molecule-of-the-week-diphenylhexatriene.html, Last Access: 18/12/2015
[37] U.S. Department of Health and Human Services, Food and Drug Administration, Center for Drug Evaluation and Research (CDER), Center for Biologics Evaluation and Research (CBER), Office of Regulatory Affairs (ORA), *Guidance for Industry. Sterile Drug Products Produced by Aseptic Processing - Current Good Manufacturing Practice:* **2004**
[38] L. Glavas, P. Olsen, K. Odelius, A.C. Albertsson, *Biomacromolecules*, 14, **2013**, p. 4150
[39] P.P. Ghoroghchian, P.R. Frail, K. Susumu, D. Blessington, A.K. Brannan, F.S. Bates, B. Chance, D.A. Hammer, M.J. Therien, *Proceedings of the National Academy of Sciences of the United States of America*, 102, **2005**, p. 2922
[40] S. Curia, A.F. Barclay, S. Torron, M. Johansson, S.M. Howdle, *Philosophical Transactions of the Royal Society of London A: Mathematical, Physical and Engineering Sciences*, 373, **2015**, p. 1
[41] C.A. Cherrington, M. Hinton, G.C. Mead, I. Chopra, *Organic Acids: Chemistry, Antibacterial Activity and Practical Applications*, in: A.H. Rose, D.W. Tempest (Eds.) Advances in Microbial Physiology, Academic Press, **1991**, pp. 87.
[42] S. Maddin, *Journal of the American Academy of Dermatology*, 40, **1999**, p. 961
[43] J. Sun Yu, A. Keun Kim, *Journal of Biomedical Science*, 17, **2010**, p. 1
[44] H.J. Arpe, *Ullmann's Encyclopedia of Industrial Chemistry, Ullmann's Encyclopedia of Industrial Chemistry: Set: Printed Fifth Edition plus Sixth Edition Electronic Release*, Wiley, **1999**
[45] D.L. Sparks, R. Hernandez, L.A. Estévez, N. Meyer, T. French, *Journal of Chemical & Engineering Data*, 52, **2007**, p. 1246

[46] J. Jennings, M. Beija, A.P. Richez, S.D. Cooper, P.E. Mignot, K.J. Thurecht, K.S. Jack, S.M. Howdle, *Journal of the American Chemical Society*, 134, **2012**, p. 4772
[47] J. Jennings, M. Beija, J.T. Kennon, H. Willcock, R.K. O'Reilly, S. Rimmer, S.M. Howdle, *Macromolecules*, 46, **2013**, p. 6843
[48] F.C. Loeker, C.J. Duxbury, R. Kumar, W. Gao, R.A. Gross, S.M. Howdle, *Macromolecules*, 37, **2004**, p. 2450
[49] M. Eriksson, L. Fogelström, K. Hult, E. Malmström, M. Johansson, S. Trey, M. Martinelle, *Biomacromolecules*, 10, **2009**, p. 3108
[50] M. Eriksson, K. Hult, E. Malmström, M. Johansson, S.M. Trey, M. Martinelle, *Polymer Chemistry*, 2, **2011**, p. 714
[51] S. Torron, M. Johansson, *Journal of Polymer Science Part A: Polymer Chemistry*, 53, **2015**, p. 2258
[52] H.E. Gottlieb, V. Kotlyar, A. Nudelman, *The Journal of Organic Chemistry*, 62, **1997**, p. 7512
[53] SITA Process Solutions, *Bubble pressure method for measuring the dynamic surface tension*, http://www.sita-process.com/information-service/process-parameter-surface-tension/bubble-pressure-method-for-measuring-the-surface-tension/, Last Access: 26/01/2016
[54] A. Noshay, J.E. McGrath, *Block Copolymers: Overview and Critical Survey*, Elsevier Science, **2013**
[55] J. Mark, *Physical Properties of Polymers*, Cambridge University Press, **2004**
[56] I.W. Hamley, P. Parras, V. Castelletto, R.V. Castillo, A.J. Müller, E. Pollet, P. Dubois, C.M. Martin, *Macromolecular Chemistry and Physics*, 207, **2006**, p. 941
[57] X. Kong, H. Qi, J.M. Curtis, *Journal of Applied Polymer Science*, 131, **2014**, p. 1
[58] A. Barclay, *Master Thesis*, School of Chemistry, The University of Nottingham, Nottingham, **2015**
[59] Y. Huang, X. Xu, X. Luo, D. Ma, *Chinese Journal of Polymer Science*, 20, **2002**, p. 45
[60] L. Zhang, A. Eisenberg, *Journal of the American Chemical Society*, 118, **1996**, p. 3168
[61] G. Rizis, *PhD Thesis*, Department of Chemistry, McGill University, Montréal, **2013**
[62] CabralH, MatsumotoY, MizunoK, ChenQ, MurakamiM, KimuraM, TeradaY, M.R. Kano, MiyazonoK, UesakaM, NishiyamaN, KataokaK, *Nature Nanotechnology*, 6, **2011**, p. 815
[63] E. Doris, F. Duconge, E. Gravel, N. MacKiewicz, B. Tavitian, Patent WO/2012/020337A1,*"Polymerized micelles for diagnosis"*, **2013**
[64] I. Rivolta, A. Panariti, B. Lettiero, S. Sesana, P. Gasco, M.R. Gasco, M. Masserini, G. Misserocchi, *Journal of Physiology and Pharmacology*, 62, **2011**, p. 45
[65] T.-F. Yang, C.-N. Chen, M.-C. Chen, C.-H. Lai, H.-F. Liang, H.-W. Sung, *Biomaterials*, 28, **2007**, p. 725
[66] M. Verbrugghe, P. Sabatino, E. Cocquyt, P. Saveyn, D. Sinnaeve, P. Van der Meeren, J.C. Martins, *Colloids and Surfaces A: Physicochemical and Engineering Aspects*, 372, **2010**, p. 28
[67] S. Kalepu, M. Manthina, V. Padavala, *Acta Pharmaceutica Sinica B*, 3, **2013**, p. 361

[68] I. Pepić, J. Lovrić, A. Hafner, J. Filipović-Grčić, *Drug Development and Industrial Pharmacy*, 40, **2014**, p. 944
[69] E.S. Lee, Y.T. Oh, Y.S. Youn, M. Nam, B. Park, J. Yun, J.H. Kim, H.T. Song, K.T. Oh, *Colloids and surfaces B: Biointerfaces*, 82, **2011**, p. 190

6 Conclusions and future investigations

This final chapter summarises the overall conclusions obtained from the research presented in this thesis. In particular, the high-pressure rheological analyses (Chapter 3) together with the potential of the new synthetic approach and the new polymers synthesised (Chapter 4 and 5).

Furthermore, aspects of possible future research that could be carried out for the continuation of the work are considered.

6.1 Conclusions

This thesis has focussed upon investigations on the use of supercritical CO_2 ($scCO_2$) to achieve new approaches that might lead to a more sustainable plastic industry.

Chapter 3 described the rheological analysis carried out on a commercially available semi-crystalline polyester; *i.e.* poly(ε-caprolactone) (PCL).
Interpretation of the viscoelastic moduli *vs* temperature graphs have been exploited for the first time on a semi-crystalline polymer under pressure, to highlight the possibility of lowering the melting point of this biodegradable polyester by adding pressurised CO_2. Hence, a new and effective methodology to assess the CO_2-induced melting point depression of semi-crystalline polymers has been described. The results correlate well with previous thermal and spectroscopic studies [1, 2], and give a rheological viewpoint to the CO_2-induced melting point depression. This could aid the modelling of this effect and support the design of lower temperature CO_2-assisted processes.
Additionally, rotational experiments were performed to determine the viscosity of PCL samples with different molecular weight (10 kg mol^{-1} and 80 kg mol^{-1} respectively). Dramatic reductions of the viscosity were observed for both polymers: at 300 bar a ~95% reduction (relative to the ambient pressure value) was obtained for the two samples.
In addition, comparisons with high-temperature viscosity studies (at ambient pressure) showed the significant improvements achieved by using $scCO_2$: the viscosity values obtained at 80 °C and 180 bar under CO_2 are comparable to those achieved at 180 °C in the absence of CO_2.
Supplementary experiments carried out under high-pressure N_2 showed that the effect of a non-plasticising gas was an increase in the viscosity, rather than a decrease.
These results highlighted the substantial advantages that high-pressure CO_2 processing of semi-crystalline polymers could provide in terms of energy saving and processing of thermally labile materials.

This learning was the starting point for the development of the next two chapters where CO_2 has been used to design a novel green lower temperature synthetic approach.

Chapter 4 described the development of a novel enzymatic low temperature approach for the preparation of functional polyesters based on renewable monomers (*i.e.* azelaic acid and 1,6-hexanediol). The use of $scCO_2$ (275 bar) allowed for the utilisation of a commercially available immobilised lipase (Novozym 435) as a catalyst. The reactions were carried out at 35 °C without pre-modification of the monomers and without using organic solvents. To the best of the author's knowledge, it is the first time that synthesis of polyesters *via* polycondensation has been carried out at such low temperatures.
Different molecular weights were targeted by carefully tuning the feed ratio of the reactants. Four different functional end-cappers were used in order to prepare poly(hexylene azelate) (PHAz) telechelics with distinctive terminal moieties.
The combined use of the supported lipase and CO_2 (and the resulting mild temperature) avoided competing side reactions involving the end-group moieties. To support this hypothesis, the same reactions were carried out in the melt without CO_2 (110 °C): these not only resulted in lower yields and uncontrolled side-reactions, but also in a reduction in the enzyme activity, which could not be efficiently recycled afterwards. Conversely, the lipase activity was not compromised during the polycondensations performed in $scCO_2$ at 35 °C.
The bio-based telechelic polymers thus prepared possess functional groups that could undergo further modification, cross-linking or chain extension processes. These possibilities were assessed through preliminary spectroscopic and thermal analyses, obtaining initial promising results.
This process could therefore lead towards a fully green, solvent-free, low-temperature route for the synthesis of renewable functional polyesters in $scCO_2$. Such an approach would be of great importance in the production of functional materials for biomedical applications. This possibility has been explored in the subsequent research chapter.

In the fifth chapter, the enzymatic low temperature approach developed in Chapter 4 has been exploited for the preparation of amphiphilic block copolymers

based on azelaic acid, 1,6-hexanediol and methoxy poly(ethylene glycol) (MPEG). Here again, the polymerisations could be carried out at 35 °C in a solvent-free CO_2 system and using Novozym 435 as a catalyst. This confirmed the versatility of these CO_2-assisted lipase-catalysed polymerisations and highlighted once again the significant prospects that CO_2-aided polyester synthesis and processing could deliver in terms of cost saving and preparation of novel materials: the use of CO_2 opens up for the design of new synthetic routes that would simply not be possible in normal (*i.e.* melt or solvent based) systems.
Additionally, the usefulness of the thus prepared copolymers was assessed through electron microscopy, light scattering, spectroscopy and surface tension studies. These analyses showed the ability of these novel bio-based polymers to act as potential nano-carriers for medical applications (*e.g.* drug encapsulation) and their possible value also as surfactants in detergents and body-care formulations.

6.2 Future work

The rheological investigations demonstrated the dramatic effect that CO_2 can have on PCL with varied molecular weight and proved that moduli *vs* temperature plots give effective information on the melting point depression under pressure; nonetheless, there are still a number of areas that have not fully been investigated here, nor in the available literature. A detailed investigation on the flow behaviour and mechanical properties of polyesters with different end-groups in CO_2 could be used to test the influence of the terminal groups on the rheological properties of the melt and of the interaction with CO_2 (are the terminal groups influencing the CO_2-induced plasticisation?). These investigations could include also the analysis of ABA block copolymers.
In addition, the analyses of mixtures containing different ratios of monomers, oligomers and polymers could give important information on high-pressure polycondensations: in principle one could follow the reactions directly in the rheometer by analysing in real time the viscosity changes. This could open up the

possibility of designing a high-pressure reaction vessel in which the torque applied by the motor to the mechanical stirrer is continuously measured, in order to obtain information on the viscosity and to stop the reaction when the desired value (and hence conversion and/or molecular weight) is reached. This would certainly be a significant step-forward in the field of CO_2-assisted polymerisations.

The low temperature enzymatic approach developed in the fourth chapter has been applied to the polymerisation of azelaic acid and 1,6-hexanediol functionalised by using four different end-cappers. Preliminary studies have been carried out to assess the reactivity of the synthesised telechelics. However, more comprehensive mechanical and application testing investigations need to be carried out to examine their real usefulness as coatings and cross-linked materials (*e.g.* adhesion, solvent, scratch and impact resistance *etc.*).

Furthermore, owing to the antiseptic properties of azelaic acid, the resulting film could be characterised by antibacterial/antiseptic properties as well. Initial bacterial growth and adhesion studies are currently in progress and are being carried out within the Faculty of Medicine & Health Sciences of the University of Nottingham (Prof Roger Bayston group).

Additionally, this lipase-catalysed polymerisation is most probably suitable also for other diacids and diols. Therefore, it would be interesting to test if different mechanical properties can be obtained when using monomers with different structures. Such investigations would reveal the real potential of this novel synthetic route.

Finally, in this research work, low molecular weights have been targeted for the purpose of producing functional polymers suitable for cross-linked materials and coating applications [3-5]. Nonetheless, high molecular weight polyesters are also a desirable class of products (*e.g.* for the production of materials with good mechanical properties) [6]. Hence, investigations on the maximum molecular weights achievable in CO_2 using Novozym 435 at different pressure and temperature conditions could deliver a new insight on the preparation of high molecular weight bio-based polyesters. Comparisons with conventional catalysts and melt processes would afford a direct evaluation of the advantages obtained in CO_2. For example, not only can the CO_2-induced plasticisation afford advantages

in term of energy saving (lower temperature), but also for a given temperature a dramatically lower viscosity might be achieved: this could lead to higher conversion and molecular weight values that result from the higher diffusivity of oligomers/polymers in the plasticised melt.

The amphiphilic copolymers based on azelaic acid, 1,6-hexanediol and MPEG described in Chapter 5 displayed interesting characteristics and self-assembly properties. However, detailed studies should be carried out in order to test their drug loading/release properties and the human-body compatibility. Furthermore, their accumulation and elimination from the body must be assessed. In this way, the real usefulness of these novel polymers for medical applications could be evaluated.

Furthermore, different diacids/diols could be investigated to understand if distinctive self-assembly and properties can be obtained by changing the building blocks of the hydrophobic segment. In addition, even if the production of bio-based PEGs has been announced [7, 8], sugar alcohol-derived hydrophilic polymers (*e.g.* poly(sorbitol) and linear poly(glycerol) [9]) could be investigated as hydrophilic blocks and impart an added value to the formulations.

Moreover, the degradation of these amphiphilic copolymers and of the telechelics presented in Chapter 4 should be inspected to determine the environmental impact of these novel polymers.

Another important aspect to consider is the separation of the polymer products described in Chapter 4 and 5 from the enzyme beads (and from the molecular sieves used to trap the water by-product). For practical reasons, in this thesis this was achieved through use of a small amount of toluene. However, our group previously showed that it is possible to exploit the CO_2-induced plasticisation of the polymer product to obtain this separation [10]: further studies need to be done to improve this process and test its large scale viability.

Finally, a general consideration regarding the energy cost of the high-pressure processes presented in this thesis has to be done. Without a doubt, the ability to prepare new materials, which may not be accessible *via* conventional high-temperature processes, represents a significant step-forward. However, the energy

cost of this synthetic approach must be carefully evaluated and compared to that of conventional high-temperature routes. These crucial examinations will provide a clear assessment of the viability of these enzymatic CO_2-aided polycondensations on a commercial scale with an industrial point of view. Such investigations are already in progress in our group. Preliminary results show that the most significant expenditure in conventional melt processing is the large amount of energy required to heat the bulk polymerisation. By contrast, compression costs for needed for CO_2 pressurisation are an order of magnitude smaller. Hence, reducing the typical working temperature from ~110 °C (or more) to 35 °C will have undoubtedly a dramatic effect in terms of energy saving.

In summary, this thesis demonstrates excellent potential for further exploitation of $scCO_2$ for a wide range of possible applications in polyester synthesis and processing.

6.3 References

[1] C.A. Kelly, K.L. Harrison, G.A. Leeke, M.J. Jenkins, *Polymer Journal*, 45, **2013**, p. 188
[2] S. Murphy, *MRes Thesis*, School of Engineering, Department of Metallurgy and Materials, University of Birmingham, **2011**
[3] M. Eriksson, L. Fogelström, K. Hult, E. Malmström, M. Johansson, S. Trey, M. Martinelle, *Biomacromolecules*, 10, **2009**, p. 3108
[4] M. Eriksson, K. Hult, E. Malmström, M. Johansson, S.M. Trey, M. Martinelle, *Polymer Chemistry*, 2, **2011**, p. 714
[5] S. Semlitsch, S. Torron, M. Johansson, M. Martinelle, *Green Chemistry*, **2016**, p.
[6] X. Kong, H. Qi, J.M. Curtis, *Journal of Applied Polymer Science*, 131, **2014**, p. 1
[7] Grand View Research, *Polyethylene Glycol (PEG) Market Analysis By Application (Medical, Personal Care, Industrial) And Segment Forecasts To 2020*, http://www.grandviewresearch.com/industry-analysis/polyethylene-glycol-peg-market, Last Access: 11/04/2016
[8] Green Chemicals Blog, *Europe explores creation of Bio-based products standards*, http://greenchemicalsblog.com/2015/03/16/europe-explores-creation-of-bio-based-products-standards/, Last Access: 11/04/2016
[9] A. Thomas, S.S. Müller, H. Frey, *Biomacromolecules*, 15, **2014**, p. 1935
[10] F.C. Loeker, C.J. Duxbury, R. Kumar, W. Gao, R.A. Gross, S.M. Howdle, *Macromolecules*, 37, **2004**, p. 2450

A Appendix 1: Additional Information for Chapter 4

A.1 ^{1}H-NMR spectra of functional PHAz polymers with DP6

As stated in Chapter 4, the ^{1}H-NMR spectra of the telechelics with a longer backbone showed also the achievement of successful polymerisations with the preparation of polymers with size within the targeted range and efficiently end-capped (Figure A.1 to Figure A.4).

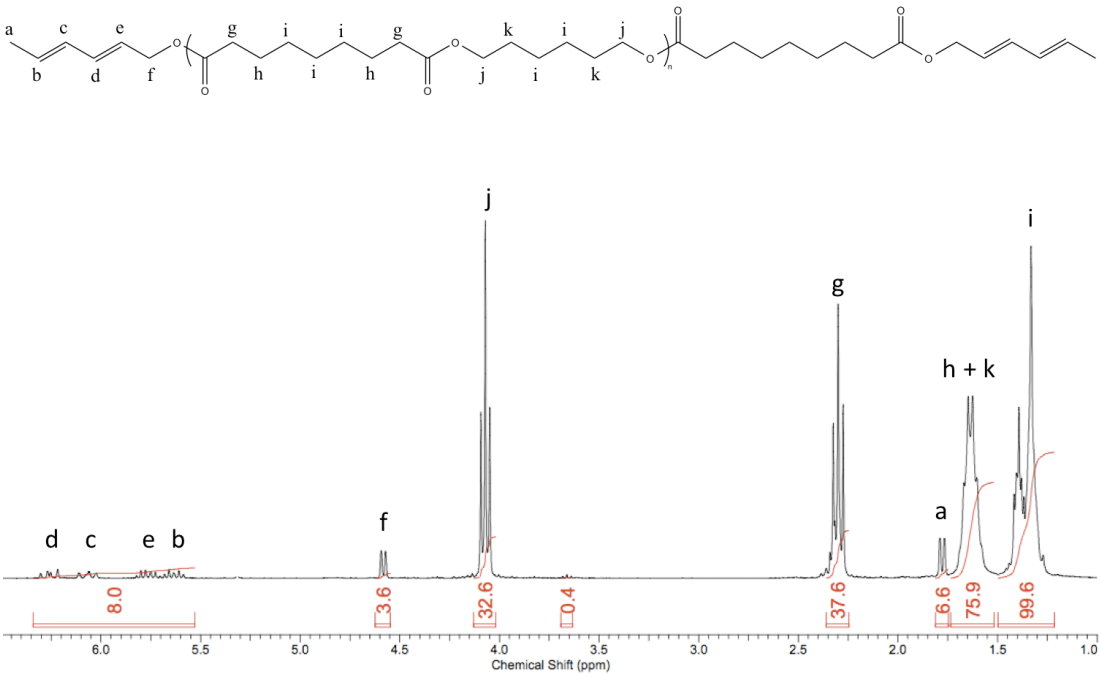


Figure A.1 - ^{1}H-NMR of PHAz-SA6: the end-capper peaks are clearly observed at around 1.75 ppm (a), 4.52 ppm (f) and between 5.50 and 6.55 ppm (b-e).

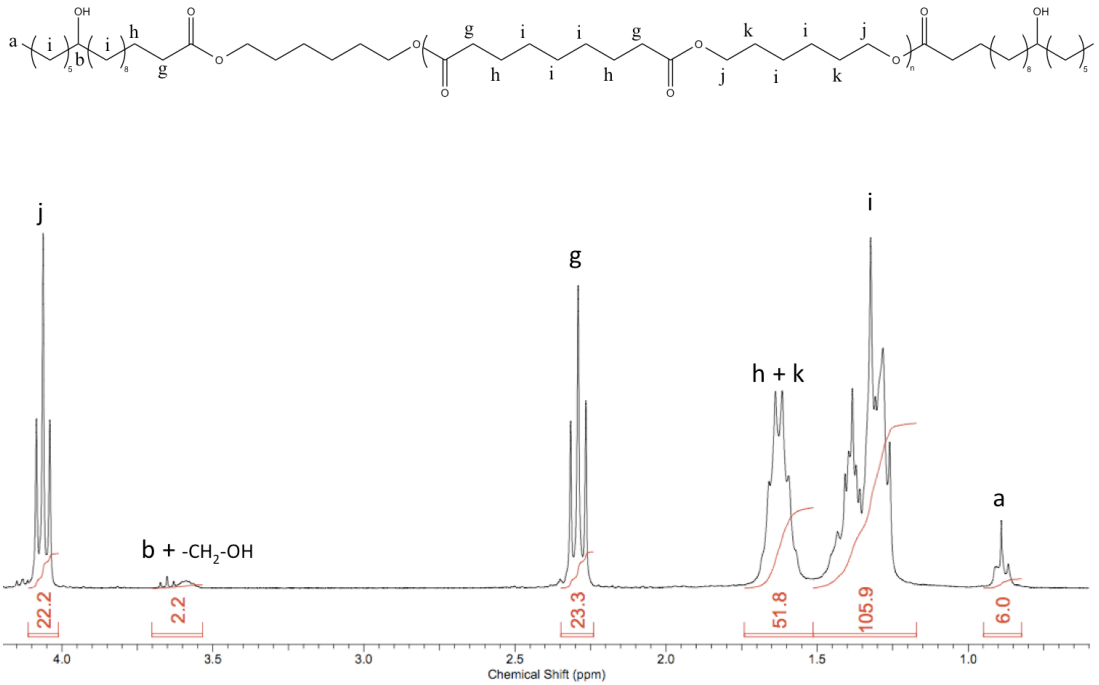


Figure A.2 – ^{1}H-NMR of PHAz-HSA6: the end-capper peaks are observed at 0.90 ppm (a), 3.60 ppm (b) and in the peak at 1.45 ppm (i). An additional small triplet that is assigned to protons adjacent to an alcohol group (either in the 1,6-hexanediol or uncapped chains) is observed at 3.65 ppm.

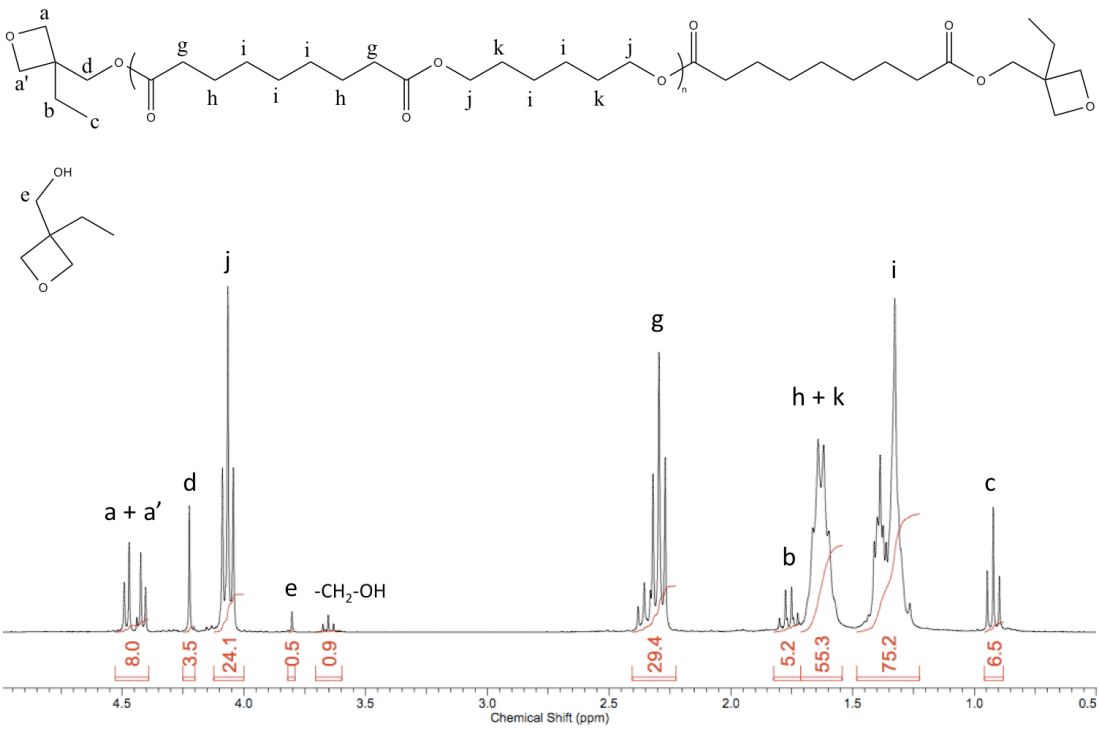


Figure A.3 - ^{1}H-NMR of PHAz-TMPO6: the end-capper peaks are observed at around 4.50 ppm (a and a'), 1.75 ppm (b), 0.95 ppm (c) and 4.25 ppm (d), a peak assigned to unreacted TMPO (<13%) is observed at 3.81 ppm (e).

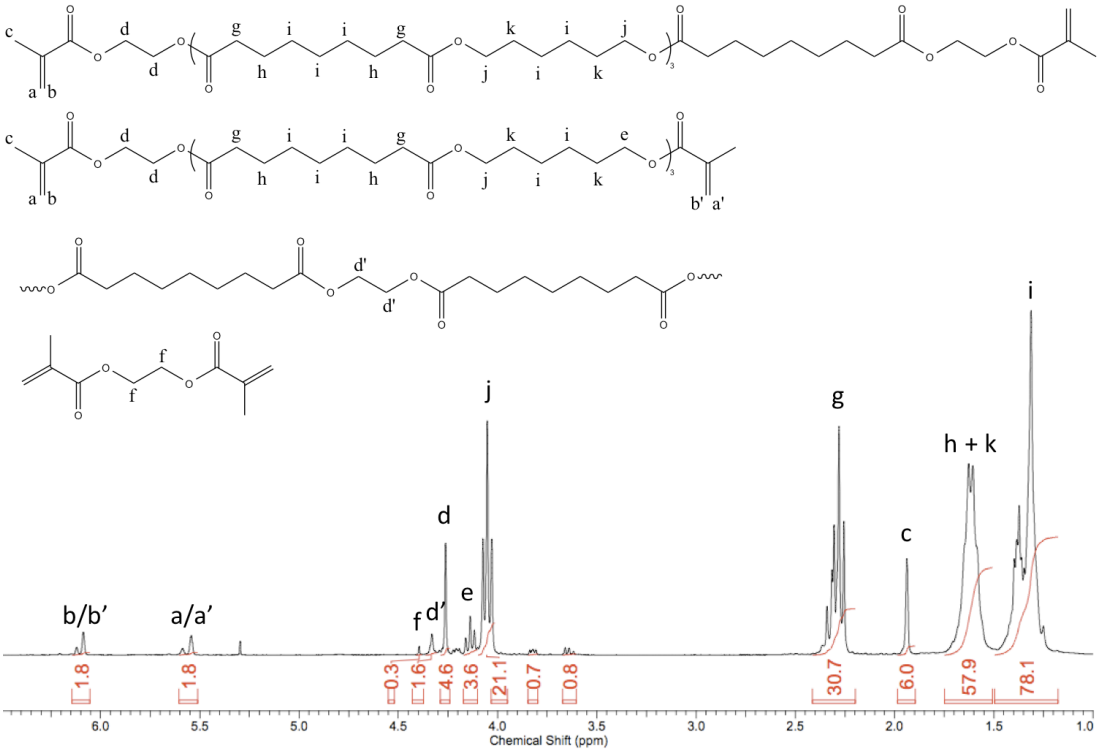


Figure A.4 – ^{1}H-NMR of PHAz-HEMA6: the end-capper signals are seen at 5.55 ppm (a and a'), 6.65 ppm (b and b'), 1.98 ppm (c) and 4.28 (d). The peak d' is assigned to ethylene glycol incorporated in the backbone rather than at the end of the chains, and the peak f is given by the EGDMA (<5%) formed by the enzyme.

A.2 ^{1}H-NMR spectra of the polymer synthesised without CO_2 in the melt at high temperature (110 °C)

The yields of the reactions carried out in the melt at 110 °C in the absence of CO_2 were quite low (40-60%). In addition to this, ^{1}H-NMR conducted on the products obtained from these reactions showed erratic integral values that did not match with the intact structures of the end-cappers: this might indicate that side-reactions involving the functionalisers moiety occurred (Figure A.5 to Figure A.8). Besides, assumption that all the chains were end-capped led to vain results on the determination of the molecular weight, which in most cases resulted considerably overestimated and incompatible with the feed ratio used in the reactions (the targeted DP was around 3). Hence, a low end-capping efficiency was generally afforded.

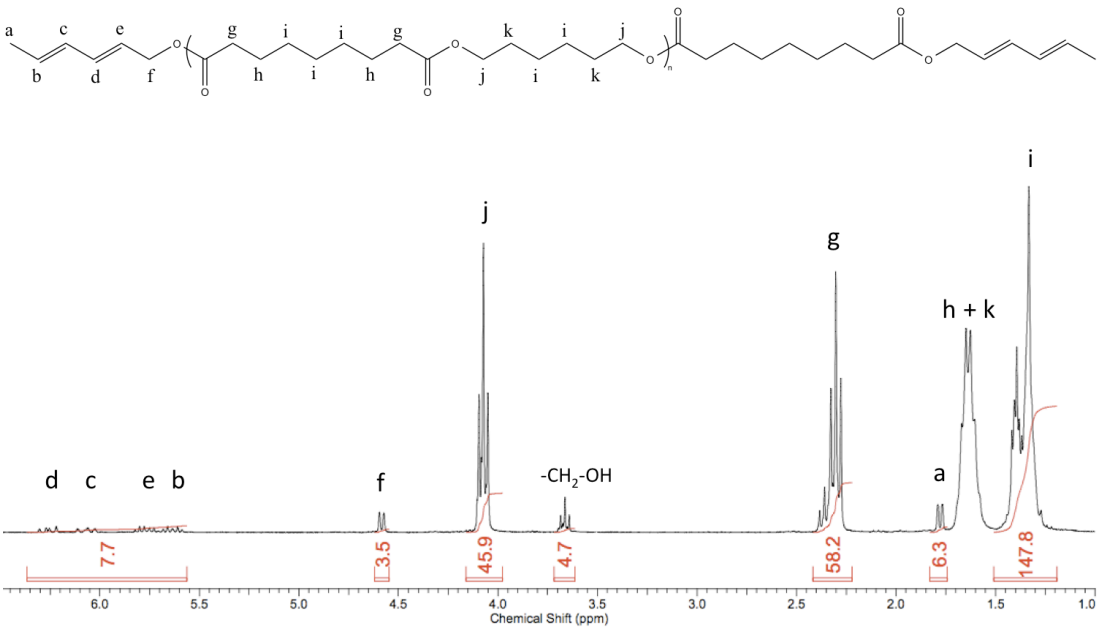


Figure A.5 - ^{1}H-NMR of PHAz-SA synthesised in the melt: the end-capper peaks are observed at around 1.75 ppm (a), 4.52 ppm (f) and between 5.50 and 6.55 ppm (b-e). The integrals attributed to the PHAz backbone are clearly overestimated considering the targeted size (DP3). This indicates a low end-capping efficiency.

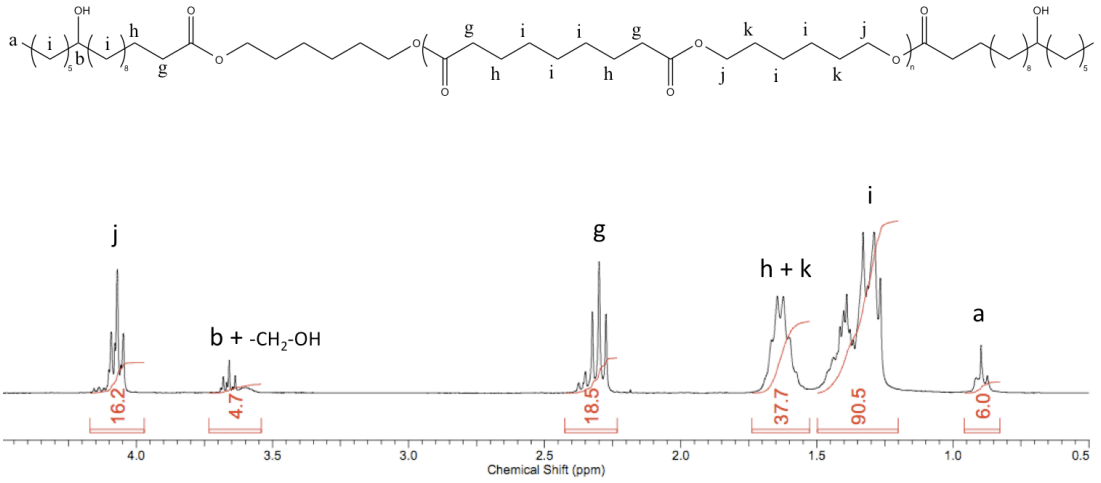


Figure A.6 - ^{1}H-NMR of PHAz-HSA synthesised in the melt: the end-capper peaks are observed at 0.90 ppm (a), 3.60 ppm (b) and in the peak at 1.45 ppm (i). The triplet that is assigned to protons adjacent to an alcohol group (either in the 1,6-hexanediol or uncapped chains) at 3.65 ppm has a much higher intensity compared to that observed for the products synthesised in CO_2. This indicates a lower monomer conversion and/or the presence of a significant amount of non end-capped chains.

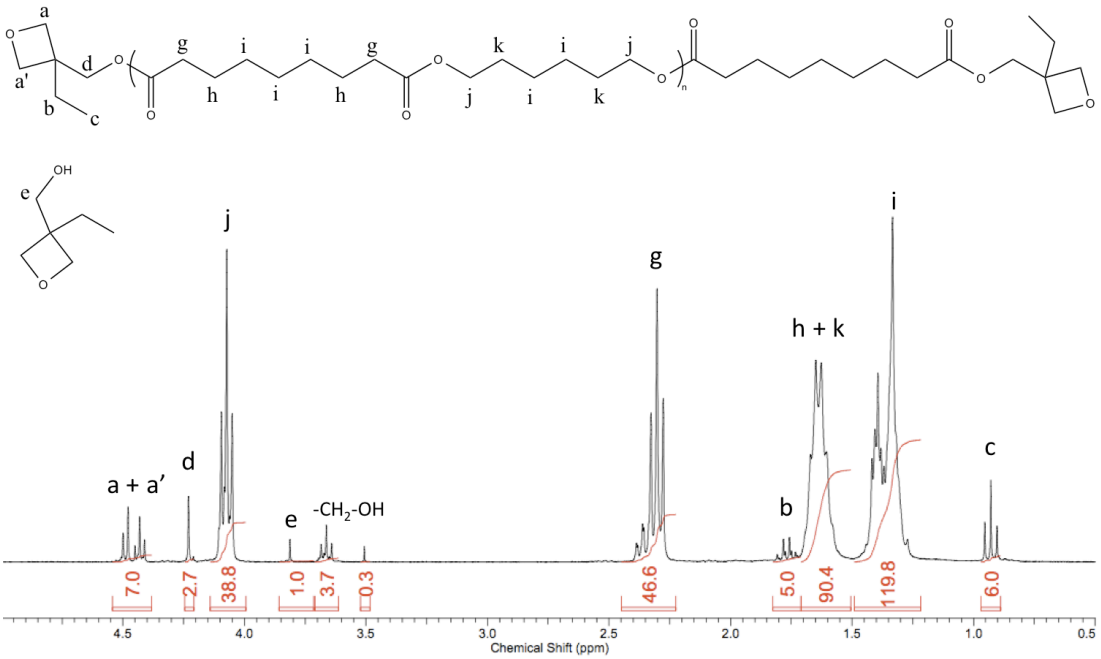


Figure A.7 - ^{1}H-NMR of PHAz-TMPO synthesised in the melt: the end-capper peaks are observed at around 4.50 ppm (a and a'), 1.75 ppm (b), 0.95 ppm (c) and 4.25 ppm (d), a peak assigned to unreacted TMPO (<13%) is observed at 3.81 ppm (e). The oxetane peaks (a+a') have a value lower than that expected; furthermore, a small peak around 3.5 ppm, which can be attributed to the formation of linear polyethers, is observed. The integrals attributed to the PHAz backbone are clearly overestimated considering the targeted size (DP3). This indicates a low end-capping efficiency.

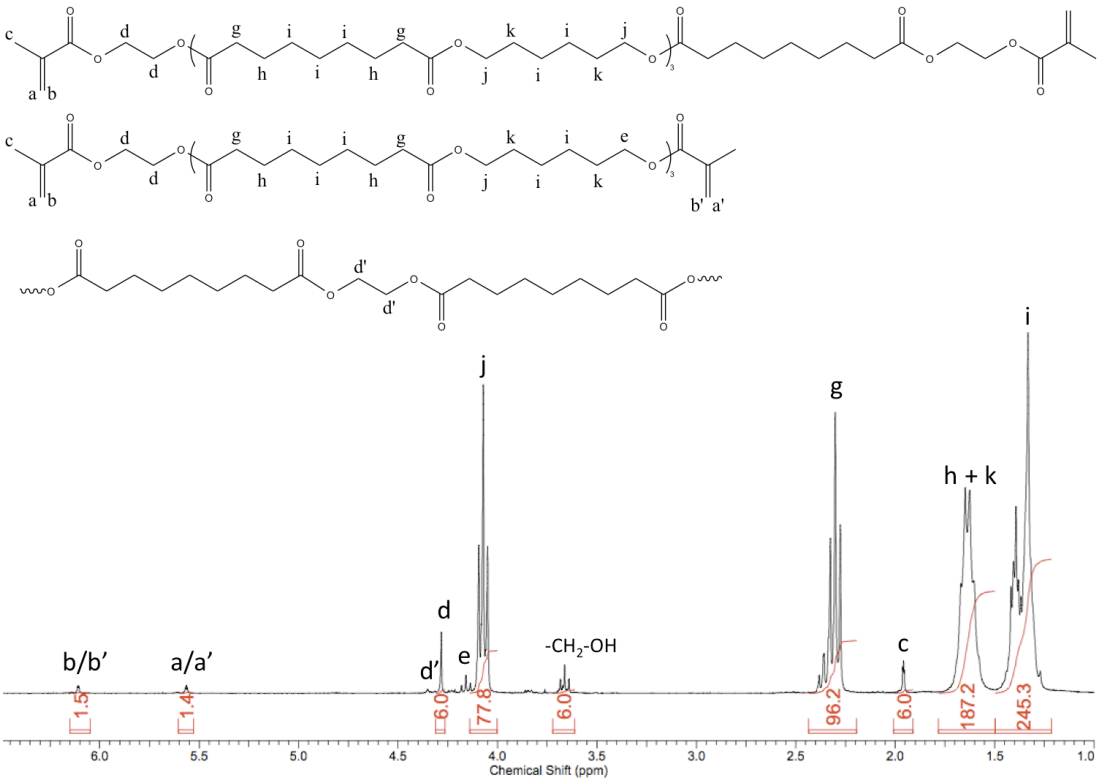


Figure A.8 - ^{1}H-NMR of PHAz-HEMA synthesised in the melt: the end-capper signals are seen at 5.55 ppm (a and a'), 6.65 ppm (b and b'), 1.98 ppm (c) and 4.28 (d). The peaks of the vinyl protons (a/a' and b/b') have a value lower than that expected; this might indicate side reactions involving this functionality. The integrals attributed to the PHAz backbone are clearly overestimated considering the targeted size (DP3). This indicates a low end-capping efficiency.

A.3 ^{1}H-NMR spectra for enzyme recycling tests (synthesis of propyl oleate)

The conversion of 1-propanol into propyl oleate was determined by monitoring the peak of 1-propanol at 3.65 ppm (a, HO-C<u>H$_2$</u>-) and comparing it to the propyl oleate peak at 4.05 ppm (b, -COO-C<u>H$_2$</u>-) (Figure A.9). As previously described, the same reaction was conducted by using: new enzyme beads, enzyme recycled from the scCO_2 reactions (used 5 times in CO_2) and enzyme used for one reaction at 110 °C (in the melt without CO_2).

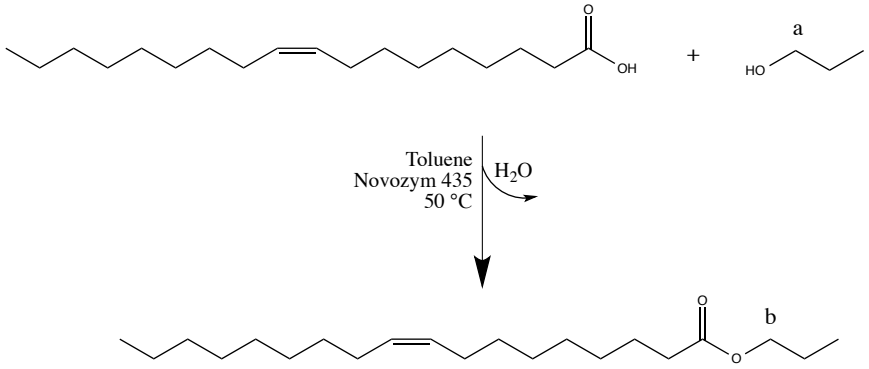


Figure A.9 - Synthesis of propyl oleate. This reaction was used to monitor the enzyme activity after the high- pressure poly-condensations. The reaction was monitored through ^{1}H-NMR by comparing the 1-propanol peak (a) at 3.65 ppm and the propyl oleate peak (b) at 4.05 ppm.

Sections of the obtained spectra are shown in the next pages (Figure A.10 to Figure A.12).

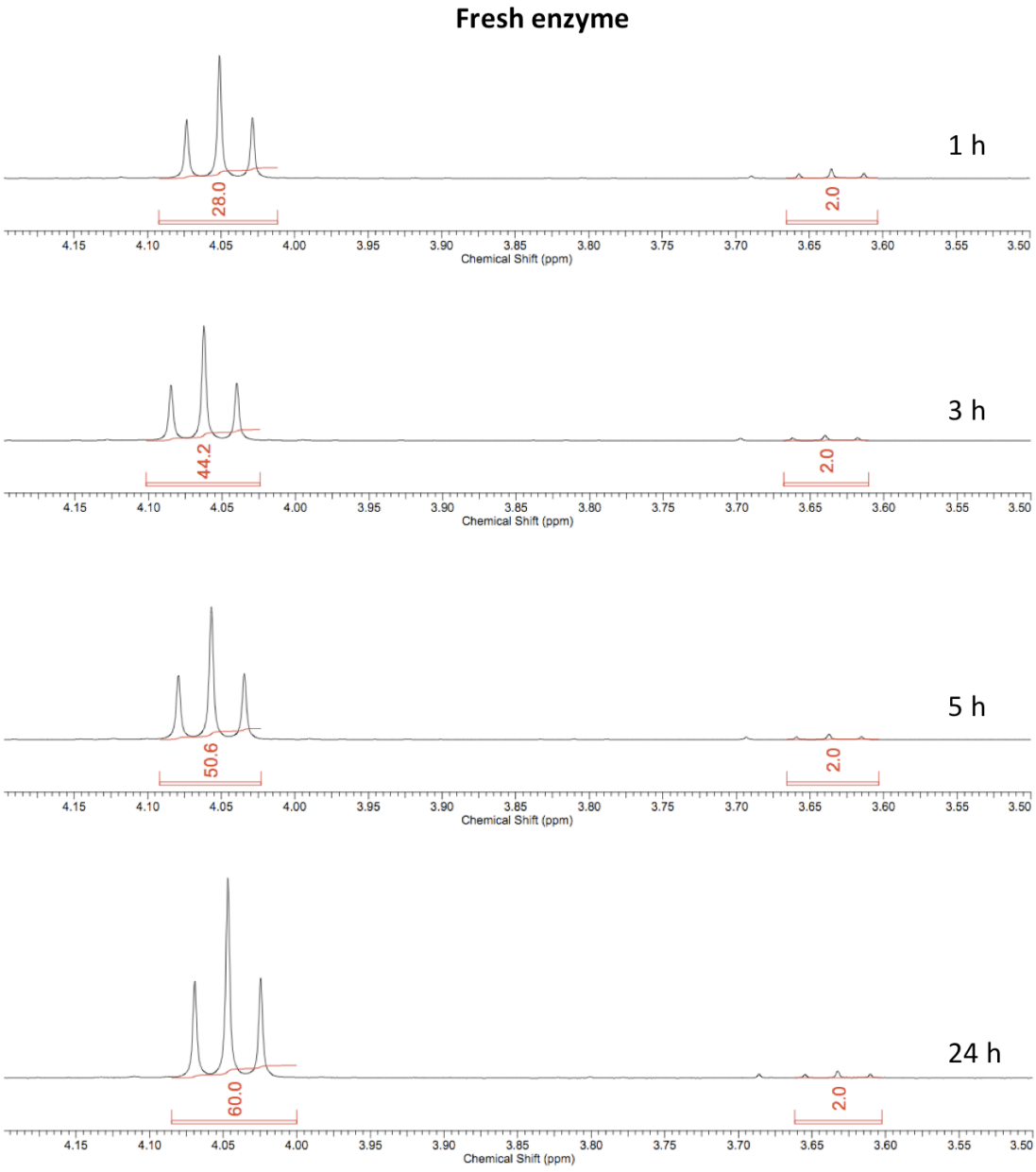


Figure A.10 – Section of the ^{1}H-NMR spectrum of propyl oleate synthesised using new Novozym 435 after 1, 3, 5 and 24 hours from the start of the reaction. The ester peak (at 4.05 ppm) grows with increasing time reaching 97% conversion at 24 hours.

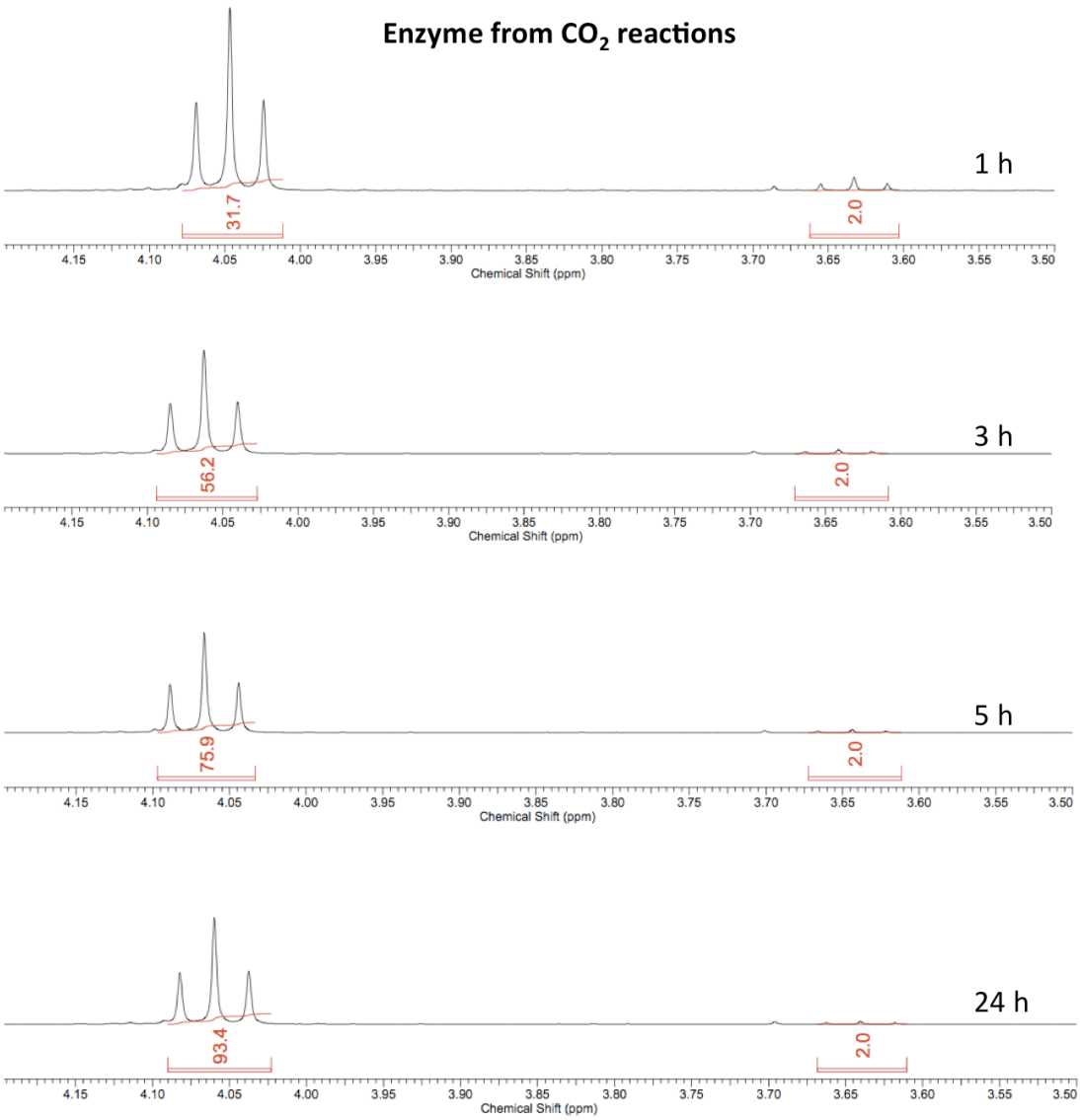


Figure A.11 - Section of the ^{1}H-NMR spectrum of propyl oleate synthesised using Novozym 435 beads used twice in CO_2 after 1, 3, 5 and 24 hours from the start of the reaction. The ester peak (at 4.05 ppm) grows with increasing time reaching 98% conversion at 24 hours.

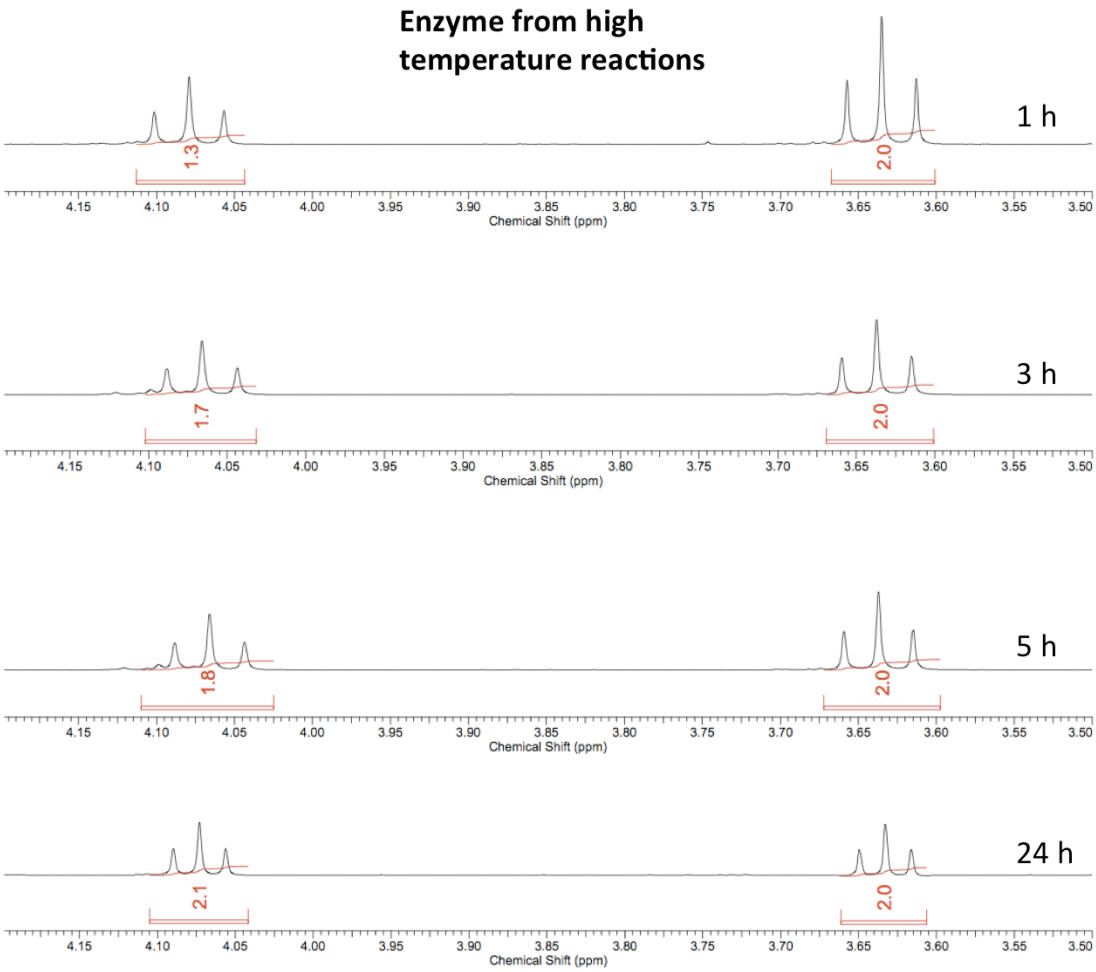


Figure A.12 - Section of the ^{1}H-NMR spectrum of propyl oleate synthesised using Novozym 435 beads used for the high temperature synthesis (110 °C) after 1, 3, 5 and 24 hours from the start of the reaction. The ester peak (at 4.05 ppm) grows with increasing time reaching 51% conversion at 24 hours.

These spectra show that the activity of CaLB is reduced after the reaction at 110 °C, whilst no changes in the conversion obtained when using new Novozym 435 and beads used in CO_2 (up to 5 times) could be detected. This confirms that the supercritical route is without a doubt more commercially sustainable and viable since not only the polymer products are not accessible through melt polycondensation, but also the enzyme can be recycled without loss of activity after the high-pressure polymerisations.

B Appendix II: Additional Information for Chapter 5

B.1 ^{1}H-NMR of MPEGs and copolymers

The ^{1}H-NMR spectra of the two different MPEGs used to end-cap the PHAz chains are shown (Figure B.1 and Figure B.2).

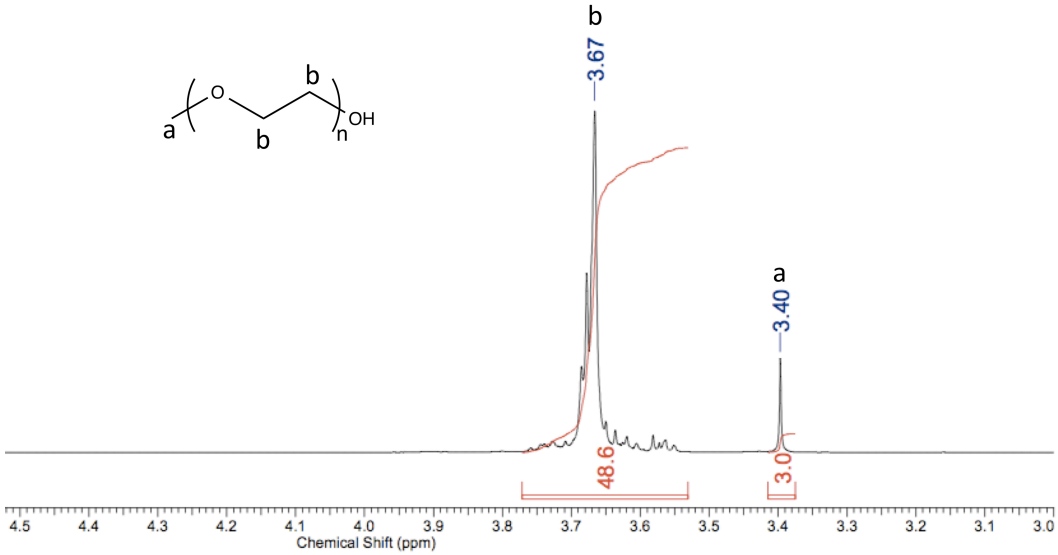


Figure B.1 - ^{1}H-NMR of MPEG550

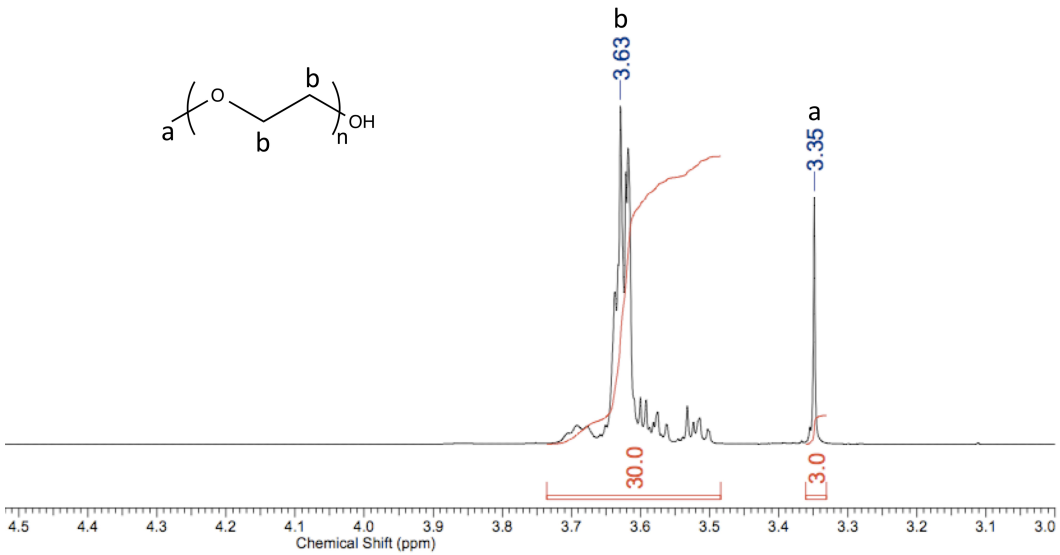


Figure B.2 - ^{1}H-NMR of MPEG350.

Integrals of the peak assigned to the MPEG backbone could be used to estimate approximate monomer conversion for all the copolymers.

The spectra of copolymers that were not shown in Chapter 5 are displayed here (Figure B.3 to Figure B.5). Integrals of the peaks at 3.38 ppm (terminal methoxy group in each of the MPEG blocks) and at 4.05, 2.28, 1.63 and 1.38-1.32 ppm (PHAz backbone protons) give a molar mass that agrees with the theoretical value (see Table 5.2 in Chapter 5).

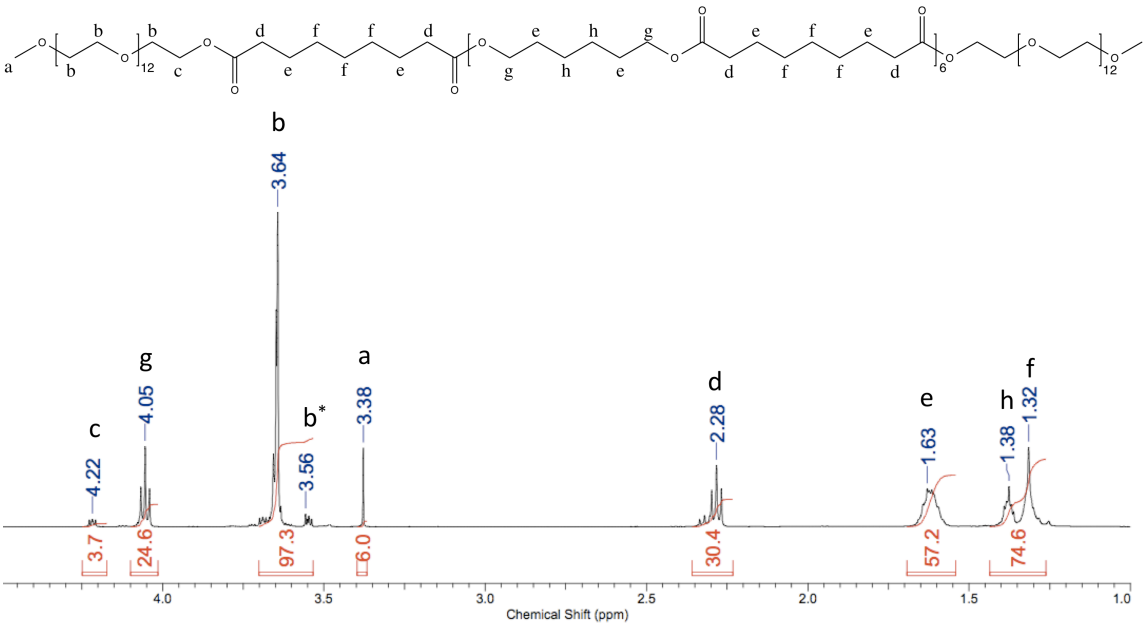


Figure B.3 - ^{1}H-NMR of polymer (b) MPEG$_{12}$-PHAz$_{6}$-MPEG$_{12}$. Integrals of the peak at 3.38 ppm (terminal methoxy group) and 4.05, 2.28, 1.63 and 1.38-1.32 ppm (PHAz backbone) can be used to estimate the average molar mass of the polymer. The peak b (3.64 ppm) is assigned to the -CH$_2$- in the MPEG backbone, while the peak b* (3.55 ppm) is assigned to the -CH$_2$- protons directly attached to the terminal methoxy group (-O-CH$_3$).

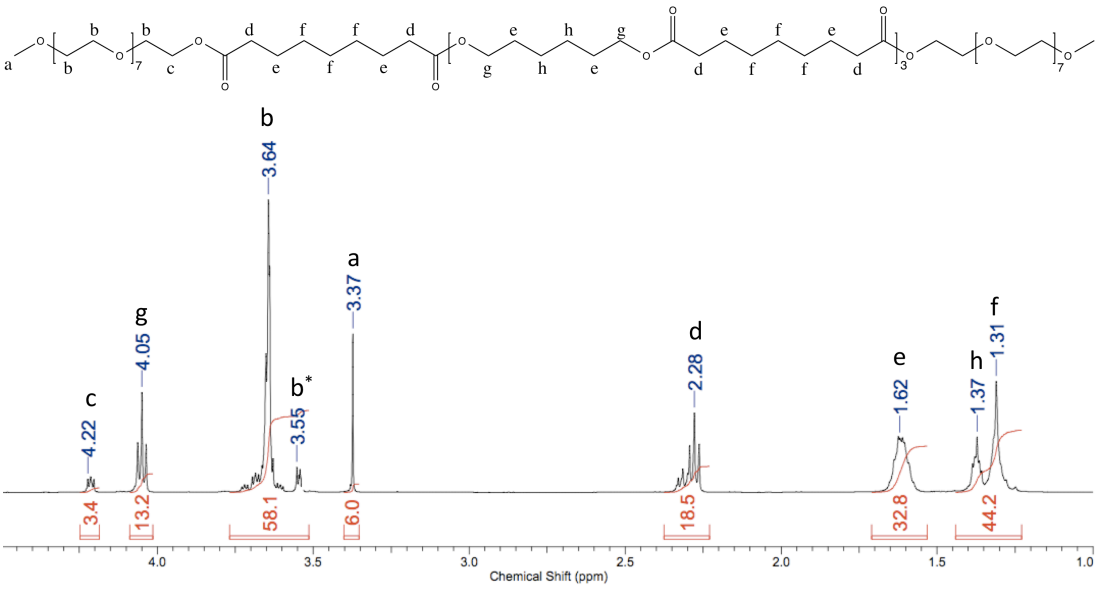


Figure B.4 - ^{1}H-NMR of polymer (c) MPEG$_7$-PHAz$_3$-MPEG$_7$.

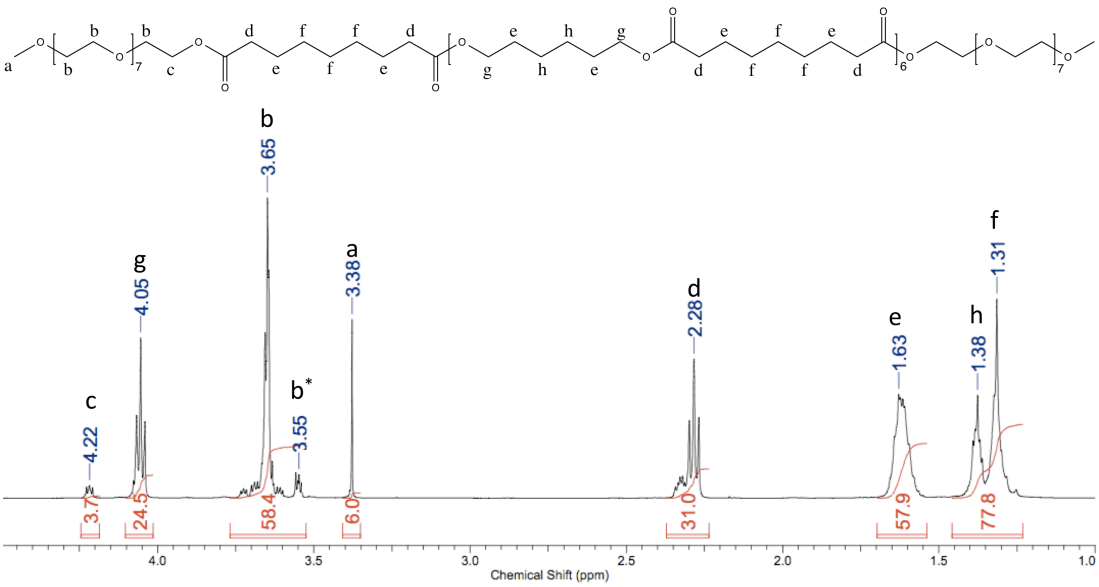


Figure B.5 - ^{1}H-NMR of polymer (d) MPEG$_7$-PHAz$_6$-MPEG$_7$.

From peak c (4.22 ppm) and a (3.38 ppm), it can be estimated that: more than 90% of the detected MPEG was attached to the polymer chains for polymers (b) MPEG$_{12}$-PHAz$_6$-MPEG$_{12}$ and (d) MPEG$_7$-PHAz$_6$-MPEG$_7$; whilst, 85% of MPEG was linked to the PHAz backbone for polymer (c) MPEG$_7$-PHAz$_3$-MPEG$_7$.

When the ^{1}H-NMR spectrum of (b) MPEG$_{12}$-PHAz$_6$-MPEG$_{12}$ is acquired in D_2O, the peaks assigned to the PHAz backbone are strongly suppressed because of the self-assembled structure in which this segment is characterised by restricted

motion (red dotted rectangles in Figure B.6); compare Figure B.6 to Figure B.3 for clarity.

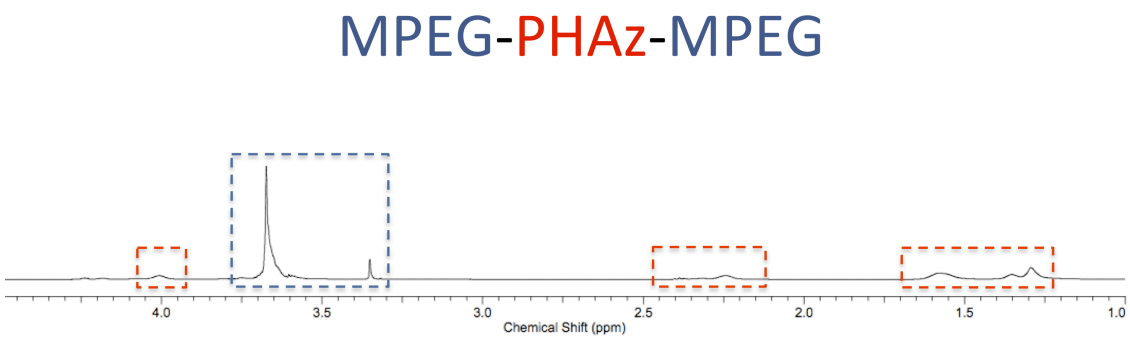


Figure B.6 - ^{1}H-NMR of polymer (b) $MPEG_{12}$-$PHAz_{6}$-$MPEG_{12}$ in D_2O. The PHAz resonances are strongly suppressed (compare to Figure B.1), whilst the MPEG peaks are clearly observed. This is due to the formation of aggregated structure with a PHAz portion with restricted motion.

B.2 DLS studies

B.2.1 Intensity and volume distribuions

Intensity and volume distribution obtained form DLS are slightly overestimated since the samples were not monodisperse (these two distributions strongly depends on the size of the particles). For this reason, the number distributions (showed in Chapter 5) matched better with the TEM images. This was more marked for samples (b) and (c) (shown) since their distributions were not monomodal (Figure B.7 to Figure B.10).

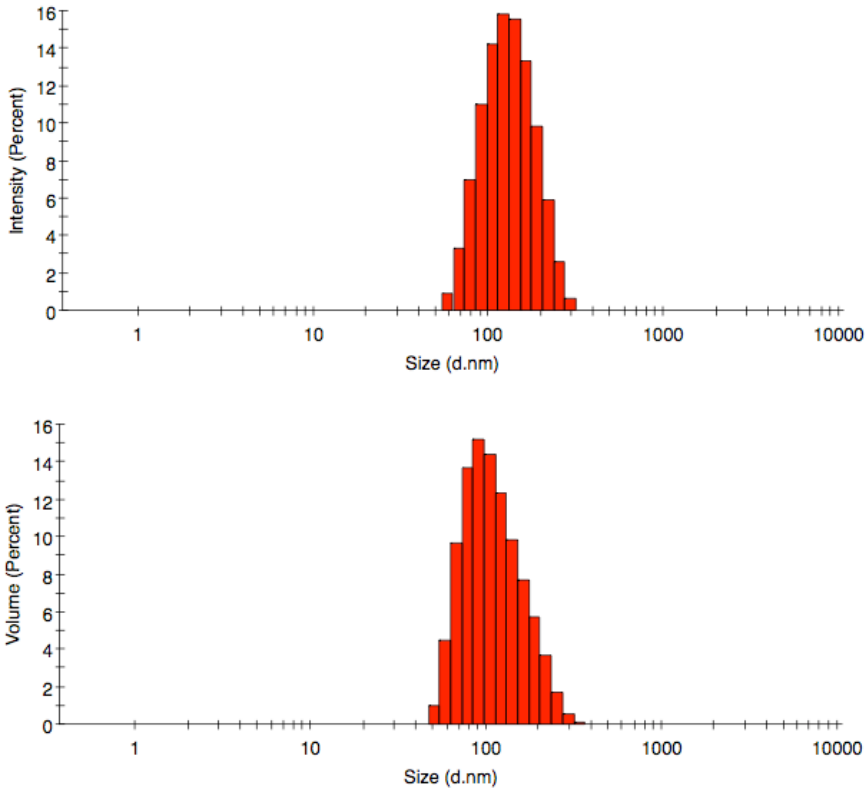


Figure B.7 – Intensity (top) and volume (bottom) distribution for (a) $MPEG_{12}$-$PHAz_3$-$MPEG_{12}$ micelles (0.1% wt in water).

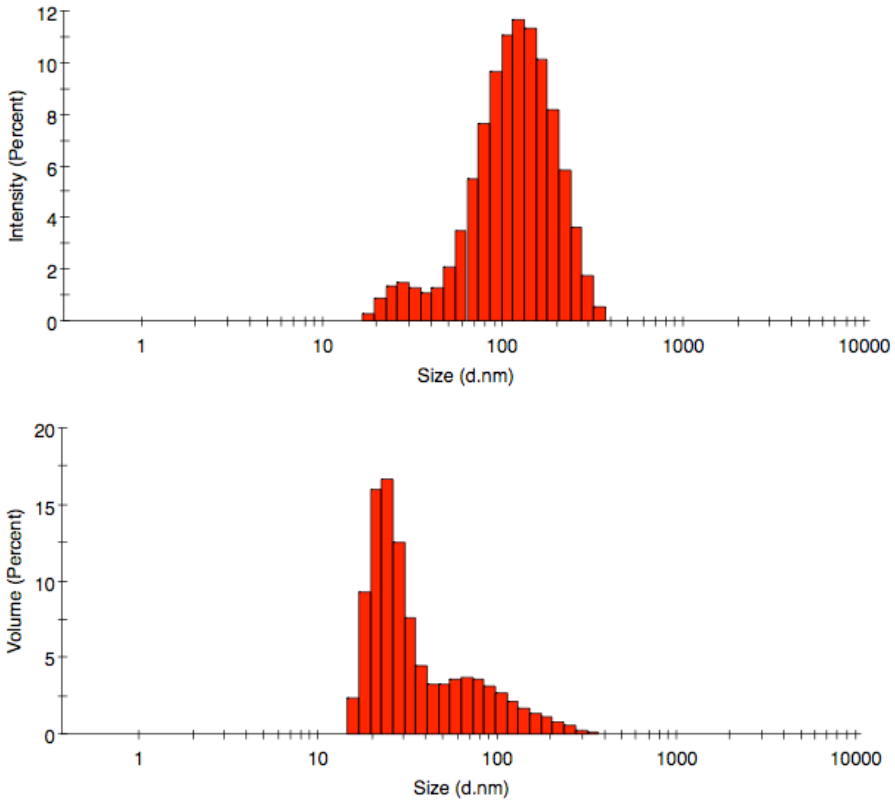


Figure B.8 - Intensity (top) and volume (bottom) distribution for (b) $MPEG_{12}$-$PHAz_6$-$MPEG_{12}$ micelles (0.1% wt in water).

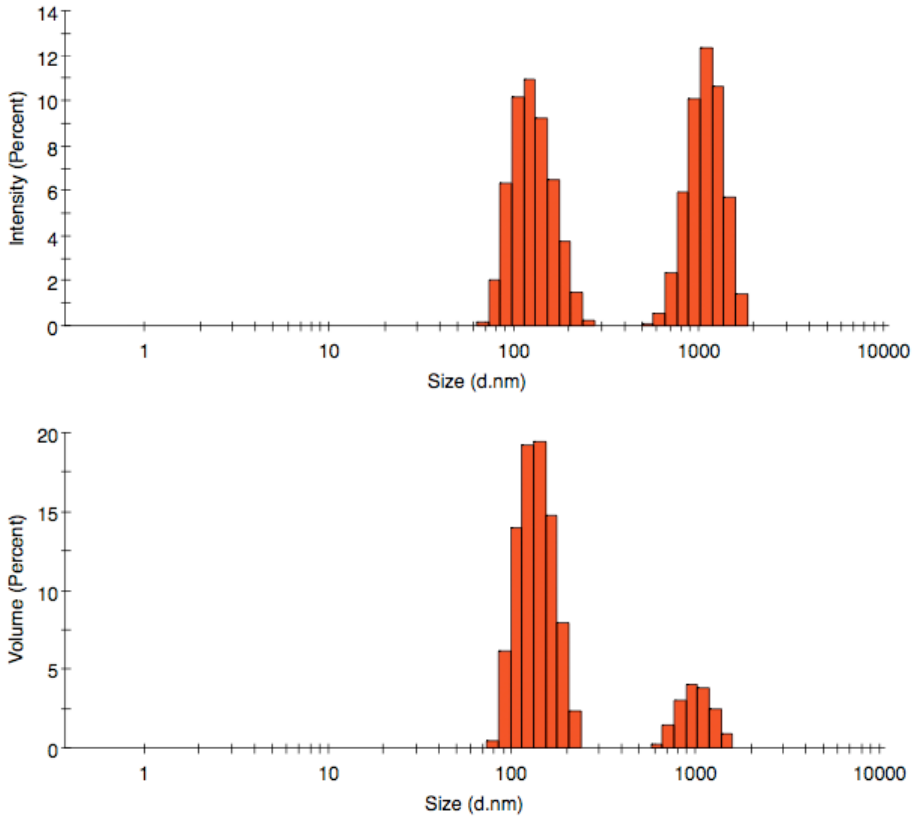


Figure B.9 - Intensity (top) and volume (bottom) distribution for (c) $MPEG_7$-$PHAz_3$-$MPEG_7$ micelles (0.1% wt in water).

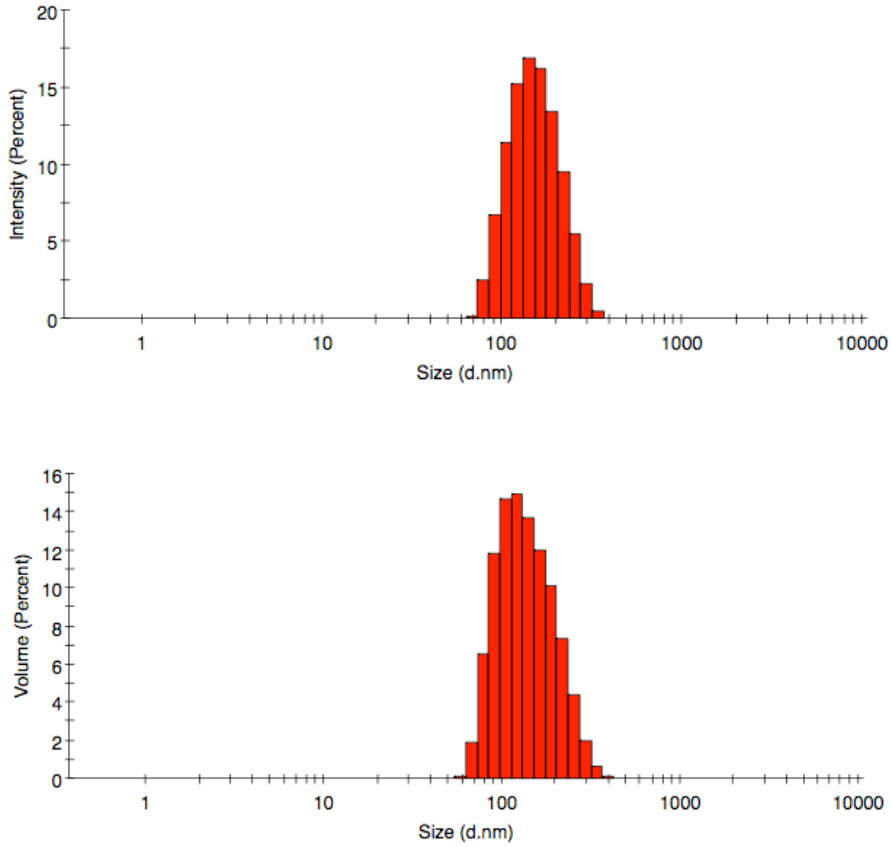


Figure B.10 - Intensity (top) and volume (bottom) distribution for (d) $MPEG_7$-$PHAz_6$-$MPEG_7$ micelles (0.1% wt in water).

B.2.2 DLS distribution of (b) $MPEG_{12}$-$PHAz_6$-$MPEG_{12}$: temperature study

The copolymer (b) $MPEG_{12}$-$PHAz_6$-$MPEG_{12}$ formed micelles with diameter around 20 nm, which are particularly interesting for medical applications. For this reason, the micellar size of this polymer was investigated further as a function of temperature. Distributions by number obtained by DLS at 30 35, 40 and 45 °C are shown (Figure B.11).

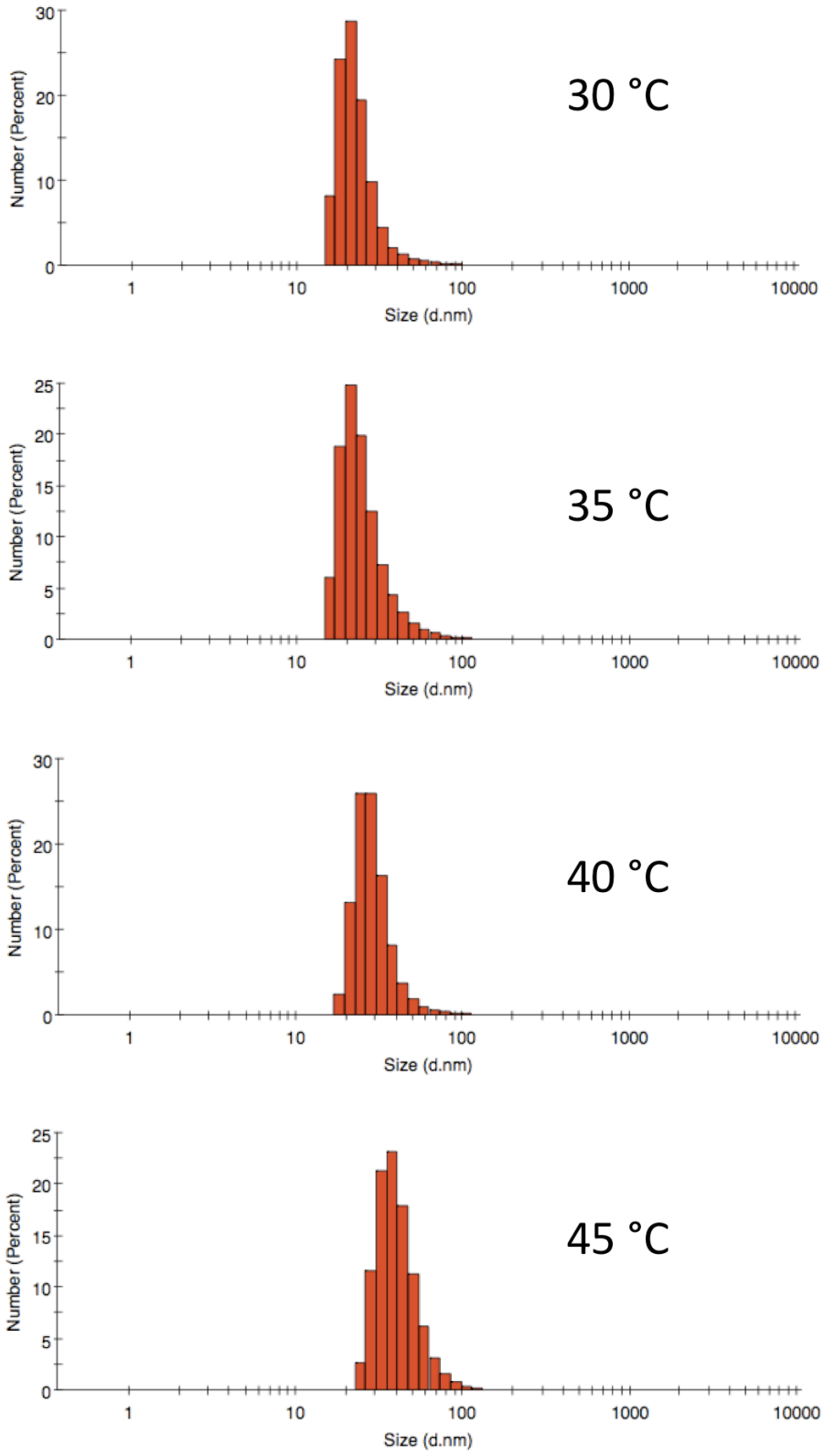


Figure B.11 – Size distribution by number of (b) $MPEG_{12}$-$PHAz_6$-$MPEG_{12}$ obtained through DLS at a range of temperature (30, 35, 40 and 45 °C top to bottom). The micellar size is shifted to higher values at higher temperatures, however the peak diameter is still below 30 nm at body temperatures.

B.2.3 DLS distribution of (b) MPEG-$_{12}$-PHAz$_6$-MPEG$_{12}$ micelles produced from nano-precipitation from DCM

Nano-precipitation from DCM was used to prepare Coumarin-6 (C6) loaded particles. Even if this solvent is not miscible with water (this might result in the formation of bigger structure, due to an increased aggregation), DCM was chosen to ensure the presence of a homogenous solution (containing C6 and the copolymer).

DLS analyses showed that the size distribution of the MPEG$_{12}$-PHAz$_6$-MPEG$_{12}$ nanoparticles prepared from DCM was not dramatically different from that obtained when using THF (Figure B.12). The distribution was slightly broader and shifted towards slightly higher values. In more detail, the peak value of the number distribution was 30.2 ± 9.3 nm (as opposed to 23.1 ± 7.3 obtained when using THF).

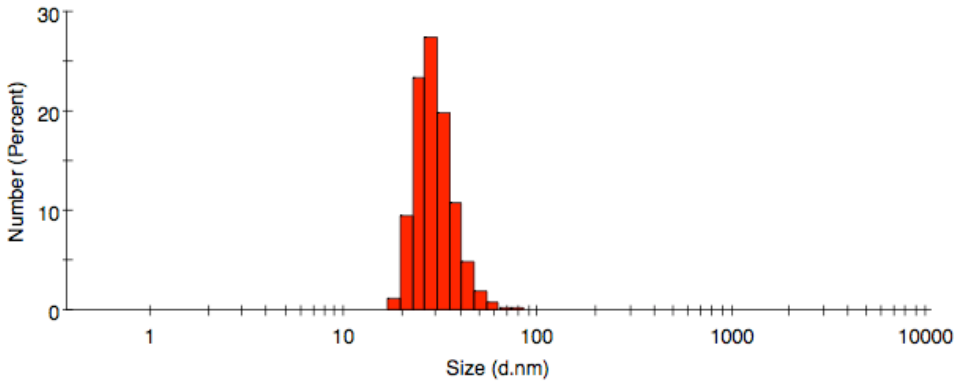


Figure B.12 - Number distribution obtained through DLS analysis (25 °C) for (b) MPEG$_{12}$-PHAz$_6$-MPEG$_{12}$ micelles (0.1% wt in water). These micelles were prepared through nano-precipitation from DCM. The average micellar size is slightly increased (30.2 ± 9.3), compared to that obtained through nano-precipitation from THF (23.1 ± 7.4 nm).

B.3 Additional TEM images

As shown in the Chapter 5, our preliminary studies confirmed the formation of self-assembled nanometric aggregates in water. Varied aggregates were observed. Additional TEM images are shown here (Figure B.13).

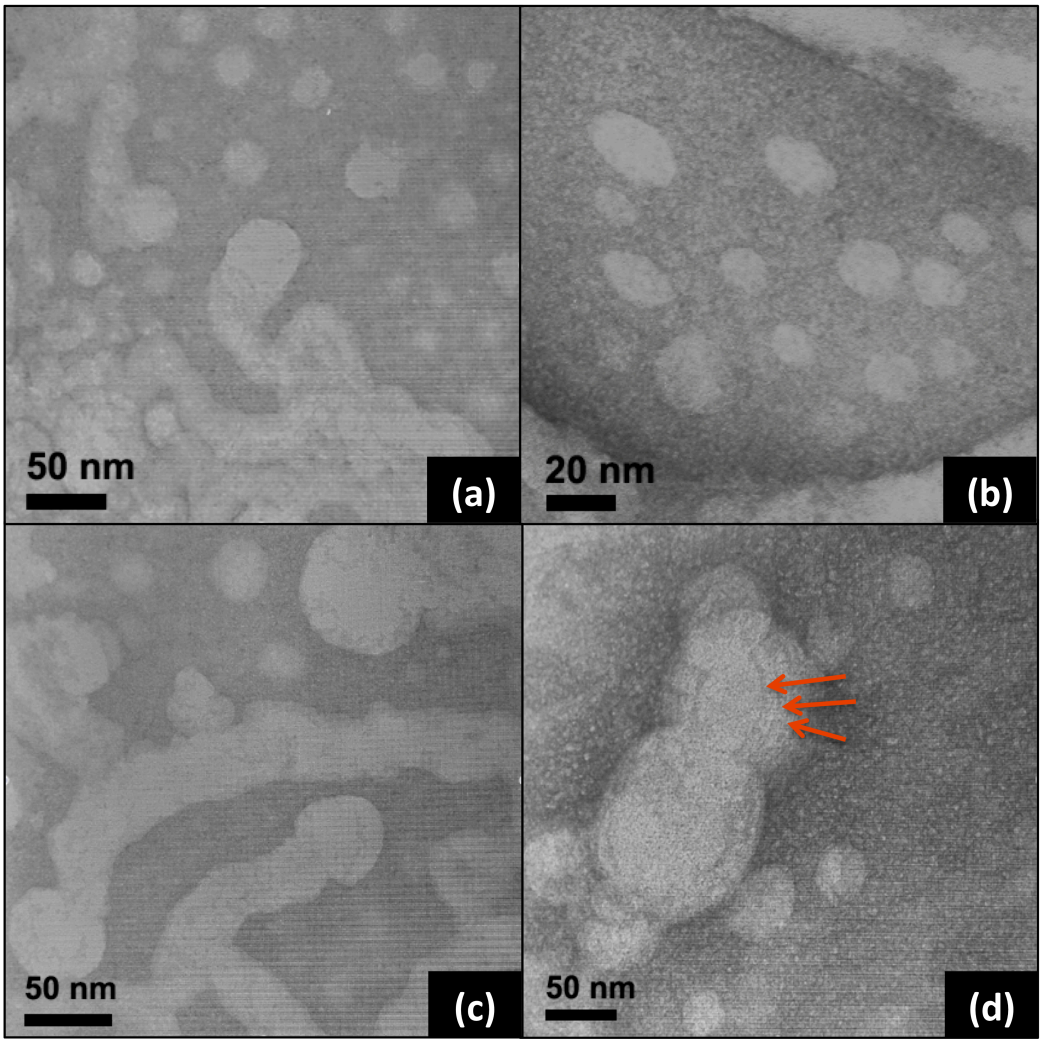


Figure B.13 - Additional TEM images (taken with negative uranyl acetate staining) of: (a) $MPEG_{12}$-$PHAz_3$-$MPEG_{12}$, (b) $MPEG_{12}$-$PHAz_6$-$MPEG_{12}$, (c) $MPEG_7$-$PHAz_3$-$MPEG_7$, (d) $MPEG_7$-$PHAz_3$-$MPEG_7$. Note the possible membrane structure (red arrows) detected in polymer (d), which might indicate the presence of vesicles.

Polymer (a) and (c) show the presence of few spherical micelles, aggregated micelles and some considerably large wormlike micelles, which can be formed upon fusion of smaller spherical micelles. Polymer (b) displays only non-

aggregated spherical micelles with diameters approximately ranging from 10 to 25 nm. Finally, the micrograph of polymer (d) shows some large aggregates where a tenuous concentric pattern is detected (red arrows), which might indicate the presence vesicles.

B.4 CMC studies

The CMC of was determined from the absorption of 1,6-diphenyl-1,3,5-hexatriene (DPH) at a fixed concentration (0.004 mM) with increasing polymer concentration. The absorbance at 362 nm *vs* concentration (% wt) for polymers (a), (c) and (d) is shown (Figure B.14 to Figure B.16). The data were fitted with a logistic growth function (red line), whilst the CMC was determined as the crossing point of the extrapolated lines at low and high concentration.

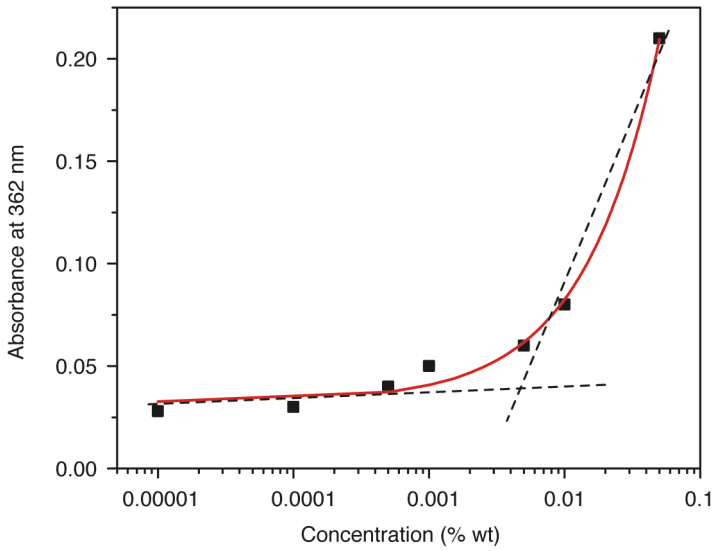


Figure B.14 – Determination of CMC by extrapolation method for polymer (a) $MPEG_{12}$-$PHAz_3$-$MPEG_{12}$.

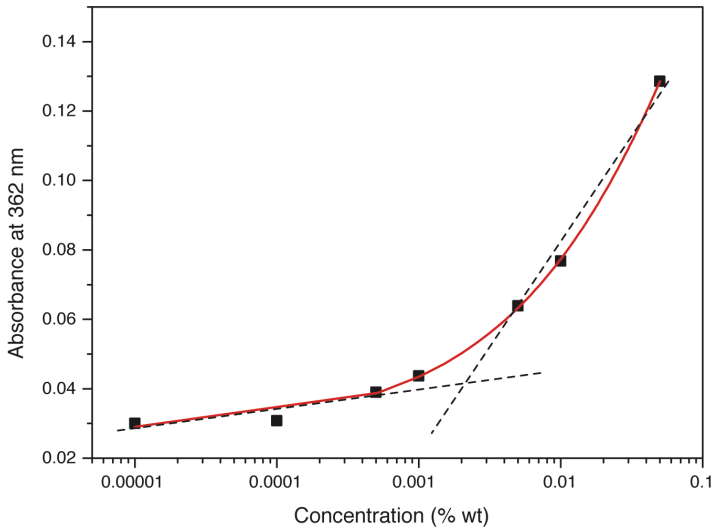


Figure B.15 – Determination of CMC by extrapolation method for polymer (c) $MPEG_7$-$PHAz_3$-$MPEG_7$.

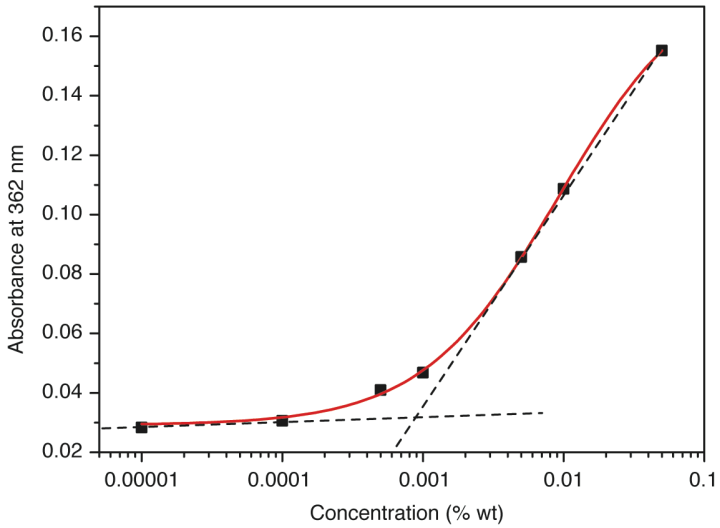


Figure B.16 - Determination of CMC by extrapolation method for polymer (d) $MPEG_7$-$PHAz_6$-$MPEG_7$.